SYNTHESIS AND ASSEMBLY OF COPPER AND COPPER (I, II) OXIDES NANOSTRUCTURES

CHANG YU

NATIONAL UNIVERSITY OF SINGAPORE

2007

SYNTHESIS AND ASSEMBLY OF COPPER AND COPPER (I, II) OXIDES NANOSTRUCTURES

CHANG YU

(B. Eng., IMPU; M. Eng., DUT)

A THESIS SUBMITTED

FOR THE DEGREE OF DOCTOR OF PHILOSOPHY

DEPARTMENT OF CHEMICAL AND BIOMOLECULAR ENGINEERING

NATIONAL UNIVERSITY OF SINGAPORE

2007

ACKNOWLEDGEMENTS

I wish to express my deepest gratitude to my supervisor, Professor Zeng Hua Chun, for his careful selection of the research topic, his invaluable direction and advice in the experiments, and his encouragement throughout the duration of this research. His dedication and preciseness in the scientific research have also greatly inspired me.

I also want to sincerely thank our group members， Mr Wei Xuming, Dr Jeyagowry T. Sampanthar, Dr Xu Rong, Mr Feng Ji, Mr Yang Huagui, Mr Low Xiongwen, Mr Liu Bin and Ms Li Jing for their timely advice and help in my experimental work. At the same time, I would like to show my sincere appreciation to Ms Lee Wei San, Mr Zhao Rui, Mr Khoo Keat Huat, Ms Tang Weng lin, Mr Teo Joong Jiat and Ms Lye Mei Ling for their tireless help in experiments.

Here I am also indebted to all the staff in the General Office and Instrument Laboratories. For technical support, I am especially grateful to Dr Li Sheng and Mdm Sam Fam Hwee Koong for XPS, Mr Chia Phai Ann and Dr Yuan Ze Liang for SEM and FESEM, Mr Mao Ning for TEM, and Mdm Khoh Leng Khim for BET. Many thanks go to Ms Lee Chai Keng and Ms Tay Choon Yen for their support in running other instruments.

TABLE OF CONTENT

SUMMARY

Copper and copper oxides (CuO and Cu_2O) are very important chemicals in assuring the qualities of our lives. This thesis reports the synthesis of metallic Cu, cuprous oxide (Cu_2O), and cupric oxide (CuO) with different nanostructures. Their structures, compositions and physicochemical properties were characterized with methods of TEM/SEM/FESEM/XRD/BET/XPS. Their crystalline growth mechanisms were also studied.

We first developed several wet-chemical methods for the synthesis of one-dimensional CuO nanostructures in water-ethanol mixed solvents at 77-82 ^oC and 1 atm. Owing to the high concentration of NaOH, the Cu^{2+} in the form of $[Cu(OH)_4]^{2-}$ transformed into CuO at 77-82 ^oC directly without passing through $Cu(OH)_2$ precursor. The crystal structure of CuO nanorods and nanoribbons has also been demonstrated. Through the experiments, the crystal growth mechanism has been discussed and various synthesis parameters have also been investigated.

Secondly, we fabricated Cu_2O products in different nanostructures under different reaction conditions. It is well known that Cu^{2+} can easily form CuO crystallites at high temperatures in a basic solution. Thus in our experiments, we systematically investigated the synthesis of Cu_2O nanostructures using acidic and basic conditions respectively. In the acidic condition, with formic acid selected as the

reductant, a full range of novel multipod frameworks of Cu_2O microcrystals was prepared and a new organization scheme for three-dimensional crystal aggregates has been elucidated, that is, faceted microcrystal subunits (6, 8, and 12 pieces) with simple cubic or face-centered cubic lattices were organized with space instruction of the formed frameworks.

We further synthesized Cu_2O crystallites in the *N,N*-dimethylformamide (DMF) solution. At high temperature, DMF was hydrolyzed into formic acid and dimethylamine. Thus the solution was in the basic condition and CuO was initially formed in the process. DMF also acted as the reductant and the capping agent for the formation of the Cu_2O crystallites. With pure DMF as the solvent, Cu_2O hollow spheres were fabricated without the assistance of solid templates. In the voiding process of the Cu_2O hollow spheres, Ostwald ripening was utilized in controlling crystallite size of shell structures, and thus resulted in effective tuning of the optical band gap energy of Cu_2O (in the range of 2.405-2.170 eV). In this reaction process, the water had a great influence on the morphology of Cu_2O.

We systematically studied the effect of water added into the Cu^{2+} DMF solution on Cu_2O morphologies after reaction at high temperatures. With the increase of water in the Cu^{2+} (0.005-0.01 M) DMF solution, the morphology of formed Cu_2O changes from hollow spheres to hollow cubes and then to large cubes. With the optimization of different parameters, Cu_2O single-crystalline hollow cubes were obtained.

Thirdly, we synthesized highly regulated ultralong copper nanowires under mild conditions, in which a high concentration of NaOH and a small amount of EDA were used to control the morphologies of Cu nanowires. The nanowires prepared were straight and highly regulated, with constant diameters in the range of 60–160 nm (mostly in 90–120 nm). The wires were ultralong, having lengths of more than 40 μm. The growth direction of these wires was along the <110>.

Finally, Chapter 9 makes a brief conclusion on the major results of the present studies related to CuO, Cu_2O and Cu nanostructures and the self-organized growth processes. Moreover, in this chapter, some suggestions for future work in this area are also provided.

NOMENCLATURE

AC	adventitious carbon
AOT	sodium bis(2-ethylhexyl)sufosuccinate
BE	binding energy (eV)
BEs	binding energies (eV)
BET	Brunauer-Emmett-Teller method
CTAB	cetyltrimethylammonium
d	distance between two planes
d_{hkl}	distance between reflection planes (hkl)
D_p	average crystalline size (nm)
DMF	*N,N*-dimethylformamide
ED	electron diffraction
EDA	ethylenediamine
EDX	Energy Dispersive X-Ray Spectroscopy
Eq.	equation
Eqs.	equations
ϕ	specimen tilted angle in transmission electron microscope analysis
FESEM	field emission scanning electron microscopy
FWHM	full width at half maximum
h	hour(s)
HRTEM	high resolution transmission electron microscope

λ	wavelength of X-ray radiation (0.1506 nm for Cu Kα radiation)
λ_e	wavelength of electron beam
PDMS	poly(dimethylsiloxane)
PEG	polyethyleneglycol
PVA	polyvinyl alcohol
PVP	polyvinylpyrrolidone,
PVS	poly(vinyl sulfate)
θ	diffraction angle in the X-ray diffraction measurements (^{o})
SAED	selected area electron diffraction
SDBS	sodium dodecyl benzenesulfonate
SDS	sodium dodecyl sulfate
T	temperature
TEM	transmission electron microscope
THF	tetrahydrofuran
TOAB	tetraoctylammonium bromide
XPS	X-ray photoelectron spectroscopy
XRD	X-ray diffraction

LIST OF FIGURES

LIST OF TABLES

PUBLICATIONS RELATED TO THE THESIS

1. J.J. Teo, Y. Chang and H.C. Zeng, Fabrications of Hollow Nanocubes of Cu_2O and Cu *via* Reductive Self-Assembly of CuO nanocrystals, **Langmuir.** 22 (2006) pp 7369-7377.

2. Y. Chang, M.L. Lye and H.C. Zeng, Large-Scale Synthesis of High-Quality Ultralong Copper Nanowires, **Langmuir,** 21 (2005), pp 3746-3748.

3. Y. Chang, J.J. Teo and H.C. Zeng, Formation of Colloidal CuO Nanocrystallites and Their Spherical Aggregation and Reductive Transformation to Hollow Cu2O Nanospheres, **Langmuir,** 21 (2005), pp 1074-1079.

4. Y. Chang and H.C. Zeng, Manipulative Synthesis of Multipod-Frameworks for Self-Organization and Self-Amplification of Cu_2O Microcrystals, **Crystal Growth & Design,** 4 (2004), pp 273-278.

5. Y. Chang and H.C. Zeng, Controlled Synthesis and Self-Assembly of Single-Crystalline CuO Nanorods and Nanoribbons, **Crystal Growth & Design,** 4 (2004), pp 397-402.

CHAPTER 1

SCOPE OF THE THESIS

Copper and copper oxide (CuO and Cu_2O) are very important chemicals, due to theirexcellent physical and chemical properties. Copper was applied in ancient time from bronze/brass cookwares, artefacts and weapon, to wires and cables in modern electrization (Calcutt, 2001; Joseph 1999; Yong et al., 2002). Cuprous oxide (Cu_2O) is a *p*-type semiconductor with a band-gap of 2.17 eV. The Cu_2O crystal has a cubic structure (SG: *Pn3m*) and has the potential applications in solar energy conversion, catalysis, crystal rectifiers, antifouling pigment and fungicide. Cupric oxide (CuO) is also a *p*-type semiconductor with a band-gap of 1.2 eV. As a unique monoxide compound with the monoclinic structure (different from normal rock-salt type structure), CuO has complex magnetic phases and forms the basis for several high-T_c superconductors and materials with giant magnetoresistance. CuO is also used for the preparation of a wide range of organic-inorganic nanostructured composites with unique characteristics, heterogeneous catalysts in many important chemical processes. It can also be used as pigment, fungicide, gas sensors, lithium battery and solar cells owing to its photoconductive and photochemical properties.

Due to their importance in our lives, we fabricated the Cu, Cu_2O and CuO

nanostructures and studied their crystal growth mechanism in this thesis. Since a Cu^{2+} salt is generally selected as the starting reactant, in this thesis, the synthetic order is the synthesis of CuO, Cu_2O and Cu nanostructures. Specifically, the objectives of this thesis are as follows:

1. Controlled synthesis of single-crystal CuO nanorods and nanoribbons in high concentration of NaOH;

2. Manipulative fabrication of Cu_2O multi-pod framework in acidic condition;

3. Fabrication of Cu_2O hollow spheres in *N,N*-dimethylformamide (DMF) basic condition;

4. Fabrication of Cu_2O hollow cubes by adjusting water volume in DMF solution;

5. Fabrication of Cu_2O nanocubes in DMF–ethanol mixed solvents;

6. The spinning of single-crystal copper nanowires.

First of all, Chapter 2 introduces the development of nanomaterials and nanotechnology. Then the crystal structures, the application and preparation of Cu, CuO and Cu_2O are introduced respectively.

Chapter 3 summarizes the general synthetic procedures in preparing Cu, CuO and Cu_2O nanostructures. The principles and methods of all used instruments (TEM/SEM/FESEM/XRD/BET/XPS) are briefly discussed and the experimental conditions usually used are also described.

In Chapter 4, we first developed several wet-chemical methods for the synthesis of one-dimensional CuO nanostructures in water-ethanol solvents at 77-82 ^{o}C at 1 atm. Owing to the high concentration of NaOH, the Cu^{2+} in the form of $[Cu(OH)_4]^{2-}$ transformed into CuO at 77-82 ^{o}C directly without passing through $Cu(OH)_2$ precursor. The crystal structures of CuO nanorods and nanoribbons are also discussed. Through the experiments, the crystal growth mechanism is discussed and various synthetic parameters are also investigated.

It is well-known that Cu^{2+} can easily form CuO at high temperature in a basic solution. In order to manipulatively synthesize Cu_2O directly from Cu^{2+}, we control the solution in acidic condition, with formic acid selected as the reductant (see Chapter 5). In this method, a range of novel multipod frameworks of Cu_2O microcrystals has been prepared and a new organization scheme for three-dimensional crystal aggregates has been elucidated, that is, faceted microcrystal subunits (6, 8, and 12 pieces) with simple cubic or face-centred cubic lattices have been organized with space instruction of the formed frameworks.

In Chapter 6, hollow Cu_2O nanospheres have been fabricated under solvothermal conditions without the assistance of solid templates. The selected solvent of DMF is not only the reductant, but it is also the capping agent for the formation of the Cu_2O crystallites. In the voiding process of the Cu_2O hollow nanospheres, Ostwald ripening is utilized in controlling crystallite size of shell structures, and thus results in effective tuning of the optical band gap energy of Cu_2O (in the range of 2.405-2.170

eV).

In the solvothermal synthesis of Cu_2O hollow spheres (Chapter 6), a small amount of water can greatly influence Cu_2O morphologies. Thus, in Chapter 7, we systematically studied the effect of water on Cu_2O morphologies. With the increase of water in the DMF, the morphology of Cu_2O changes from hollow spheres, to hollow cubes and then to large cubes. With the optimization of the different parameters, Cu_2O single-crystal hollow cubes have been obtained.

In Chapter 8, using low-cost starting chemicals, the large-scale synthesis of highly regulated ultralong copper nanowires can be achieved under mild conditions, in which a high concentration of NaOH and a small amount of ethylenediamine (EDA) are used to control the morphologies of Cu nanowires. The nanowires prepared are straight and highly regulated, with constant diameters in the range of 60–160 nm (mostly in 90–120 nm). The wires are ultralong, having lengths of more than 40 μm. The growth direction of these wires is along the <110>.

Finally, Chapter 9 concludes with the major results of the present studies related to Cu, CuO and Cu_2O nanostructures and the self-organized growth processes. Some suggestions for future work in this area are also provided.

CHAPTER 2

LITERATURE REVIEW

2.1 Nanomaterials and Noanchemistry

Stone, bronze, iron: Civilization has always been defined by Man's relationship with materials (Hampden-Smith and Interrante, 1998). Nowadays, materials science is a hot topic in scientific research and has witnessed substantial progress in the synthesis, characterization and understanding of materials from atomic dimensions to nanoscales (Averback et al., 1991).

Nanostructured materials may be defined as those materials whose structural elements—clusters, crystallites or molecules—have dimensions in the 1 to 100 nm range (Moriarty, 2001). When the particle size of materials is reduced to nanoscale, the interactions among the particles are intensified owing to the tremendous specific surface area. Therefore, the intrinsic properties such as electronic, magnetic, optical, physical and chemical properties of the materials have been found to be very different from those of the bulk form (Ozin, 1992). For example, small clusters of transition metal atoms have been found to have reactivities that are considerably larger than those of the bulk metal and vary by orders of magnitude with size (Ozin, 1992).

Over the past decade, huge advances have been achieved both in the synthesis of size-tunable, monodipersed nanoclusters and in the development of techniques for their assembly into well-ordered nanostructured solids (Moriarty, 2001). Considering

the composition, application and research development, nanomaterials can be generally categorized into the groups as follows (Xu[4], 2004(b)):

A) Carbon nanotubes;

B) Semiconductors (Si, Ge, GaP, GaAs, GaSb, InP, InAs, InSb, CdS, CdSe, CeTe, ZnS, ZnSe, ZnTe, PbS, PbSe and PbTe);

C) Ceramics (Al_2O_3, TiO_2, SiO_2, ZrO_2, CeO_2, SiC and composites of these compounds, such as zeolite, amorphous aluminosilicate, etc);

D) Metals and metal alloys (Au, Pt, Pd, Ru, Ag, Co, Ni, Fe, Cu, Ag-Pd, Co-Ni, Fe-Co, Pt-Pd, M50 steel, etc);

E) Metal hydroxides and oxides ($Mg(OH)_2$, MgO, Fe_2O_3, Co_3O_4, ZnO etc).

As one of the main branches of solid-state chemistry, nanochemistry is concerned with the research on syntheses, structures and properties of nanomaterials (Suryanarayana and Koch, 1999). Nanochemistry began from the preparation of the uniform colloids. With the development of colloid chemistry and preparation of a large amount of nano-sized compounds, the special characteristics and properties of these nanomaterials were recognized, and therefore more studies have been focused in this field. It is well known that the properties of materials depend on its composition, size and shape of particles. Thus the objective of nanochemistry is to develop the novel nanomaterials, to control size and shape of nanoparticles, and further to enhance their properties and functions.

The development of nanochemistry has passed through two stages in the past

twenty years. The first stage is the preparation of uniform colloids, including metal oxide or non-oxide, and composite. The influences of pH values and concentrations of all kinds of ions on particles size and shape were completely investigated (Matijević, 1993). The second stage is the fabrication of all kinds of nanostructures, including one-dimensional nanotubes, nanowires, nanorods and nanoribbons, two-dimensional self-assembly superlattice devices, and three-dimensional nanocubes, hollow spheres, hollow cubes, multi-pod nanocrystals et al. Many new fabrication methods are developed.

2.1.1 Nanostructures

2.1.1.1 Nanowires, nanorods, nanobelts and Nanotubes

One-dimensional structures are always the focal point in nanochemistry, owing to the difficulties in the synthesis or fabrication of these structures with well-controlled dimensions, morphology, phase purity, and chemical composition. A variety of novel chemical methods have been developed for fabricating 1D nanostructures in the past several years. These methods can be summarized into i) 1D crystal growth of anisotropic crystallographic structures; ii) use of various templates (including "soft template" of capping reagent) to direct the formation of 1D nanostructures; iii) introduction of a liquid-solid interface to reduce the symmetry of a seed; iv) self-assembly of 0D nanostructures; v) size reduction of a 1D microstructures (McCann et al., 2005; Remskar, 2004; Tang[1] and Kotov, 2005; Wu[5] et al., 2002; Xia et al., 2003). The synthesized 1D solid nanomaterials include WS_2, MoS_2, ZnS, NbS_2, TaS_2, HfS_2,

ZrS_2, Te, Se, VO_x, TiO_2, Al_2O_3, GaN, GaAs, InGaAs, Au, Co, Fe, Si etc. (McCann et al., 2005; Remskar, 2004; Tang[1] and Kotov, 2005; Wu[5] et al., 2002; Xia et al., 2003).

2.1.1.2 Hollow spheres and hollow cubes

The fabrication of monodispersed hollow structures (including hollow spheres and hollow cubes) has also attracted interests in past several years, owing to their different structural, optical, electrical, thermal and surface properties from those of their sold forms. Applications of materials of this kind are diverse, including capsules for drug delivery, artificial cells, low dielectric constant materials, acoustic insulation, photonic crystals, shape-selective adsorbents, catalysts, fillers and so on (Caruso[1] and Caruso, 1998; Caruso[1] et al., 2001(a); Caruso[2] et al., 2001; Collins et al., 2003; Gou and Murphy, 2003; Hentze et al., 2003; Naik et al., 2003; Park[1] et al., 2003; Sun[3] et al., 2002(a), 2003(a); Sun[3] and Xia, 2002(b, c); Torimoto et al., 2003; Wang[12] et al., 2004; Yang[4] et al., 2003; Yin[2] et al., 2001; Zhong et al., 2000).

Concerning the fabrication of hollow nanomaterials, there have been two main categories of preparative methods: (i) the template-directed synthesis, and (ii) the emulsion synthesis. The basis of the template-directed synthesis is adsorption of nanoparticles or polymerization on modified polymeric (e.g., polystyrene) (Caruso[1] and Caruso, 1998; Caruso[1] et al., 2001(a); Caruso[2] et al., 2001; Göltner, 1999; Liang[2] et al., 2003; Valtchev, 2002; Wang[2] et al., 2002; Yang[4] et al., 2003; Yin[2] et al., 2001; Zhong et al., 2000) or inorganic (e.g., SiO_2) (Kamata et al., 2003; Kim[2] et al., 2003; Kim[3] et al., 2002; Mandal et al., 2000; Torimoto et al., 2003) template surface and

subsequent removal of the template by calcinations or dissolution with solvents. Recently a novel sacrificed silver cube templating method is developed for fabrication of hollow cubes, but the formed materials are only limited to Au, Pd and Pt metal (Sun[3] et al., 2002(a), 2003(a); Sun[3] and Xia, 2002(b, c)). In emulsion synthesis, the solution is emulsified and the adsorption or reaction then takes place on the surface of sol droplets (micelles) to form the hollow spheres. This method can also be viewed as another version of templating, and after reaction, the "soft" template can be removed directly from the formed hollow spheres (Collins et al., 2003; Dinsmore et al., 2002; Hentze et al., 2003; Hu[2] et al., 2003; Kulak et al., 2002; Li[7] et al., 2003(a); Naik et al., 2003; Park[1] et al., 2003; Wu[3] et al., 2003; Yang[1] and Zeng, 2004(a); Yang[2] and Zhu, 2003).

2.1.1.3 Multi-pod nanostructures

It is well known that the applications of materials might associate with the complexity of material structures. Thus the fabrication of more complex multi-pod nanostructures has currently received much attraction (Chen[5] et al., 2002; Ito, 1998(a); Jun et al., 2001, 2002; Lao et al., 2002; Li[5] et al., 2003(a); Manna et al., 2000, 2003; Sun[2] et al., 2002; Wan et al., 2003). Of all the multi-pod materials, the formed tetrapod-branched crystals generally occur in group II-VI semiconductors, such as ZnO (Ito, 1998(a); Lao et al., 2002; Sun[2] et al., 2002; Wan et al., 2003), CdS (Chen[5] et al., 2002; Ito, 1998(a); Jun et al., 2001), CdSe (Ito, 1998(a); Manna et al., 2000) and CdTe (Ito, 1998(a); Manna et al., 2003). These crystals have two kinds of crystal structures,

that is, cubic zinc blend (ZB) and hexagonal wurtzite (W) (Ito, 1998(a)). These tetrapod structure has a ZB type core with four {111} facets and four W type pods then extend from the four {111} facets, due to the identical structure of cubic BZ {111} facets and hexagonal W ±(0001) facets (Ito, 1998(a)). In addition, tetra-pod CuCl with BZ type crystal structure was also synthesized (Li[5] et al., 2003(a)).

2.1.1.4 Self-assembled superstructures

Self-assembly is the autonomous organization of components into patterns or structures without human intervention (Whitesides and Grzybowski, 2002). The self-assembly of nanoparticles is an attractively "bottom-up" method for the synthesis of superstructures and nanodevices. In the past several years, self-assembly attracted great interests due to following reasons. The first, self-assembly is one of the practical strategies for constructing the nanostructures. The second, self-assembly is common to many dynamic, multicomponent systems, such as electronic devices, diatom biosilica, bilayered membranes, photonic crystals and liquid crystals et al (Black et al., 2000; Dumestre et al., 2004; Fudouzi and Xia, 2003; Geissler and Xia, 2004; Jacobs et al., 2002; Sumper, 2002; Trau, 1997; Whitesides and Grzybowski, 2002; Wijnhoven and Vos, 1998). The self-assembled nanostructures include 2-D and 3-D superlattices with two kinds of driving forces, that is, static and dynamic. Generally, the self-assembly process involves the preparation of colloidal nanocrystals (NCs) of controlled composition, size, shape and internal structures, and the manipulation of these materials into ordered NC assemblies (Superlattices) (Murray et al., 2001).

At present, self-assembly is mainly used in magnetic crystals, photonic crystals and semiconductors. The assembled nanostructured materials include Co,

$Co_{core}Ag_{shell}$ nanoparticles, Fe, Ni, Fe_2O_3, Fe_3O_4, PbSe, TiO_2, CdSe, Diatom Biosilica, Silica, polystyrene particles etc (Bala et al., 2004; Black et al., 2000; Dumestre et al., 2004; Fudouzi and Xia, 2003; Hyeon, 2003; Jiang[1] et al., 2003(a); Kim[4] et al., 2005; Murray et al., 2001; Puntes et al., 2001; Sumper, 2002; Trau et al., 1997; Wijnhoven and Vos, 1998; Zaitseva et al., 2005).

2.2 Crystal structure, application and synthesis of copper (Cu)

2.2.1 Crystal structure and application of copper (Cu)

Copper is reddish, with a bright metallic luster. The crystal structure of copper metal is face-centred cubic (fcc). The group lattice is *Fm3m* with a_o = 3.607 Å (Buchanan, 1997). Figure 2.1 is the ball-line model of cubic structure of Cu metal.

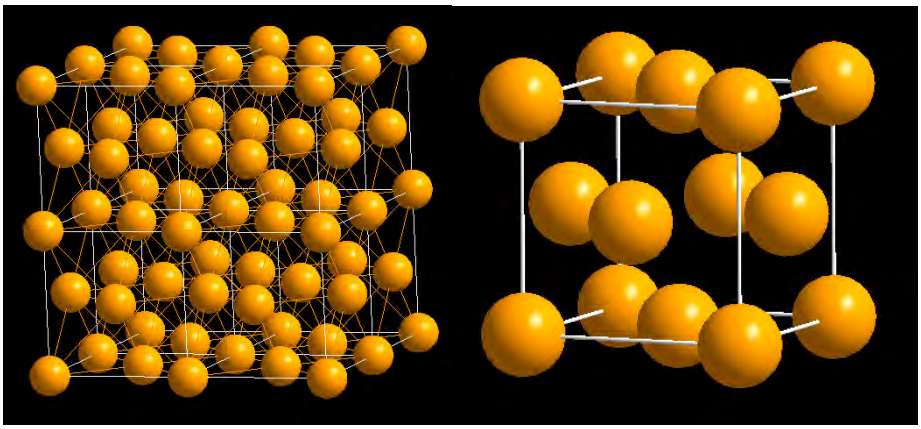

Figure 2.1 Crystal structure of metallic Cu: group lattice: *Fm3m*; a_o = 3.607 Å.

Copper is malleable, ductile and corrosion resistant. It is an excellent conductor of heat and electricity. In the past two centuries, copper helped us realize several waves of industrial revolution. With an annual production of more than 15

million tons and more than 60% of the total amount used in the electrical industry, It can be said that the copper cable supports our modern electrical industry and our modern life. Table 2.1 lists some of the reasons why copper and copper alloys are vital to the major types of application that benefit from combinations of the attributes described (Calcutt, 2001; Joseph 1999; Yong et al., 2002).

2.2.2 Synthetic strategies for metallic copper nanostructures

Metallic copper has been used in a wide variety of commercial applications, especially in the modern electrical industry. With the requirement of small size and development of the nanometer technique, its properties can be enhanced by processing it into various nanostructures with well-controlled dimensions and aspect ratios. In the past decade, various forms of metallic copper nanostructures have been synthesized, including nanoparticles, nanowires, nanotubes, and nanorods. The methods include electrochemical deposition, vapor deposition, reverse micelles et al. The fabrication of element copper nanostructures is reviewed in the following sections.

2.2.2.1 Sol-gel formation of copper nanoparticles

The sol-gel method is one of the approaches to prepare well-dispersed nanoparticles and homogenous thin films by tailoring the structure of a primary precursor in which metal atoms distribute uniformly. This method is mainly based on the hydrolysis and polycondensation of a metal alkoxide, which ultimately yields hydroxide or oxide under certain conditions. To obtain homogeneous macromolecular

Table 2.1 Attributes and Applications of Copper and Copper Alloys.

Property	**Industry/Type of Application**
Aesthetics	Architecture, sculpture, jewellery, clocks, cutlery.
Bactericide	Door hardware, marine internal combustion engines, and crop treatments.
Biofouling resistance	Hydraulic and marine engineering, metalworking, aerospace, power generation, shipbuilding, offshore oil and gas platforms.
Corrosion resistance	Plumbing tubes and fittings, roofing, general and marine engineering, shipbuilding; chemical engineering, industrial processes including pickling, etching and distilling; domestic plumbing, architecture, desalination, textiles, papermaking.
Ease of fabrication	All of the above plus printing.
Electrical conductivity	Electrical power generation, transmission and distribution, communications, resistance welding, electronics.
Environmental friendliness	Essential for health of humans, animals and crops
Fungicide	Agriculture, preservation of food and wood.
Low temperature properties	Cryogenics, liquid gas handling, superconductors.
Mechanical strength/ductility	General engineering, marine engineering, defence, aerospace.
Non-magnetic	Instrumentation, geological survey equipment, minesweepers, offshore drilling.
Non-sparking	Mining and other safety tools, oxygen distribution.
Elasticity	Electrical springs and contacts, safety pins, instrument bellows, electronic packaging.
Thermal conductivity	Heat exchangers and air-conditioning/refrigeration equipment, automotive radiators, internal combustion engines, mining.

oxide networks for qualified nanomaterials in sol-gel process, controlling experimental conditions such as pH, solution concentration, and temperature etc is essential (Wang[13] et al., 2003(a)).

The conventional sol-gel methods are also the most important ones to generate metallic copper nanoparticles when reductants were added into the Cu^{2+} solution. Compared with oxides or hydroxides, metal particles are generally active and therefore aggregate to form large particles. Dhas et al. (1998) synthesized copper nanoparticles by refluxing the copper (II) hydrazine carboxylate aqueous solution at 80 ^{o}C for 3 h. The metallic copper clusters present irregular shaped particles (200-250 nm), having sharping edges and facets. It is obviously difficult to synthesize very fine and homogeneous copper particles owing to the high surface energy of copper metal. In order to control the morphology and particles size of copper particles, polymers, surfactants and organic complexes were usually added in the sol-gel synthesis process.

Complexes are helpful in controlling the Cu particle size and morphology in the synthesis process. Hsu et al. (1990) firstly generated cubic metallic copper particles in the $Cu(NO_3)_2$ solution with urea as a complex compound. The size of copper cubes ranged 1-10 μm. Henglein (2000) formed colloidal copper particles (20-100 nm) with the γ-irradiation of the aqueous solutions of $KCu(CN)_2$, which also contained methanol or 2-propanol as OH scavenger. Complexes can greatly decrease the concentration of free cations in the solution, and at the same time, many complexes can form special structures, like the “nanoreactors”, to influence the particle size and morphology, e.g., the dendrimer structure of poly(amidoamine) (PAMAM) complex. The PAMAM

dendrimer is important in the synthesis of Cu nanoclusters. After complexation within various surface modified PAMAM dendrimers, copper (II) ions were reduced by hydrazine or sodium borohydrite to zero-valent dendrimer-copper nanocomposite (Balogh and Tomalia, 1998; Zhao et al., 1998, 1999). More importantly, Cu cluster size ranging from 1 to 2 nm can be controlled by varying the size of the host-dendrimer nanoreactor. A family of diaminobutane (DAB) core, poly(propylene imine) dendrimers were coordinated to Cu(II) to form DAB-Am(n)-Cu(II) complexes (Floriano et al., 2001). The complexes were reduced to DAB-Am_n-$Cu(0)_{cluster}$ with $NaBH_4$. It was found that the size of the nanoclusters is a function of the *n/x* ratio of the DAB-Am_n-$Cu(II)_x$ precursors, with high monodispersity.

Recently, with the development of molecular biology, the space structures of some biomolecules have been illustrated, e.g., DNA and some peptides, and its complicated structures can be also developed as nanobioreactors for nanostructured materials (Banerjee et al., 2003; Becerril et al., 2004; Monson and Woolley, 2003). Monson and Woolley (2003) deposited Cu metal onto surface-attached DNA, forming nanowire-like structures that are around 3 nm tall. In this process, the Cu^{2+} initially associated with DNA and reduced by ascorbic acid to form a metallic copper sheath around DNA. A sequenced histidine-rich peptide nanotubes were also adopted as the templates. Cu nanocrystals with high packing density were uniformly coated on the histidine-incorporated nanotubes (Banerjee et al., 2003).

Polymers and surfactants are widely used to control the particle size and morphology in the synthesis of nanomaterials. The polymers used in the synthesis of

copper particles include polyvinyl alcohol (PVA), polyvinylpyrrolidone (PVP), polyethyleneglycol (PEG), poly(dimethylsiloxane) (PDMS) and poly(vinyl sulfate) (PVS) (Cao[2] et al., 2003; Henglein, 2000; Huang et al., 1997; Kapoor and Mukherjee, 2003; Kumar et al., 2001(b); Liu[2] et al., 2003; Savinova et al.,1988; Yen et al., 2003). The addition of polymers can greatly increase the resistance of the cation diffusion in solutions and therefore decrease the copper particle size. For example, Huang et al. (1997) synthesized copper nanoparticles by reduction of copper (II) acetate in water or in 2-ethoxyethanol in the presence of PVP. The average size varied from 6.6 to 22.7 nm in ethoxyethanol and from 15.5 to 30.2 nm in water. As the most important conductive wires in the electrical industry, the synthesis of one-dimensional nanorods or nanowires attracts great attention in materials chemistry. Liu[2] et al. (2003) synthesized the copper nanoparticles, copper 1D array nanoparticles wrapped in PVP and nanorods by adjusting the concentration of copper ion and PVP and the refluxing time. In the reaction, PVP was used as a surface modified reagent as well as a soft template. Cao[2] et al. (2003) prepared junctions of copper nanorods with polymer-surfactant (PEG-CTAB) added together into the $CuCl_2$ solutions. The reaction conducted at 100 ^{o}C and potassium borohydride was used as reductant. In the process, the micelles of the cationic surfactant CTAB are usually rod-shaped and the linear polymer chains normally present random coil structures in the solution. Since there exist interactions (e.g., strong hydrophobic interaction, Van der Waals force and electrostatic interaction) between water-soluble polymer and cationic surfactant, the surfactants associating with the polymer chains form micellar aggregates at a rather

low concentration. Thus the supermolecular aggregates form in the solution with the coils of PEG chains as the core, around which are rod-shaped cetyltrimethylammonium (CTAB) micelles. Such aggregates composed of polymer coil and rod-shaped micelles can act as templates for the precipitation of Cu due to the interaction of Cu^{2+} with them (Cao[2] et al., 2003).

In order to synthesize the long copper nanowires, Liu[6] et al. (2003(c)) added the surfactant of sodium dodecyl benzenesulfonate (SDBS) in the Cu(II) glycerol complexes solution in the presence of reductant of phosphite at 120 ^{o}C. The copper nanowires had preferred [110] growth direction with average diameters of ~85 nm and lengths of several hundreds micrometers. The SDBS and CTAB are commonly used surfactants in synthesizing copper particles (Cao[2] et al., 2003; Liu[6] et al., 2003(c); Wu[4] and chen, 2004).

2.2.2.2 Micelles or microemulsion method

Reverse micelles are thermodynamically stable mixtures of water, oil, and surfactants where the water regions are separated from oil by a monolayer of surfactants. Due to the amphiphilic nature of the surfactant, numerous disordered or partially ordered phases are formed, depending on temperature and surfactant concentration (Lisiecki and Pileni, 1995(a)). The widely used reverse micelle system to synthesize metallic copper particles is sodium bis(2-ethylhexyl)sufosuccinate (AOT)/water/isooctane or AOT/water/cyclohexane, and sodium borohydrate or hydrazine is reductant in the reaction (Cason et al., 2001; Lisiecki and Pileni, 1993,

1995(a) (b); Lisiecki et al., 2000(a), (b), (c); Pileni and Lisiecki, 1993; Pileni et al., 1998; Salzemann et al., 2004; Tanori and Pileni,1997). The water content *w* (*w* = $[H_2O]/[AOT]$) is a very important factor to influence the Cu particle size. With the value of *w* from 1 to 20, the Cu nanoparticles generally distribute in the range of 2-20 nm. The concentration of AOT also greatly influences the Cu particle size. When the [AOT] increases, the nanoparticle size of copper decreases (Lisiecki and Pileni, 1995(a); Pileni and Lisiecki, 1993). In this reaction system, Salzemann et al. (2004) changed the hydrazine content R (R = $[N_2H_4]/[Cu(AOT)_2]$) from 3 to 15, and copper nanocrystals favor formation of various isotropic and anisotropic shapes. Cubes, flat triangles, pentagons, and elongated forms are thus observed. Through adjusting the parameters, reverse micelles method can be used in fabricating 1D Cu nanostructures. Lisiechi et al. (2000 (a)) fabricated Cu truncated decahedral cylinder with R = 3 and *w* = 30. When water was replaced with the NaCl aqueous solutions (0-2.4 mM), Cu cylinders or rods were also fabricated (Lisiecki et al., 2000(b), (c); Pileni et al., 1998). The other used microemulsion systems include tetraoctylammonium bromide (TOAB)/water/tetrahydrofuran (THF) and DBS/water/toluene systems (Chen[2] and Sommers, 2001; Guo et al., 1999). The sizes of resulting Cu nanoparticles are in 1-2 and 4.0 nm respectively. Recently, Song et al. (2004) developed new reverse micelles system in obtaining Cu nanoparticles, that is, bis(ethylhexyl)hydrogen phosphate (HDEHP)/water/n-heptane (or n-octane or n-hexane). All of the obtained Cu particles were spherical with a diameter 50-60 nm.

The colloidal copper particles were also prepared in the sodium dodecyl

sulfate (SDS) normal micelles system. Below the cmc, the obtained products were an interconnected network of either oxide or pure copper aggregates. Above the cmc, the syntheses showed the formation of elongated particles or spherical copper particles. The size of the particles decreases with the increase in the surfactant concentration. The particle size ranged from 2 to 7 nm (Lisiecki et al., 1996).

2.2.2.3 Electrochemical deposition

Electrochemical deposition has been used to synthesize nanomodulated ceramic superlattices (Switzer et al., 1990, 1992, 1994; Switzer and Golden, 1993***),*** quantum-confined metal/semiconductor nanocomposites (Switzer et al., 1997), and copper (I) oxide film (Zhou and Switzer, 1998).

As the most important interconnector in the electric industry, the fabrication of metallic copper 1D nanowires and nanotubes has been fully developed in this method (Gao[2] et al., 2002; Konishi et al., 2003; Li[4] et al., 2004; Molares et al., 2001 (a) (b); Pang et al., 2003; Wang[11] et al., 2004). The templates applied are porous alumina membrane (PAM) and polycarbonate filter (PC). In this method, the diameters of Cu nanowires were controlled with pore sizes of the templates and range from 30 to 500 nm. Furthermore, with adjusting of the parameters, Cu nanotubes have also been fabricated (Li[4] et al., 2004; Wang[11] et al., 2004).

2.2.2.4 Aerosol formation of Cu or its oxide particles

Chemical vapor deposition is a very attractive way to obtain Cu aerosol

particles. Nasibulin et al. (2001(b)) prepared Cu nanoparticles by thermal decomposition of copper acetylacetonante $Cu(acac)_2$ vapor using a vertical flow reactor at ambient nitrogen pressure. The experiments were performed in the precursor vapor pressure range of 0.06-44 Pa at furnace temperatures of 431.5 ^{o}C, 596.0 ^{o}C, and 705.0 ^{o}C. At 431.5 ^{o}C, the number average size of the primary particles increased from 3.7 nm to 7.2 nm with the increasing precursor vapor particles pressure from 1.8 to 16 Pa. Choi and Park (2004) selected $Cu(etac)[P(OEt)_3]_2$ as a precursor and free-standing copper nanowires with diameters of 70-100 nm were fabricated on Si (111) surface at temperatures below 300 ^{o}C. The copper nanowires exhibited high purity and crystallinity with [111] orientation.

Vacuum vapor deposition (VVD) was also adopted to synthesize Cu nanoparticles (Liu[6] and Bando, 2003 (a) (b)). Copper has a melting point of 1083 ^{o}C, but it starts to evaporate from around 800 ^{o}C at a low pressure of 1.0×10^{-4} Pa. The Cu vapor generated deposited and grew into the shape of a rod at low temperature area. Besides, the Cu vapor aerosol can be produced by sputtering source and then deposited on the silicon nitride at ultra-high vacuum of 3×10^{-8} Torr (Olynick et al., 1995, 1996). The average particle size is about 10 nm. At a high vacuum of 10^{-7} Torr range in the TEM chamber, Cu nanorods were also fabricated by electron beam irradiation (Wang[7] et al., 2004). It is assumed that the electron beam irradiation results in the evaporation of Cu and a temperature gradient on the substrate where the highest temperature is located at the centre of the converged e-beam. The Cu nanorods are straight with diameters ranging from 40 to 50 nm. Vitulli et al. (2002) evaporated copper metal in a

Sylvania W/Al_2O_3 crucible at a pressure of 10^{-4} Torr. The copper aerosol was co-condensed with acetone at liquid nitrogen temperature. The Cu powders obtained range from 3 to 4 nm.

2.2.2.5 Solid state reaction

In solid state reaction, the morphology of metallic copper is controlled by the precursor. Hamada et al. (1992) reduced the precursor of copper (I) oxide with hydrogen to synthesize metallic copper at 69-111 ^oC. The precursor particles, having an average size of 0.46, 0.62 and 1.26 μm respectively, were produced by reducing Fehling's solutions of different concentrations with glucose. The resulting copper particles retained the original morphology of the oxides. Hsu et al. (1990) also obtained Cu particles by reducing precursor with hydrogen gas at 150 -200 ^oC, but the precursor was uniform spherical particles of copper (II) basic carbonate. In order to preserve particle integrity, the precursor powders were coated with small (~ 10 nm) silica particles (Ludox HS or 130M) before reduction with hydrogen (Hsu et al., 1990).

In order to fabricate the 1D copper nanowires, $Cu(OH)_2$ nanobelts was also used as the precursor and the template. The transformation took place at 300-600 ^oC in a vacuum of 3×10^{-8} Torr. The decomposition follows the $Cu(OH)_2$ to CuO, to Cu_2O, and then to Cu (Wang[13] et al., 2003(c)). Multiwall carbon nanotubes (MWNTs) have also been used as templates to synthesize Cu nanowires (Hwang et al., 2003). In this method, the MWNTs were at first treated with H_2SO_4/HNO_3 (3/2 by volume) for 3 h, which resulted in the carboxylic acid groups being generated on the surface of

MWNTs. Subsequently, functionalized MWNTs were suspended in $Cu(NO_3)_2$ solution. With hydroquinone being added, the Cu deposited on the surface of MWNTs. The final MWNTs-encapsulated Cu nanowires range from 50 to 150 nm and the lengths are up to several micrometers.

2.3 Crystal structure, application and synthesis of cupric oxide (CuO)

2.3.1 Crystal structure and application of cupric oxide (CuO)

Among various 3d transition metals and their derivatives, cupric oxide (CuO, tenorite) is a unique monoxide compound (in monoclinic phase, different from normal rock-salt type structure) and the group lattice is C2/c (a_o = 4.684 Å, b_o = 3.425 Å, c_o = 5.129 Å, β = 99.47 °, JCPDS file no. 05-0661) (Bush et al., 2002). Figure 2.2 shows the structure of monoclinic structure of CuO.

As one of the important chemical materials, CuO has been used in many industrial fields. The CuO based heterogeneous catalysts have been used in many important chemical processes (Ramírez-Ortiz et al., 2001; Wang[4] et al., 2002; Wang[9] et al., 2002 (a)), such as degradation of nitrous oxide (Blanco et al., 2004; Bennici et al., 2005; Jiang[2] et al., 2004; Wojciechowska et al., 2004; Zhu[2] et al., 2004(a)), selective oxidation of ammonia (Olofsson et al., 2004), oxidations of carbon monoxide (Jung et al., 2004; Na-Ranong et al., 2003), and removal of dimethyl ether, methanol and phenol (Bravo et al., 2004; Fenoglio et al., 2004; Matter et al., 2004; Papavasillou et al., 2004; Sun[1] et al., 2004; Udrea et al., 2003).

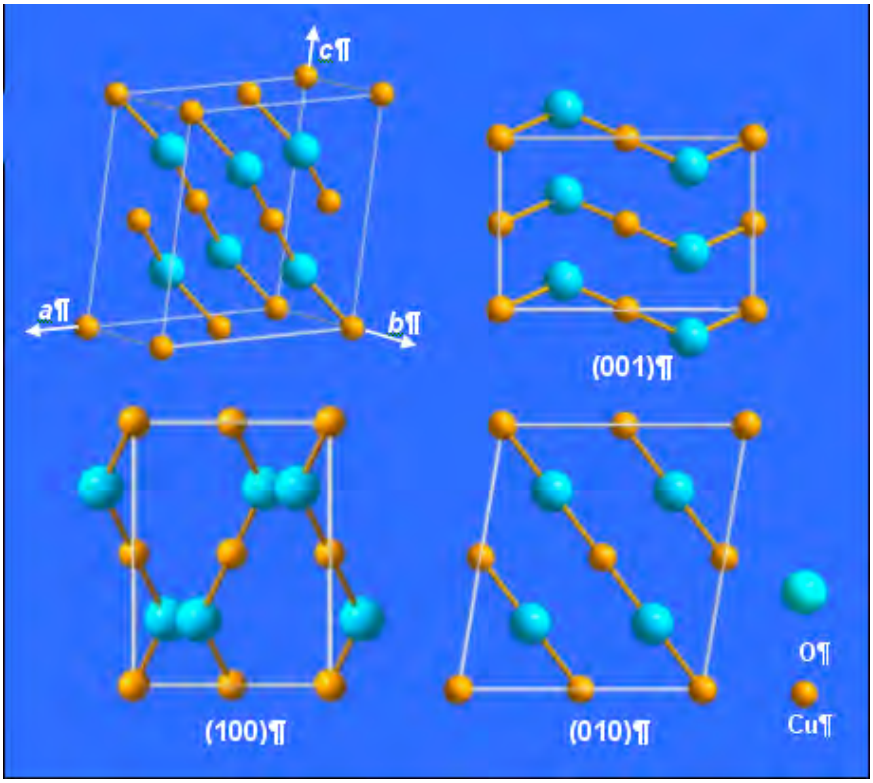

Figure 2.2 Crystal structure of cupric oxide (CuO): group lattice: *C2/c*; a_o = 4.684 Å, b_o = 3.425 Å, c_o = 5.129 Å, β = 99.47 °.

Furthermore, CuO has complex magnetic phases and forms the basis for several high-T_c superconductors and materials with giant magnetoresistance (Borgohain and Mahamuni, 2002(a); Bush et al., 2002; Kuzmenko et al., 2001; Prabhakaran et al., 1999; Zheng et al., 2000). When CuO particles were prepared to nanoscales, the antiferromagnetic transition temperature reduced dramatically from bulk temperature of 230 K to 50 K (Zheng et al., 2004). As a *p*-type semiconductor (E_g = 1.2 eV), its surface conductivity changes in the presence of various donor-acceptor couples. Thus CuO can be used as a kind of conductance sensor material (Cruccolini et al., 2004). It can also be used as an additive to increase the conductivity of the ceramics (Nishiyama et al., 2004).

CuO is also used in preparation of a wide range of organic-inorganic nanostructured composites and ceramics that possess unique characteristics such as high thermal and electrical conductivities as well as high mechanical strength and high-temperature durability (Brookshier et al., 1999; García-Martínez et al., 1993; Huang et al., 1995; Kumar et al., 2001(a); Ramírez-Ortiz et al., 2001). CuO is also used as pigment, fungicide, metallurgy reagent, gas-sensors, magnetic storage media, electronics, lithium batteries, and solar cells owing to its photoconductive and photochemical properties(Borgohain and Mahamuni, 2002(a); Brookshier et al., 1999; Bush et al., 2002; Cao[1] et al., 2003(a); Carnes et al., 2002; García-Martínez et al., 1993; Hong et al., 2002; Hsieh et al., 2003; Huang et al., 1995; Jiang[1] et al., 2002; Kumar et al., 2000, 2001(a); Kuzmenko et al., 2001; Lee[2] et al., 1997; Ramírez-Ortiz et al., 2001; Vorobyova et al., 1999; Wang[4] et al., 2002; Wang[8] et al., 2002; Wang[9] et al., 2002 (a), 2003(b); Wu[2] et al., 2002; Xu[2] et al., 2002; Xu[3] et al., 1999; Yu[4] et al., 2000).

2.3.2 Synthesis of cupric oxide

Because of the above-mentioned fundamental and practical reasons, the synthesis of nanostructured CuO has attracted considerable attention, and various methods to synthesize CuO crystals have been developed. The morphologies range from nanoparticles (0D) to 1D CuO nanostructures.

2.3.2.1 Sol-gel formation of CuO nanoparticles

Sol-gel approach is commonly used in synthesizing the nanostructural materials. It has advantages of the simplicity of the synthetic steps, the flexibility of the solution chemistry, the low temperatures required for treatments, and the small investment in equipment. In this method, the crystalline CuO particles were synthesized by mixing the $Cu(NO_3)_2$ solution and NaOH solutions at a higher temperatures (Lee[2] et al., 1997; Li[2] and Chang, 2004). In the process, Lee[2] et al. (1997) adopted the Controlled Double-Jet Precipitation (CDJP) technique and the $Cu(NO_3)_2$ and NaOH solutions were simultaneously introduced by peristaltic pumps into the CDJP reactor which already contained 100 ml of deionized water and kept at the desired reaction temperature. At 50 ^oC, ellipsoid-type CuO crystals were obtained while at 90 ^oC, CuO needles were subsequently formed. Li[2] and Chang (2004) synthesized the CuO nanoparticles by directly mixing the $Cu(NO_3)_2$ and NaOH solutions at 80 ^oC. The CuO nanoparticles obtained have a needle-like shape.

Copper acetate is a commonly used salt to synthesize CuO nanoparticles and the reactions include the titration with NaOH solution (Liang[3] and Zhu, 2004; Wang[4] et al., 2002; Zhu[3] et al., 2004(a)) and direct hydrolysis at high temperature (Kumar et al., 2000, 2001(a); Zhu[3] et al., 2004(b))**.** In order to control the morphologies of prepared CuO nanoparticles, several organic capping agents were added in the reaction system, e.g., CTAB, PVA, PEG, and glacial acetic acid and the morphologies included nanoparticles, needle-like plates and polycrystalline micrometer spheres.

2.3.2.2 Decomposition of precursor

Cu (II) cation easily forms basic precursors in a basic solution at a low temperature, which include $Cu(OH)_2$, $Cu_2(OH)_2CO_3$, and $Cu_2Cl(OH)_3$. These precursors can be transformed to CuO at high temperature. In this method, CuO paticles with different sizes were obtained (Carnes et al., 2002; Fan et al., 2004; García-Martínez et al., 1993; Huang et al., 1995).

In recent years, the fabrication of one dimensional nanostructures has attracted considerable attention owing to their special shape-dependent properties. In this method, the precursors are also the templates for final CuO products. Many works have been done to fabricate 1D CuO nanostructures by preparing 1D precursors (Du and Tendeloo, 2004; Lu[1] et al., 2004; Wang[9] et al., 2003 (a, b); Wen et al., 2003; Xu[2] et al., 2002; Zhang[3] et al., 2004; Zhu[1] et al., 2004). In these reactions, capping agents of ammonium, urea and PEG were adopted to control the 1D precursors. If these precursors were heated in air, the CuO formed can perfectly maintain the 1D polycrystalline structures of their precursors (Lu[1] et al., 2004; Wen et al., 2003; Zhang[3] et al., 2004). If the precursors were heated in deionized water, the CuO obtained was single crystal and with a nanoleaflet shape (Lu[1] et al., 2004).

2.3.2.3 Thermal oxidation method

Metallic copper can also be used to directly synthesize CuO through the oxidation at a high temperature. Jiang[1] et al. (2002) heated the copper grid directly in

air at 400, 500 and 600 ^{o}C respectively and the formed uniform CuO nanowires were controlled with diameters in the range of 30-100 nm and with lengths up to 15 μm. In the process, Cu at first was oxidized to Cu_2O and then to the CuO product. Hsieh et al. (2003) also adopted this method to fabricate CuO nanowires on the surface of a copper foil. In order to perfectly control the morphology of CuO nanowires, the copper foil was initially electrodeposited with some Cu nuclei as the template for the CuO crystal growth. Besides metallic copper, CuS nanowires were also used as templates and transformed to Cu_xO (x = 1, 2) nanowires at 400 ^{o}C in the presence of O_2. Although they are polycrystalline, they are remarkable uniform (Wang[8] et al., 2002). In addition, CuO nanoparticles can also be coated on the surface of some substrate, e.g., SiO_2, TiO_2, carbon nanotubes, by directly heating $Cu(Ac)_2$ and $Cu(NO_3)_2$ salts adsorbed on the surface of substrates at a high temperature (Brookshier et al., 1999; Wu[2] et al., 2002; Yu[4] et al., 2000).

2.3.2.4 One-step solid-state reaction method

Xu[3] et al. (1999) adopted the one-step solid-state reaction method to synthesize monoclinic CuO nanoparticles, in which $CuCl_2{\cdot}2H_2O$ and NaOH were mixed and grounded using a molar ratio of 2:5 for 30 min and the CuO particles are with an average size of 12 nm. It was found that the CuO powder sample was stable at room temperature, but when the sample was pressed into pellets, it became unstable. Besides, they discovered that the grains in the pellets grew with time. The particle size increased from 12.1 nm to 16.4 nm after 4 days. The method is very simple, but the

sample is the mixture of CuO and NaCl. In order to obtain CuO nanorod, Wang[9] et al. (2001, 2002(a)) added surfactant PEG 400 in this reaction. The process was carried out at the room temperature for a short synthetic time. The average diameter of obtained CuO nanorod is *ca.* 8 nm. The formation of the CuO nanorods was due to the assemblage of CuO nanoparticles along the chain structures of PEG.

2.3.2.5 Solvothermal method

The solvothermal method is also used in the synthesis of CuO nanostructures (Cao[1] et al., 2003(a); Hong et al., 2002; Yang[3] and Gao, 2004). Hong et al. (2002) developed a convenient alcohothermal route to synthesize CuO nanoparticles with a average diameter of 3-9 nm by using copper acetate ($Cu(Ac)_2$) as the starting reactant at mild conditions. In their work, it was found that the role of the organic solvent of ethanol is critically important for the present low temperature (110–150 °C) decomposition of $Cu(OAc)_2$ to CuO. This is because the esterification reaction readily occurred between $(OAc)^-$ and ethanol under alcohothermal conditions. In order to synthesize 1D CuO nanorods and nanotubes in hydrothermal method, Cao[1] et al. (2003(a)) adopted the surfactant of CTAB in a NaOH high-concentration solution. Owing to the presence of $[Cu(OH)_4]^{2-}$, the CuO nanorods and nanotubes were fabricated directly and the resultant nanorods and nanotubes were longer than 1-5 μm.

2.3.2.6 Electrochemical method

CuO nanocrystals of three different sizes 3.5, 6.5, and 10.0 nm were synthesized by Borgohain and Mahamuni (2002(a)) via a novel electrochemical route, in which acetonitrile and tetrahydrofuran mixed in the ratio of 4:1 and the capping agent TOAB served as the electrolyte. With this method, chiral films of CuO were deposited onto achiral (001) surface of single-crystal Au (Switzer et al., 2003; Kothari et al., 2004). In this process, chiral precursors, such as tartaric acid, the amino acids of alanine and valine, were used to dictate the chiral structure of CuO films. This study provides a noval approach to develop materials with chiral structures.

2.4 Crystal structure, application and synthesis of cuprous oxide (Cu_2O)

2.4.1 Crystal structure and application of cuprous oxide (Cu_2O)

Cuprous oxide (Cu_2O) is a *p*-type semiconductor with a band-gap of 2.17 eV. The space group of Cu_2O crystal is *Pn3m* (a_o = 4.267 Å, JCPDS file no. 05-0667) (Chen[4] et al., 2003). Figure 2.3 is the ball-line model of cubic structure of Cu_2O.

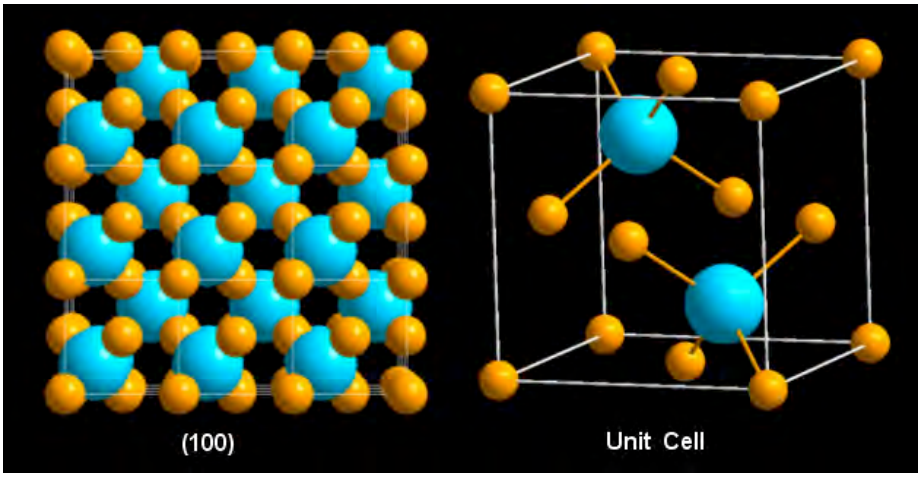

Figure 2.3 Crystal structure of cuprous oxide (Cu_2O): group lattice: *Pn3m*; a_o = 4.267 Å.

As a *p*-type semiconductor, Cu_2O crystal has attracted much interest in applications. Bulk Cu_2O has the large excitonic binding energy (140 meV) and therefore presents a well-defined series of excitonic features in the absorption and luminescence spectrum at a low temperature. Thus Cu_2O is widely studied as a potential material in the solar cells for low-cost photovoltaic power generation (Borgohain et al., 2002(b); Musa et al., 1998). There are several advantages for Cu_2O in this application: (i) it is nontoxic; (ii) it has a theoretical solar cell conversion efficiency of 18%; (iii) there is an abundance of copper; (iv) the semiconductor layer formation process is simple (Musa et al., 1998). At present, the studies are concentrated on the preparation of transparent conducting oxide (TCO)/Cu_2O heterojunction solar cells consisting of a Cu_2O thin film or sheet combined with a TCO thin film, such as ZnO, In_2O_3, SnO_2 , CdO or TiO_2 (Hames and San, 2004; Minami et al., 2004; Katayama et al., 2004; Siripala et al., 2003).

Cu_2O is also an important catalyst and can be used in cyclohexane oxidation, Barbier Reaction, Ullmann-type amination coupling and thermal decomposition of ammonium perchlorate et al (Medina-Valtierra et al., 2003; Sinha and Roy, 2004; Ramírez-Ortiz et al., 2001; Son et al., 2004; Zhu[4] et al., 2004). In most industrial processes of cyclohexanone, cyclohexanol or adipic acid production， the used inorganic or organic acids can be or can evolve into toxic byproducts. Recent result shows that Cu_2O–CuO film fabricated on the glass fibers has a high catalytic activity at low temperatures for these reactions, for example, there is a good selectivity of 37%

for cyclohexanol production at 300 °C (Medina-Valtierra et al., 2003). In the known Grignard-Barbier reaction, a reagent combination of SnO and catalytic Cu_2O promotes the reaction of allyl halides with aldehyde, cyclic monoketone, 1,2-diketone, 1,3-diketone, and anhydride, leading to corresponding homoallylic alcohols having exclusive γ-regioselectivity (Sinha and Roy, 2004). The particle size is also a key factor to influence the catalytical activity. When nanosized uniform Cu_2O coated Cu nanoparticles were used as the catalyst in the Ullmann-type amination reactions of imidazole with various aryl chlorides， the reactions proceeded quickly. The high catalytic activity of the reaction seems to result from the high surface area derived from the nanoparticles (Son et al., 2004).

Cu_2O has many special physical and chemical properties and therefore is used as the composites and reactants for some special industrial materials. Cu_2O has a high melting point of 1235 °C, so Cu_2O based cermets can endure a very high temperature, for example, Cu/Cu_2O cermets was regarded as a possible replacement anode material for high temperature electrolysis, especially for aluminum electrolysis (Shao et al., 2004). Adding Cu_2O can improve the efficiency of photocatalysis of TiO_2, the same as doping noble metal inside, such as Pd, Pt and Au. The mechanism is that Cu_2O can accelerate the rate of transferring electron to oxygen, resulting in a large number of holes which can degrade the organic matters (Li[3] et al., 2004). Cu_2O powder is also the reactant for some composites, such as SiC/Cu and Al_2O_3/Cu. In the reaction process, Cu_2O were reduced into Cu nanoparticles on the surface of composites (Zhang[4] et al., 2004; Liang[1] et al., 2004). Cu_2O is also an excellent gas sensor material. When Cu_2O

(1.0 w%) is screen-printed on the surface of α-Al_2O_3, the composite shows maximum sensitivity factor (SF) of 165, 296 and 78 for CO, H_2 and LPG gases (1000 ppm each), respectively, at an optimum operating temperature of 450 ^oC (Morea et al., 2004). Cu_2O has been also used as the antifouling pigment, fungicide and pigment (Lossin and Westhoff, 1997; Wayne-Richardson, 1997). The properties of Bose condensation of excitons and photoconductivity at low temperatures have always attracted attention (Marchetti et al., 1997).

2.4.2 Methods of preparation of copper (I) oxide

Cuprous oxide (Cu_2O) is a *p*-type semiconductor with a band-gap of 2.17 eV. The Cu_2O crystal has a cubic structure (SG: *Pn3m*) and has potential applications in solar energy conversion, catalysis, crystal rectifiers, antifouling pigment, fungicide et al. Many methods in the synthesis of Cu_2O have been reported. According to the different necessities, Cu_2O can be prepared as particles, nanowires, and a layer on the copper or a polymer surface, or can be dispersed on the support such as alumina, MgO or glass.

2.4.2.1 Sol-gel formation of Cu_2O nanoparticles

Sol-gel method is a common method to synthesize Cu_2O long ago (Mcfadyen and Matijević, 1973). Cu_2O particles were prepared by reducing copper tartrate complex with glucose. This action is widely used in the analytical determination of

saccharides. The morphology of Cu_2O changed from cubes, to cuboctahedra, and then to octahedra with the increase of the concentration of glucose. The average size of particles in this method was about 1 μm. In order to decrease size of the particles, surfactants and polymers were adopted in the aqueous solution, for example, CTAB, PEG, PVP (Chen[3] et al., 2002; Gou and Murphy, 2003, 2004). The size of Cu_2O nanocubes prepared was decreased to 25 nm. Orel et al. (2003) heated solutions of copper (II) acetate in ethylene glycol (EG) and tetraethylene glycol (TEG) and the uniform spheres were obtained from aggregation of nano-sized copper (I) oxide.

Cu_2O crystals have a cubic structure. With copper acetate and copper citrate used as precursors, the reduced Cu_2O crystals have a hexa-pod and octa-pod structures (Chen[4] et al., 2003; Wang[3] et al., 2003). The pods grew along <100> and <111> directions. Matijević (1994) also prepared the hexa-pod Cu_2O crystals in the $CuCl_2$ aqueous solution, and the added EDTA with 0.02 M might play a role in the formation of this structure. Zhu[5] et al. (1994) also prepared Cu_2O in the presence of a CH_3COOH/CH_3COONa buffer pair. However, the product is nanocrystalline powders of Cu_2O with a particle size of 14 nm, not a multi-pod structure. The reason may be the application of the surfactant of SDS. In addition, the reaction took place at 80 ^oC with the radiation of a 70000 Ci ^{60}Co γ-ray source.

The synthesis of 1D nanowires or nanorods has attracted a considerable attention owing to their special chemical and physical properties. Wang[9] et al. (2002(d)) selected PEG (Mw 20000) as a capping agent to synthesize Cu_2O nanowires

in the following process. PEG and $CuCl_2$ were dissolved in water and NaOH was added dropwise into the solution. Then the formed $Cu(OH)_2$ was reduced by N_2H_4. The formed Cu nanowires were relatively straight and long, with diameters of about 8 nm and the lengths ranging from 10 to 20 μm, which resulted in a very large aspect ratio. Cao[1] et al. (2003(a)) prepared Cu_2O nanowires and nanorods by reducing the complex of $[Cu(OH)_4]^{2-}$ and at the same time, the surfactant of CTAB was used in the process. Xiong et al. (2003(b)) developed a new strategy to fabricate Cu_2O nanowires, in which a complicated complexes with several linear-aligned copper cations of $[Cu_3(dmg)_2Cl_2]_n^{2n+}$ was used as precursors and glucose was the reductant. Dong et al. (2001) found that the organic additives added had an important influence on the formation mechanism of the Cu_2O particles and could lead to different microstructures of the resultant Cu_2O crystallites. When they prepared the Cu_2O by the reduction of aqueous $CuSO_4$ with hydrazine, the addition of CTAB to the reaction solution could induce the formation of cubic Cu_2O single crystals, while glucose resulted in the formation of spherical polycrystals.

Muramatsu and Sugimoto (1997) prepared uniform spherical Cu_2O particles with an average diameter of 0.27 μm by aging a 0.5 M CuO suspension containing 0.5 mol dm^{-3} N_2H_4 and 3 wt% deionized gelatin for 3 h at 30 ^oC. In this method, the reaction rate had a great influence on the morphology of Cu_2O. With $Cu(OH)_2$ instead of CuO, the Cu_2O particles were polydispersed ones due to the high solubility of $Cu(OH)_2$. The pH value was also a key factor to influence the Cu_2O morphology. When pH<9, the polydispersed Cu_2O particles formed since more Cu^{2+} ions dissolved

out from CuO particles. High pH value ca. 10 led to the formation of metallic Cu due to the too high reducing activity of hydrazine. Gelatin inhibited the direct reduction of CuO by N_2H_4. When reducing freshly prepared $Cu(OH)_2$ with N_2H_4 in water at room temperature, the nanocubes and nanooboxes were obtained (Wang[12] et al., 2004). When ammonium was added in the starting solution, the freshly prepared $Cu(OH)_2$ were nanowires. After these nanowires were reduced with N_2H_4, the obtained Cu_2O maintain the morphology of $Cu(OH)_2$ templates (Wang[9] et al., 2003(a)).

Ram and Mitra (2001) prepared Cu_2O nanocrystals of 10–30 nm in size by reducing Cu^{2+} to Cu with $NaBH_4$ and then transformed into Cu_2O in an aqueous solution at 80-100^{o}C. The formed Cu_2O was in a new orthorhombic crystal structure with lattice parameters a = 0.421 nm; b = 0.324 nm and c = 0.361 nm.

2.4.2.2 Vacuum vapor deposition and oxidization of copper

To synthesize nanosized Cu_2O particles by the oxidization of copper, the size of metallic copper particle is a key factor. Many researchers (Balamurugan and Mehta, 2001(a, b); Deki et al., 1998; Kellersohn et al., 1995; Yanagimoto et al., 2001 (a, b)) prepared nano-sized metallic copper with vacuum vapor deposition technique for the synthesis of nano-sized Cu_2O particles. Kellersohn (1995) initially obtained the nanostructured copper by means of inert gas aggregation of copper vapor. Then the formed copper was oxidized for less than 2 h at 150 ^{o}C and with an oxygen pressure of 800 mbar. The prepared Cu_2O particles have a mean diameter of 9 nm. Recently, a

conventional activated reactive evaporation (ARE) method has been used for preparing the Cu_2O nanoparticles (Balamurugan and Mehta, 2001(a)). The thermally evaporated copper with high purity (99.999%) passed through oxygen plasma. The deposition chamber having a base pressure of 5×10^{-6} Torr was maintained at 5×10^{-3} Torr by admitting oxygen. The formed Cu_2O nanoparticles deposited on cleaned glass substrates and were in the size range of 8-100 nm. Balamurugan (2001(b)) also prepared Cu_2O thin film in this method. The films deposited at room temperature (30^oC) have a predominant Cu_2O cubic phase, and those deposited at 150-200^oC have a single Cu_2O cubic phase. The average crystallite size was varied from 4.9 to 9.0 nm by changing oxygen flow rate and substrate temperature.

In recent years, nano-sized semiconductor and metal particles embedded in solid dielectric matrices have attracted an increasing interest because of novel applications as photonics and electronics devices based on quantum size effects and their high third-order non-linear susceptibility. Deki (1998) dispersed Nano-sized Cu_2O particles in nylon 11 films by a thermal relaxation technique. In this method, metallic copper was vaporized and deposited on the surface of Nylon 11 thin film at a pressure of 2.0×10^{-5} Torr. Then The Cu/nylon 11 laminated films were heat-treated at 100 °C for 30 min in N_2 and in air. The dispersed Cu_2O particles were relatively homogeneous in size, and the mean size of the Cu_2O particles increased from 3.2 to 6.3 nm in diameter upon increasing amount of Cu deposition. Yanagimato et al. (2001 (a, b)) dispersed Cu_2O nanoparticle in NH_2-terminated poly(ethylene oxide) matrix by means of the same method. The mean size of the Cu_2O nanoparticles could be

controlled from 2.5 to 3.5 nm in diameter by changing the amount of initial Cu deposition.

2.4.2.3 Electrochemical method

Electrochemistry is an attractive technique for materials synthesis. Electrodeposition can be used to deposit a variety of materials such as ceramics, semiconductors, superlattices, and superconductors. A wide range of semiconductors have been electrodeposited, e. g. quantum dots of CdSe, epitaxial films of CdTe on InP and epitaxial layers of GaAs (Golden et al., 1996). Cu_2O has also been electrochemically deposited onto several substrates (Borgohain, 2002(b); Ermakova et al., 1986; Golden et al., 1996; Liu[4] et al., 2003; Mahalingam et al., 2002; Ono et al., 1999; Puzakov and Ermakova, 1991).

Golden et. al. (1996) electrodeposited the Cu_2O films on stainless steel and indium tin oxide by reducing copper (II) lactate in an alkaline solution. At the pH value of 9, the orientation of the Cu_2O film is [100], while at the pH value of 12, the orientation changes to [111]. Borgohain (2002(b)) synthesized Cu_2O nanocrystals by a modified electrochemical route, in which the electrolytic bath consisted of a mixture of acetonitrile (CH_3CN) and THF in the ratio of 4:1. The supporting electrolyte, TOAB is served as a stabilizer. The Cu_2O nanoclusters formed have average diameters of 2.0±0.5 and 8.0±2.0 nm by applying for current densities of 50 and 2 mA/cm^2 respectively. I

The shape of nanostructures is one of the important factors which can determine the physical and chemical properties of the nanostructures. In order to fabricate Cu_2O nanowires, the porous alumina membrane (PAM) and polymer membrane have been used as templates and the Cu_2O are deposited in the pores of the templates in this method (Kenane and Piraux, 2002; Leopold et al., 2002; Oh et al., 2004). After removing of templates, Cu_2O nanowires are obtained. In this process, the diameters of nanowires can be determined with the pore sizes of the templates.

2.4.2.4 Thermal method

In this method (Palkar et al., 1996), the copper citrate precursor and copper oxalate precursor were prepared first by means of rapid liquid dehydration and precipitation respectively. The liquid dehydration process involves fast nucleation of fine particles from an aqueous solution of copper citrate. Distilled acetone was used as dehydrating agent since it has a high solubility for water but not for copper citrate. The precipitation of copper oxalate was conducted in a solution of copper acetate at a constant pH of 2.0. Two kinds of precursors obtained was calcined to produce copper oxide.

Heating the citrate precursor at 250 °C results in a mixture of Cu_2O and CuO. The percentage of Cu_2O in the mixture was found to decrease when either the calcination temperature or the calcinations time was increased. But when the particle size of Cu_2O is below the 25 nm, the percentage of Cu_2O remains approximately

constant. The result possibly indicates the existence of a critical particle size of 25 nm for Cu_2O. When Cu_2O particles are smaller than 25 nm， they are more stable than the CuO. Heating of oxalate precursor provides the same results.

2.4.2.5 Simple boiling method

In this method (Fernando et al., 2002), 99.99% pure copper plates (3×3 cm^2) were cleaned with sandpaper to remove the outer layers of the copper sheets. Thereafter the copper plates were mechanically polished until a mirror like surface was obtained. Then the plates were thoroughly cleaned and immersed in a 10^{-3}M $CuSO_4$ solution and boiled to obtain Cu_2O layers on the surface of the copper plate. Boiling time controlled the amount of Cu_2O formed on the copper substrate. The oxide formed in grams per unit area (g cm^{-2}) on the copper substrate was determined by measuring the difference of the weight of the copper plates before and after boiling. During the boiling, a fixed volume of $CuSO_4$ solution was maintained to provide the same experimental conditions for different preparations. The pH of the $CuSO_4$ solution was measured before and after boiling using a Horiba pH meter. The layers consist of Cu_2O phase with a thickness of about 1.4 μm for 60 minutes boiling in $CuSO_4$ solution.

2.4.2.6 Hydrothermal method

Kinoshita and Nakano (1967) prepared large Cu_2O crystal by means of

hydrothermal method. In the autoclave, a seed crystal and source crystal, which were made by the melting method, were set at the top and the bottom. About 90-95% of the volume of the autoclave was filled with 0.1 to 1 M aqueous solution of sodium hydroxide. The seed temperature was set between 300°C and 350°C, and the source temperature was kept 30-50°C higher than the seed temperature. A large crystal was formed on the seed crystal, and one or two hundreds of small crystals were obtained on the inner wall of the autoclave, respectively, after one hundred hours' growth under these conditions. The size of individual crystals grown on the inner wall of the autoclave even reach about 1×1 mm^2 in cross section and 1-2 mm in length.

2.5 Summary

As one of the most important elments in the world, copper and copper oxides (CuO and Cu_2O) have been thoroughly studied. So much is known now about their structures, preparations, properties and application; with the development of nanochemistry, so much is still being learned or to be learned. The new development will continuously change our life and bring us into the new times.

CHAPTER 3

EXPERIMENTAL METHODS

3.1 Materials preparation

In this study, the synthesis of CuO, Cu_2O and Cu nanostructures is the main objective. Figure 3.1 is the schematic drawing of the contents of Chapters 4–8.

In Chapter 4, we adopted a water-alcohol solvent system to prepare CuO nanocrystals. With the titration of the $Cu(NO_3)_2$ solution into a high concentration of NaOH solution at the mild conditions (77–82 °C, 1 atm), Cu^{2+} was rapidly transformed to $Cu(OH)_2$ and then to CuO under a pseudo-steady-state operation. In the condition, the one-dimensional (1D) CuO nanorods and nanoribbons were fabricated.

In Chapters 5–7, a solvothermal method was used to synthesize Cu_2O nanostructures. In Chapter 5, the reaction was conducted in the ethanol-water system at 150–220 ^oC and formic acid was used as the reductant. In this acidic condition, Cu^{2+} was directly reduced into Cu_2O single-crystalline multipod structures. In Chapters 6–7, DMF was used as a solvent and the reductant. Owing to the hydrolysis of DMF at high temperature, the solutions were basic and therefore, the CuO precursor formed initially in the process. When the solvent was pure DMF, the Cu_2O hollow spheres were prepared from the aggregation of the CuO precursors (Chapter 6). In Chapter 7, a small

amount of deionized water (0.3–0.5 mL) was added into the DMF solution. Under this condition, the Cu_2O hollow cubes were formed. At the same time, the DMF-ethanol solvent system was adopted in the reaction, and the Cu_2O nanocubes were then fabricated with this solvent system.

In Chapter 8, the Cu nanowires were fabricated in the NaOH aqueous solution (3.5–15 M) at 40–100 ^{o}C. In this process, EDA was adopted as a chelate agent and hydrazine was used as the reductant.

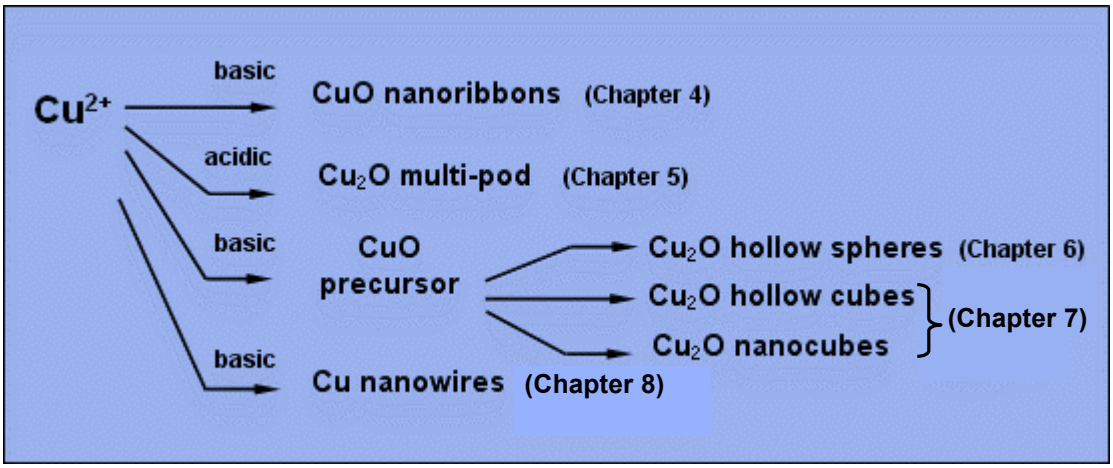

Figure 3.1 The schematic drawing of the content of the thesis.

3.2 Characterization methods

3.2.1 Powder X-ray diffraction (XRD)

The crystallographic information of all samples in PhD work was investigated by powder XRD (Shimadzu XRD-6000, Cu Kα radiation, λ = 1.5406 Å). Each sample was prepared in the form of a fine homogeneous powder and a thin smooth layer of the samples mounted on a non-crystalline substrate such as a glass slice was fixed in the

path of X-rays. As each powder sample contained a large amount of fine particles, the sample could be orientated in every possible direction relative to the beam of X-rays and the diffracted rays corresponded to all sets of planes in the crystals. The XRD patterns with diffraction intensity versus 2θ were recorded, usually selecting a special 2θ range for different kinds of samples in the range of 10 ^{o} to 95 ^{o} at a scanning speed of 2 ^{o} min^{-1}.

The powder XRD pattern is a very important method for the crystal analysis. (1) It can be used for the identification of an unknown crystalline material. Through comparison of measured XRD pattern with the Powder Diffraction File (Joint Committee on Powder Diffraction Standards. Swarthmore, USA), we can confirm the composition and the crystal structure of the unknown crystalline material. (2) The well-known Bragg's equation can be used to determine the interlayer space of the crystals (Azarof and Buerger, 1958; Brundle et al., 1992; Cullity, B.D., 1978; Feldman and Mayer, 1986):

$$d_{hkl} = \lambda / (2\sin\theta) \quad (3.1)$$

where d_{hkl} is the distance between reflection planes (hkl);

λ is the wave length of X-ray (Cu Kα radiation, λ = 1.5418 Å);

θ is the diffraction angle.

(3) The Debye-Scherrer formula can be used to estimate the average crystallite size (t) in the range of 5–100 nm, as seen in Equation (3.2):

$$t = 0.9 \lambda / (FWHM \times \cos\theta) \quad (3.2)$$

here FWHM means the full width at half maximum and can be measured directly by XRD (Cullity, 1978; Azarof and Buerger, 1958).

3.2.2 Transmission electron microscopy (TEM)

In TEM analysis, a highly focused and monoenergetic electron beam was used to bombard the sample specimen. The transmitted electrons form images on a fluorescent screen, which provide morphological features and atomic arrangements of the nanostructured materials. For high resolution transmission electron microscopy (HRTEM), several beams are scattered by the crystal in different directions interfere to form a "lattice image". Picometer-scale imaging provided by HRTEM is essential for nanomaterials science (Bulle-Lieuwma et al., 1991; Wang[13], 2000, 2003(b)). During the specimen preparation, a small amount of CuO, Cu_2O or Cu sample (about 3 mg) was usually dispersed by 2 mL deionized water or ethanol and the mixture was stirred in a ultrasonic water bath for 10–30 min at room temperature, and then a few drops of such solution mixture were spread on a copper grid coated with carbon films for analysis in a JEM-2010 electron microscopy (200 kV) or FEI Tecnai-G^2 (200 kV).

3.2.3 Selected area electron diffraction (SAED)

The principle of electron diffraction (ED) is the same as X-rays diffraction, and when a focused beam of electrons passes through a crystal, diffraction will occur if

the Bragg's equation (3.1) is fulfilled. The diffraction pattern is obtained on the fluorescent screen, as in TEM analysis, which is usually normal to the incident beam direction. The diffraction image is diffraction spots or rings on the screen for different samples. Based on the SAED pattern, the crystallinity of the selected sample can be obtained. If a large number of randomly oriented crystallites are covered, ring patterns will be obtained. With fewer crystallites present in the selected aperture, the "rings" lose their continuity and a spotty ring pattern results. Furthermore, a single crystal will give rise to a regular and ideally symmetrical arrangement of diffraction spots, each of which has a different value of *hkl*. The pattern is solved by relating distances and angles in the crystal lattice by the equation:

$$(D/2)d = L\lambda_e = \text{camera constant} \tag{3.3}$$

where D is the ring diameter and thus D/2 is the distance from any spot to the centre of the pattern. d is the lattice plane spacing, L is the effective camera length, and λ_e is wavelength of the electron beam (Fultz and Howe, 2001).

3.2.4 Scanning electron microscopy (SEM)

SEM is invaluable for surveying materials under high magnification and providing information on particle sizes and shapes, texture and surface details of powders or solid pieces. When electron beam is continuously swept across the specimen at high speed, the specimen is irradiated and in turn produces secondary or backscattered electrons. When these backscattered electrons are detected and the

signals are sent to the amplifier, the final image is built up from the number of electrons emitted from each spot on the sample. In order to improve the conductivity of the samples, some of theSEM samples are coated with a very thin layer of platinum by a sputter coater. Besides giving the images of the samples, SEM can also provide information on the elemental composition of materials imaged as well, with Energy Dispersive X-Ray Spectroscopy (ED). As the electron beam of the SEM is scanned across the sample surface, it generates X-ray fluorescence from the atoms in its path. The energy of each X-ray photon is characteristic of the element which produces it. The EDS microanalysis system collects the X-rays, sorts and plots them by energy, and automatically identifies and labels the elements responsible for the peaks in this energy distribution. In order to produce clearer, less electrostatically distorted images, Field Emission Scanning Electron Microscopy (FESEM JSM-6700F)) was used in this work as well. For FESEM, a field-emission cathode in the electron gun of a scanning electron microscope provides narrower probing beams at low electron energy, resulting in both improved spatial resolution and minimized sample charging and damage.

3.2.5 X-ray photoelectron spectroscopy (XPS)

XPS is widely used to investigate the chemical composition of surfaces because of its ability to explore the first few atomic layers and assign chemical states to the detected atoms. XPS works by irradiating the sample surface *in vacuo* with monoenergetic soft X-rays and causing photoelectrons to be ejected from the inner

orbits of the atoms. Binding energy (BE), which is defined as the energy of attraction between the electron and the nucleus, can be measured by this technique. Each element has a unique BE and for a given electron in the same element the BE changes with different chemical combinations. Therefore this method can be used for surface chemical species identification. As the number of electrons ejected is proportional to the quantity of the element, the peak areas or peak heights can be used (with appropriate sensitivity factors) to determine the compositions of the surface. Chemical states can also be made from exact measurement of peak positions and separations. In this work, samples were examined in AXIS Hsi (Kratos Analytical) using a mono Al Kα X-ray source (1486.6 eV) at a constant dwell time of 100ms and a pass energy of 40.0 eV. The core-level signals were obtained at a photoelectron take-off angle (α, measured with respective to the sample surface) of 90°. The X-ray source was run at a reduced power of 150W (15 kV and 10 mA). The presure in the analysis chamber was maintained at 1.33×10^{-8} Pa or lower duing each measurement. All BEs were referred to the C 1s peak (BE = 284.7 eV) arising from adventitious hydrocarbon. Prior to the peak deconvolution, X-ray satellites and inelastic background (Shirley-type) were subtracted for all spectra. To simplify data processing, the FWHM within the same core level of an element was fixed to be the same during the peak deconvolution process (by Newton's method), and all peaks were set to be Gaussian type. The atomic ratio was estimated by assuming the integrated baseline, homogeneous surface layer, and using Perkin-Elmer sensitivity factors (Wagner et al., 1979).

3.2.6 Surface area analysis

In this work, the Brunauer-Emmett-Teller (BET) method was used to measure the total surface area of some prepared samples through the BET equation (Brunauer et al., 1938, 1940):

$$\frac{1}{W(\frac{P_0}{P}-1)} = \frac{1}{W_m C} + \frac{C-1}{W_m C}(\frac{P_0}{P}) \tag{3.4}$$

where W is the weight of gas absorbed at the reletive presure P/P_0 and W_m is the weight of adsorbate constituting a monolayer of surface coverage, and C is a contant with a range of 50 - 250 when mitrogen is used as the adsorbate at -196 ^{o}C. W_m and C can be calcualted from the intercept and slope of a linear plot of $1/W[(P_0/P)-1]$ vs. P/P_0. The surface area is thus the product of W_m and the cross-sectional area of each nitrogen molecule under the experiemntal conditions. In our experiments, the BET surface area was obtained from 6-point adsorption data in the relative (P/P_0) arange of 0.05 to 0.35 in a Quantachrome NOVA-1000 apparatus. Full adsorption and desorption isotherm of nitrogen on our samples were determined at various pressures and the pore volume and pore-size distribution were calculated with the Barret-Joyner-Halenda (BJH) method (Barrett et al., 1951). It should be noted that all the samples were degassed at 100 ^{o}C overnight in a pure nitrogen stream before each measurement.

CHAPTER 4

CONTROLLED SYNTHESIS AND SELF-ASSEMBLY OF SINGLE-CRYSTALLINE CuO NANORODS AND NANORIBBONS

4.1 Introduction

As mentioned in Chapter 2, cupric oxide (CuO, tenorite) is a unique monoxide compound (in monoclinic phase) for both fundamental investigations and practical applications, so various methods for synthesizing CuO nanostructures have been developed. Nonetheless, these investigations were mainly devoted to fabrication of nanoparticles (zero-dimension) (García-Martínez et al., 1993; Huang et al., 1995). Following a large number of reported preparations of nanoparticles, investigation on fabrication of 1D CuO nanostructures has also started (Hsieh et al., 2003; Jiang[1] et al., 2002; Lee[2] et al., 1997; Wang[8] et al., 2002; Wang[9] et al., 2002 (a), 2003(b); Wu[2] et al., 2002; Xu[2] et al., 2002). But the reported wet processes can only produce straight short CuO needles, or the polymer (PEG), templates (carbon nanotubes) and high temperatures are used in the process. Moreover, there is no subsequent report of controlled growths of CuO nanorods or (flexible) nanoribbons via solution reactions, especially with control of both morphology and dimension. The objective of this

chapter is aimed at developing “newer and softer” synthetic routes to fabricate 1D nanostructures of CuO and systematical studying the effects of process parameters on their morphologies and dimensions.

4.2 Experimental section

4.2.1 Materials preparation As summarized in Table 4.1, there were six major synthetic schemes used in the current work: (A) 40 mL of $Cu(NO_3)_2{\cdot}3H_2O$ (0.01 M, in pure ethanol) was slowly added to 40 mL of NaOH (0.5 M, in pure ethanol) solution under stirring in a Teflon flask at 65 °C with a rate of 0.1 mL/min using a mechanically pumped syringe. The resultant product was then aged together with mother liquor at the same temperature for 12 and 36 h, respectively. (B) 40 mL of $Cu(NO_3)_2{\cdot}3H_2O$ (0.01 M, in pure ethanol) was slowly added to 40 mL of NaOH (0.5 M, in pure ethanol) solution in the Teflon flask at 77 °C with a rate of 0.1 mL/min. After this, 40 mL of deionized water was added to the above flask at a rate of 0.2 mL/min. The resultant product was then aged together with mother liquor at the same temperature for 0, 20, and 60 h, respectively. (C) 40 mL of $Cu(NO_3)_2{\cdot}3H_2O$ (0.03 M, in pure ethanol) was slowly added to 40 mL of NaOH (0.5 M, in pure ethanol) solution in the Teflon flask at 78 °C with a rate of 0.2 mL/min. After this, 60 mL of deionized water was added to the above flask at a rate of 0.1 mL/min. The resultant product was then aged together with mother liquor at the same temperature for 0, 6, 30, 63, 126 h, respectively. (D) 20 mL of $Cu(NO_3)_2{\cdot}3H_2O$ (0.08 M, in pure ethanol) was slowly added to 20 mL of NaOH (0.5 M, in pure ethanol) solution in the Teflon flask at 78 °C with a rate of 0.1 mL/min. After this, 40 mL of deionized water

was added to the above flask at a rate of 0.1 mL/min. The resultant product was then aged together with mother liquor at the same temperature for 0 and 16 h, respectively. (E) 20 mL of $Cu(NO_3)_2 \cdot 3H_2O$ (0.01 M, in pure ethanol) was slowly added to 20 mL of NaOH (0.5 M, in pure ethanol) solution in the Teflon flask at 81 °C with a rate of 0.2 mL/min. After this, 20 mL of deionized water was added to the above flask reactor. The system was aged for 3 h, after which 40 mL of $Cu(NO_3)_2 \cdot 3H_2O$ (0.02 M, in pure ethanol) and 40 mL of NaOH (0.5 M, in pure ethanol) were injected simultaneously at the same rate of 0.1 mL/min. The resultant product was then aged together with mother liquor at the same temperature for 0, 15, and 39 h, respectively. (F) 40 mL of $Cu(NO_3)_2 \cdot 3H_2O$ (0.02 M, in pure water) was slowly added to 40 mL of NaOH (5 M, in pure water) solution in the Teflon flask at 82 °C with a rate of 1.0 mL/min. Another 40 mL of the same $Cu(NO_3)_2 \cdot 3H_2O$ solution was then injected into the flask reactor at a rate of 0.3 mL/min. Accompanying with the Cu^{2+} addition (40 + 40 mL), a total of 16 g of solid NaOH was added to the flask reactor to keep the NaOH concentration at 5 M (at a rate of 0.4 g of NaOH pellets per 2 mL of Cu^{2+} injection). The resultant product was then aged together with mother liquor at the same temperature for 0, 20, 40, and 90 h, respectively. In all the above methods, a water-cooled refluxer unit was mounted on top of the Teflon flask during the experiments to prevent solvent loss. After each experiment, CuO nanocrystals were separated by centrifugation at a speed of 6000 rpm for 10 min, and washed with deionized water repeatedly. Finally, the solid samples were dried under vacuum overnight at room temperature.

Table 4.1 Experimental procedures and product results.

Expt.	Preparation procedure	Results
A	40 mL of NaOH (0.5 M [a]) + 40 mL of Cu^{2+} (0.01 M [a]) at 0.1 mL/min and 65 ^{o}C,aged for 12-36 h	Amorphous product
B	40 mL of NaOH (0.5 M [a]) + 40 mL of Cu^{2+} (0.01 M [a]) at 0.1 mL/min and 77 ^{o}C, + 40 mL of H_2O at 0.2 mL/min and 77 ^{o}C, aged for 0-60 h	Short nanorods, breadth = 5-8 nm
C	40 mL of NaOH (0.5 M [a]) + 40 mL of Cu^{2+} (0.03 M [a]) at 0.2 mL/min and 78 ^{o}C, + 60 mL of H_2O at 0.1 mL/min and 78 ^{o}C, aged for 0-126 h	Short nanorods, breadth = 8-10 nm
D	20 mL of NaOH (0.5 M [a]) + 20 mL of Cu^{2+} (0.08 M [a]) at 0.1 mL/min and 78 ^{o}C, + 40 mL of H_2O at 0.1 mL/min and 78 ^{o}C, aged for 0-16 h	Short nanorods, breadth = 10-15 nm
E	20 mL of NaOH (0.5 M [a]) + 20 mL of Cu^{2+} (0.01 M [a]) at 0.2 mL/min and 81 ^{o}C, + 20 mL of H_2O, aged for 3 h; then 40 mL of NaOH (0.5 M [a]) + 40 mL of Cu^{2+} (0.02 M [a]) both at 0.1 mL/min and 81 ^{o}C, aged for 0-39 h	Long nanoribbons, breadth = 8-10 nm; Long nanorods (after aging)
F	40 mL of NaOH (5 M [b]) + 40 mL of Cu^{2+} (0.02 M [b]) at 0.1 mL/min and 82 ^{o}C, + 40 mL of Cu^{2+} (0.02 M [b]) at 0.3 mL/min and 82 ^{o}C, during which 16 g of NaOH was also added, aged for 0-90 h	Nanoribbons, nanoplatelets, nanosheets (maximum area = 500 × 1000 nm)

[a] in pure ethanol. [b] in deionized water.

4.2.2 Materials characterization The crystallographic information of the samples was investigated by powder XRD. The XRD patterns with diffraction intensity versus 2-theta were recorded in a Shimadzu X-ray diffractometer (model 6000) with Cu K_α radiation (λ = 1.5406 Å) from 5° to 65° at a scanning rate of 2° min^{-1}. The investigation with HRTEM and SAED were carried out on a JEM-2010 with an electron kinetic energy of 200 kV. SEM images were taken with a JSM-5600LV to examine the morphology of nanocrystals prepared..

4.3 Results and Discussion

Under the reaction conditions used in method A, only a small quantity of amorphous precipitate was resulted (checked with XRD method; not shown), which indicates that a water-free reaction medium is not suitable to form crystalline CuO. With the water added in method B, nanocrystalline CuO precipitates can be generated. In Figure 4.1, typical XRD patterns for this sample series are displayed. The major peaks located at 2θ values of 30° to 65° correspond to the characteristic diffractions of monoclinic phase CuO (JCPDS card no. 5-0661) (Kuzmenko et al., 2001), verifying that the CuO products are phase-pure. As the aging time increases, the diffraction peaks become higher and steeper apparently, which signifies that the crystallinity of CuO improves with a longer aging treatment in solution [B (60 h) vs B (0 h), Figure 4.1]. The rodlike crystal morphology of this series of samples is shown in Figure 4.2. Without any aging, CuO crystallites with breadths in the range of 5–8 nm are weakly aggregated together [B (0 h)], indicating strong intercrystal interactions due to their small crystal

sizes although they can be separated rather easily into monodispersed ones in more dilute suspensions.

With a higher concentration of copper and water in the reaction solution, on the other hand, larger CuO nanorods can be prepared. In the sample series of C, well faceted rods in the breadth range of 8–10 nm are readily formed, as shown in Figure 4.2 [C (6 h)]. The CuO nanorods are monodispersed, and their breadths are uniform while the length is varied in the range of 20–50 nm. After 30–126 h aging, the crystallinity is further increased (see Figure 4.1), and their crystal morphology is also displayed in Figure 4.2 [C (63 h)]. The steady increase in rod-breadth is also illustrated in the sample series D, where the cation concentration and subsequent water added are increased further (see Experimental Section). As shown in Figure 4.2 [D (16 h)], the rod breadths are changed to a range of 10–15 nm, although the growth in length was not very appreciable (their XRD patterns in Figure 4.1). The crystallite morphology is now changed to a more platelet-like type due to the increase in breadth.

Different from the previous wet methods that produced the CuO in sharp needlelike morphology (Cao[1] et al., 2003(a); Lee[2] et al., 1997; Wang[9] et al., 2003(b)), the current approach is able to provide 1D CuO nanorods with a constant breadth and well faceted boundaries. In the above syntheses (B to D series), the breadth and length of CuO nanorods can be controlled via changing either the reaction time or reactant concentrations (including water). In addition to the general confirmation of CuO phase, the XRD patterns of Figure 4.1 also provide information on crystal orientations. In

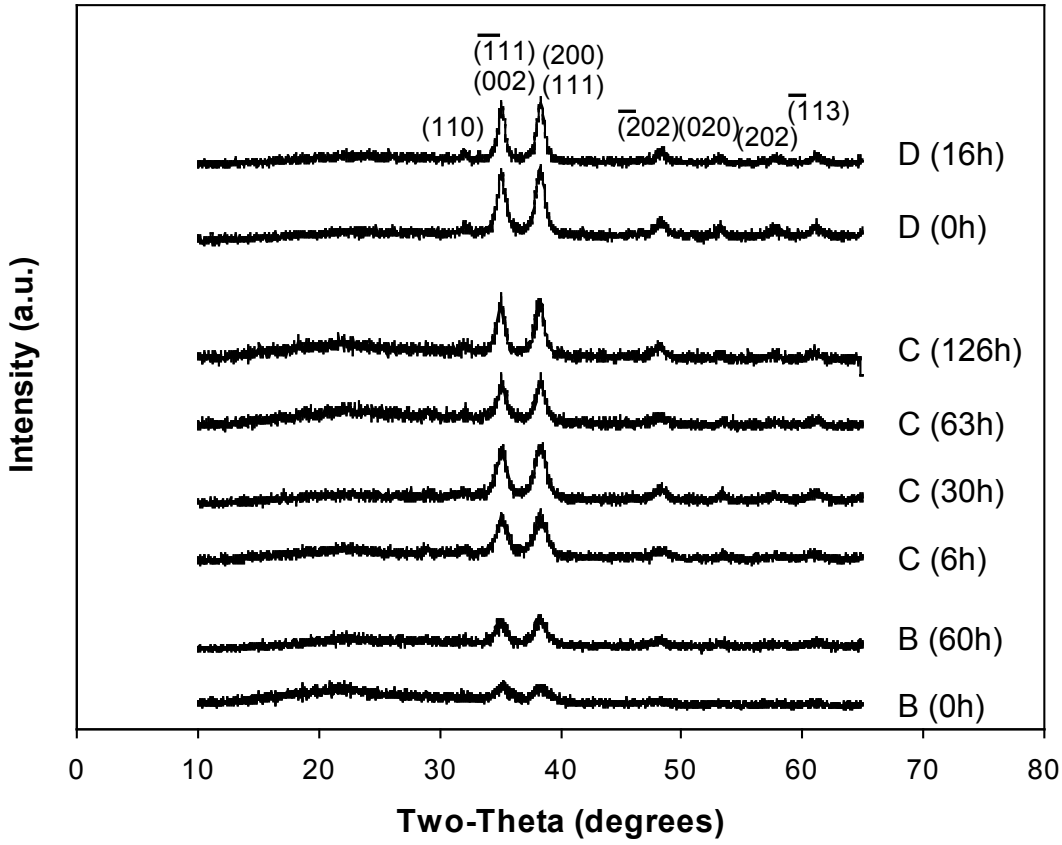

Figure 4.1 Representative XRD patterns of the sample series of B, C, and D; samples of series of A are essentially amorphous; the hump at 2θ = 22–23° is due to the diffraction of glass sample holder.

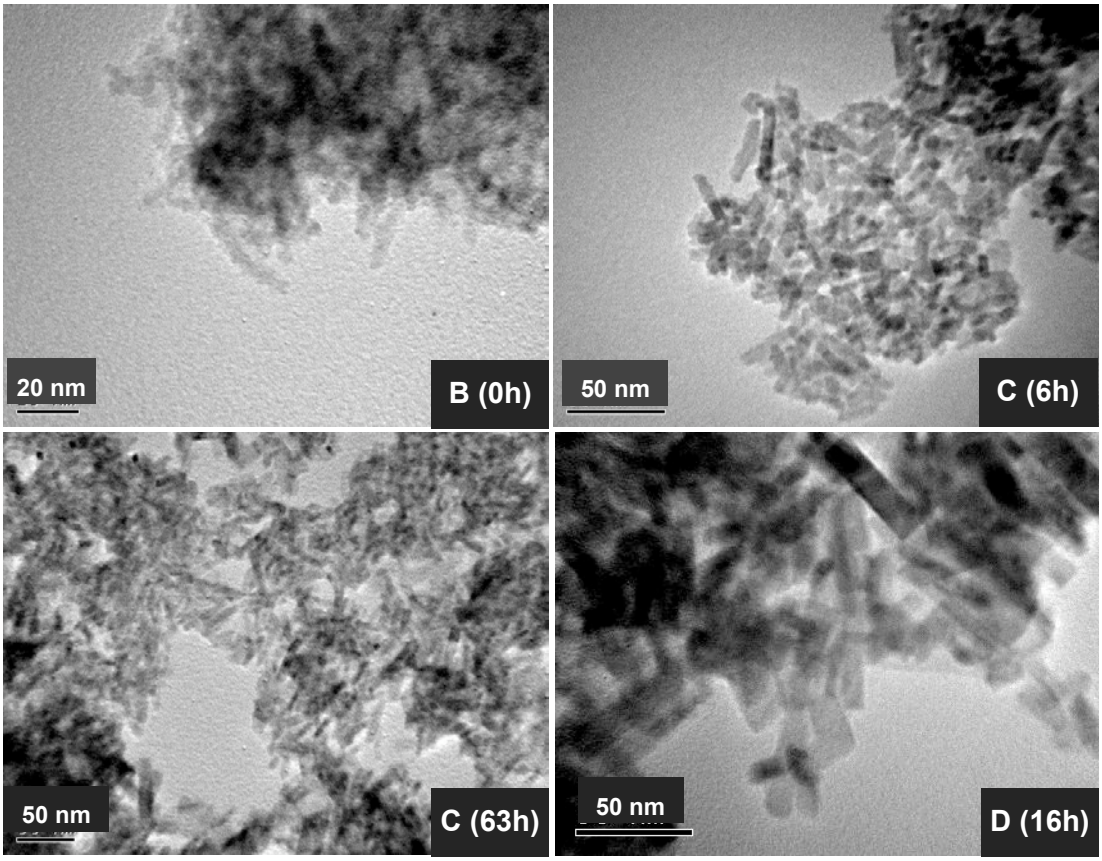

Figure 4.2 Representative TEM images of CuO nanorods synthesized from B, C, and D series of experiments (aging time is also indicated).

particular, low Miller-indexed (002) and (200) reflections are among the strongest, which indicates that they are preferential crystal planes of the nanorods. The monoclinic CuO belongs to a space group of $C2/c$ (a_o = 4.6837 Å, b_o = 3.4226 Å, c_o = 5.1288 Å, β = 99.54°) (Kuzmenko et al., 2001). In Figure 4.3 A, a representative ED pattern and its related CuO nanorod are displayed. The diffraction pattern can be indexed to the [001] zone spots. The CuO nanorods prepared in this work are single crystalline, and they are grown along a preferred direction of ⟨010⟩. It is noted that this growth anisotropy is different from those reported in the literature (Cao[1] et al., 2003(a); Jiang[1] et al., 2002; Wang[9] et al., 2002 (a), 2003(b)). For example, preferred growths along both [111] and [$\bar{1}$11] have been elucidated very recently in the growth of CuO nanorods on the oxidation of copper substrates in air at elevated temperatures (Jiang[1] et al., 2002). On the other hand, the growths along [001] and [111] have also been observed, respectively, in the CuO nanowhiskers/nanorods synthesized with solidstate reactions and wet-chemical reactions in the presence of a nonionic surfactant (PEG 400) (Wang[9] et al., 2002 (a), 2003(b)). On the basis of our ED investigation, it is known that the dimensional hierarchical sequence in our CuO nanorods is $[010]_{\text{length}} > [100]_{\text{breadth}} > [001]_{\text{thickness}}$, since most nanorods used their {001} planes for settlement during the TEM sample preparation. While the majority of nanorods in this work show round growing heads (i.e., round {010} planes), a considerable amount of the rods is bounded with {110} facets, especially for those with a small aspect ratio. Some of these short nanorods are exampled in Figure 4.6 and 4.12 **(**which will be further addressed shortly), noting that the interplanar angle between two {110} surface is

107.8° (see Figure 4.3 B). Figure 4.3 C is the bead-line model of the CuO (001) surface, which can also illustrate the interplanar angle of 107.8° between two {110} surface. The above crystal habits (i.e., low Miller indexed planes) in our CuO nanorods are consistent with those observed in CuO macroscopic crystals obtained from a high temperature melt growth (melt maintained at 1060 °C for 1–3 h, then cooled to a subsolidus temperature of 600 °C) where Bi_2O_3 and PbF_2 were used as solvents (Bush et al., 2002), although there is a substantial reduction in dimension from the millimeter scale down to the current nanometer regime, as well as a drastic synthetic temperature change (e.g., 77–82 °C in our current work). Nonetheless, the growth anisotropies observed in the two cases are quite different, which can be attributed to the compositional variation in the growth environment, as surface reactivity of crystals can be altered easily with the chemical species and solvents.

There are a number of roles that NaOH plays in the synthesis. First, it combines with $Cu(NO_3)_2$ to form $Cu(OH)_2$, which is then decomposed to CuO and water:

$$Cu(NO_3)_2 \cdot 3H_2O + 2NaOH \longrightarrow CuO + 2NaNO_3 + 4H_2O \qquad (1)$$

Under our synthetic conditions, the formation of a green $Cu(OH)_2$ intermediate precipitate was not observed, since heating was provided to accelerate this decomposition. Second, NaOH is a strong electrolyte, and it may neutralize the surface charges of the CuO nanorods, preventing them from possible crystallite

aggregation. Third, the high-concentration NaOH used may create diffusion layers on certain surfaces of CuO nanorods, which may create an additional growth anisotropy allowing only energetically favorable crystallographic planes to grow. As demonstrated in experiments A to D, the reactants in an alcoholic environment are not reactive, and thus the formation of CuO nanostructures (eq 1) is strongly dependent on the reaction medium. In the syntheses B to D, as a confirmation, the reaction was activated by slowly adding water to the alcohol-based reactant mixtures (see Experimental Section).

The above methods (B to D) generally give short CuO nanorods with a small aspect ratio (defined hereafter as the length-to-breadth ratio). To fabricate CuO nanorods (or wires/ribbons) with a higher aspect ratio, an additional synthetic step was introduced. In method E, the growth can be divided into two steps: (i) preparing CuO nanorods as starting seeds (this step is similar to methods B to D), and (ii) injecting chemical reagents ($[Cu^{2+}]$ and $[OH^-]$) simultaneously at an extremely low rate.

Figure 4.4 displayed the XRD patterns for this sample series. Compared with Figure 4.1, it verifies that the CuO products are phase-pure. As shown in Figure 4.5**,** monodispersed CuO nanorods (wire-like) in 100% morphological yield from a few hundred nanometers to 1 μm in length can be prepared when no further aging was carried out. It is important to note that the breadths (in the range of 5–15 nm) of these nanorods are surprisingly uniform throughout an entire length and with an exceptionally large aspect ratio, in contrast to the previously obtained short needlelike

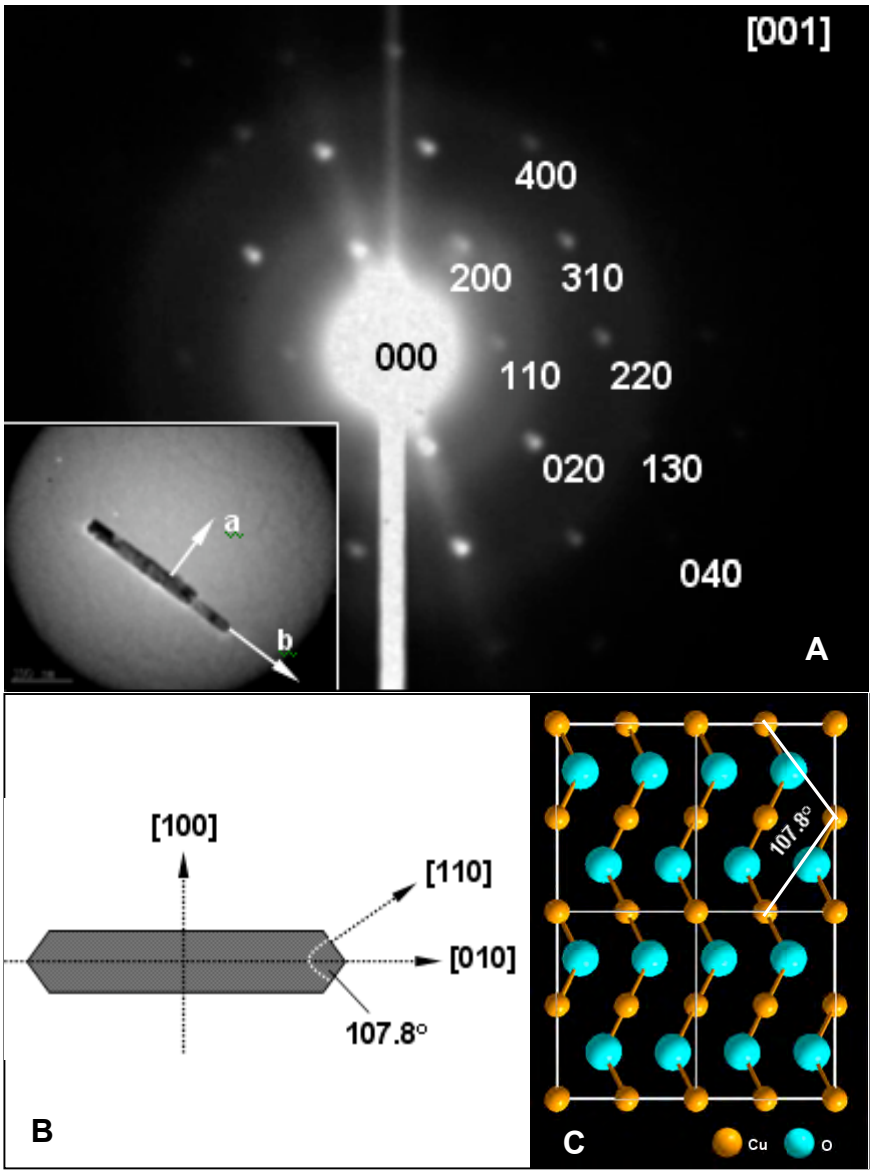

Figure 4.3 (A) SAED pattern and TEM image of a CuO nanorod (inset, which faceted with two {110} planes along + *b*-axis) prepared from F experiment (20 h, Figure 4.12); (B) Illustration indicates the nanorod crystal orientation in the real space; (C) the bead-line model of the CuO (001) surface.

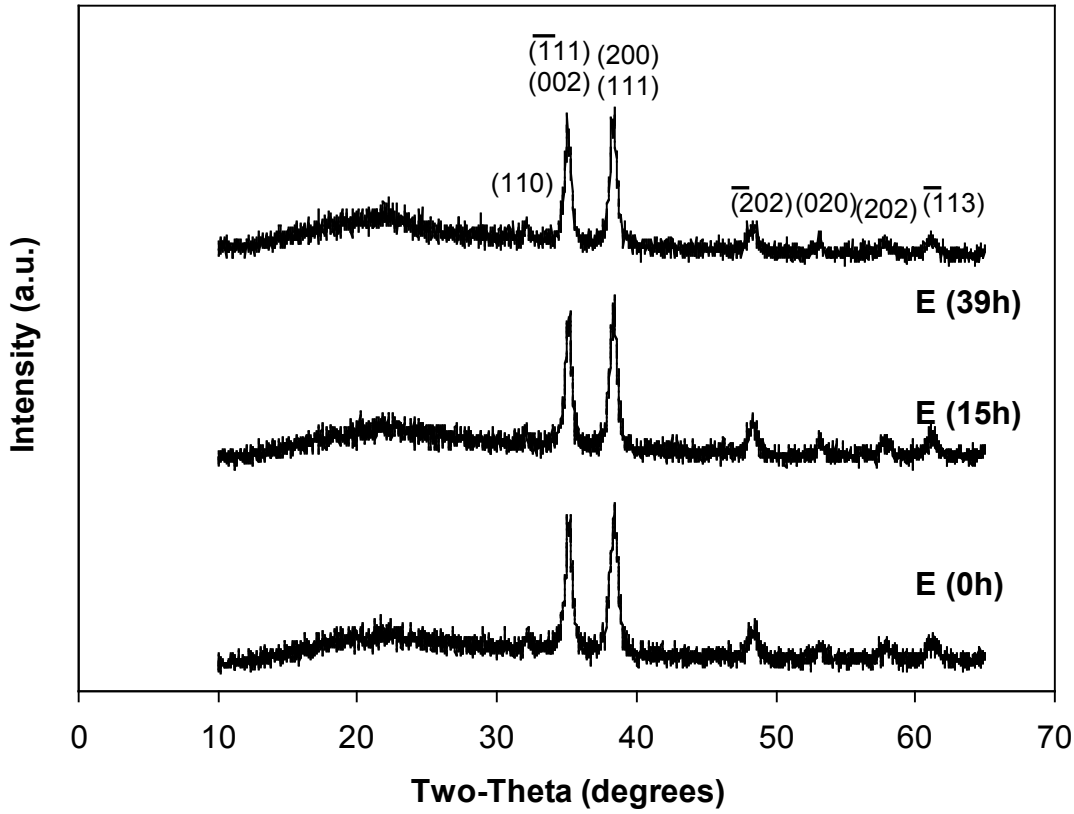

Figure 4.4 XRD patterns of the sample series E with and without aging treatments; the hump at 2θ = 22–23° is due to the diffraction of glass sample holder.

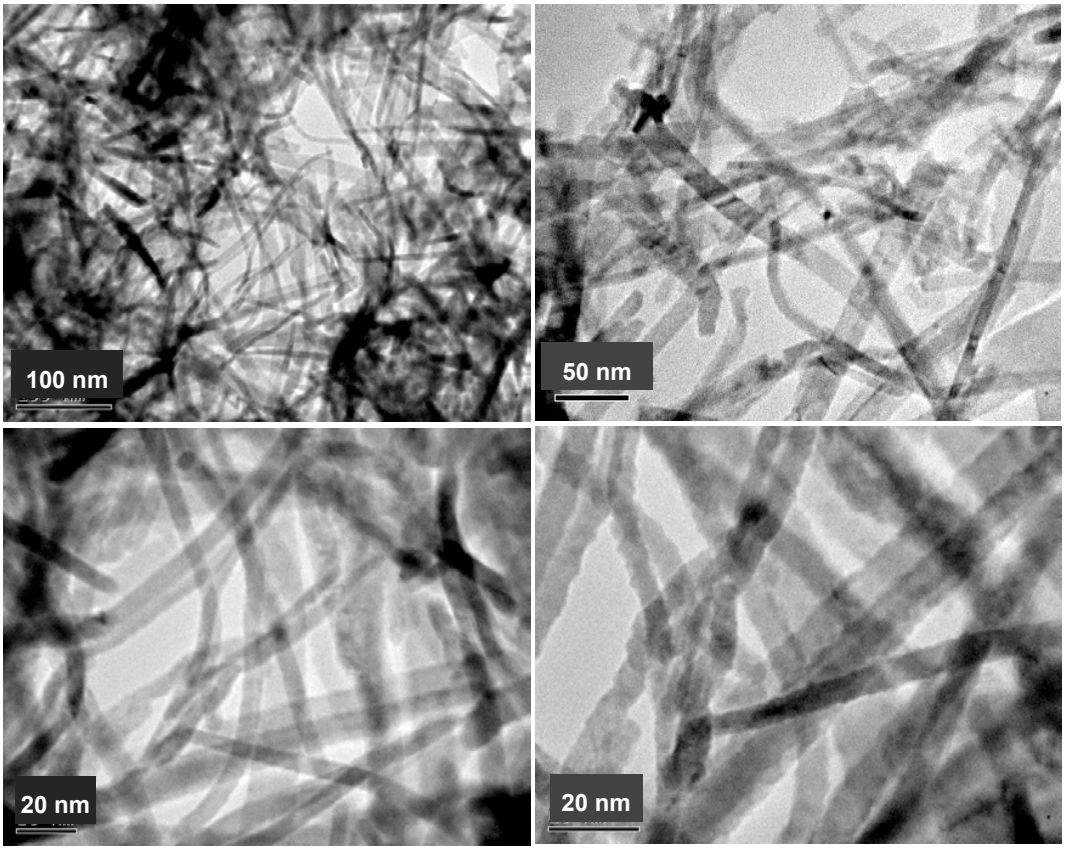

Figure 4.5 Representative TEM images of CuO nanoribbons synthesized from the E series of experiments without aging treatment.

morphology (Cao[1] et al., 2003(a); Lee[2] et al., 1997; Wang[9] et al., 2003(b)). This observation suggests that the growth in step (ii) can actually be considered as a steady-state (or pseudo-steady-state) operation in which the low concentration of Cu^{2+} and slow addition of the reagents are the two crucial prerequisites to the observed unidirectional growth. Apparently, in view of the constant breadths attained, the actual nanorod length along the ⟨010⟩ directions can be further manipulated with the amounts of reagents added within a reasonable time frame if even longer nanorods are targeted.

On the other hand, with a prolonged aging introduced to the synthesis, method E may invite additional modifications of the resultant nanorods (ribbons). In Figure 4.6, some of these morphological variations are illustrated. In general, the CuO samples give more rodlike morphologies (compared to those without aging, Figure 4.5) after aging treatment, which may be attributed to an operation of Ostwald ripening. As shown in Figure 4.6(i), the breadths of the nanorods become less uniform upon the aging; large ones become even larger, and small ones become even smaller, causing a greater size-contrast among the nanorods. Furthermore, overgrowth on the surface planes of existing CuO nanorods can be observed (See Figure 4.7). More interestingly, shorter CuO nanorods recreated from the above ripening process can self-assemble into a two-dimensional netted structure [Figure 4.6 (iii and iv)]. As depicted in Figure 4.8, there are three different modes of attachment. The short nanorods are attached to one another using their low Miller-indexed crystal planes, {001}, {100}, and {110} surfaces, respectively. This type of crystallite growth has been well known in

recent years, and can be described as a cementing process or an "oriented attachment" in nanoscale regime in which a larger crystal structure is formed from smaller ones by direct joining of suitable crystal planes (Kolthoff and Noponen, 1938; Kolthoff and Eggertsen, 1941, 1954; Penn and Banfield, 1998). The examples observed in the recent years include TiO_2 nanocrystallites, β-$Co(OH)_2$ nanoplatelets, ZnO nanorods, and α-MoO_3 nanoforks (Chemseddine et al., 1999; Liu[1] and Zeng, 2003; Lou and Zeng, 2003; Pacholski et al., 2002; Penn and Banfield, 1998; Sampanthar and Zeng, 2002).

In the netted structures of Figure 4.6 (iii and iv), attachment with two {110} crystal planes results in a turning of nanorod alignment and an angle of 107.8° departing two different sets of nanorods in the planar networks (Figure 4.8d). The required crystal facets of {110} in this self-attachment are indeed present in the short nanorods [Figure 4.6(ii) and Figure 4.12] due to the slower growth. A careful TEM examination on the net-structure with higher magnifications indeed confirms the attachment of the {110} planes (See Figure 4.9). To the best of our knowledge, the structure shown in Figure 4.6 (iii and iv) serves as a first example for formation of netted assemblies from primary metal oxide nanorods.

The synthesis with method F was to test the effect of NaOH on the final CuO morphologies. The phase pure CuO samples are confirmed with the XRD analysis (See Figure 4.10), which also shows that the crystallinity of the samples can be improved further with aging under the studied conditions. In SEM images of Figure 4.11, the overall appearance of CuO samples is displayed as a function of aging time. In general,

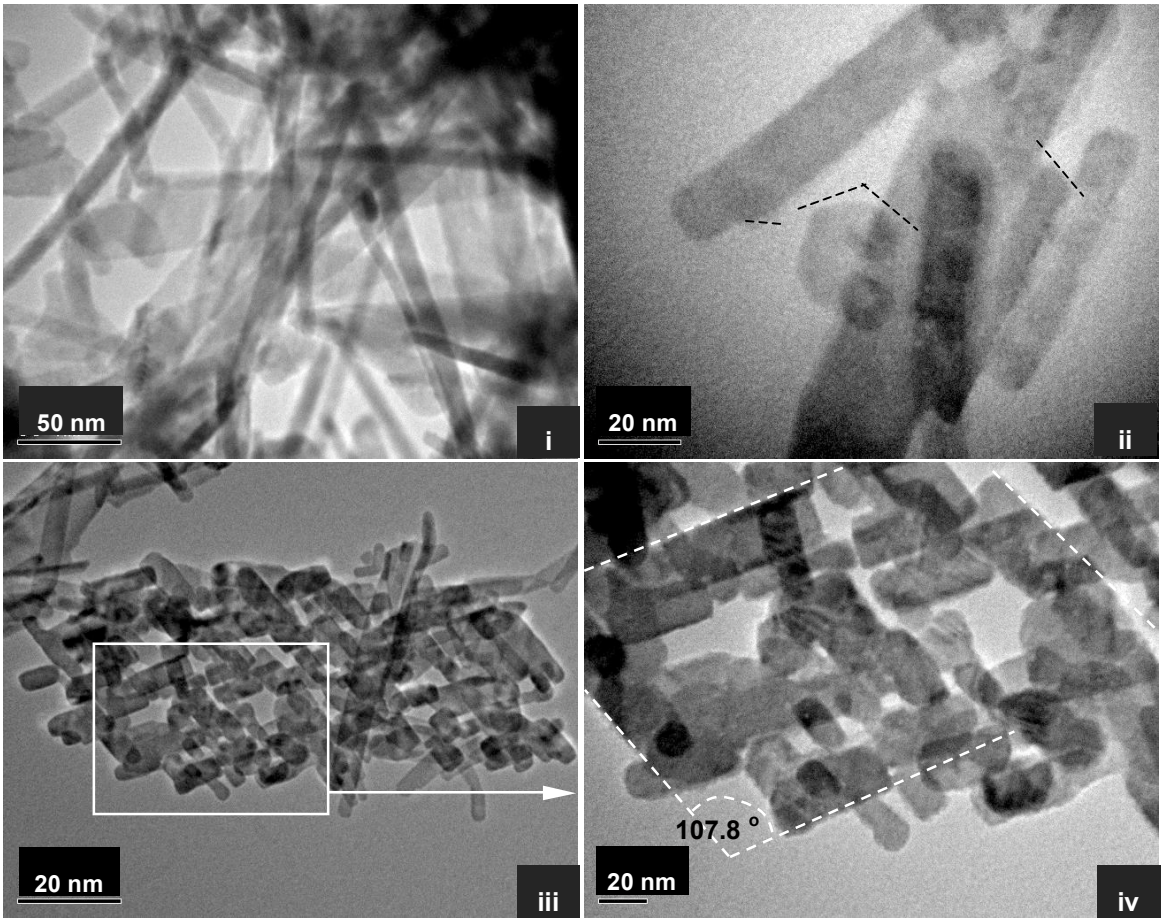

Figure 4.6 Representative TEM images of CuO nanoribbons synthesized from the E series of experiments with an aging treatment of 15 h: (i) a more rodlike morphology (compare to Figure 4.5), (ii) overgrowth on the existing rods; black dashed lines indicates the {110} crystal planes, (iii) oriented attachment of some short rods, and (iv) a detailed view of (iii); also see Figure 4.8.

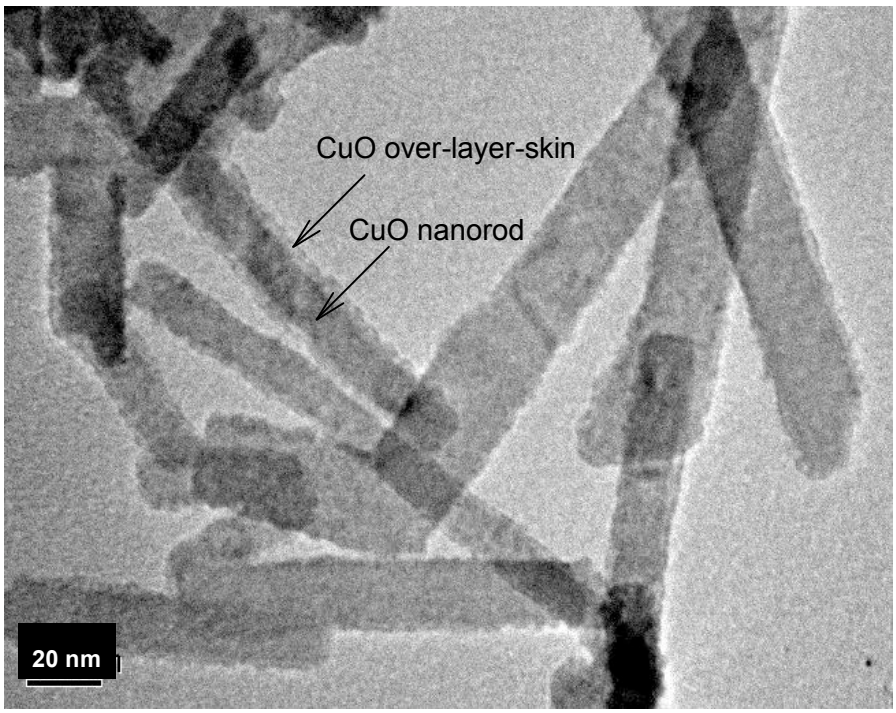

Figure 4.7 TEM image of sample E with prolonged aging of 39 h to indicate the overgrowth of CuO on the existing nanorods.

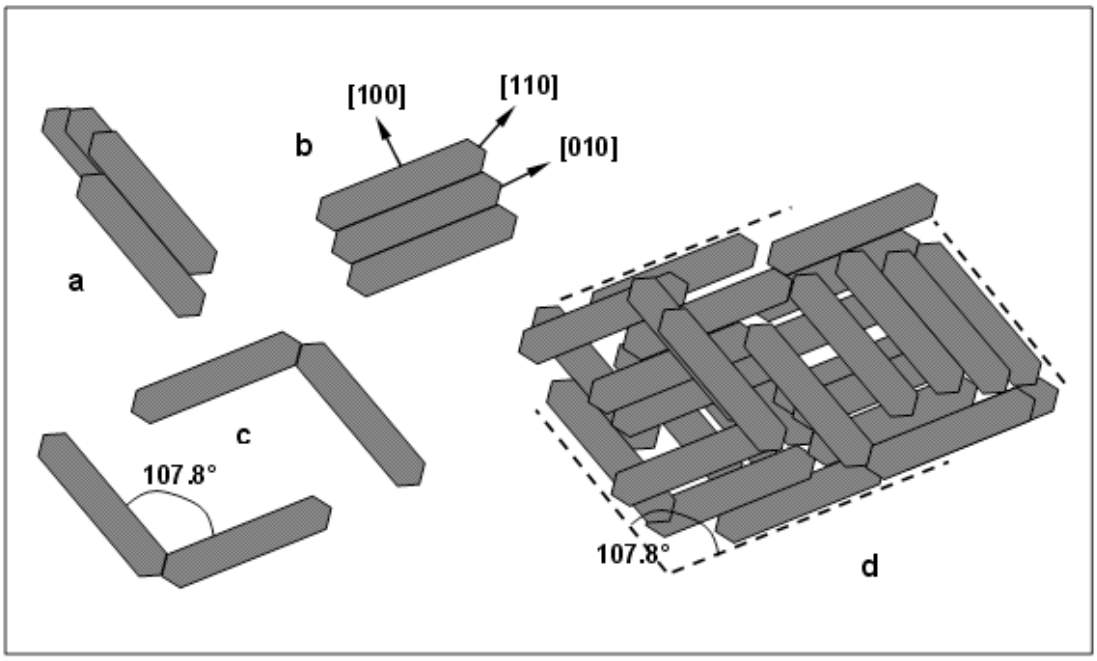

Figure 4.8 Schematic illustration of two-dimensional assembly of short CuO nanorods using their (a) top crystal planes {001}, (b) side crystal planes {100}, and (c) end crystal planes {110}; the final combination of the above oriented attachments is indicated in (d) [refer to Figure 4.6 (iii and iv)].

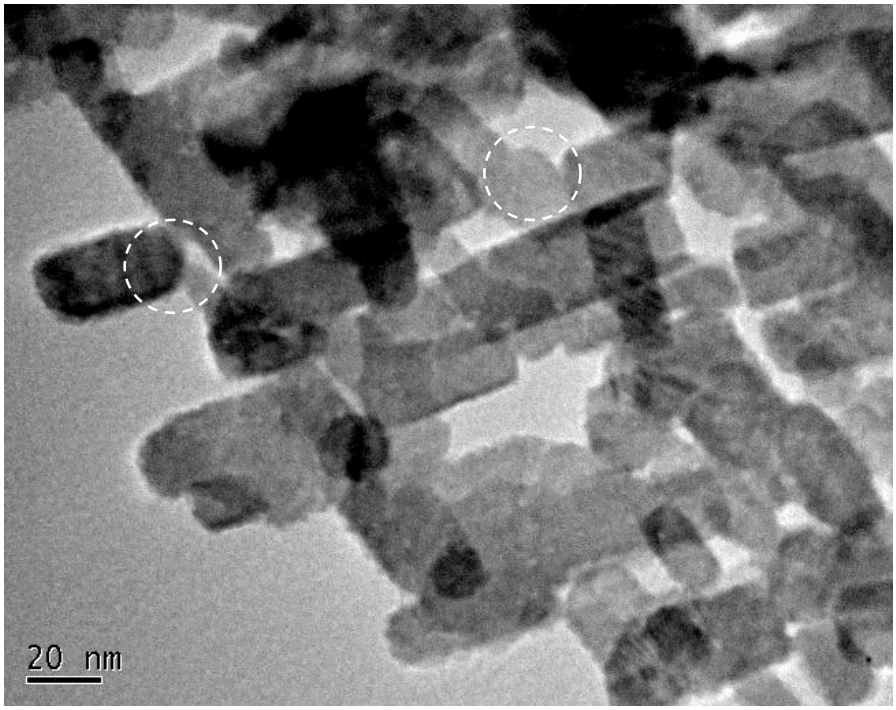

Figure 4.9 TEM image of the detailed {110} plane-attachment (indicating in circled area) among CuO nanorods in the netted structure (15 h aging in experiment series E, also see Figure 4.6 and Figure 4.8).

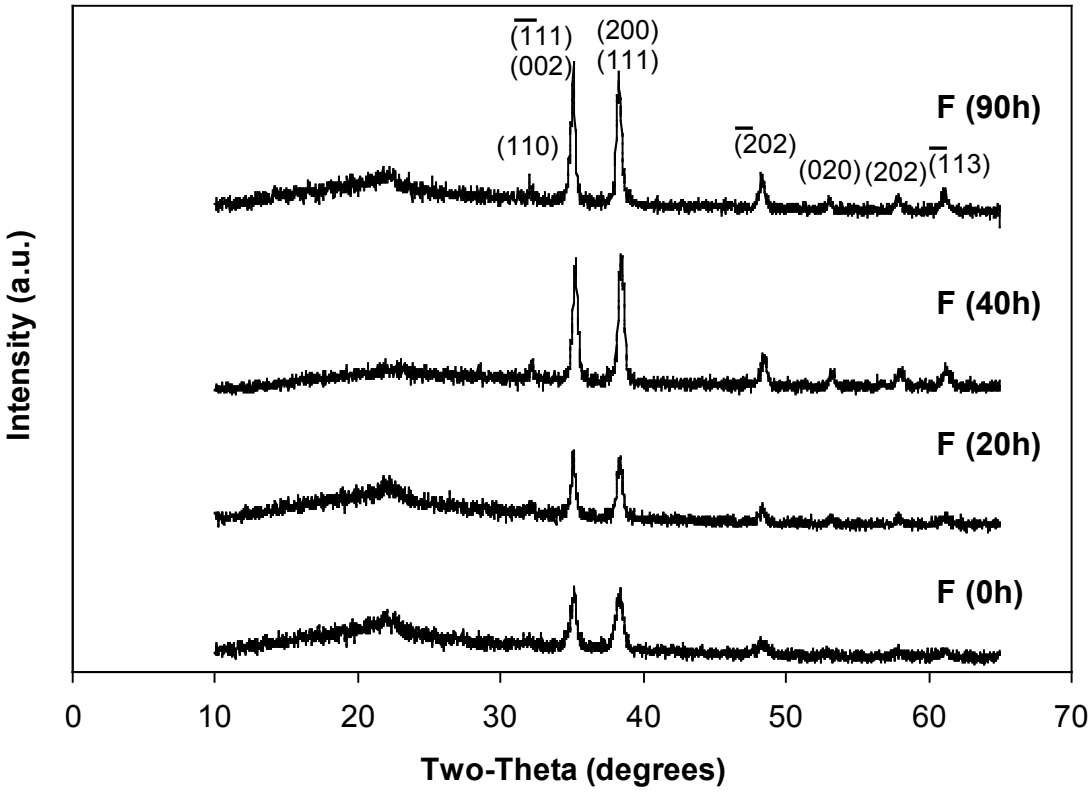

Figure 4.10 XRD patterns of the sample series F with or without aging treatment; the hump at 2θ = 22–23° is due to the diffraction of glass sample holder.

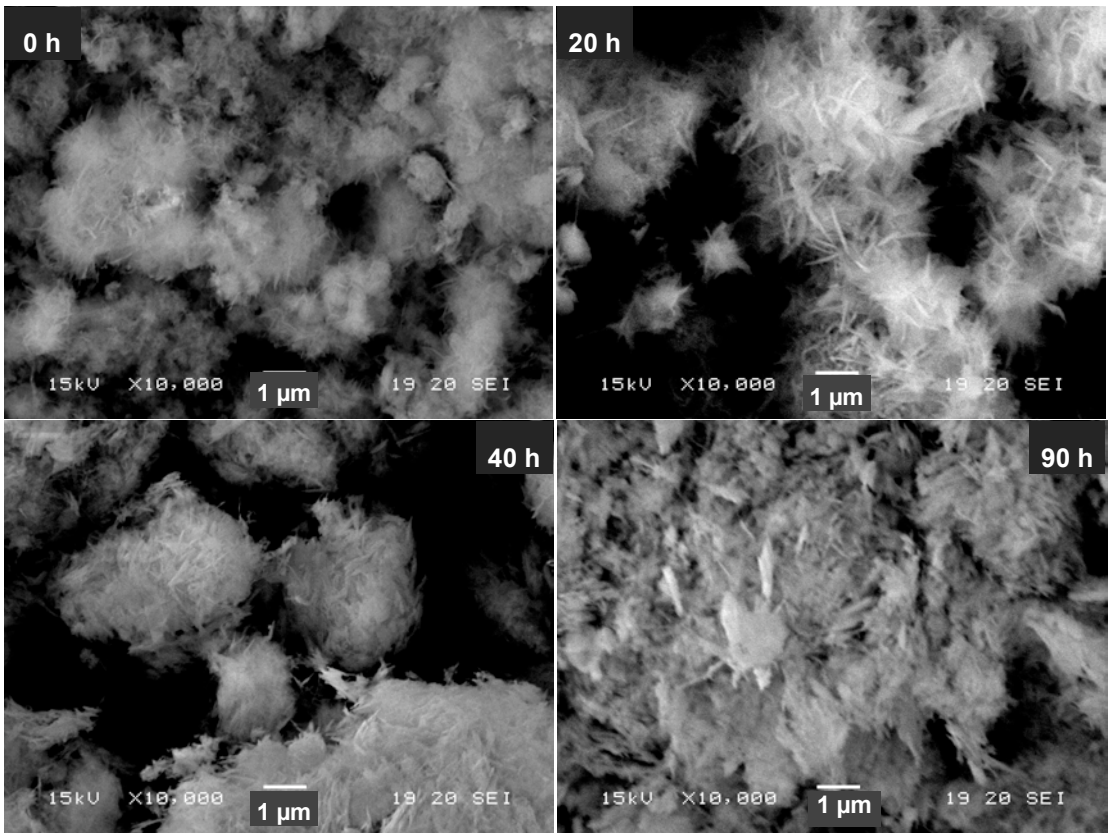

Figure 4.11 SEM images of the sample series F with different aging times.

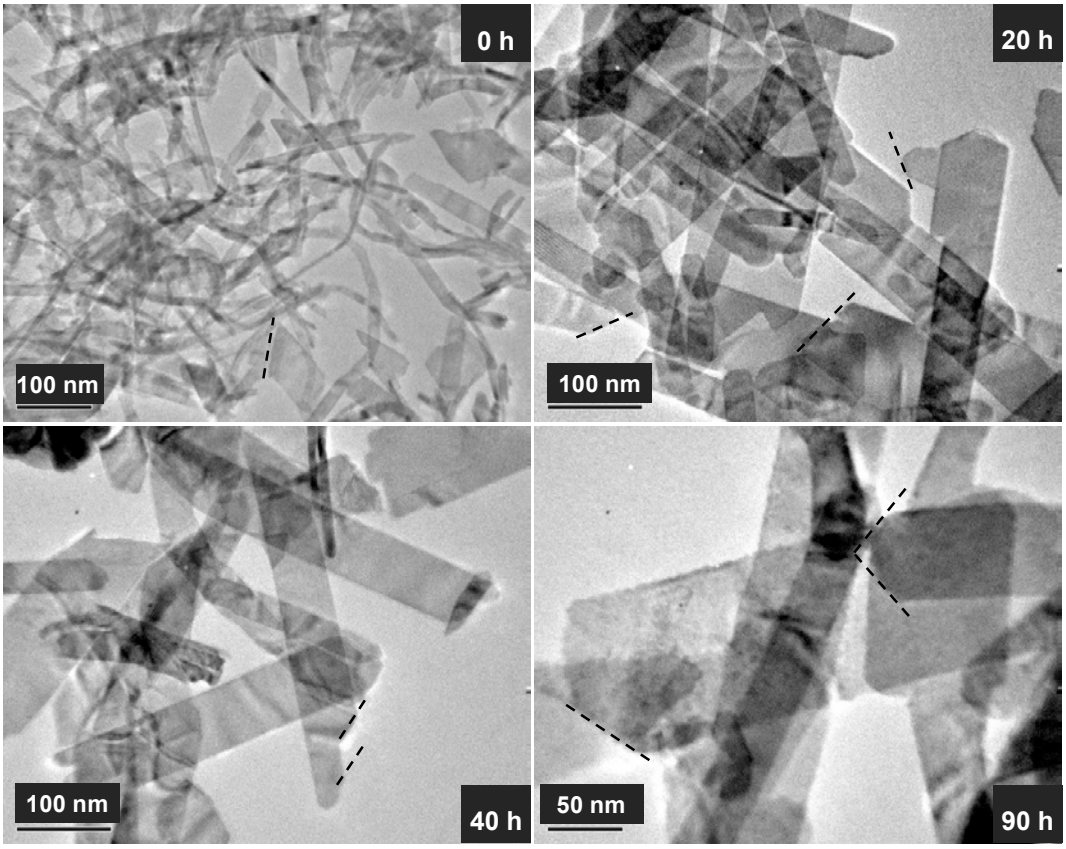

Figure 4.12 TEM images of the sample series F with different aging times. Black dashed lines illustrate the {110} crystal planes.

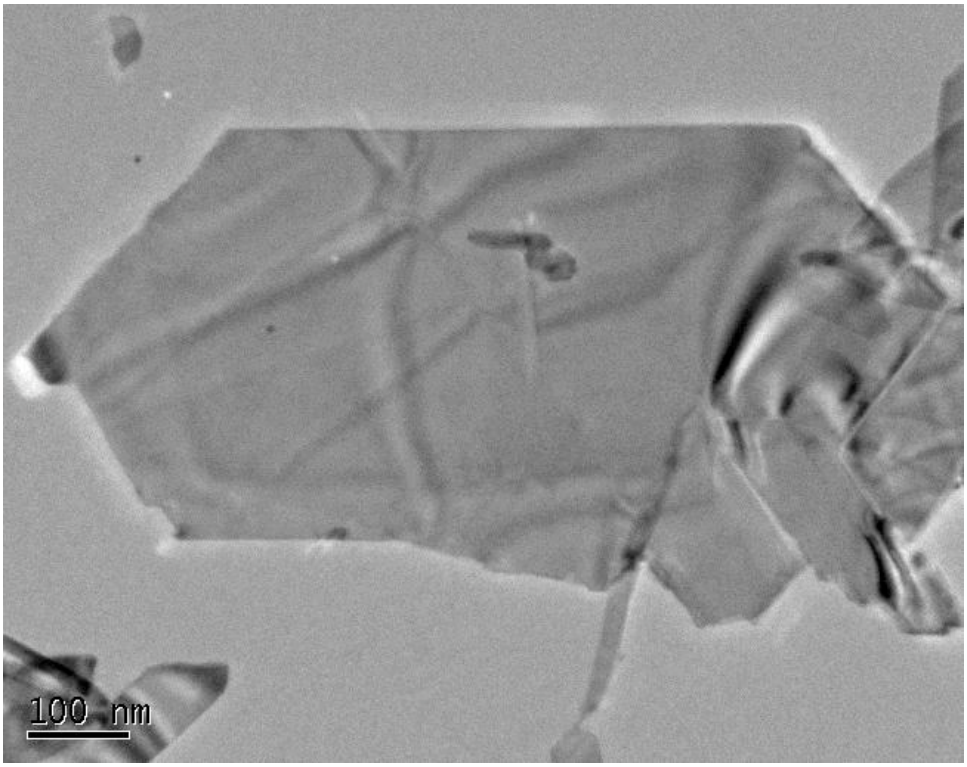

Figure 4.13 TEM image of a sheet-like CuO nanostructure with “wrinkles” from the experiment F (40 h aging).

the as-prepared CuO nanostructures have a length longer than 1 μm without a prolonged aging. Their morphology changes from needlelike to fiberlike, and then to a more platelet-like aggregate prior to the acetone dispersion. The TEM images of dispersed CuO samples of Figure 4.11 are reported respectively in Figure 4.12. Without aging, the CuO sample gives a ribbonlike (rather than rodlike) morphology. Compared to those in Figure 4.5, the growth along the ⟨100⟩ directions in method F is much faster. For example, in addition to the nanoribbons, small platelets of CuO with an average area of 80 × 90 nm are also present (0 h, Figure 4.12). With additional aging treatments in a concentrated NaOH environment, the breadth of the nanorods can be gradually increased (20, 40, and 90 h, Figure 4.12). Upon this breadth expansion, the one-dimensional nanorods should also be viewed as two-dimensional platelets, since sheetlike CuO as large as 500 × 1000 nm has been prepared (See Figure 4.13). After aging for 40 hours, the CuO crystallites are well faceted and the {110} crystal planes can be clearly observed, which also verifies the self-assembly mechanism of Figure 4.8. Nonetheless, due to the high concentration of NaOH in the solution, no "oriented attachment" is observed among the crystallites, as fewer chances are left for the CuO nanorods to make direct contact and coupling.

4.4 Conclusion

In summary, one-dimensional CuO nanostructures in rod, wire, ribbon, platelet, and sheet morphologies can be fabricated with the present wet-chemical

methods in which a water-ethanol mixture is used as solvent. At low reaction temperatures and normal atmospheric pressure, single-crystalline monodispersed CuO nanorods with a selected breadth in the range of 5–15 nm can be prepared by simply changing the starting copper ion concentration. It has been found that the preferential growth direction of nanorods is ⟨010⟩. Rigid or flexible long nanorods and nanoribbons up to 1 μm can also be prepared with a two-step continuous process in which seeding and length growth can be further controlled under a pseudo-steady-state operation. Upon the aging treatment, morphology of the pristine nanorods can be further modified. Overgrowth and rod shortening due to Ostwald ripening have been observed. At the same time, the resultant short nanorods can self-assemble into a two-dimensional netted structure using their {001}, {100}, and {110} crystal planes. Nanoplatelets or sheets of CuO can also be synthesized with a high concentration solution of NaOH in which the growth along ⟨100⟩ becomes more pronounced. A wide variety of synthetic methods and process parameters investigated in this work allow us to fabricate CuO nanostructures with flexibility for morphological and dimensional control.

CHAPTER 5

MANIPULATIVE-SYNTHESIS OF MULTIPOD FRAMEWORKS FOR SELF-ORGANIZATION AND SELF-AMPLICATION OF Cu_2O MICROCRYSTALS

5.1 Introduction

Cuprous oxide (Cu_2O) has a cubic structure (space group: *Pn3m*). Even in the simplest cubic structural symmetry, the Cu_2O prepared in solution phase also shows that crystal habit changes from cubic through cuboctahedral to octahedral as the average particle size increases (Kinoshita and Nakano, 1967; Mcfadyen and Matijevic, 1973). The actual cause of this evolution sequence has not been revealed for more than 30 years, although Cu_2O microcrystals had been prepared into hexa-pod-like whiskers (Chen[4] et al., 2003), after investigations of multipod crystals of other materials such as CdSe, CaS, MnS, etc (Gao[1] et al., 2002; Lu[2] et al., 2001; Manna et al., 2000).

In this chapter, the synthesis of cuprous oxide (Cu_2O) mltipod frameworks in acidic solution was investigated. To attain certain programmability or predictability of this type of crystal organization, understanding the process fundamentals is a crucial

prerequisite. We synthesized a range of novel Cu_2O multipod frameworks that include octa-pods, two types of dodeca-pods, and hexa-pods, as summarized in Figure 5.1.

5.2 Experimental section

5.2.1 Materials preparation More than 60 growth experiments were carried out in this work to get a general pattern of Cu_2O multipod framework formation and microcrystal self-organization. In a typical growth experiment, the starting solution of copper was prepared by mixing 30-100 (mostly 30) mL of 0.005-0.015 (mostly 0.010) M copper nitrate solutions [$Cu(NO_3)_2 \cdot 3H_2O$ dissolved in C_2H_5OH-H_2O solvents at a varied volume ratio of EtOH:H_2O = 100:0% to 70:30%] and 1.5-4.5 (mostly 1.5) mL of pure formic acid. Prior to the reaction, the solution mixture was sonicated in an ultrasonic water bath for 5 min. The reactions were carried out with a Teflon-lined stainless steel autoclave in an electric oven at 150-220 (mostly 180) °C for 1.25-5 (mostly 2) h. After the reaction, the autoclave was taken out from the oven and cooled in tap water. Thereafter, the dispersions were purified by centrifugation-redispersion cycles, with each successive supernatant being decanted and replaced with ethanol.

5.2.2 Materials characterization The obtained Cu_2O products were characterized with scanning electron microscopy (SEM), energy-dispersive X-ray spectroscopy (SEM/EDX, JSM-5600LV), and powder XRD (Shimadzu XRD-6000, Cu KR radiation) (Lou and

Zeng, 2003; Sampanthar and Zeng, 2002).

5.3 Results and Discussion

The crystallographic structure and chemical composition of all microscale multipod frameworks and microcrystals of Cu_2O synthesized in this work were confirmed with the XRD method (space group: *Pn3m*, a_o = 4.267 Å, PDF file 05-0667; see Figure 5.2). In Figure 5.1, major branching patterns of Cu_2O are summarized as a function of solvent composition and starting reagent concentrations. In principle, the observed first-order fractal growth occurs at synthetic conditions far from thermodynamic equilibrium where the chemical perturbation may play an important role. On the basis of our growth experiments, it is clear now that the branching is extremely sensitive to the chemical environment provided which, in turn, determines the final crystal organization and crystal morphology.

Under synthetic conditions with low water contents, Cu_2O crystal branching takes place along all orientations of <111>, which results in the formation of eight-pod frameworks (type (i), Figure 5.1). This type of branching has also been independently observed with another chemical route using glucose as a reducing agent (Wang[3] et al., 2003). Some representative SEM images of Cu_2O microcrystals synthesized with a water content in the range of 5-10 vol % are displayed in Figure 5.3. In Figure 5.3a,b, the octa-pod microcrystals are bounded with low Miller index crystal planes of {110};

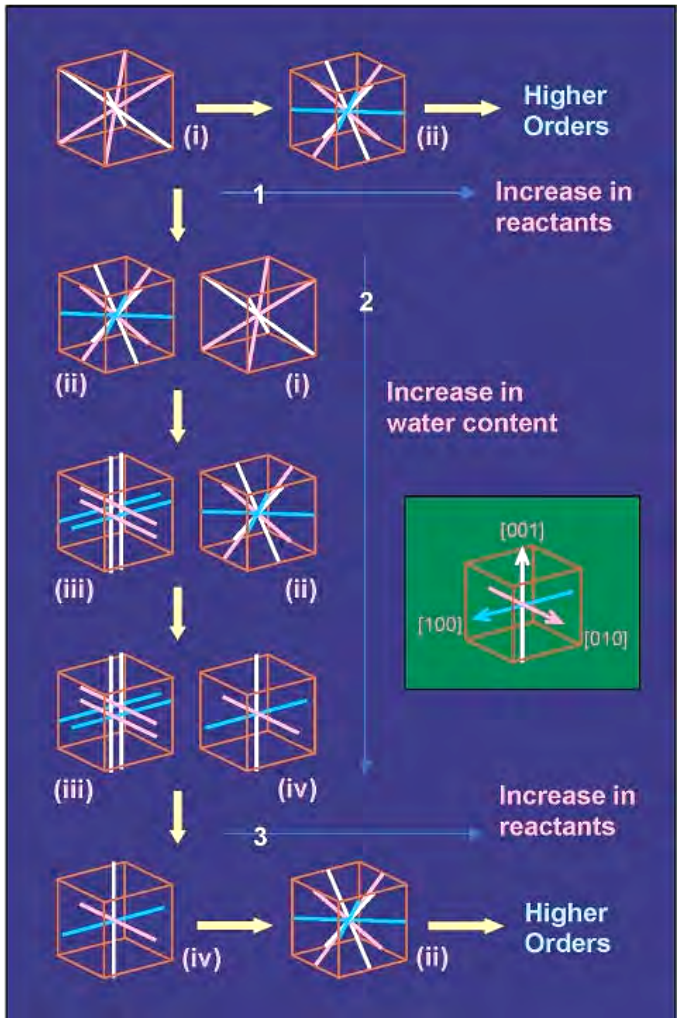

Figure 5.1 A summary flowchart of various branching fashions (inset indicates the coordinate system) of Cu_2O microcrystals under the current synthetic conditions: (i) 8-pod branching along <111> directions; (ii) 12-pod branching along <110>; (iii) 12-pod branching along <100> directions; and (iv) 6-pod branching along <100> directions. Colored lines within a cubic box are all equivalent (just to enhance the visibility).

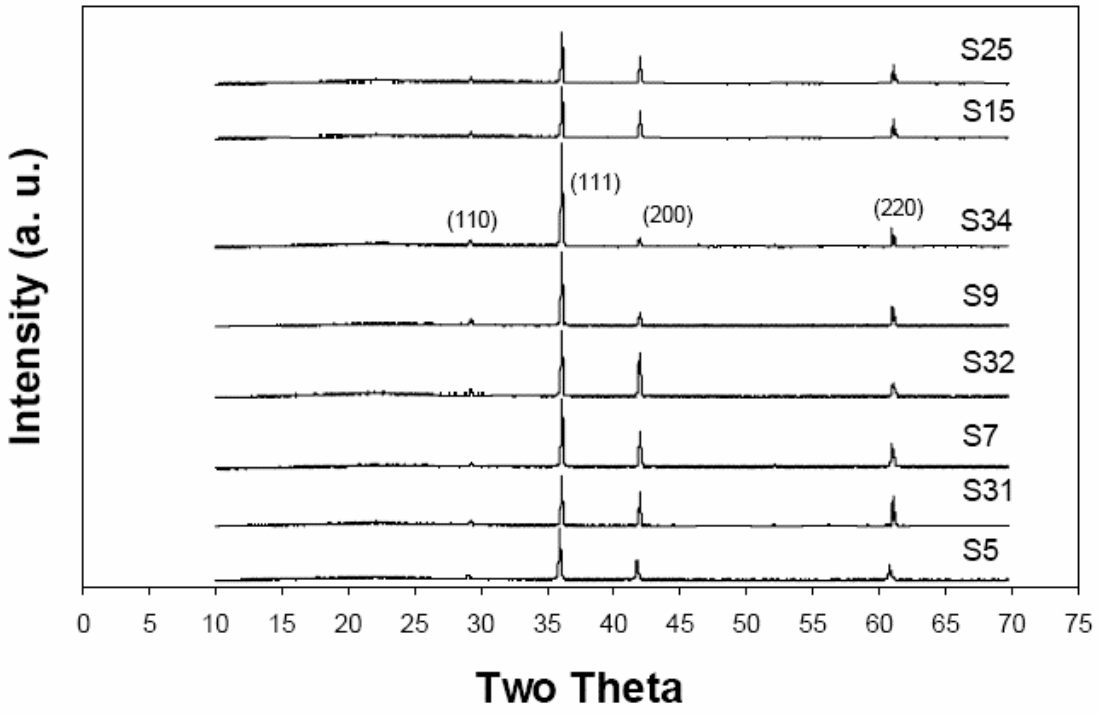

Figure 5.2 Representative XRD patterns of synthesized Cu_2O samples with different branching crystal morphologies (S5 to S34 are sample numbers.): S5 = Figure 5.3c,d; S7 = Figure 5.5a-d; S9 = hexa-pods (type (iv)); S15 = hexa-pods (type (iv)); S25 = Figure 5.7; S31 = Figure 5.3a,b; S32 = Figure 5.5e,f; S34 = hexa-pods (type (iv)). Note that there are variations in the reflection peak intensity, and the relative intensities of the reflection peaks are indeed proportional to the crystallographic planes observed in the samples.

a total of 12 {110} facets can be clearly observed along the pod surfaces, while their robust growing tips along <111> are each terminated with three crystal planes of {100}. When the water content is reduced, the {110} planes get less stable, and they are gradually replaced with the {100} planes. Interestingly, this type of growth leads to self-organization of cubic microcrystals on the preexisting octa-pod frameworks. In Figure 5.3c, enlargement of the multipods is pronounced owing to the change of plane stability. As a result, eight small cubes are developed respectively from the octa-pods, giving rise to a set of crystal aggregates (eight cubes per aggregate). More interestingly, one may also view this process as self-organization of crystal subunits according to a predefined space allocation. These microcrystals are packed in a simple cubic lattice (inset, Figure 5.3), showing a so-called “cube-within-cube” or “crystal-within-crystal” arrangement. At higher reaction temperatures, the stacking process can be accelerated, as reported in Figure 5.3d, where the flattened subunits are readily observed after only 1.25 h. At 1 vol % water, the eight-piece-crystal aggregates can be synthesized in a high population under the similar preparative conditions. It should be mentioned that centralized crystal porosity can be created in a closing up process (dice-like crystals, Figure 5.3c,d), and elimination of this space will generate a smooth symmetric cube which is 8 times as large as its initial building components. Alternatively, this synergetic growth can be viewed as a self-amplification of cube structure. When the water content is further reduced (<1 vol %), only individual cubical crystals can be obtained (see SEM images in Figure 5.4). This observation reveals that except for the {100} planes other crystallographic planes are not stable under the water-free

conditions.

With an increase in either reagent concentration or water content (paths 1 and 2, Figure 5.1), dodeca-pod frameworks can be fabricated. This type (type (ii), along 12 <110> directions, Figure 5.1) of branching can be considered as a general result of increasing surface reactivity of {110} planes. Figure 5.5 shows some frameworks of this type and their related microcrystal assemblies prepared at higher starting reagent concentrations (path 1, Figure 5.1). Two basic sets of building units can be observed: elongated (Figure 5.5b) and symmetrical polyhedra (Figure 5.5c). The crystal subunits are bounded with low Miller index planes {100}, {110}, and {111}, although some of crystal surfaces are not so smooth due to the rapid growth (Figure 5.5d). In Figure 5.5c, for example, 12 crystal subunits are attached to 12 corners of a large cuboctahedral cage (i.e., a {100}-face-truncated octahedron), noting that each small crystal itself is a truncated cube ({110} for cube edges and {111} for cube corners). These subunits are packed into a face-centered cubic lattice, if considering that the center of the framework (seed crystal) is one of the units. The intracrystal porosity is also present; six holes are formed in the square planes (each is formed by four crystal subunits) and eight in the triangular planes (each is formed by three crystal subunits), noting that elimination of the in-plane porosity will lead to formation of larger crystal cuboctahedra. In the same way, the tips of 12 elongated crystal pods also give a cuboctahedral cage, as illustrated in Figure 5.5d. This type of branching can also be attained by increasing water content (path 2, Figure 5.1). For example, similar crystal assemblies had been prepared with water content of 15 vol % in the starting solution

(Figure 5.5 e,f). Under this condition, the crystals are better faceted; the elongated arms are similarly bounded with {100}, {110}, and {111} surfaces.

When water content in the synthesis is further increased, a new type of dodeca-pod branching emerges. Designated as type (iii) in path 2 of Figure 5.1, the branching has two extruding pods (2 × 6 in total) along each principal crystallographic axis. Figure 5.6 shows this double-dagger-like morphology, accompanied by the presence of type (ii) microcrystals. At the used experimental conditions, stable crystal surfaces of type (ii) (Figure 5.6 c,d) are mainly the {111} planes that are substantially different from those reported in Figure 5.5 where {100} and {110} are predominant. It is interesting to note that with the {111} facets each crystal building block in fact is a small crystal octahedron, and an integration of these building units (12 pieces in total) via edge sharing is fitted well within a larger crystal octahedron, as illustrated in inset of Figure 5.6c. Similar to those in Figure 5.5c, the octahedral subunits of Figure 5.6c,d are also packed into a face-centered cubic lattice if one considers the central seed as a subcrystal. On the other hand, connecting all the “dagger tips” in type (iii) frameworks also leads to a larger piece of octahedron. Therefore, the synthetic conditions therein favor the octahedral formation, which is an underlying chemistry governing both type (ii) and (iii) structures in this multimode growth where the branching rates along <100> and <110> directions are comparable. At a lower reaction temperature (150 °C), type (iii) branching mode can be selected with a fine-tuning of preparative parameters, as shown in Figure 5.7. Due to the low synthetic temperature, the crystal facets of these multipods are not as smooth as those in Figure 5.6.

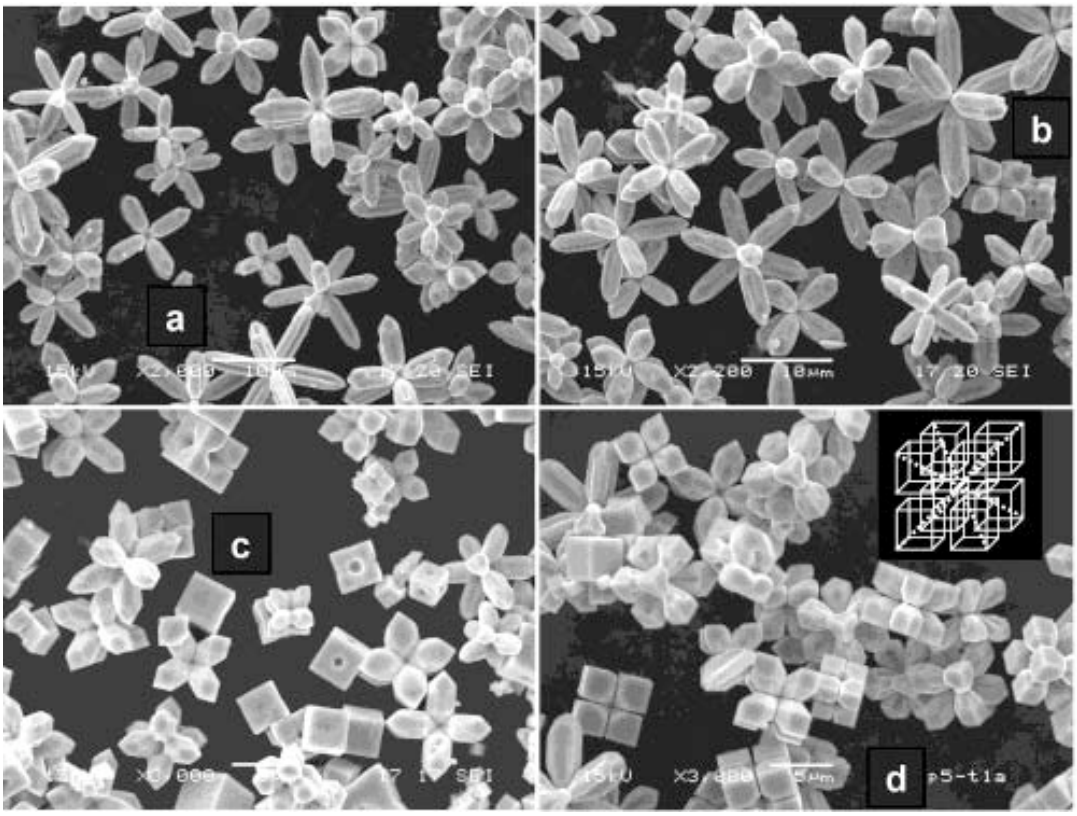

Figure 5.3 Type (i) multipod frameworks and crystal assemblies: (a and b) prepared with 30 mL of 0.005 M Cu^{2+} solution (water at 10 vol %) and 1.5 mL of formic acid at 180 °C (2 h); (c) prepared with 30 mL of 0.005 M Cu^{2+} solution (water at 5 vol %) and 1.5 mL of formic acid at 180 °C (2 h); and (d) prepared with 30 mL of 0.005 M Cu^{2+} solution (water at 5 vol %) and 1.5 mL of formic acid at 220 °C (1.25 h). Inset indicates the stack of eight face-sharing cubical subunits according to the space provided by type (i) framework.

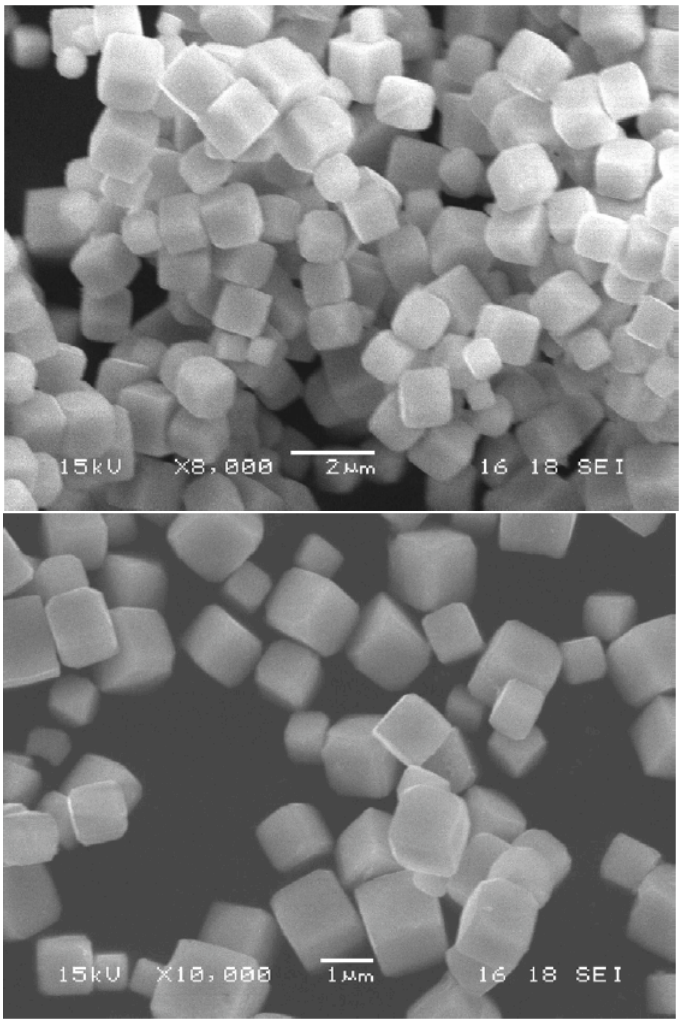

Figure 5.4 SEM images of single-cubes of Cu_2O synthesized without water in the ethanol solution.

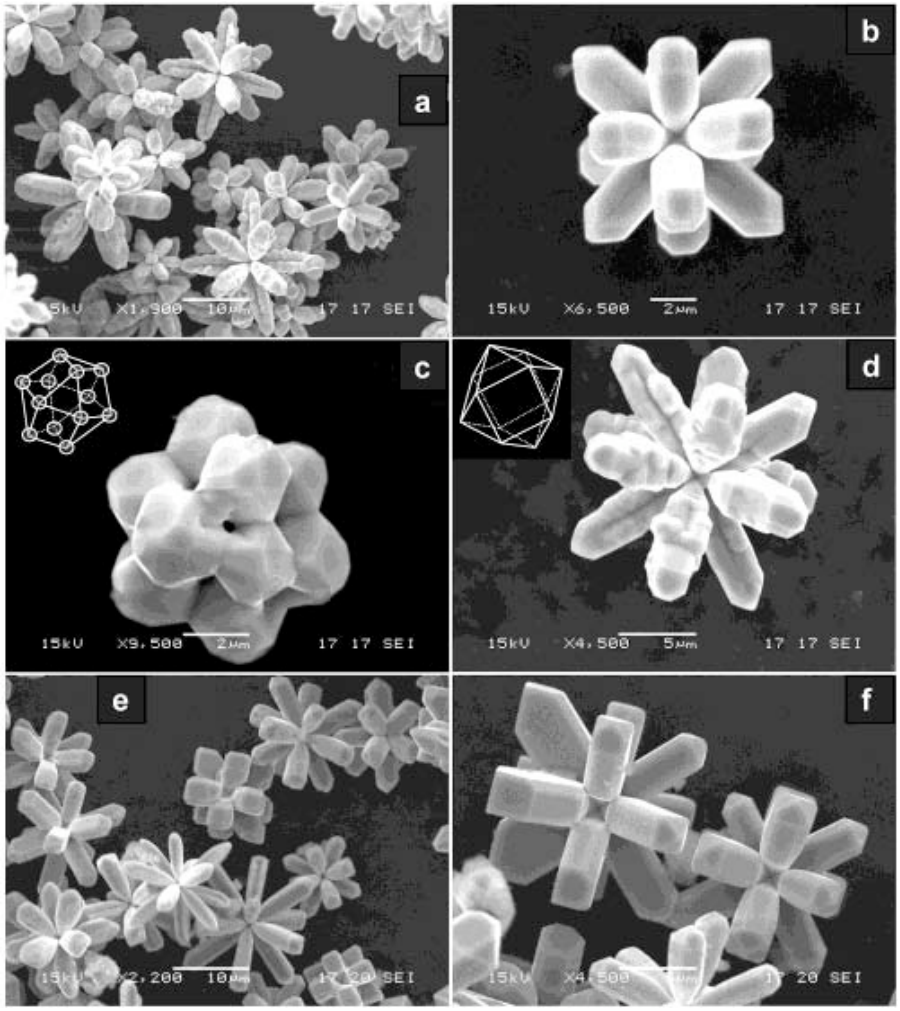

Figure 5.5 Type (ii) multipod frameworks and crystal assemblies: (a-d) prepared with 30 mL of 0.015 M Cu^{2+} solution (water at 5 vol %) and 4.5 mL of formic acid at 180 °C (2 h); and (e and f) prepared with 30 mL of 0.010 M Cu^{2+} solution (water at 15 vol %) and 1.5 mL of formic acid at 180 °C (2 h). Insets indicate the cuboctahedral cages in type (ii) structures.

At even higher water concentrations, type (iv) branching becomes attainable, often appearing together with the type (iii) microcrystals (path 2, Figure 5.1). By manipulating synthetic conditions, however, single-phase hexa-pod frameworks or their microcrystal "stacks" can be prepared, as reported in Figure 5.8a,b and Figure 5.8c,d, respectively. Since the crystal morphological evolution records the process history, rich dynamic information has been stored in the crystal morphology. The pods formed in the initial growth are normally bounded with 12 {100} planes (Figure 5.8a,b; instead of four {110} planes (Chen[4] et al., 2003)). Compared to those of the reported hexa-pods (Chen[4] et al., 2003), the central cores and arms of the hexa-pods from our synthesis (Figure 5.8) are much smaller and more complex, which allows us to trace the branching process. More importantly, an enlargement of hexa-pods has been pursued in this work for the first-time when the concentration of starting reagent is increased (e.g., Figure 5.8c,d; the volume of formic acid was changed to 4.5 mL). Once again, the crystal subunits in this case are faceted with the {111} planes, resulting in a face-centered close packing of crystal octahedra where the interconnectivity is generated by edge sharing. In some cases, the crystal-building units are fused together, giving rise to a larger octahedral crystal (six times larger) with a total of eight intracrystal holes on the centers of {111} planes. Instead of the type (iv) frameworks, furthermore, type (ii) crystal assemblies can be prepared with higher reactant concentrations (such as an increase in Cu^{2+} ions), as indicated in path 3 of Figure 5.1. For example, similar octahedral crystal assemblies to those reported in Figure 5.6c,d have been prepared with 0.015 M Cu^{2+} over a water range of 22 to 30 vol

% while keeping other synthetic parameters unchanged.

It has been reported that in many cases the fractal aggregates are normally polycrystalline or even in an amorphous state (Deutscher andLereah, 1988; Kniep and Busch, 1996; Lereah et al., 1991; Shang, 1996; Vicsek, 1992; Zhang[2], 1990). In contrast, the crystal assemblies of all types in the present study are single-crystalline. The overall crystal symmetry is strictly followed for both branching and assembly, which is further evidenced in the self-creation and self-elimination of the intracrystal porosity. In Figure 5.9, the void spaces created within cube assembly and octahedron assembly are due to rapid growths of the outer crystal planes ({100} for Figure 5.9a, and {111} for Figure 5.9b). These observations reveal that the assembly of crystals occurs inwardly, i.e., from the outside branches toward a framework center (also refer to Figure 5.3c,d).

On the basis of the above findings, it is understood that the surface reactivity (i.e., the fastest growing plane or direction) of Cu_2O microcrystals takes the following sequence in response to the increase in water content: {111}, {110}, and then {100}. In agreement with this change, the overall crystal assemblies show a crystal evolution from cube to cuboctahedron, then to octahedron. An explicit description on the relationship among the adopted morphologies is now available. In particular, the formation of Cu_2O microcrystals can be divided into the following temporal steps: (1) fractal growth of multipod frameworks from a nucleation center (space expansion), (2) attachment of microcrsytal building blocks (space occupation) according to the space instruction of the frameworks, and (3) formation of larger crystal polyhedrons when

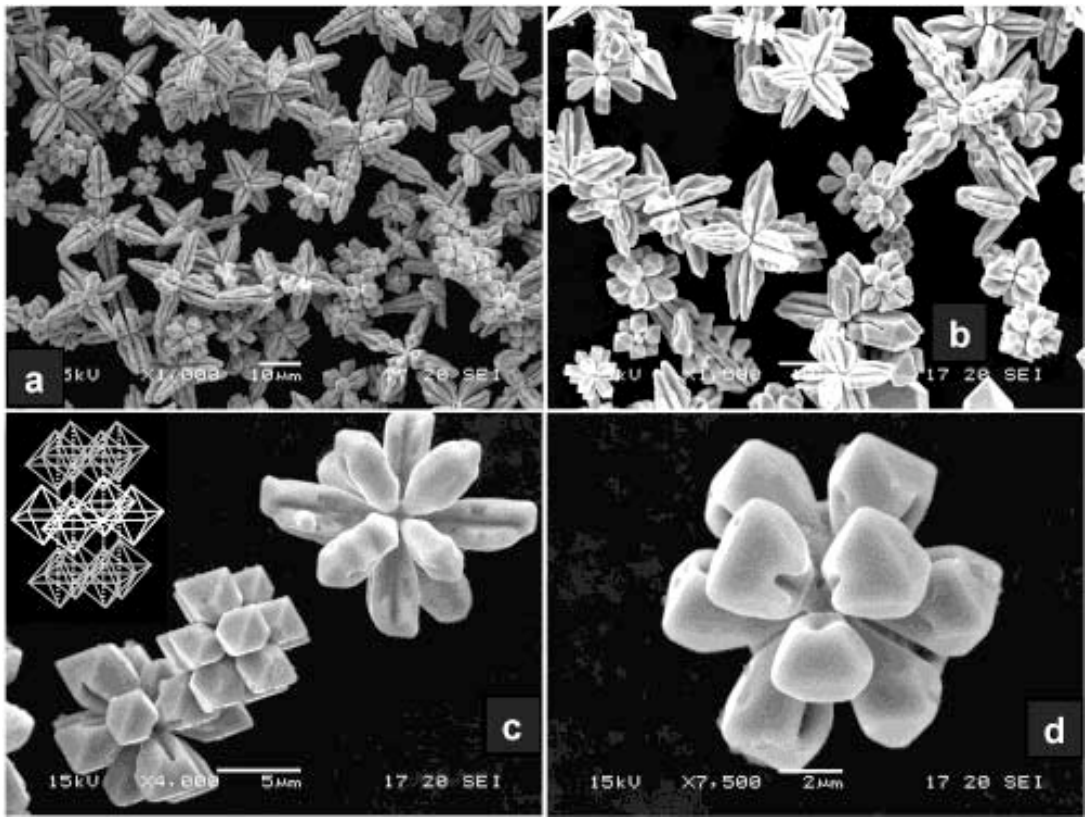

Figure 5.6 Mixed phase of type (ii) and type (iii) multipod frameworks and crystal assemblies prepared with 30 mL of 0.010 M Cu^{2+} solution (water at 20 vol %) and 1.5 mL of formic acid at 180 °C (2 h): overall mixed phase (a and b), and detailed views on crystal assemblies of type (ii) with 12 octahedral building blocks (c and d). Inset indicates an ideal stack of twelve edge-sharing octahedral subunits along the [001] direction.

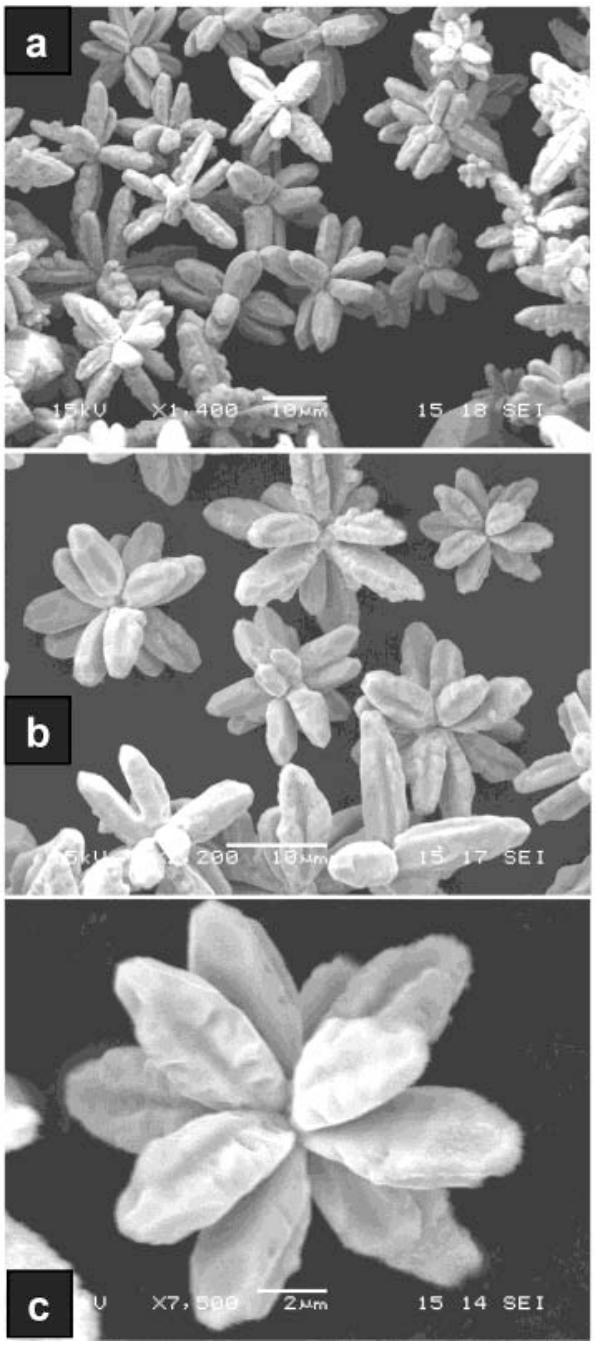

Figure 5.7 Type (iii) crystal assemblies prepared at 150 °C (5 h) with 30 mL of 0.015 M Cu^{2+} solution (water at 21 vol %) and 1.5 mL of formic acid. SEM images were taken with increasing magnifications (a-c).

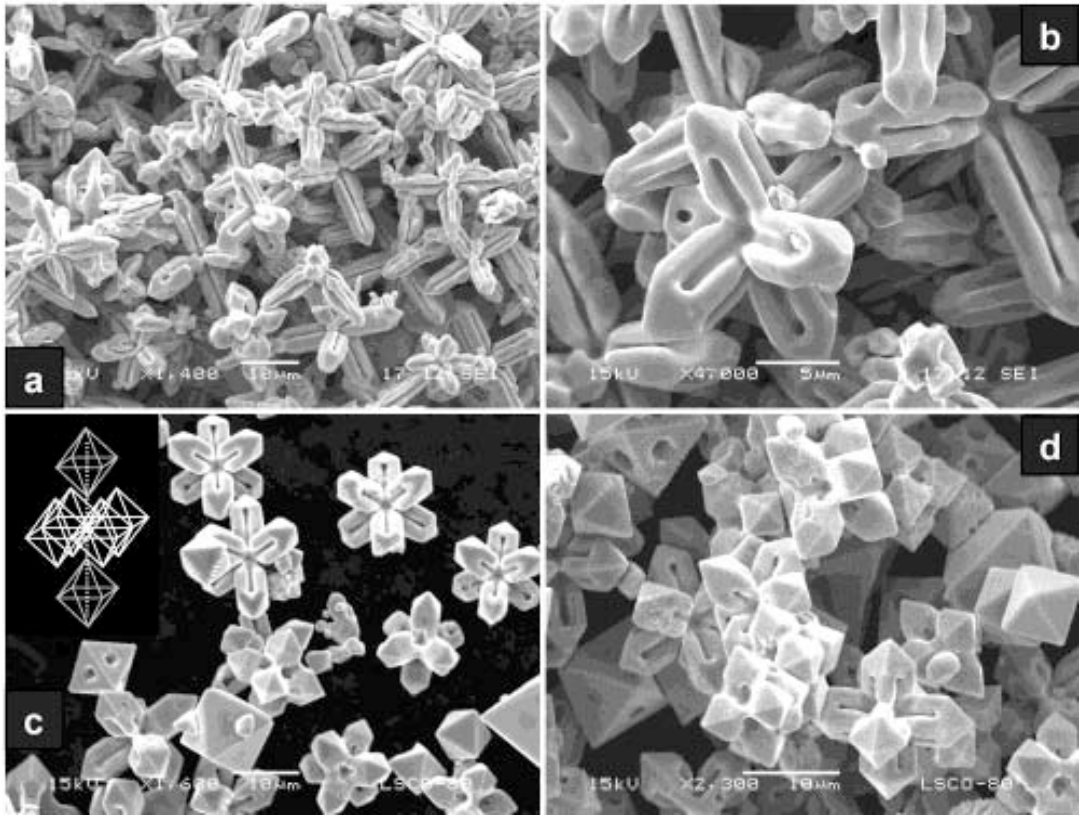

Figure 5.8 Type (iv) multipod frameworks and crystal assemblies: (a and b) prepared with 30 mL of 0.010 M Cu^{2+} solution (water at 22.5 vol %) and 1.5 mL of formic acid at 185 °C (2 h); and (c and d) prepared with 30 mL of 0.010 M $^{2+}$ solution (water at 22.5 vol %) and 4.5 mL of formic acid at 180 °C (1.5 h). Inset indicates an ideal stack of six edge-sharing octahedral subunits along the [001] direction.

intracrystal porosity is eliminated (space optimization). Resembling many natural dynamic processes (Whitesides and Grzybowski, 2002), the above three steps represent a "simple-complex-simple" morphological replication at different scales. Because the formation of Cu_2O solid results from the redox reactions between Cu^{2+} cations and formic acid in solution, the observed morphological evolution reflects a growth rate change in response to the variation of nutrient supply (or degree of supersaturation) in a batch reaction environment, as well as to the changes of ionic constituents (such as Cu^{+} and/or O^{2-}) on various surface planes that interact with liquid chemical species during the growth.

Since a framework is started from a common central core, individual microcrystals are grown simultaneously. This observation explains why all the crystal building blocks within a crystallite have similar sizes. Hence, the present stacking scheme is primarily determined by the first-order fractal growth. This finding may be further applied to other material systems. For instance, the supported hierarchical mesophase crystals of hybrid organic silane along with surfactants had been synthesized and the formation of hierarchically ordered structures had been explained with multiplication and self-similar growth (Tian et al., 2003(a, b)). Although a mechanism involving a stepwise nucleation from the edges of previous crystal has been proposed to explain the construction of high order octahedral structures (Tian et al., 2003(a, b)), the origin of the initial nucleation process (i.e., the first order) in that study has remained unknown. In this regard, our present findings have shed light on

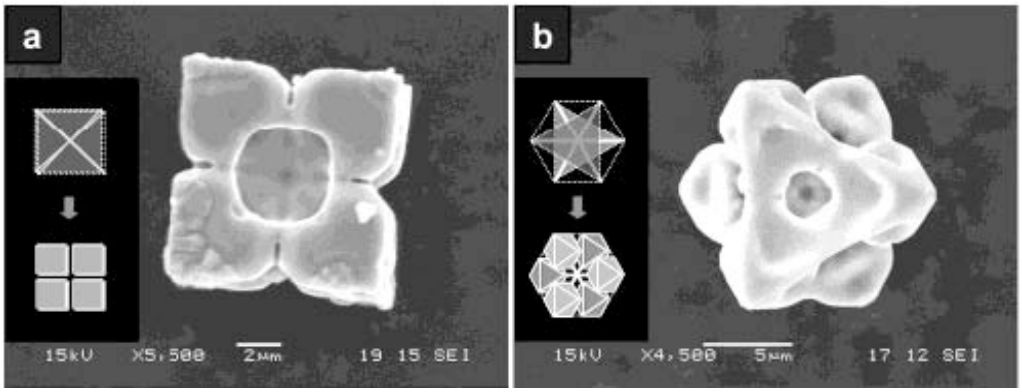

Figure 5.9 Intracrystal cavities created within 8-cubical-crystal assembly (a: type (i), viewed along the [100] axis) and 6-octahedral-crystal assembly (b: type (iv), viewed along the [111] axis). Insets indicate the framework formation and attachment of subunit crystals.

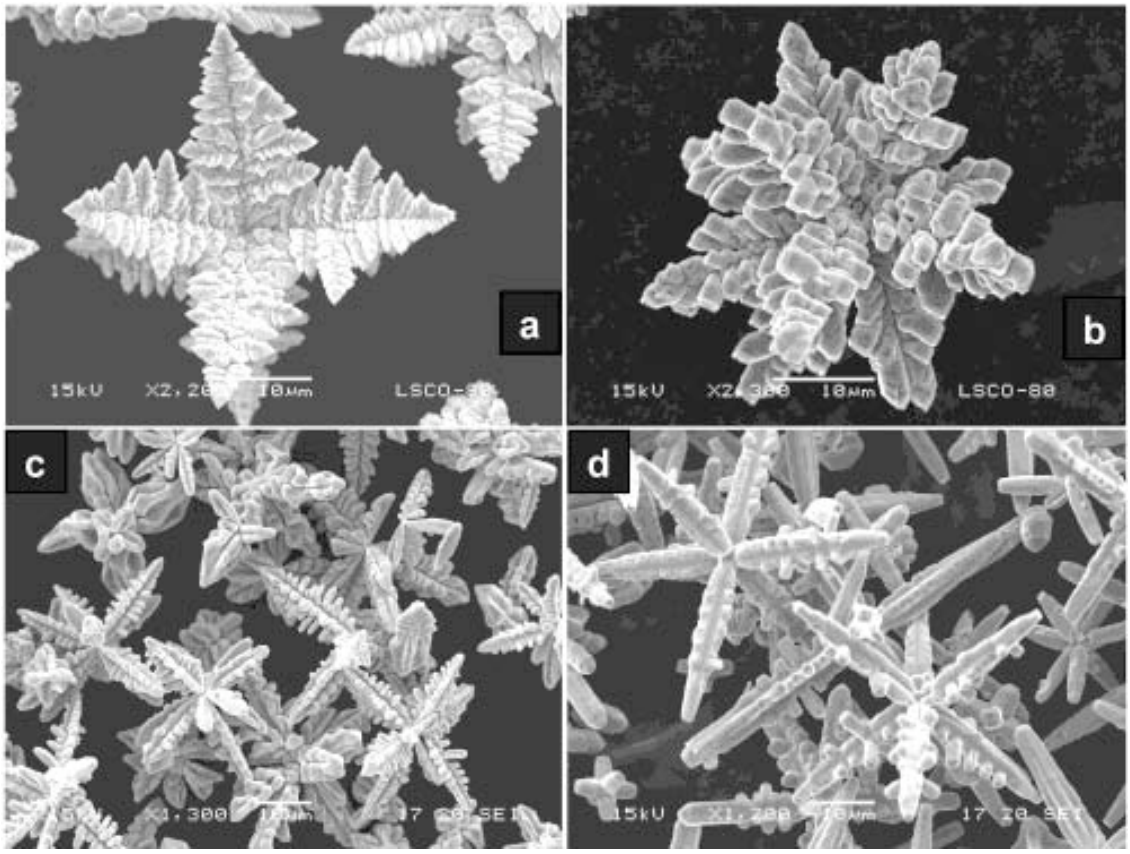

Figure 5.10 Higher-ordered multipod frameworks and crystal assemblies: (a, type (i)) prepared with 30 mL of 0.050 M Cu^{2+} solution (water at 5 vol %) and 4.5 mL of formic acid at 180 °C (1.5 h); (b, type (ii)) prepared with 30 mL of 0.030 M Cu^{2+} solution (water at 5 vol %) and 4.5 mL of formic acid at 180 °C (1.5 h); (c, type (iii)) prepared with 30 mL of 0.015 M Cu^{2+} solution (water at 22 vol %) and 1.5 mL of formic acid at 180 °C (2 h); (d, type (iv)) prepared with 30 mL of 0.050 M Cu^{2+} solution (water at 30 vol %) and 4.5 mL of formic acid at 180 °C (2 h).

general aspects of the initial nucleation process.

The primary objective in the present work was to examine the first-order organization of Cu_2O microcrystals according to the space allocation provided by crystal framework. With highly isotropic crystal systems, such as the one investigated herein, more complex geometrical crystal assemblies with predefined space locations are still possible. In particular, higher order growths may still adopt this "packing scheme" where a similar but larger framework built from dendritic expansion may serve as a space provider for higher-order organizations (Zeng[2] and Lim, 1998), depending on the actual supply of nutrient chemicals and other growth conditions. In Figure 5.10, for example, some of our preliminary results are displayed. Under low water conditions, higher-order branching growths on type (i) framework can be realized with higher concentrations of the starting reagents (Figure 5.10a), noting that the second-and third-order dendritic arms in this structure are also pointing to the <111> directions of the first-order. Similarly, multilevel hierarchical structures of types (ii), (iii), and (iv) have also been prepared respectively with a higher degree of supersaturation of reactants and increasing water content (Figure 5.10b,c,d). Due to increase in complexity, attachment of Cu_2O crystal building blocks onto these higher ordered frameworks appears to be challenging, as controlling the interdendritic space is a crucial step.

5.4 Conclusion

In summary, a variety of multipod frameworks of Cu_2O microcrystals can be prepared through careful control of synthetic parameters such as water content, reagent concentrations, and reaction time and temperature. In particular, the Cu_2O microcrystals tend to grow into cubical, cuboctahedral, and octahedral morphologies, respectively, with an increase in water content in the synthesis. More importantly, three-dimensional microcrystals can be organized into simple cubic or face-centered cubic lattices according to space instruction of the formed frameworks. This self-organizing scheme can be viewed in the following steps: (i) fractal growth of multipod frameworks from a nucleation center (space expansion), and (ii) attachment of microcrystal building units (space occupation). The resultant microcrystal stacks (step (ii)) also provide a base for generation of intracrystal porosity and crystal self-amplification. Various crystal morphologies of Cu_2O microcrystals can be well correlated to their respective multipod frameworks, including higher ordered hierarchical organizations of crystals.

CHAPTER 6

FORMATION OF COLLOIDAL CuO NANOCRYSRTALLITES AND THEIR SPHERICAL AGGREGATION AND REDUCTUIVE TRANSFORMATION TO HOLLOW Cu_2O NANOSPHERES

6.1 Introduction

In this chapter, a novel method for fabricating hollow spheres was developed, in which DMF was selected solvent and therefore the reaction took place in basic condition. In the reaction process, the colloidal CuO nanocrystallites formed first, and then aggregateed and were reduced to Cu_2O hollow spheres. In this chapter, we will also demonstrate that chemical composition, structure, and photoelectronic properties of semiconductor nanoparticles can be step-wise controlled by forming and gathering primary nanocrystallites, solid-solution redox reaction, and subsequent crystallite aging and solid evacuation. In particular, a process mechanism has been revealed for the synthesis of cuprous oxide Cu_2O (a *p*-type semiconductor with a band gap of 2.17eV) nanospheres: (i) formation of CuO nanocrystallites; (ii) spherical aggregation of primary CuO crystallites; (iii) reductive conversion of CuO to Cu_2O; and (iv) crystal aging and hollowing of Cu_2O nanospheres. For the first time, a wealth of colorful

Cu_2O hollow nanospheres, with variable E_g in the range of 2.405-2.170 eV, has been fabricated using the current one-pot synthetic approach.

6.2 Experimental section

6.2.1 Materials preparation In our typical single-step experiments, 30 mL of 0.005-0.010 M $Cu(NO_3)_2$ solution [a certain quantity of $Cu(NO_3)_2 \cdot 3H_2O$ was dissolved in organic solvent DMF to make a stated concentration] was sealed in a Teflon lined stainless steel autoclave with 50 mL capacity and then heated at different temperatures (150, 160, 170, and 180 ^oC) for different times to form Cu_2O nanoproducts. In a typical two-step experiment, the above-mentioned solution was heated at 140-150 ^oC for 22-40 h and then continuously heated at 180 ^oC for 8-42 h. After reaction, the autoclave was cooled with tap water and the Cu_2O products were washed with pure ethanol for 3 times and then dried in a vacuum system. Table 6.1 shows the detailed experimental parameters.

6.2.2 Materials characterization The crystallographic information of the samples was investigated by powder XRD (Shimadzu, model XRD-6000, Cu K_α radiation λ = 1.5406 Å). Morphological investigation was carried out with TEM (Joel model JEM-2010, 200 kV), and SEM (Joel model JSM-5600LV). The UV-Visible absorption spectra of suspensions of Cu_2O hollow nanospheres synthesized with different reaction times were measured by a UV-VIS-NIR scanning spectrophotometer (Shimadzu, model UV-3101 PC; with ethanol as a solvent).

6.3 Results and Discussion

Figure 6.1 illustrates the synthetic process developed in the present work and the related color changes upon reaction process time. The evolution of the crystal morphology of samples at 150 ^{o}C is reported in Figure 6.2A. In this TEM study, it is found that the product formed within the first 4h comprises small nanocrystallites in both CuO and Cu_2O phases, which was confirmed with powder XRD; CuO space group: C2/c; a_o = 4.684 Å, b_o = 3.425 Å, c_o = 5.129 Å, β = 99.47 ^{o}, JCPDS file no. 05-0661; Cu_2O space group: *Pn3m*, a_o = 4.267 Å, JCPDS file no. 05-0667) ; Figure 6.3), and some of these crystallites have attached each other into spherical aggregates (Figure 6.2B) with diameters in the range of 100-200 nm. Other dispersive nanocrystallites have also eventually gathered, accompanying with a phase transformation form CuO to Cu_2O (i.e., reductive transforming reaction; confirmed with XRD, Figure 6.3), after longer reaction (Figure 6.2 C,D). The crystallite agglomeration was then followed by solid core evacuation, as evidenced in Figure 6.4. The TEM image contrasts show that hollowing takes place gradually in the central cores of Cu_2O nanospheres, where the lighter central parts correspond to the void spaces. The selected area electron diffraction (SAED; Figure 6.4D) rings are relatively sharp and can be assigned perfectly to polycrystalline Cu_2O. It is then understood that the nanospheres of Cu_2O did not undergo further chemical reactions, but went through a re-crystallization process (i.e., Ostwald ripening) in the core evacuation. Although

Table 6. 1 A list of experiments conducted in the present work.

Sample No.	$[Cu^{2+}]$	Temperature (^{o}C)	Time (h)
1	0.010	150	4
2	0.010	150	9
3	0.010	150	14
4	0.010	150	23
5	0.010	150	35
6	0.010	150	50
7	0.010	160	2
8	0.010	160	4
9	0.010	160	10
10	0.010	160	15
11	0.010	160	27
12	0.010	160	40
13	0.010	170	1.5
14	0.010	170	3.25
15	0.010	170	4
16	0.010	170	6
17	0.010	180	2
18	0.010	180	3
19	0.005	180	4
20	0.010	180	4
21	0.010	180	7
22	0.010	180	8
23	0.010	180	9
24	0.010	180	10
25	0.010	180	12
26	0.010	180	13
27	0.010	180	14
28	0.010	180	15
29	0.010	180	17
30	0.010	180	20
31	0.010	180	25
32	0.010	180	30
33	0.010	180	33
34	0.010	180	36
35	0.010	150 + 180	22 + 8
36	0.010	150 + 180	22 + 10
37	0.010	150 + 180	22 + 11
38	0.010	150 + 180	24 + 8
39	0.010	150 + 180	24 + 10
40	0.010	150 + 180	24 + 11
41	0.010	150 + 180	26 + 42

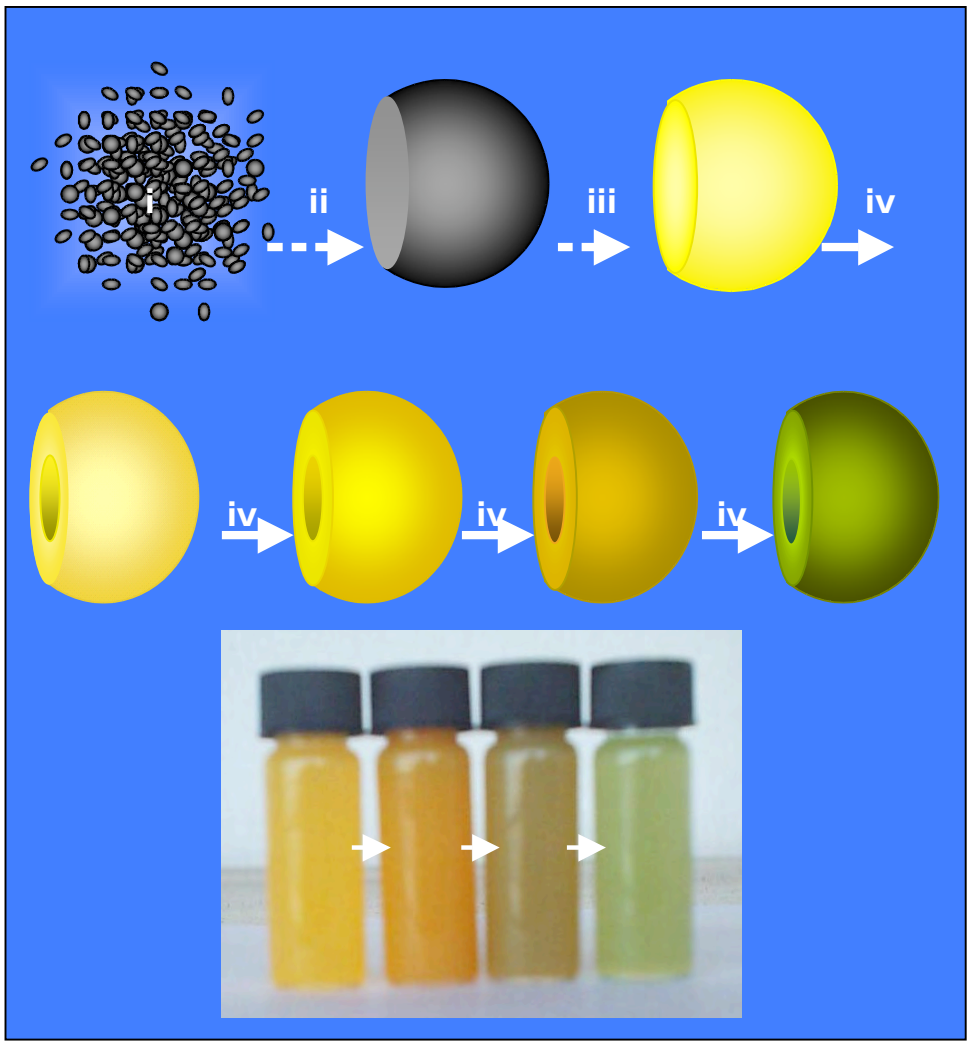

Figure 6.1 The synthetic flowchart developed in the present work: (i) formation of primary CuO nanocrystallites, (ii) spherical aggregation of CuO, (iii) reductive conversion of CuO to Cu_2O, and (iv) crystallite growth and cavity formation. Inset shows the color change of a series of hollow Cu_2O nanospheres formed from the experiments: 30 mL of $[Cu^{2+}]$ = 0.010 M at 180 ^{o}C for 4, 7, 10 and 14 h respectively.

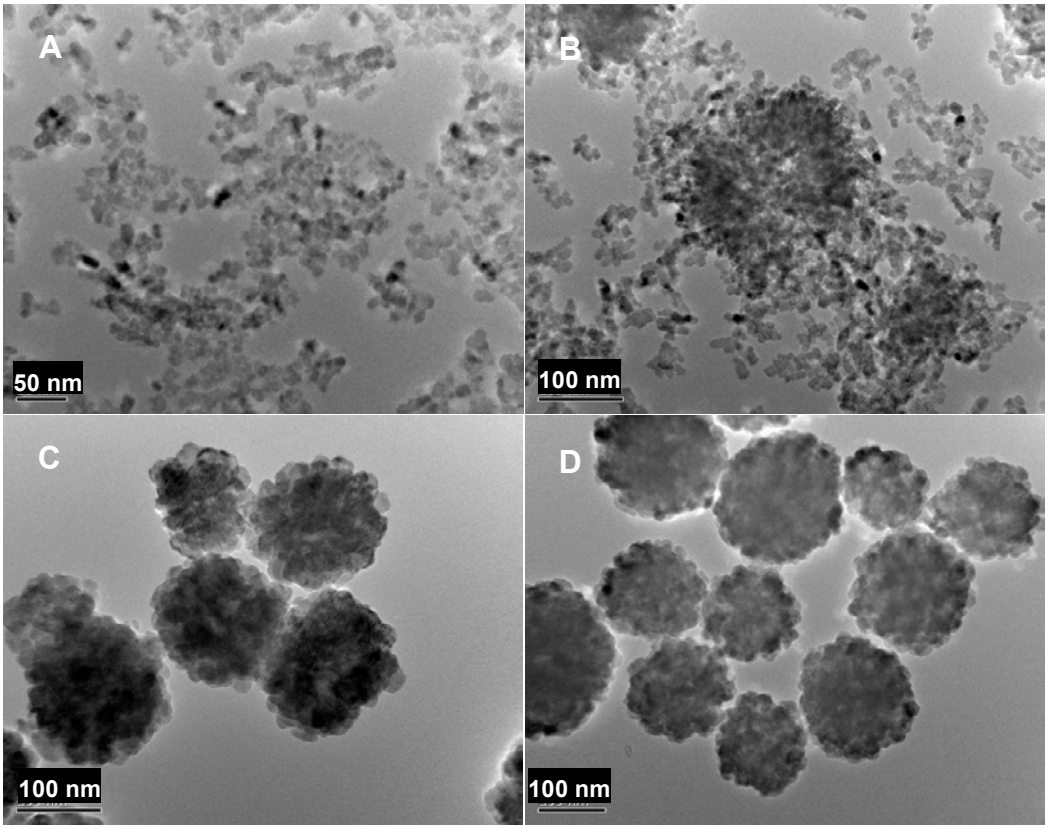

Figure 6.2 Formation of primary CuO nanocrystallites, spherical aggregation of CuO nanocrystallites, and chemical reduction of CuO to Cu_2O: TEM images of the samples prepared after different reactions times (A & B: 4 h; C: 14 h; and D: 23h) at 150 ^{o}C; Starting solution: $[Cu^{2+}]$ = 0.010 M, 30 mL.

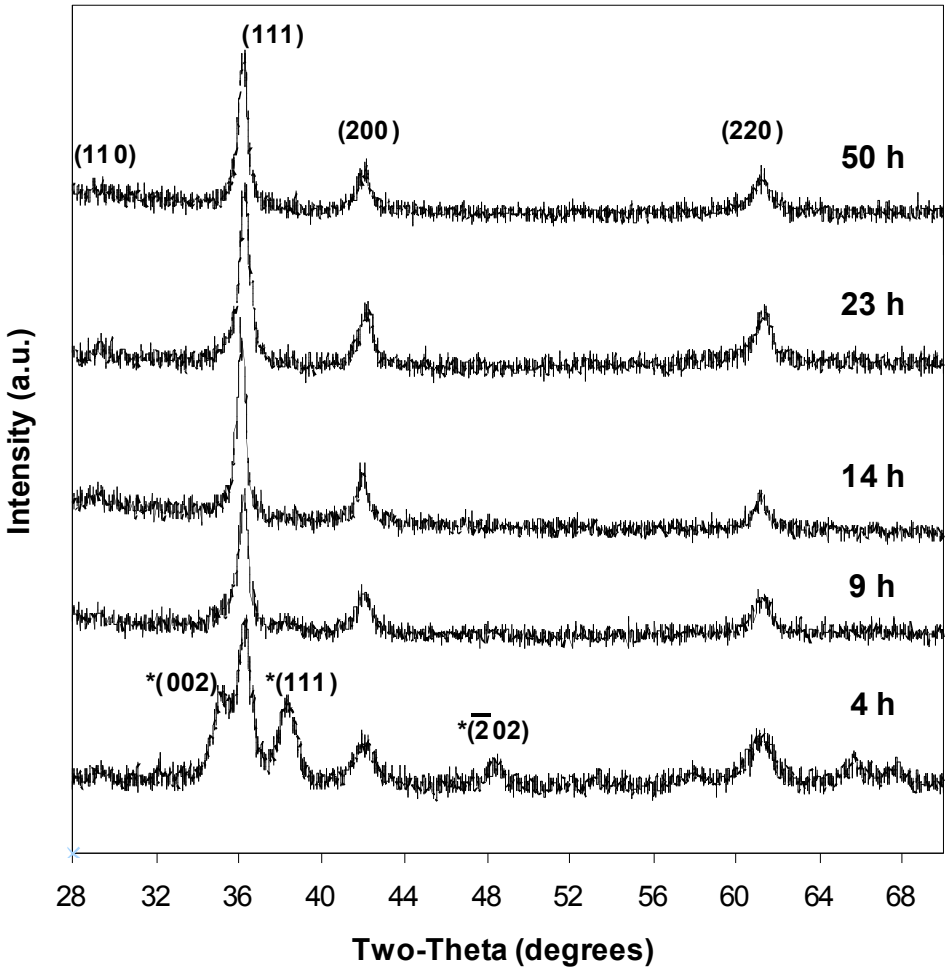

Figure 6.3 XRD patterns of samples synthesized after different reactions times (4 h to 50 h) at 150 ^{o}C: showing the phase transformation of CuO to Cu_2O at 150 ^{o}C. Starting solution: $[Cu^{2+}]$ = 0.010 M, 30 mL. Symbol * indicates the diffraction peaks from unconverted CuO phase.

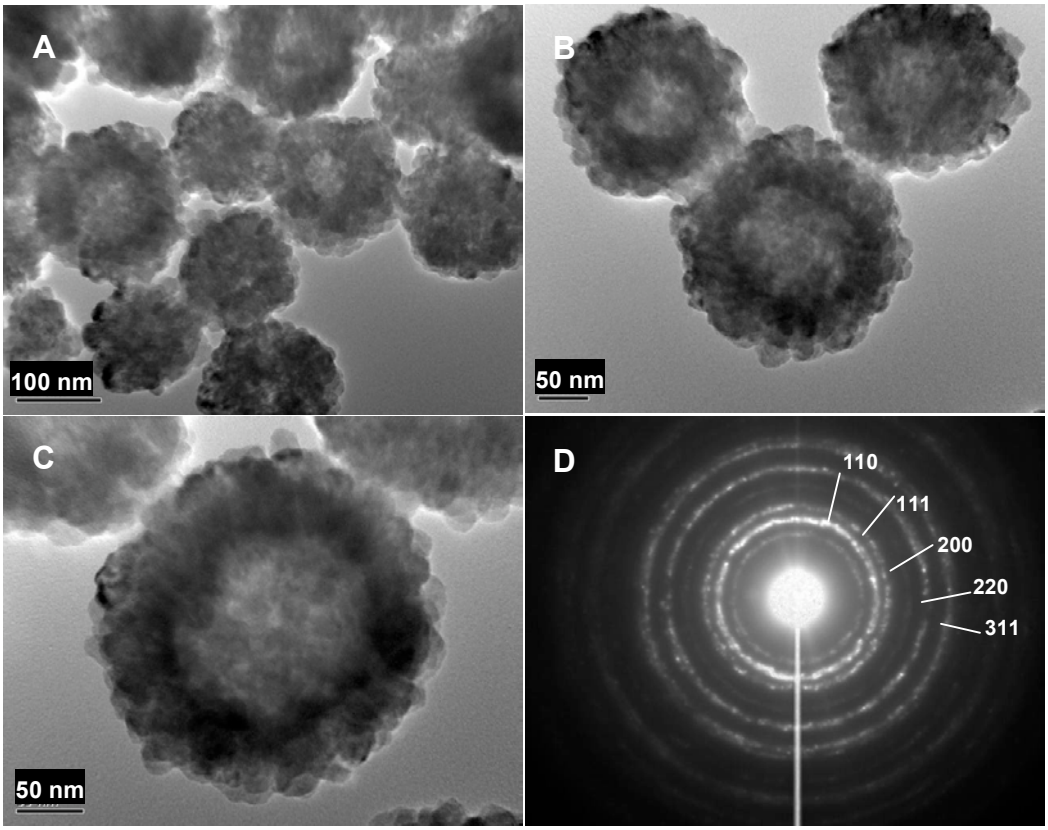

Figure 6.4 The core hollowing process in Cu_2O nanospheres: TEM images of the samples prepared after different reactions times at 150 ^oC (A & B: 35 h; C: 50 h; and D is the SAED pattern of the sphere shown in C); Starting solution: $[Cu^{2+}]$ = 0.010 M, 30 mL.

the formation of smaller crystallites is kinetically favored during the initial agglomeration, larger crystallites are thermodynamically favored (Ostwald, 1897). In Figure 6.4, indeed, the void space in the Cu_2O nanospheres is getting bigger with aging time. This is because the smallercrystallites located at central cores have higher surface energy and they tend to relocate themselves to the shell parts during the Ostwald ripening. On the basis of the above results, the process steps can be summarized: (i) formation of CuO nanocrystallites, (ii) spherical aggregation of primary CuO crystallites; (iii) reductive conversion of CuO nanospheres to Cu_2O; and (iv) crystal aging and evacuation of Cu_2O cores *via* Ostwald ripening.

Since no strong reducing agents were added in our starting solution, it is thought that DMF solvent has been working as a weak reducing agent in the synthesis; the chemical reactions are proposed as follows:

$$HCON(CH_3)_2 + H_2O \longrightarrow HCOOH + NH(CH_3)_2 \quad (6.1)$$

$$Cu^{2+} + H_2O + 2NH(CH_3)_2 \longrightarrow CuO_{(s)} + 2NH_2(CH_3)_2^{+} \quad (6.2)$$

$$2CuO_{(s)} + HCOOH \longrightarrow Cu_2O_{(s)} + H_2O + CO_2 \quad (6.3)$$

The formations of the solid phases in eqs (2) and (3) have been confirmed in the above XRD/SAED investigations. Apparently, the formic acid HCOOH in eq (1) is a reducing agent generated from hydrolysis of DMF (water molecules from $Cu(NO_3)_2 \cdot 3H_2O$, Experimental Section). As a simple confirmation for this reaction, it is noted that the starting copper solutions were indeed turned to basic and had a stink

odor of amines after hydrolysis of DMF (Liu[5] et al., 2003; Pastoriza-Santos and Liz-Marzán, 2000; Yu[2] et al., 1990).

The above chemical and physical processes can be accelerated when a higher process temperature is used. For example, the conversion of CuO to Cu_2O had been largely completed after 4 h of reactions at 160-170 ^oC (Figure 6.5-6.7). Based on our XRD results, it is noted that the sample synthesized at 180 ^oC for only 2 h has already been primarily in monovalent phase Cu_2O (Figure 6.8). When the reaction was prolonged to 3 h, t he remaining divalent phase was transformed almost completely to Cu_2O. When the reaction was continued for 20 h, however, a small amount of metallic copper appeared (Figure 6.8), indicating there was time limit to obtain phase-pure Cu_2O, which, interestingly, may also provide a way for fabricating Cu-Cu_2O composite nanospheres though this is not the prime effort of our present study.

The crystal morphologies of the above samples are further examined in Figure 6.9 (180 ^oC). In addition to the early phase conversion to Cu_2O, the core hollowing also takes place much faster (4 h, Figure 6.9), since the Ostwald ripening is more efficient at higher temperatures. In this regard, the phase conversion and core hollowing virtually proceed simultaneously at higher temperatures, and the process boundary between the phase conversion and core evacuation is no longer clear. In good agreement with the XRD findings, the shells of nanospheres indeed become thinner and less compact when some of the Cu_2O crystallites were reduced to metallic copper (20 h, Figure 6.9).

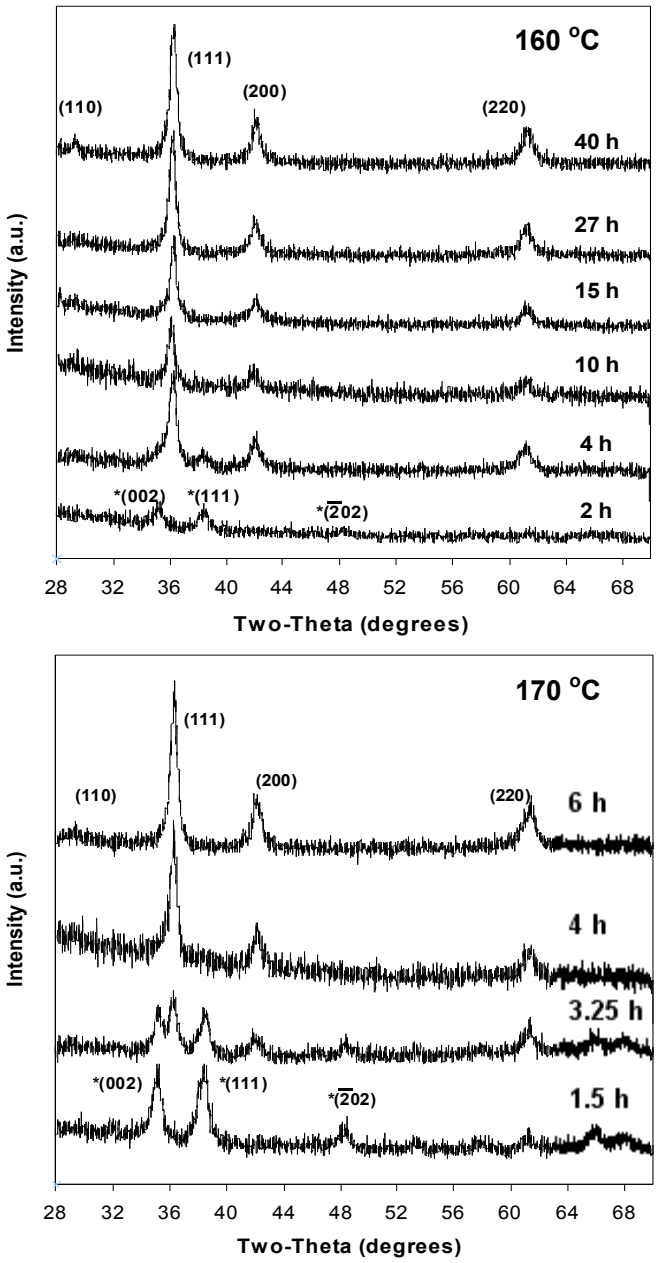

Figure 6.5 XRD patterns of samples synthesized after different reactions times at 160 ^{o}C and 170 ^{o}C: showing the phase transformation of CuO to Cu_2O at 160 ^{o}C and 170 ^{o}C. Starting solution: $[Cu^{2+}]$ = 0.010 M, 30 mL. Symbol * indicates the diffraction peaks from initial CuO phase.

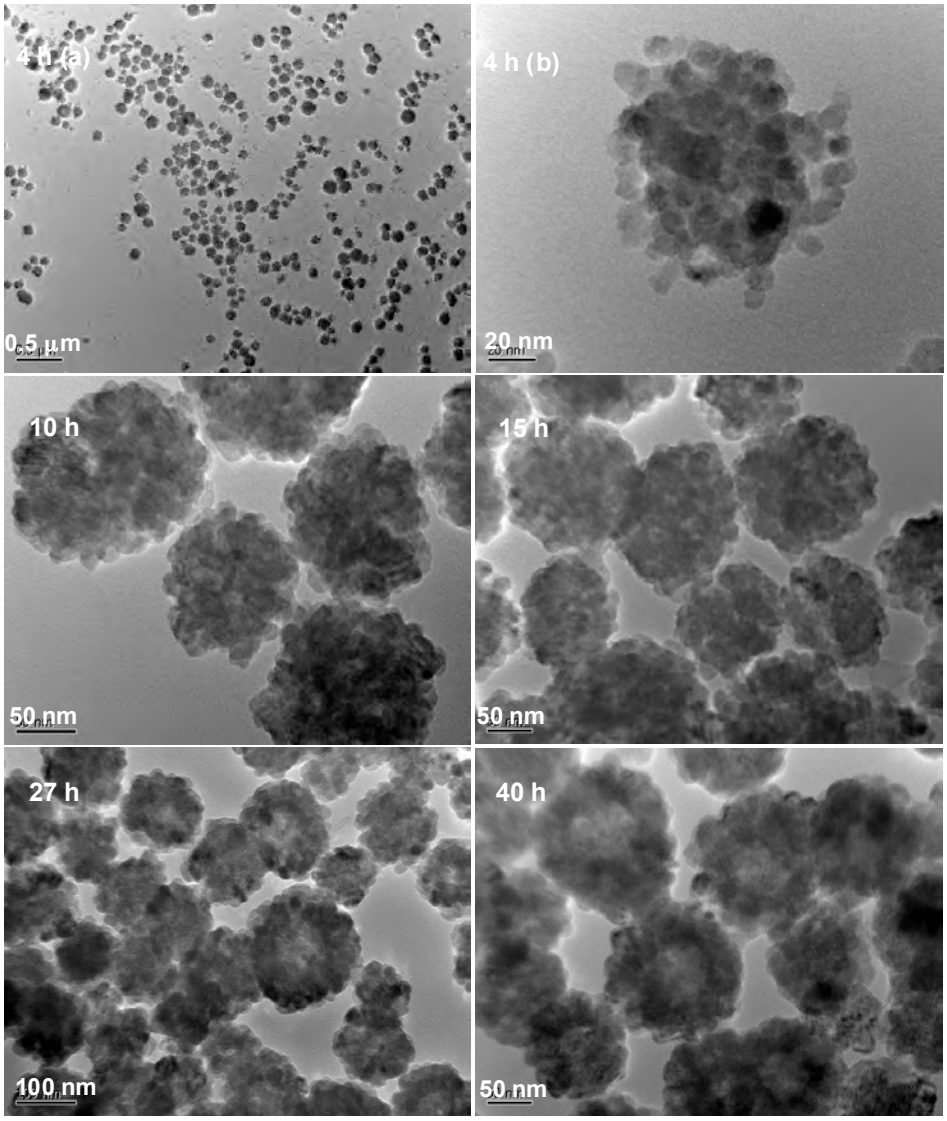

Figure 6.6 TEM images of the samples prepared after different reactions times (4 to 40 h) at 160 ^{o}C; Starting solution: [Cu^{2+}] = 0.010 M, 30 mL. 4 h (a) and (b): solid phases are Cu_2O (major) and CuO; 4 h (a): overall distribution of the aggregation; 4 h (b): an individual aggregate (one of those in 4 h (a)) which contains smaller crystallites. The images for 10 h, 15 h, 27 h and 40 h show the hollowing process of the Cu_2O nanospheres.

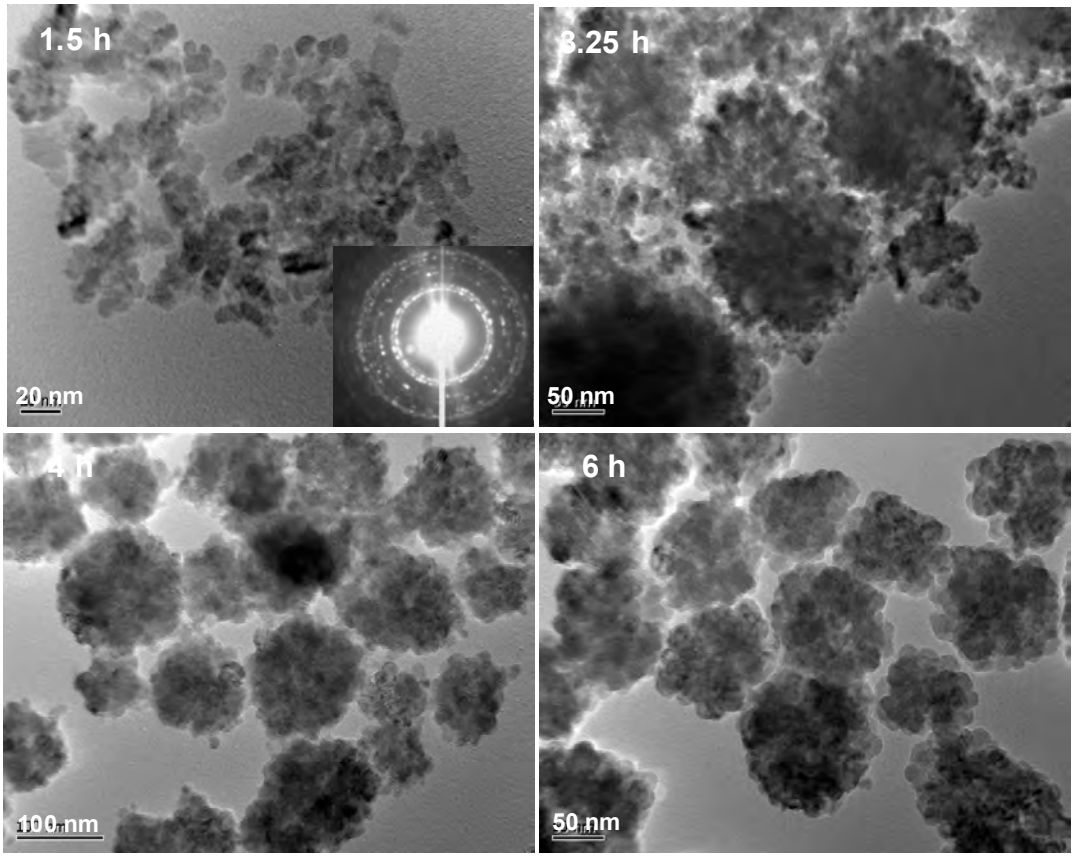

Figure 6.7 TEM images of the samples prepared after different reactions times (1.5 to 6 h) at 170 ^{o}C; Starting solution: [Cu^{2+}] = 0.010 M, 30 mL. Solid phase(s): CuO (1.5 h); Cu_2O + CuO (3.25 h); Cu_2O (4 h and 6 h). TEM image of 1.5 h: weakly aggregating CuO crystallites (inset: SAED pattern of the CuO crystallites). TEM images from 3.25 h to 6 h: showing an aggregation process for formation of solid Cu_2O nanospheres.

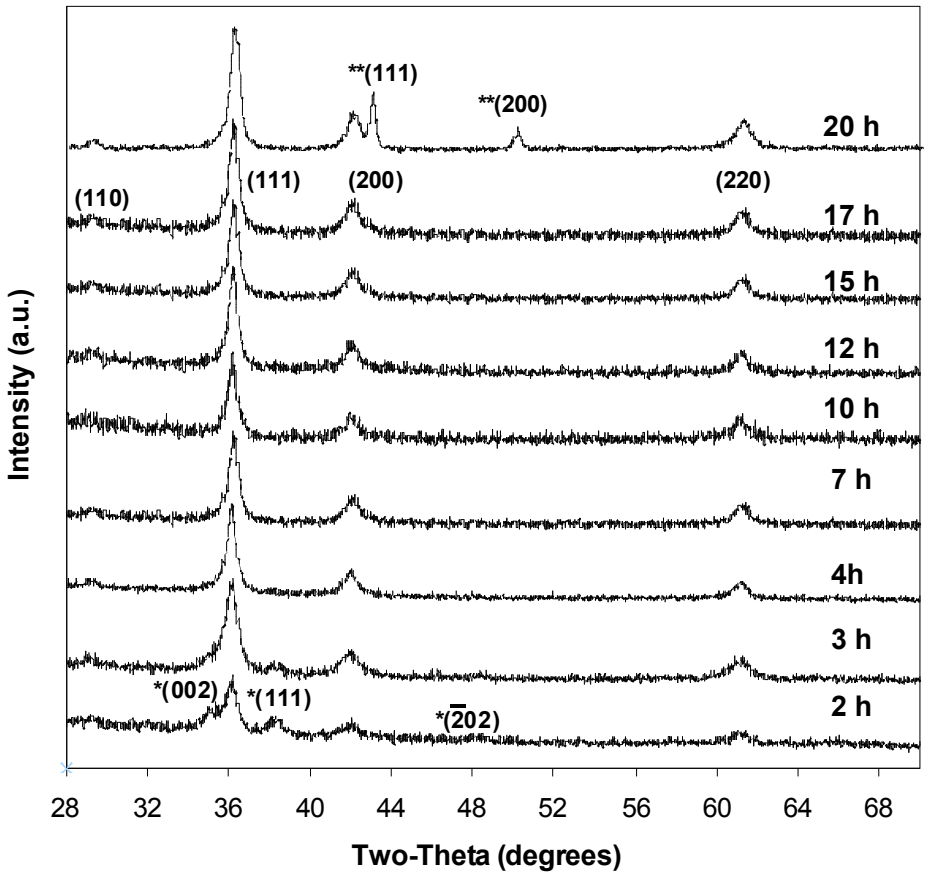

Figure 6.8 XRD patterns of samples synthesized after different reactions times at 180 ^{o}C: showing the phase transformation of CuO to Cu_2O at 180 ^{o}C. Starting solution: $[Cu^{2+}]$ = 0.010 M, 30 mL. Symbol * indicates the diffraction peaks from initial CuO phase, and symbol ** indicates the diffraction peaks from the metallic Cu phase formed during the final reduction.

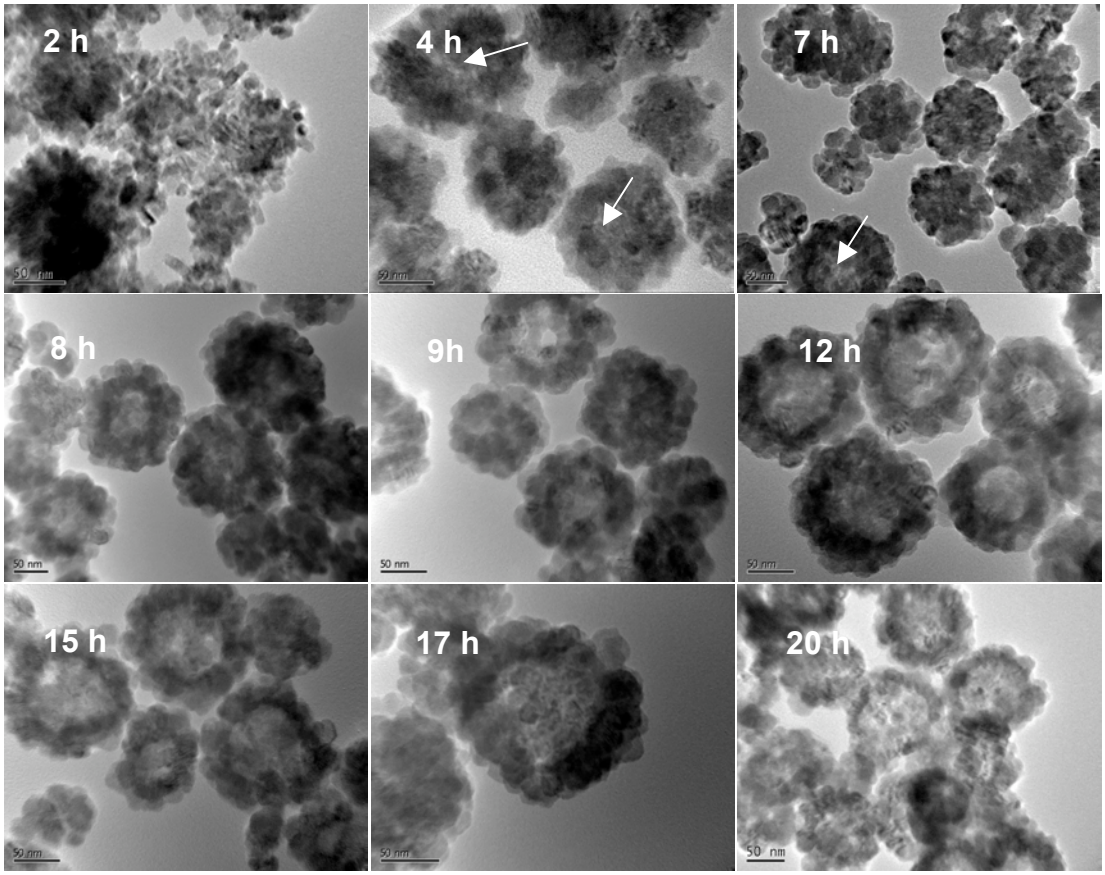

Figure 6.9 TEM images of the samples prepared after different reactions times (2 to 20 h) at 180 ^{o}C; Starting solution: [Cu^{2+}] = 0.010 M, 30 mL. White arrows indicate observable hollow spheres in some short reaction time cases (4 h and 7 h); all bar scales = 50 nm.

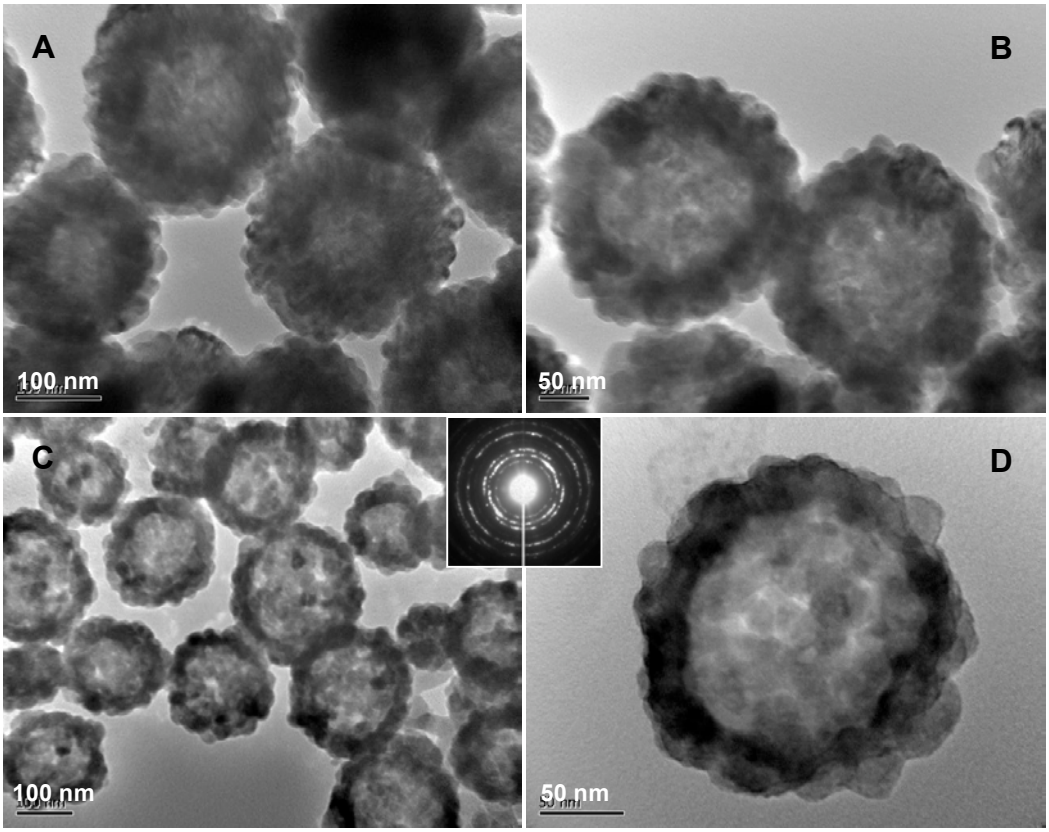

Figure 6.10 TEM images of the samples prepared with two-step heating routines (A: 150 °C for 22 h+180 °C for 8 h; B: 150 °C for 24 h+180 °C for 10 h; C & D: 150 °C for 26 h+180 °C for 42 h); Starting solution: $[Cu^{2+}]$ = 0.010 M, 30 mL. The inset is a SAED pattern (essentially Cu_2O type) from the spheres shown in C (Note: due to a prolonged reduction reaction in this synthesis, aggregated metallic copper was also detected in other parts sample (not shown) in addition to the Cu_2O hollow spheres).

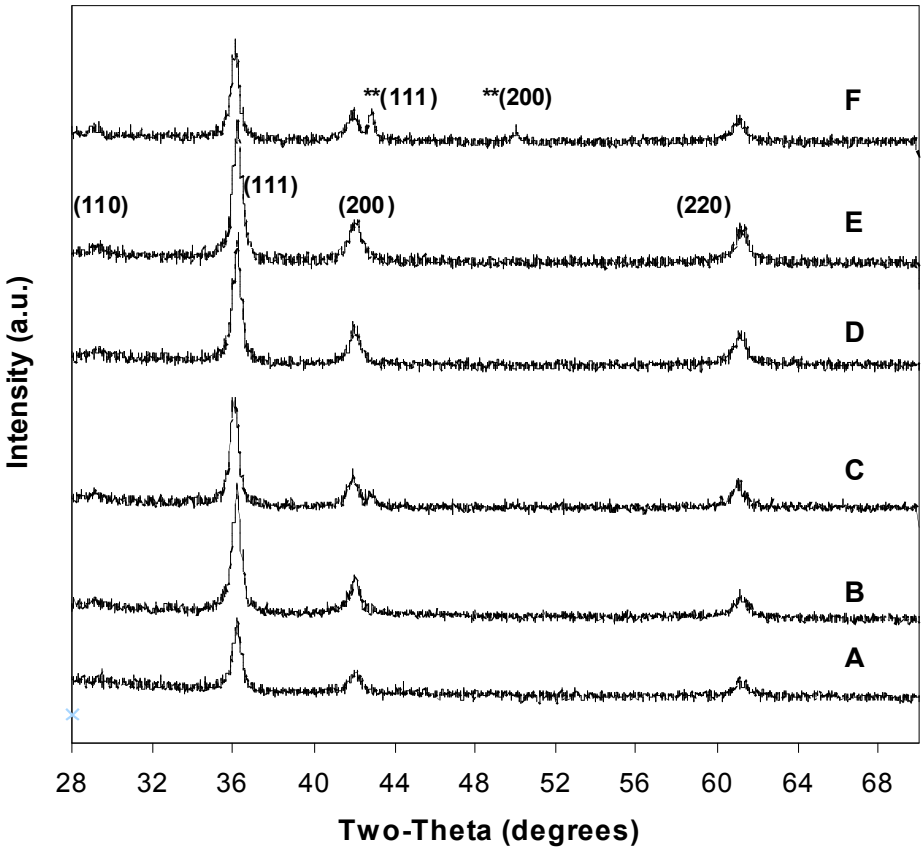

Figure 6.11 XRD patterns of hollow Cu_2O nanospheres synthesized with the two-step method: (A). 150 °C for 22 h + 180 °C for 8 h; (B). 150 °C for 22 h + 180 °C for 10 h; (C). 150 °C for 22 h + 180 °C for 11 h;. (D). 150 °C for 24 h + 180 °C for 8 h; (E). 150 °C for 24 h + 180 °C for 10 h; (F). 150 °C for 24 h + 180 °C for 11 h. Starting solution: $[Cu^{2+}]$ = 0.010 M, 30 mL. S symbol ** indicates the diffraction peaks from the metallic Cu phase formed during the final deep reduction.

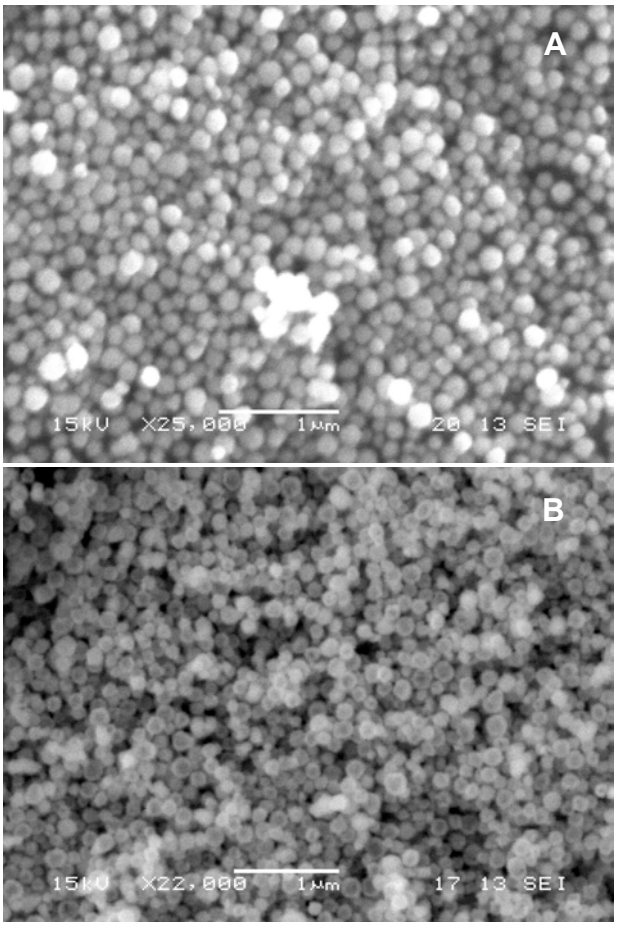

Figure 6.12 SEM images of the samples prepared with different reaction conditions (A: 150 °C for 50 h; B: 150 °C for 24 h+180 °C for 11 h); Starting solution: $[Cu^{2+}]$ = 0.010 M, 30 mL.

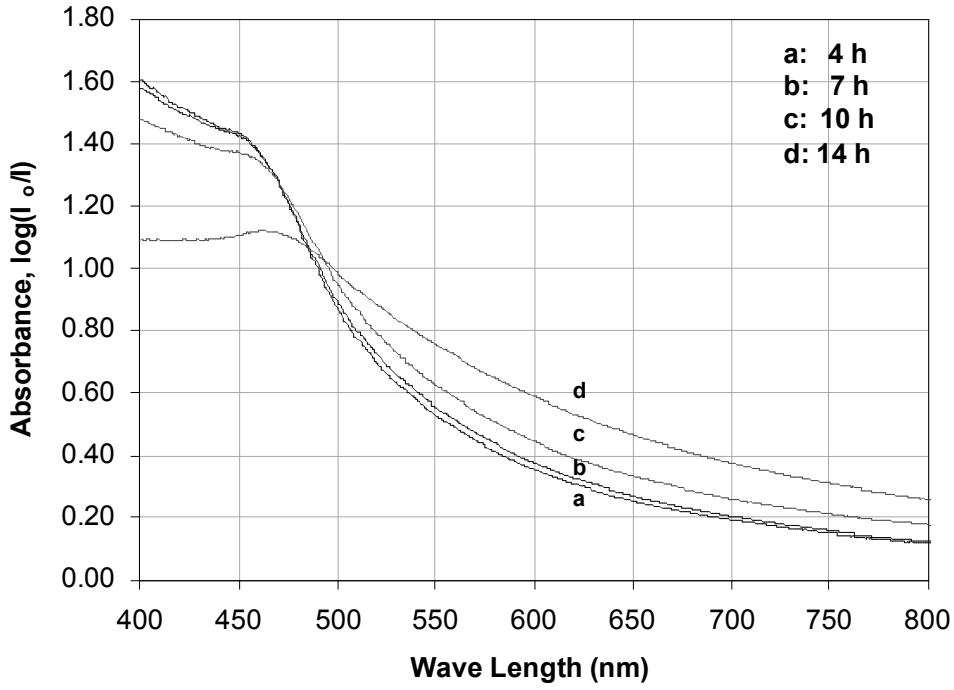

Figure 6.13 Representative UV-visible absorption spectra: measured for four Cu_2O samples synthesized at 180 ^oC for 4, 7, 10, and 14 h, respectively. Starting solution: $[Cu^{2+}]$ = 0.010 M, 30 mL.

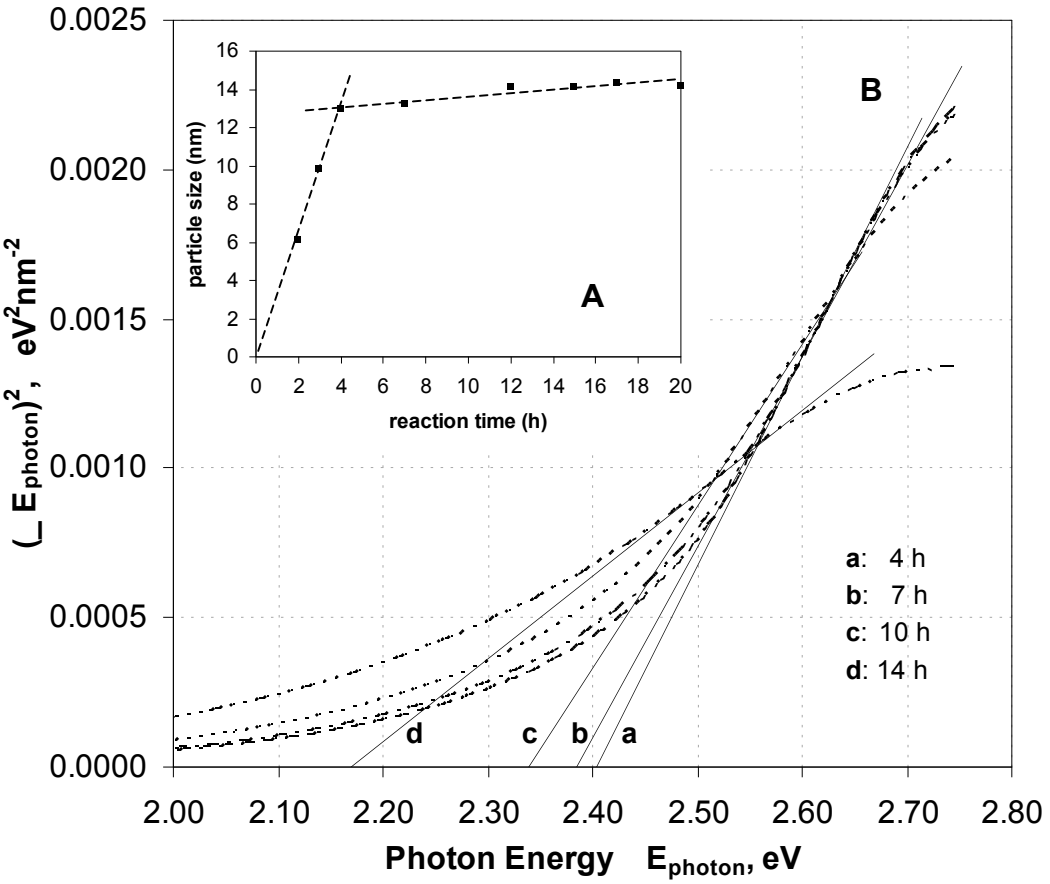

Figure 6.14 A: Deduced crystallite size from the Debye-Scherrer method (based on (111) reflection of Cu_2O phase; data from Figure 6.8). B: Representative plots of $(\alpha E_{ploton})^2$ versus E_{ploton} for the direct transition; band gap energies of hollow Cu_2O nanospheres obtained by extrapolation to $\alpha = 0$ (the samples were diluted in ethanol solvent in these measurements; see Figure 6.13). Except for variation in reaction time, other experimental parameters were kept identical for all these samples: $[Cu^{2+}] = 0.010$ M, 30 mL, and 180 ^{o}C.

Although the reaction rate and mass transfer rate are both increased at higher temperatures, it is found that the hollow nanospheres formed at 180 °C (Figure 6.9) are not as round as those prepared at 150 °C (Figure 6.4). To obtain a better shape control, a combined approach has been developed taking advantage of the temperature effect. This method is based on the following observations: (i) a low process temperature is suitable for forming symmetrical Cu_2O nanospheres (Figure 6.2); and (ii) a high process temperature is suitable for rapid core evacuation (Figure 6.9). Some hollow nanospheres prepared with this two-step method are presented in Figure 6.10 (also See Figure 6.11). It can be seen that the longer the cumulative time, the emptier the cores are [Figure 6.10A (22 h + 8 h) vs. Figure 6.10B (24 h + 10 h)]. It is clear that the samples synthesized are emptier than those synthesized at 150 °C (50 h, Figure 6.4C) while the time can be shortened significantly. With the present methods, high product uniformity and a 100% morphological yield can be attained early via controlling reaction time, even up to formation of the Cu-Cu_2O composites (outer diameters in 100-200 nm, SEM, Figure 6.12).

In parallel to the core hollowing, nanocrystallite size in shell structure can be further controlled and thus optical band gaps of Cu_2O hollow spheres can be fine-tuned. In order to examine this effect, the crystallite size upon aging time was further quantified with the Debye-Scherrer equation (Cheetham and Day, 1987). It should be mentioned that since relative intensities of XRD peaks for Cu_2O phase did not change in all our samples, data deduced with this method should be highly reliable. As shown

in Figure 6.14A, the Cu_2O crystallite growth rate rises sharply in the initial stage (2 h and 3 h). The rate then becomes much slower over the range of 4-20 h, but an increasing trend is definitely observable. To correlate crystallite size to the optical band gaps, UV-Visible absorption spectra of the hollow Cu_2O nanospheres prepared with different reaction times were measured (Figure 6.13), and a classical Tauc-approach was employed to estimate their optical energy band gaps (Tsunekawa et al., 2000). It has been found that the $n = {}^1/_2$ (allowed direct transition) gives the best description for all absorption measurements. Figure 6.14B shows four representative plots of $(\alpha E_{photon})^2$ versus E_{photon} based on the direct transition. The extrapolated value (the straight lines to the x-axis) of E_{photon} at $\alpha = 0$ gives an absorption edge energy corresponding to E_g = 2.405 eV (4 h), 2.385 eV (7 h), 2.340 eV (10h), and 2.170 eV (14 h) respectively. When the reaction time is 14 h, the optical band gap obtained herein is essentially equal to that of the natural single crystal Cu_2O reported in literature (2.1722 eV) (Matsumoto et al., 1996). The quantum confinement threshold of Cu_2O nanocrystallites is therefore ca 14 nm (14 h, Figure 6.14A) in these nanospheres. In excellent agreement with the above band gap measurements, the colloidal solutions of these Cu_2O nanospheres show a series of color changes upon the process time of the present approach (inset, Figure 6.1). The observed color varies from bright yellow to orange, brown, and green, when the size of Cu_2O crystallites was gradually increased along the simultaneous hollowing process.

6.4 Conclusion

In summary, a new chemical approach has been devised to fabricate cuprous oxide Cu_2O hollow nanospheres without the assistance of solid template. Based on the growth experiments and materials characterization, it is understood that the formation mechanism comprises four different steps: (i) generation of primary nanocrystallites of CuO; (ii) spherical gathering of the primary CuO; (iii)reductive conversion of CuO to Cu_2O; and (iv) crystal aging of Cu_2O and formation of hollow nanospheres. In the final step (iv), Ostwald ripening has been utilized in controlling crystallite size of shell structures, and thus for effective tuning the optical band gap energy of Cu_2O (in the range of 2.405-2.170 eV). Considering their unique hollow structure and facile tuning in band gap energy, the prepared Cu_2O nanospheres can be potentially used for harvesting solar energy in the visible range. The solid-solution redox reactions devised in this chapter may also be extendable to future fabrication of Cu-Cu_2O nanocomposites.

CHAPTER 7

FABRICATIONS OF HOLLOW NANOCUBES OF Cu_2O AND Cu *VIA* REDUCTIVE SELF-ASSEMBLY OF CuO NANOCRYSTALS

7.1 Introduction

Two novel methods had recently been developed for fabrications of nanostructures with interior voids. The first method, illustrated in Figure 7.1a, relies on a three-dimensional (3D) aggregation of primary nanocrystallites, followed by a solid evacuation through Ostwald ripening (Yang[1] and Zeng, 2004(b)). The second method (Figure 7.1b), in which tiny nanocrystallites are gathered two-dimensionally (2D) fulfilling certain crystallographic requirements (i.e., oriented attachment), provides a direct means for construction of hollow structures through a *plane-by-plane* mechanism (Yang[1] and Zeng, 2004(c)). In Chapter 6, the Cu_2O hollow spheres have been fabricated with the first method (Figure 7.1a and Figure 6.1).

In this chapter, we fabricated Cu_2O hollow nanocubes with the third method (depicted in Figure 7.1c). As a first reported case, the present synthetic method is virtually a combination of both "oriented attachment" and "Ostwald ripening" processes. In the first stage, nanocrystallites undergo oriented attachment to form a well-defined geometrical structure (e.g., cube). In the second stage, solid evacuation

takes place in the central part of the shape-defined aggregate *via Ostwald ripening*, resulting in single-crystal hollow nanocubes. Although the syntheses of single-crystal hollow nanocubes of Cu_2O have been reported (Gou and Murphy, 2003; Wang[12] et al., 2004), the hollowing mechanism of Cu_2O has so for remained unknown. With this new fabrication of Cu_2O hollow nanocubes (Figure 7.1c), we are able to explain for the first time the formation mechanism.

7.2 Experimental section

7.2.1 Materials preparation In a typical experiment, 30 mL of 0.005-0.010 M $Cu(NO_3)_2{\cdot}3H_2O$ solution [a certain quantity of $Cu(NO_3)_2{\cdot}3H_2O$ was dissolved in organic solvent DMF to make a stated concentration] and 0.10-0.60 mL of deionized water were mixed and sealed in a Teflon-lined stainless steel autoclave with 50 mL capacity and then heated at different temperatures (150, 160, 170, 180, 190, 200, and 210 ^oC) for different reaction times to form Cu_2O nanoproducts. In some experiments, 0.004-0.020 g $NaNO_3$ was also added in the solution to adjust the morphology of Cu_2O nanoproducts. Table 7.1 shows the detailed experimental parameters. In addition to using the DMF-water, Cu_2O nanocubes were also synthesized with a Cu^{2+} solution in DMF-ethanol cosolvent. Briefly, 30.0 mL of 0.005 or 0.010 M $Cu(NO_3)_2{\cdot}3H_2O$ in a DMF and ethanol mixed solvent [The volume ratio DMF to ethanol was changed from 29:1 to 4:26, note that there was a small amount of water inherited from the starting $Cu(NO_3)_2{\cdot}3H_2O$ salt; shown in Table 7.2] were sealed in the above autoclave and then heated at 160 and 180 ^oC in order to produce Cu_2O. In some experiments, $NaNO_3$ salt (mostly 0.01 g) was also added as a mineralizer. In a two-step synthesis of Cu nanocubes, the autoclave was firstly heated at 180 ^oC for 6 h, and consecutively heated at 200 ^oC for 1-2 h, as detailed in Table 7.2.

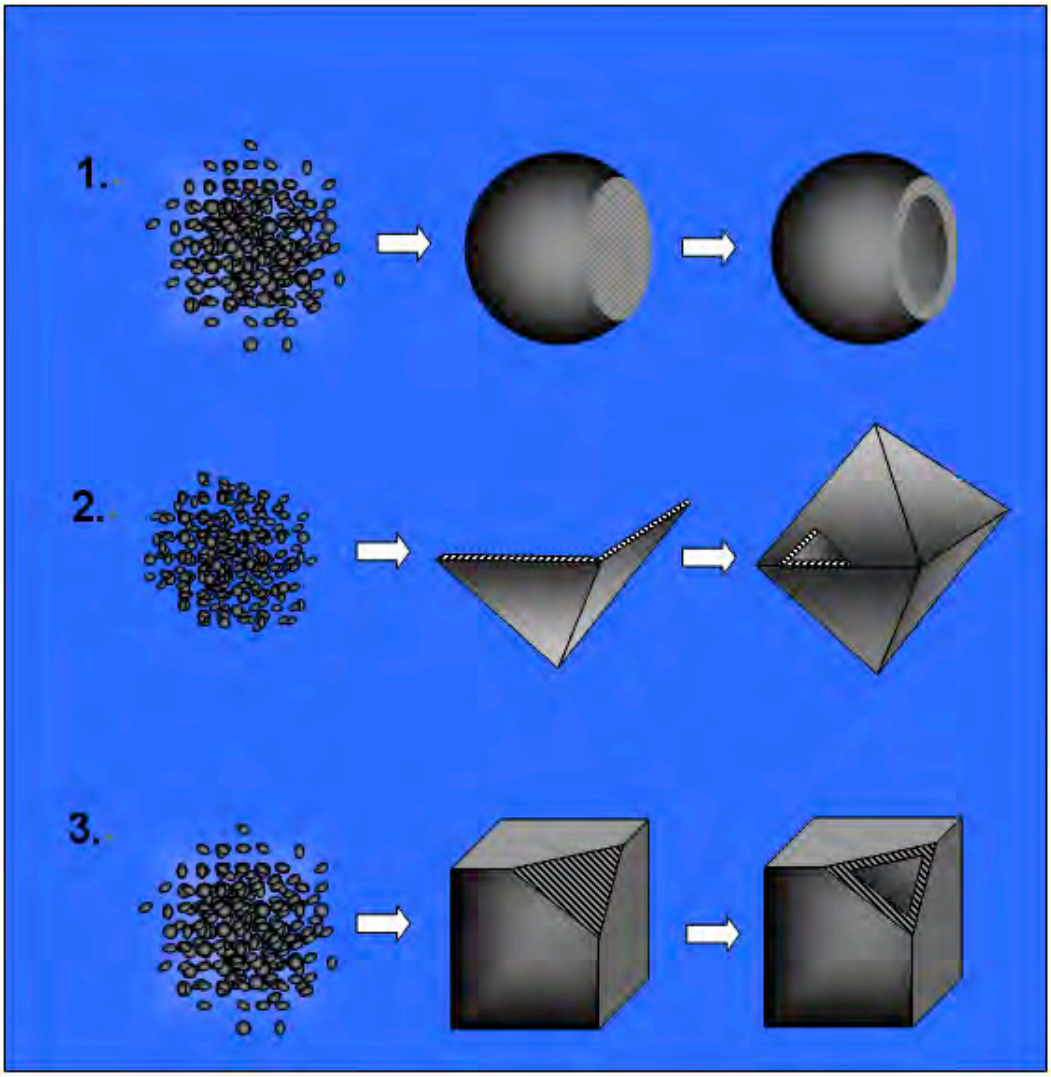

Figure 7.1 Three different types of synthetic methods for generation of hollow nanostructures: (1) random aggregation of nanocrystallites and core hollowing via Ostwald ripening, resulting in polycrystalline nanospheres; (2) two-dimensional oriented attachment for formation of thin crystal planes and constructuion of hollow octahedra in a plane-by-plane manner; and (3) three-dimensional oriented attachment for solid nanocubes and creation of hollow interiors by Ostwald ripening. Hashed areas indicate the solid parts of nanostructures.

Table 7. 1 A list of experiments conducted in the DMF-water cosolvent.

Expt. No.	Cu^{2+} (mol/L)	H_2O (mL)	$NaNO_3$ (g)	Temp.(^oC)	Time (h)
1	0.01	0.3	0.008	190	10
2	0.01	0.3	0.02	190	10
3	0.01	0.3	0.1	190	10
4	0.01	0.3	0.004	150	40
5	0.01	0.3	0.01	150	40
6	0.01	0.3	0.02	150	40
7	0.005	0.3	0.01	160	48
8	0.005	0.3		170	26
9	0.005	0.3	0.01	170	26
10	0.005	0.5		170	26
11	0.005	0.5	0.01	170	26
12	0.005	0.5	0.02	170	26
13	0.005	0.3		180	15
14	0.005	0.3	0.01	180	15
15	0.005	0.4		180	15
16	0.005	0.4	0.01	180	15
17	0.005	0.5		180	15
18	0.005	0.5	0.01	180	15
19	0.005	0.4		190	11
20	0.005	0.5		190	11
21	0.005	0.6		190	11
22	0.005	0.4		200	6.5
23	0.005	0.5		200	6.5
24	0.005	0.6		200	6.5
25	0.005	0.4		210	5.5
26	0.005	0.5		210	5.5
27	0.005	0.6		210	5.5
28	0.005	0.4		210+180	2.5+10
29	0.004	0.1		210	5.5
30	0.004	0.2		210	5.5
31	0.004	0.3		210	5.5
32	0.003	0.1		210	5.5
33	0.003	0.2		210	5.5
34	0.003	0.3		210	5.5
35	0.003	0.4		210	5.5
36	0.003	0.5		210	5.5
37	0.003	0.6		210	5.5
38	0.005	0.5		200	1.5
39	0.005	0.5		200	2
40	0.005	0.5		200	2.5
41	0.005	0.5		200	3
42	0.005	0.5		200	3.5
43	0.005	0.5		200	4.5
44	0.005	0.5		200	5.5
45	0.005	0.5		200	7

Table 7.2 A list of experiments conducted in DMF-ethanol cosolvent.

Expt. No	DMF:Ethanol (mL)	Molar ratio DMF:Ethanol	Cu^{2+} (mol/L)	$NaNO_3$ (g)	Temp.(^oC)	Time (h)
1	29:1	21.87:1	0.005		160	16
2			0.005		180	4
3			0.005		180	7
4	27:3	6.79:1	0.01		160	16
5			0.005		160	16
6			0.005		180	4
7			0.005		180	7
8			0.005		180	10
9			0.005		180	20
10	26:4	4.90:1	0.005		180	10
11			0.005		180	20
12	24:6	3.01:1	0.01		160	16
13			0.01		180	4
14			0.005		180	7
15			0.005		180	10
16			0.005	0.01	180	7
17	20:10	1.51:1	0.01		160	16
18			0.01		180	4
19			0.005		160	16
20			0.005		180	4
21			0.005		180	7
22			0.005	0.01	180	7
23			0.005	0.01	180	10
24	15:15	1:1.33	0.01		180	4
25			0.005		160	16
26			0.005		180	4
27			0.005		180	7
28			0.005		180	10
29			0.005		180	20
30	10:20	1:2.65	0.01		180	4
31			0.005		160	16
32			0.005		180	2
33			0.005		180	3
34			0.005		180	4
35			0.005		180	6
36			0.005		180	10
37			0.005		180	20
38			0.005		180 ^oC 6 h + 200 ^oC 1 h	
39			0.005		180 ^oC 6 h + 200 ^oC 1.5 h	
41			0.005		180 ^oC 6 h + 200 ^oC 2 h	
42	4:26	1:8.62	0.01		180	4
43			0.005		160	18
44			0.005		180	4
45			0.005		180	6
46	30:3	7.54:1	0.01		160	36
47			0.01		160	48
48			0.01		180	5

7.2.2 Materials characterization The crystallographic information of the samples was investigated by powder XRD (Shimadzu, model XRD-6000, Cu K_α radiation λ = 1.5406 Å). Morphological investigation was carried out with TEM/SAED (Joel model JEM-2010, 200 kV; and HRTEM, Philips FEI Tecnai-G^2, 200kV), SEM (Joel model JSM-5600LV), FESEM/EDX (Joel model JSM-6700LV). Surface analysis for the samples was performed using XPS (also used for Auger electron spectroscopy (AES) measurement), Kratos Analytical model AXIS-Hsi] with a monochromated Al Kα X-ray source (1486.6 eV).

7.3 Results and Discussion

7.3.1 Composition and morphology of products

A series of experiments was first carried out to narrow down some synthetic parameters for hollow-cube formation (Table 7.1). The crystal structure of all prepared products was investigated with XRD method (Figure 7.2). All recorded XRD peaks can be assigned to the cubic symmetry of Cu_2O ($Pn\bar{3}m$: a_o = 4.26 Å; JCPDS no. 03-0892), Confirming that all the products are phase-pure Cu_2O. The composition of the prepared Cu_2O products was also checked with EDX technique, which shows that the atomic ratio of Cu to O is indeed close to 2:1 (e.g., 65.7:30.0, Figure 7.3) in our Cu_2O samples.

In the present synthesis, hollow nanocubes of Cu_2O were formed with the addition of suitable amount of water in DMF solution; what is a key to the cubic morphology. Figure 7.4 shows the morphology of prepared Cu_2O hollow cubes at 200 ^oC for 6.5 h, with 0.50 mL deionized water in 30 mL of 0.005 M Cu^{2+} DMF solution

(Exp. 23, Table 7.1). It is observed that the Cu_2O products formed are of cubic structures (FESEM images: Figure 7.4A, B), and there is a void space in the center of each cube (TEM images: Figure 7.4C, D). The measured size distribution of the hollow cubes in Figure 7.4C, D is about 200 ± 30 nm, indicating that the hollow cubes are monodispersed in size. Quite interestingly, surfaces of these hollow cubes are not particularly smooth, suggesting that they might be made from an aggregation of smaller particles which will be addressed shortly. Apart from the TEM investigation, the hollow interior is also confirmed with FESEM method. For instance, one small pinhole or two through central space can be easily observed on the edges or corners of these nanocubes (Figure 7.5), although the inner void of hollow cubes is sealed rather completely. These pinholes may serve exchange channels for chemical constituents inside and outside the cubes when employing them as nanoreactors. Depending on the synthetic parameters, furthermore, hollow nanocubes with edge lengths smaller than 100 nm can also be prepared with the present method (Figure 7.4E,F).

The crystal orientation and crystallinity of Cu_2O hollow cubes were further studied with HRTEM/SAED method. Figure 7.6B shows an electron diffraction pattern of a Cu_2O hollow cube (Figure 7.6A). In the measurement, the electron-beam was injected along the [001] direction and the spot array has a four-fold symmetry that can be indexed with *hk0* (i.e., [001] zone spots, in accordance to the extinction rule of electron diffraction of space group *Pn3m*). As indicated by the clear diffraction spots, all the hollow cubes are nearly single-crystalline, and bounded with six crystal planes {100}, {010} and {001}. Figure 7.6C shows the HRTEM image of the edge area of such a hollow cubes. The crystallinity within a crystallite block is high, although there are intercrystallite mismatches (e.g., splitting of spots, Figure 7.6B). The lattice fringe

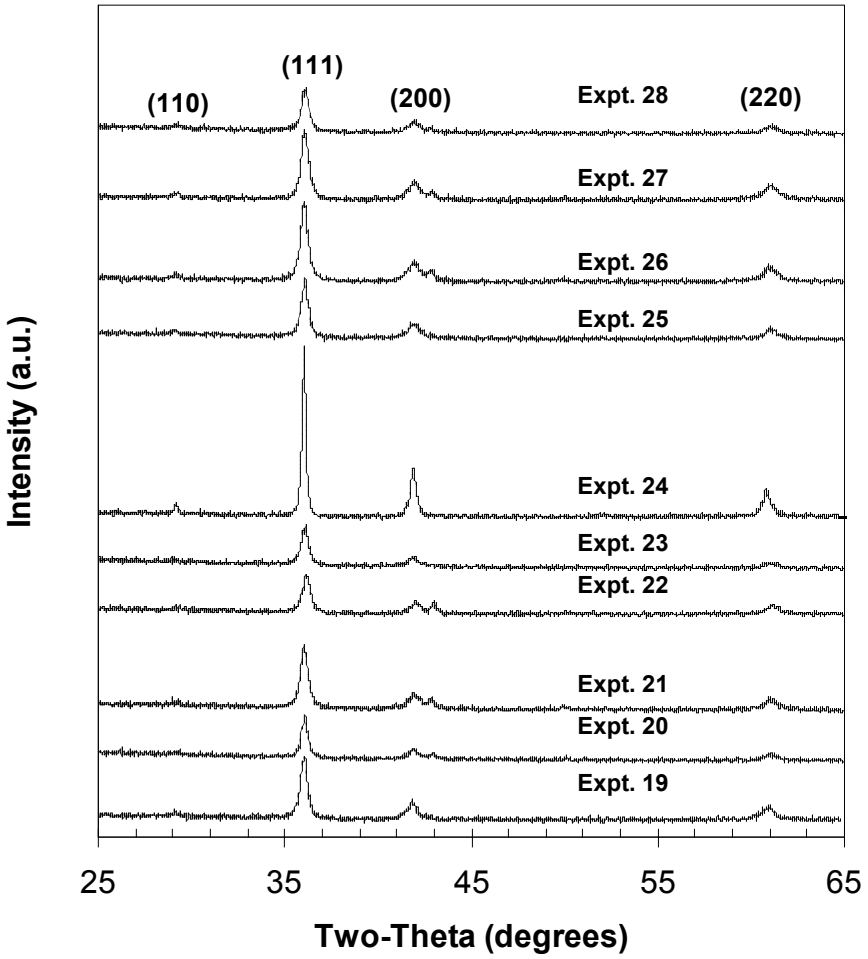

Figure 7.2 Representive powder XRD patterns of some selected Cu_2O nanoproducts (Expt. 19-28, Table 7.1).

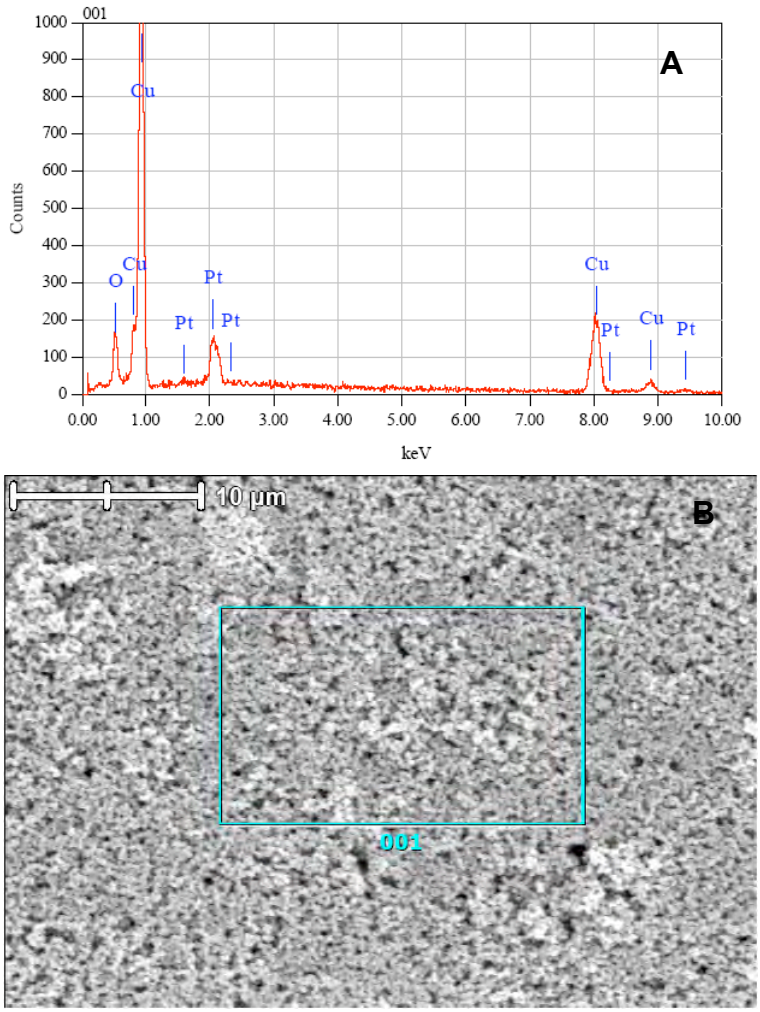

C. EDX analysis result of Cu_2O hollow cubes (Expt. 20, Table 7.1)

Element	(keV)	Mass %	Error %	Atom %
O K	0.525	8.61	0.12	29.8
Cu K	8.040	75.44	0.91	65.7
Pt M	2.048	15.95	0.43	4.5
Total		100.00		100.00

Figure 7.3 (A) the EDX Spectrum and (B) FESEM image of sample prepared at 190 ^{o}C for 11 h with 0.5 ml of water in solution (Expt. 20, Table 7.1); (C) the EDX analysis result of above-mentioned sample.

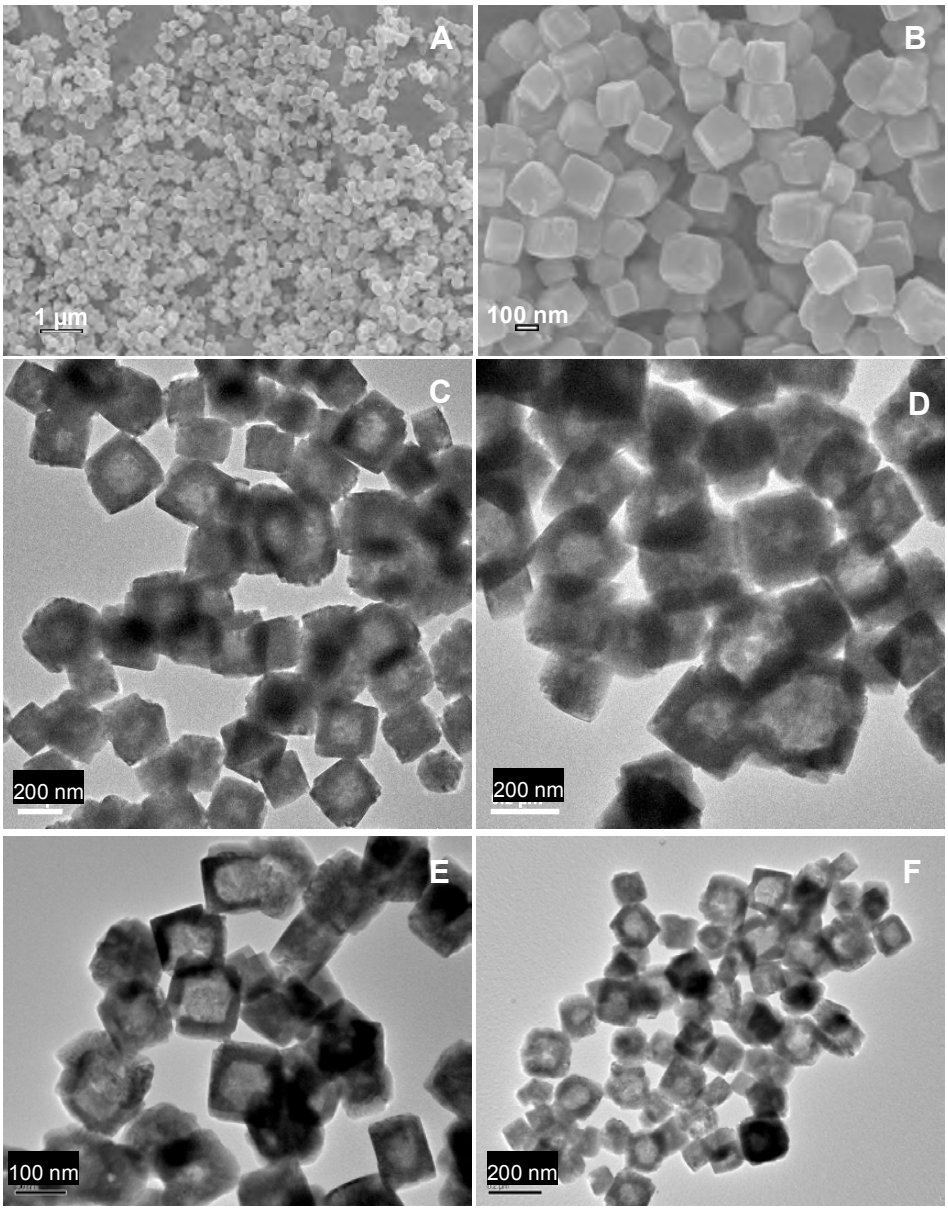

Figure 7.4 FESEM images (A and B) and TEM images of as-prepared Cu_2O hollow Cubes; experimental condition: 30 mL of [Cu^{2+}] (0.005 M in DMF) + 0.50 mL of H_2O at 180 ^oC for 15 h (Expt. 17, Table 7.1). TEM images (E and F) of smaller Cu_2O hollow nanocubes; experimental condition: 30 mL of [Cu^{2+}] (0.005 M in DMF) + 0.40 mL of H_2O at 180 ^oC for 15 h (Expt. 15, Table 7.1).

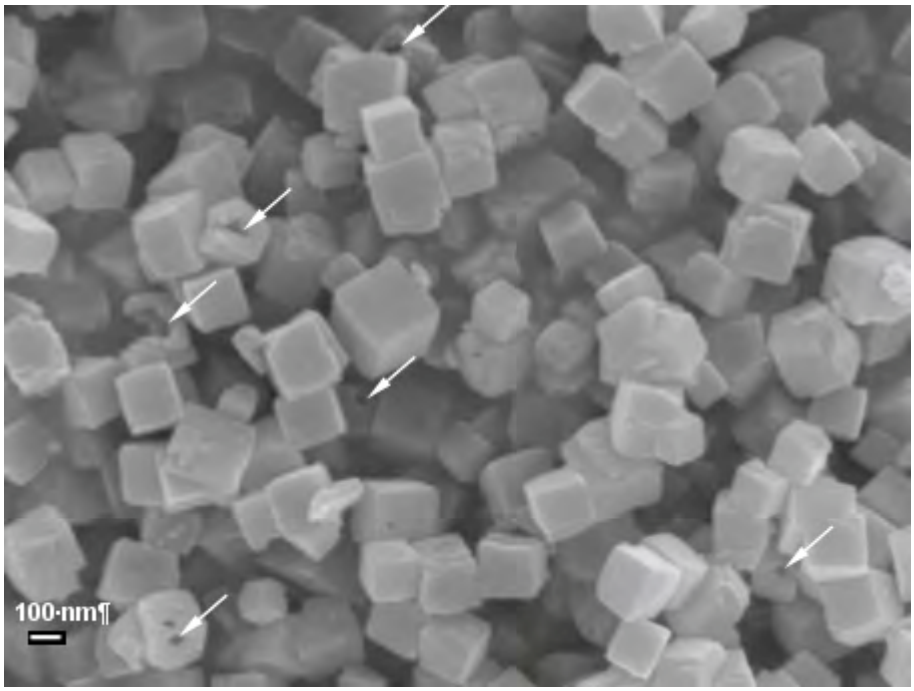

Figure 7.5 FESEM images of Cu_2O hollow Cubes prepared at 190 ^oC for 11 h with 0.5 ml of water in solution (Expt. 20, Table 7.1). Some arrows show the pinholes of hollow cubes.

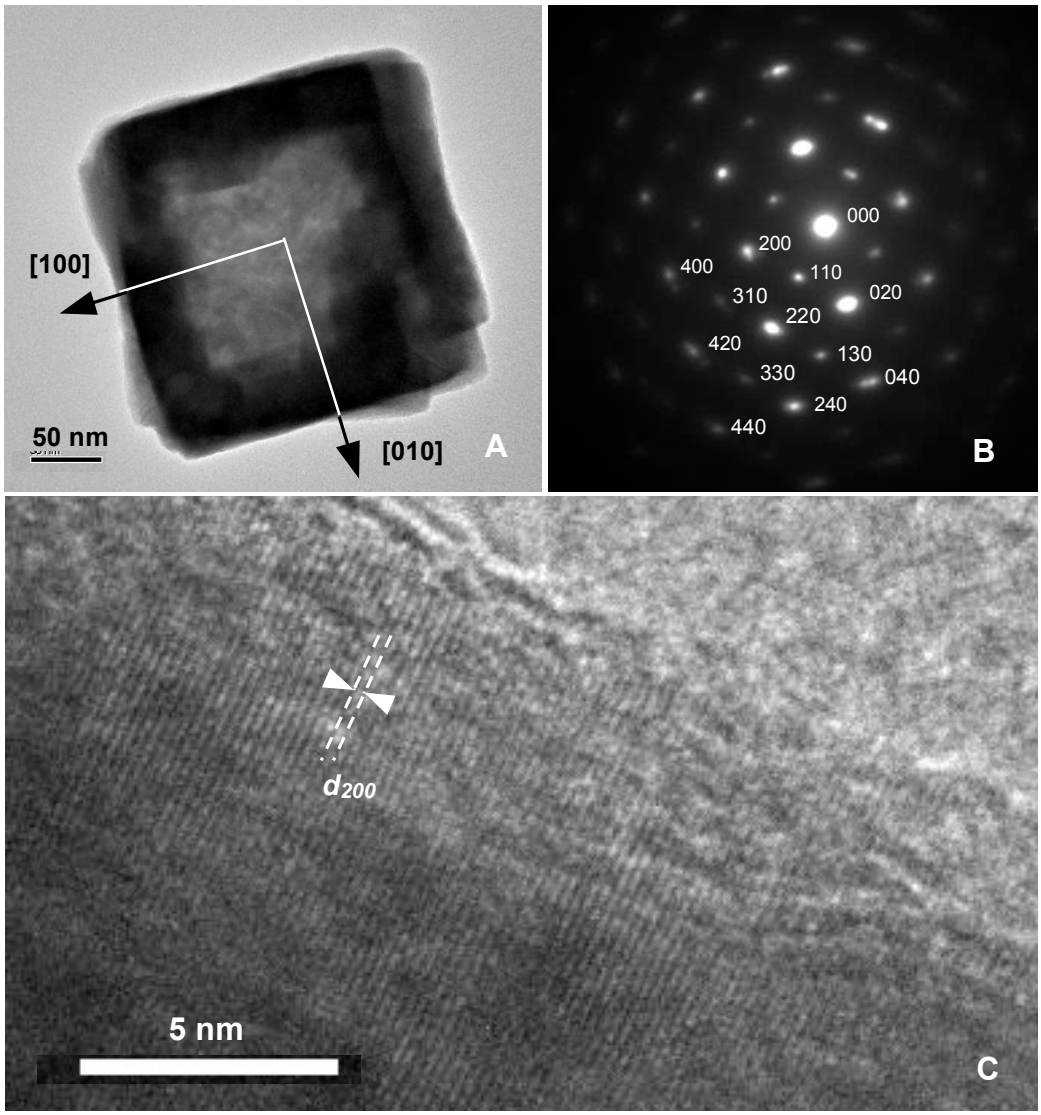

Figure 7.6 (A and B) TEM image of a Cu_2O hollow Cube and its SAED pattern. Experimental condition: 30.0 mL of [Cu^{2+}] (0.005 M in DMF) + 0.50 mL of H_2O at 180 ^oC for 15 h (Expt. 17, Table 7.1). (C), HRTEM image of a Cu_2O hollow Cube. Experimental condition: 30.0 mL of [Cu^{2+}] (0.005 M in DMF) + 0.50 mL of H_2O at 200 ^oC for 6.5 h (Expt. 23, Table 7.1).

of d_{200} is about 2.13 Å, which is in good agreement with 2.12 and 2.14 Å reported in literature (JCPDS files of 03-0892 and 34-1354).

7.3.2 Growth process of Cu_2O hollow cubes

The growth process of Cu_2O hollow cubes was investigated in detail at different reaction times and temperatures (Table 7.1). Figure 7.7 displays a series of evolutional XRD patterns of the samples investigated. The solid products formed after 1.5-2.0 h of reactions are phase-pure CuO. With a longer reaction time of 2.5-3.0 h, the product becomes a mixture of CuO and Cu_2O. This mixture is then converted into phase-pure Cu_2O over a reaction time range of 3.5-6.5 h. However, when the time exceeds 7.0 h, metallic copper (Cu^0) appears in the product as a secondary phase, indicating the reduction of CuO has been overdone at this reaction time.

Corresponding to the above phase evolution, time-dependent crystal morphology of the samples was reported in Figure 7.8 and 7.9. At a short reaction time of 1.5 h, TEM images show that CuO nanocrystallites self-aggregate to oval-shaped structures with the lengths of about 80-150 nm (Figure 7.8A, B); the CuO phase of these crystallites is also confirmed in the polycrystalline ED rings (inset, Figure 7.8A). TEM images of Figure 7.8C-F illustrate the morphology of product formed at an intermediate reaction time corresponding to the formation of CuO and Cu_2O mixture (2.5 h; also refer to Figure 7.7). It is interesting to note that partially converted Cu_2O crystallites formed at this reaction time are aligned into square-like frames (Figure 7.8C), which lays down the base for a nanocube structure (Figure 7.8D). It is further noted that there are plenty of intercrystallite spaces present in these premature cubic structures (Figure 7.8D). Two resulting Cu_2O nanocubes of this kind are displayed in

Figure 7.8E, F, together with their small starting CuO crystallites. During this process, the CuO crystallites are reduced and attached simultaneously to form cubic structures, noting that the resulting Cu_2O cubes at this stage are not compact, as indicated in the TEM image contrasts. After 3.5 h of reaction (Figure 7.9A, B), initial CuO nanocrystallites have been significantly reduced, whereas the cubical shape of Cu_2O has been largely established. Over the next two hours of reaction (at 5.5 h), hollowing and recrystallization processes take place with Ostwald ripening, through which a central space is created (Figure 7.9C, D).

From the above XRD and TEM analyses, it can be understood that the formation process of Cu_2O hollow cubes comprises the following three consecutive steps: (i) production of primary CuO nanocrystallites; (ii) reductive formation of loosely packed cubic aggregates of Cu_2O from the preformed CuO crystallites; and (iii) evacuation of central crystallites and perfection of Cu_2O hollow nanocubes through Ostwald ripening mechanism.

7.3.3 Surface compositional analysis of products

On the basis of XRD/TEM/SAED findings, we know that the CuO crystallites are reduced and aggregated simultaneously to Cu_2O nanocubes in the above formation process (2.5-3.5 h; Figure 7.7 and 7.8; the step (ii)). In order to have a better understanding of this growth mechanism, the surface compositional analysis was conducted.

XPS spectra of Cu $2p_{3/2}$ for the samples over this transforming process are displayed in Figure 7.10, and the binding energies (BEs) of different chemical species are listed in Table 7.3. In general, Cu $2p_{3/2}$ spectra can be deconvoluted into 2 peaks

(except for the sample at 1.5 h). The BEs at 933.8, 933.5 and 933.5 eV measured in our samples agree well with the reported values of CuO in a range of 933.4 to 933.9 eV (Brookshier et al., 1999; Espinós et al., 2002; Wagner et al., 1979; Wang[4] et al., 2002; Wang[9] et al., 2002(a), 2003(b); Xu[3] et al., 1999; Zhu[3] et al., 2004(a)), and the BEs at 932.7, 932.5 and 932.5 eV are also close to the reported data of Cu_2O of 932.4 or 932.5 eV (Espinós et al., 2002; Fernando et al., 2002; Wagner et al., 1979; Wang[9] et al., 2002(d)). Therefore, the evolution of peak areas in these samples reveals a gradual transformation from CuO to Cu_2O (Table 7.3). Through this surface analysis, more quantitative compositional information can now be obtained. The starting Cu^{2+} in DMF initially forms pure CuO crystallites (100%) at 1.5 h. When the reaction time is increased to 2.5 h, the product is a mixture of CuO and Cu_2O, and the surface molar ratio of CuO to Cu_2O is *ca* 4:1 (Cu^{2+}: Cu^{+} = 0.80:0.20; Table 7.3). When the reaction time is longer than 3.5 h, the main phase of products becomesCu_2O, and the molar ratio of CuO to Cu_2O is changed to 1:4 (Cu^{2+}: Cu^{+} = 0.18:0.72 at 3.5 h, and 0.21:0.79 at 6.5 h, Table 7.3). According to the XRD patterns of these samples (Figure 7.7), however, the formed bulk products are all pure Cu_2O if the reaction time is longer than 3.5 h. Therefore, it should be deduced that a small fraction of surface Cu_2O was oxidized to CuO during the sample drying and handling under normal ambient conditions.

Table 7.3 Cu binding energies (eV) and their relative contents (in parenthesis).

Samples	CuO	Cu_2O
1.5 h	933.77	
2.5 h	933.77 (0.80)	932.65 (0.20)
3.5 h	933.47 (0.18)	932.54 (0.82)
6.5 h	932.52 (0.21)	932.48 (0.79)

Figure 7.11 displays the O 1s XPS spectra measured for the samples discussed above, and their deconvoluted BEs are listed in Table 7.4. The lowest BEs of O 1s (the lattice O^{2-}) are in the range of 529.12-529.30 eV for samples at 1.5 h, 2.5 h and 3.5 h, which is consistent with the literature data of CuO (529.5 eV) (Chen[4] et al., 2003; Wang[9] et al., 2002(a); Xu[3] et al., 1999). The second peaks at 529.99-530.66 eV indicate the formation of Cu_2O phase. It should be mentioned that the lattice oxygen O^{2-} for CuO phase is not detectable in the sample prepared at 6.5h due to its small quantity.

Table 7.4 Binding energies (eV) of O 1s of different chemical species and their relative Contents (in parenthesis).

Sample	CuO	Cu_2O	$OH^-$and/CO_3^{2-}	H_2O
1.5 h	529.22 (0.47)		531.21 (0.41)	533.00 (0.12)
2.5 h	529.30 (0.50)	530.66 (0.20)	531.57 (0.23)	532.89 (0.07)
3.5 h	529.12 (0.05)	529.99 (0.42)	531.52 (0.36)	532.97 (0.18)
6.5 h		530.18 (0.44)	531.52 (0.38)	532.95 (0.18)

Auger electron spectra of Cu L_3VV are also important in characterizing Cu^+ and Cu^{2+} oxidation states of the samples. Figure 7.12 shows a comparison between the Cu 2p and Cu L_3VV spectra for the above four different samples. From the Cu L_3VV spectra, the main kinetic energies (KEs) are 918.2, 918.1, 917.1 and 917.1 eV for samples prepared at 1.5 h, 2.5 h, 3.5 h and 6.5 h, respectively. For the sample prepared at 1.5 h, the Cu $2p_{3/2}$ BE of 933.8 eV and KE of 918.2 eV agree respectively with the reported values of 933.7 eV and 918.1 eV of CuO phase (Espinós et al., 2002; Wagner et al., 1979). For the sample prepared at 2.5 h, as mentioned in Figure 7.10, the Cu $2p_{3/2}$ spectrum have two BE peaks at 933.8 eV and 932.7 eV, respectively, which correspond to surface phases of CuO and Cu_2O (in a smaller quantity, Table 7.3). In this observation, the position of the KE in Cu L_3VV spectrum for this sample is around

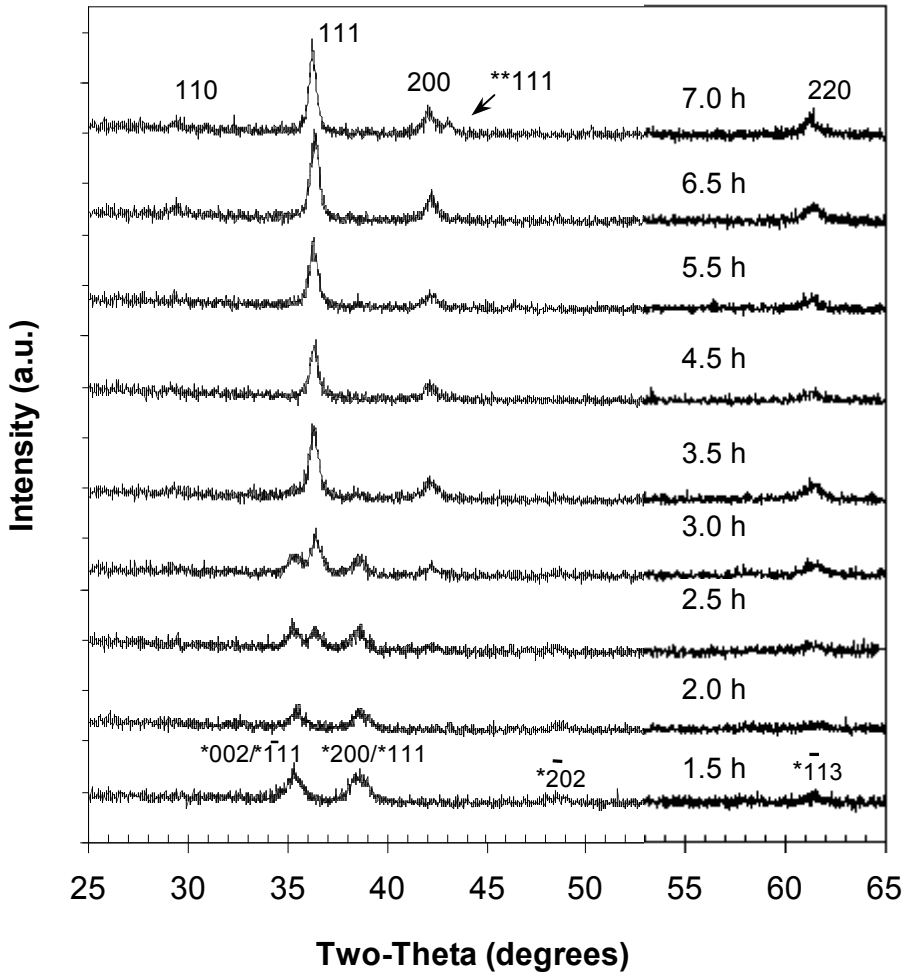

Figure 7.7 Powder XRD patterns of nanoproducts synthesized at 200^{o}C with different reaction times. Experimental condition: 30.0 mL of [Cu^{2+}] (0.005 M in DMF) + 0.50 mL of H_2O at 200 ^{o}C for 1.5 h to 7 h. Single-asterisk (*) denotes the CuO phase whilst the double-asterisk (**) represents the metallic Cu component.

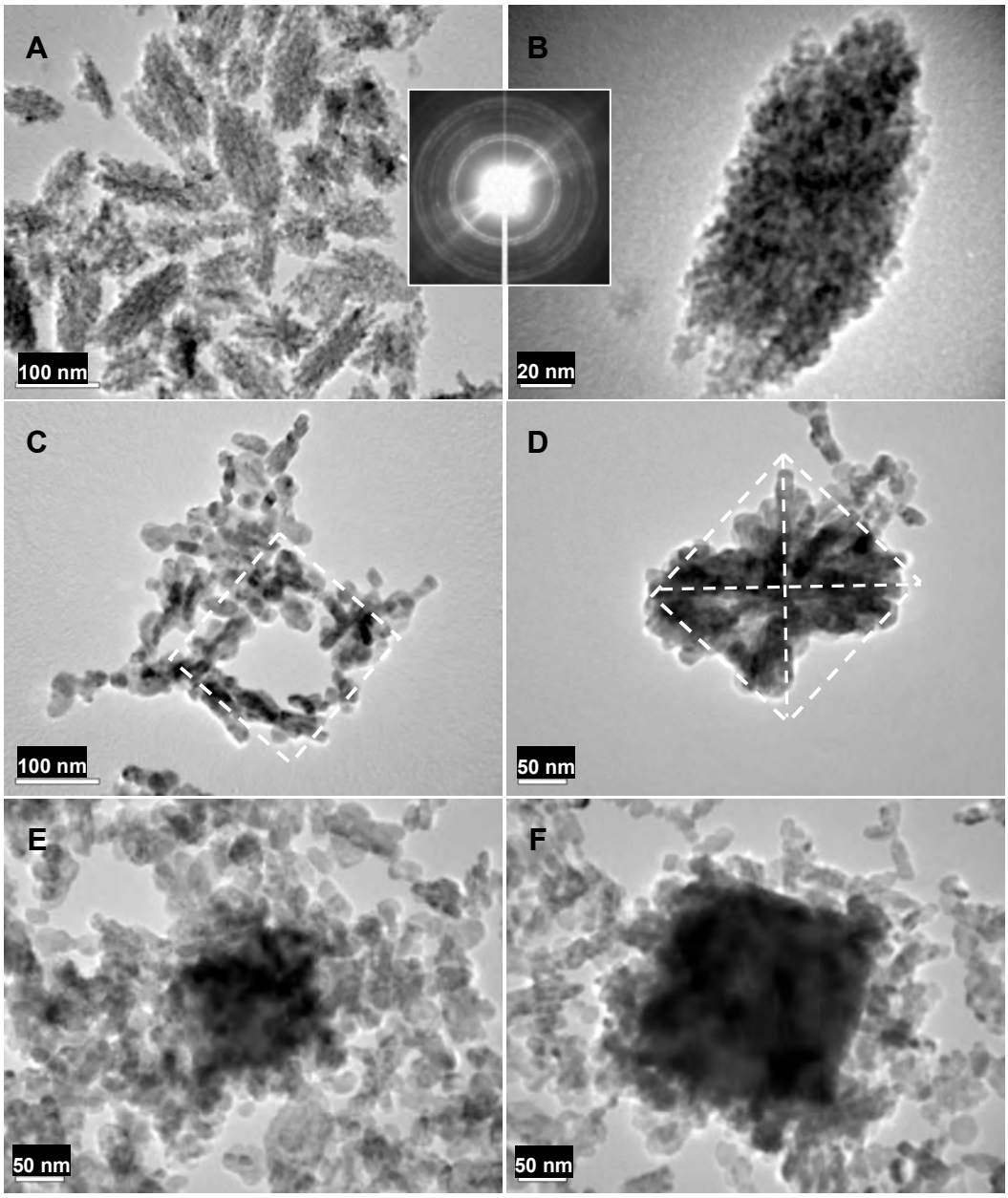

Figure 7.8 (A and B) TEM images of CuO nanoproducts prepared at 200 ^{o}C for 1.5 h. (C to F) TEM images of mixture of CuO and Cu_2O nanoproducts prepared at 200 ^{o}C for 2.5 h. Other experimental parameters: 30.0 mL of [Cu^{2+}] (0.005 M in DMF) + 0.50 mL of H_2O. The XRD patterns of the two samples can be seen in Figure 7.7.

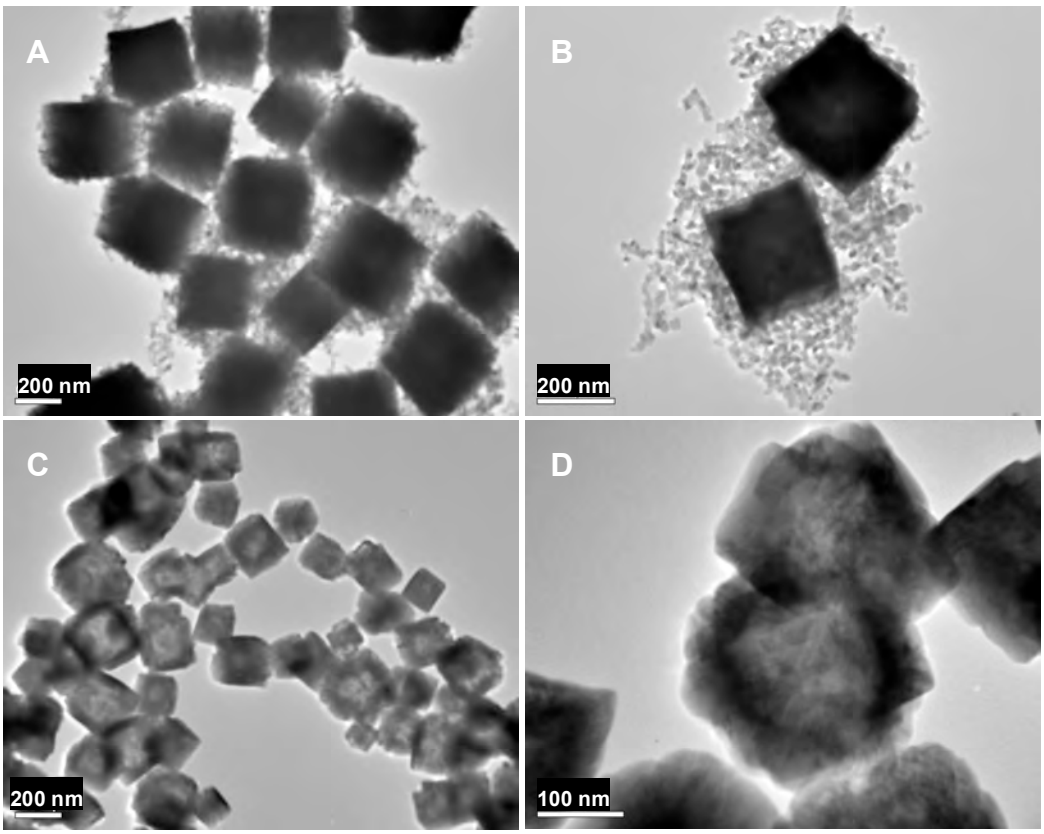

Figure 7.9 (A and B) TEM images of mixture of CuO and Cu_2O nanoproducts prepared at 200 ^oC for 3.5 h. (C and D) TEM images of mixture of CuO and Cu_2O nanoproducts prepared at 200 ^oC for 5.5 h. Other experimental parameters: 30.0 mL of [Cu^{2+}] (0.005 M in DMF) + 0.50 mL of H_2O. The XRD patterns of the two samples can be seen in Figure 7.7.

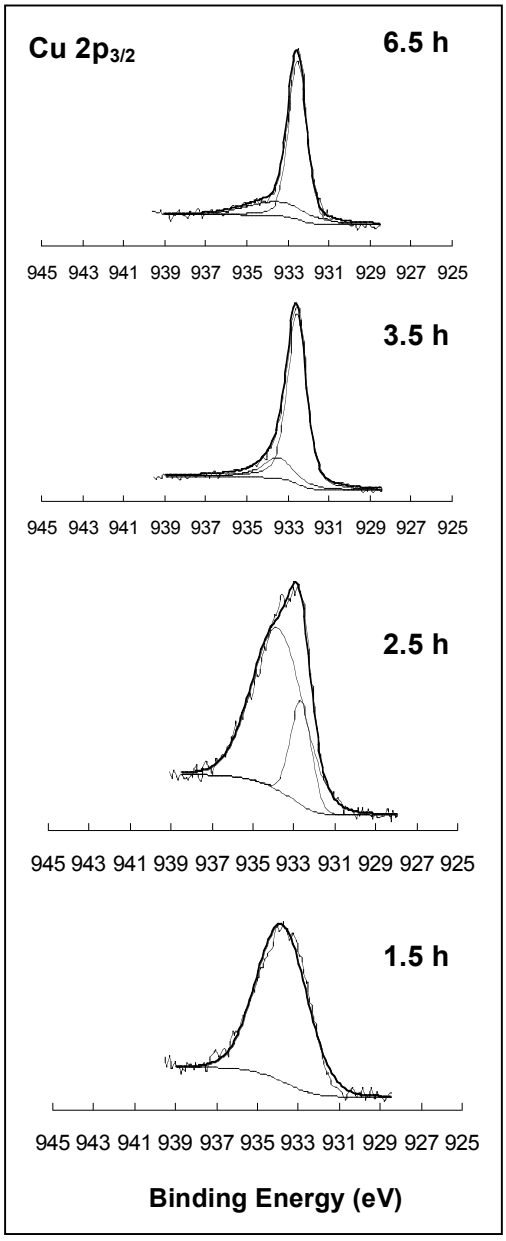

Figure 7.10 XPS spectra of Cu $2p_{3/2}$ for samples synthized at 200 ^{o}C for different reaction time (1.5 h to 6.5 h). Other experimental parameters: 30.0 mL of [Cu^{2+}] (0.005 M in DMF) + 0.50 mL of H_2O. The XRD patterns of these samples can be seen in Figure 7.7.

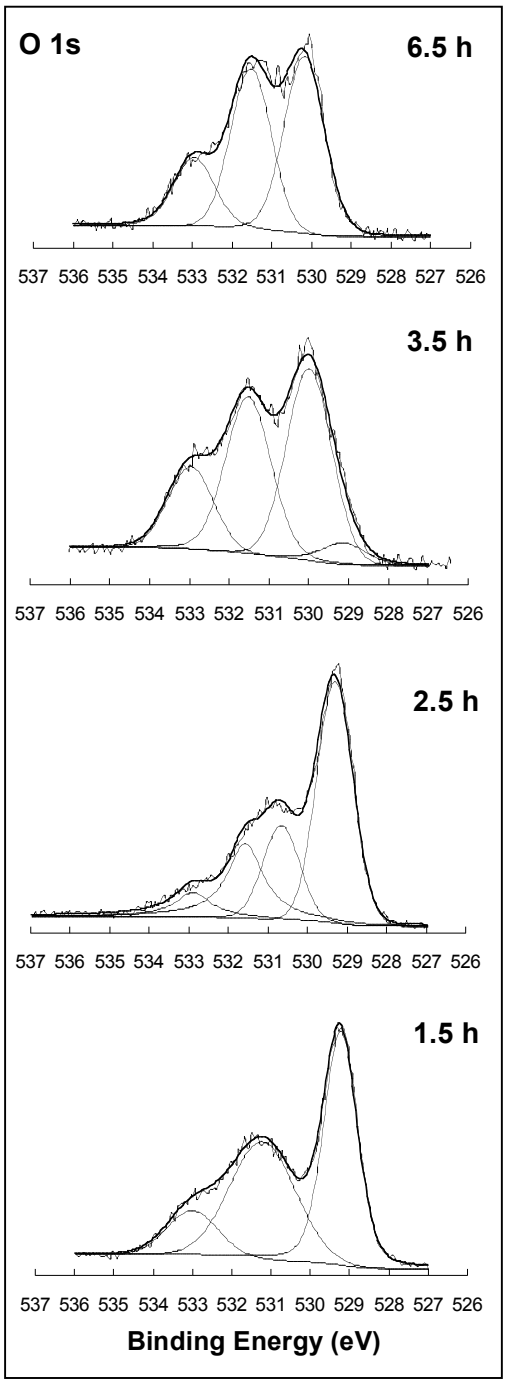

Figure 7.11 XPS spectra of O 1s for samples synthized at 200 °C for different reaction time (1.5 h to 6.5 h). Other experimental parameters: 30.0 mL of [Cu^{2+}] (0.005 M in DMF) + 0.50 mL of H_2O. The XRD patterns of these samples can be seen in Figure 7.7.

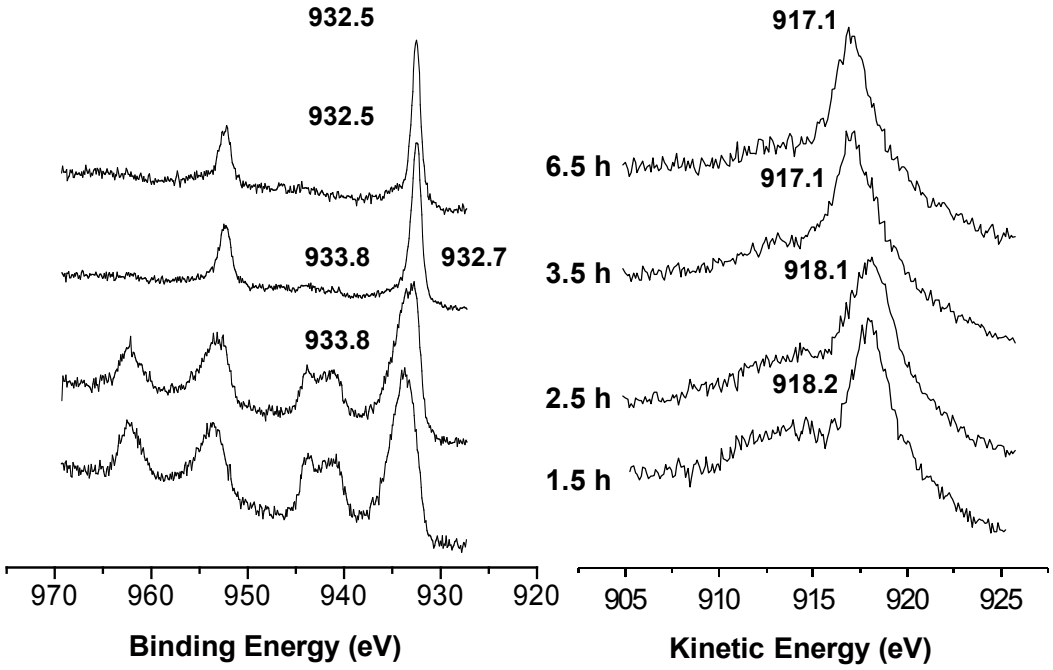

Figure 7.12 Comparison of Cu 2p spectra and Cu L_3VV spectra for nanoproducts synthized at 200 ^oC for different time (1.5 h to 6.5h). Other experimental parameters: 30.0 mL of [Cu^{2+}] (0.005 M in DMF) + 0.50 mL of H_2O. The XRD patterns of these samples can be seen in Figure 7.7.

918.1 eV for CuO (Wagner et al., 1979), noting that there is a significant peak broadening due to the transient nature of this sample. When the reaction time is prolonged to 3.5 h and 6.5 h, the BEs are 932.5 and 932.5 eV, and the KEs are 917.1 and 917.1 eV respectively. These values once again indicate that the two samples with reaction time of 3.5 h and 6.5 h are primarily in Cu_2O phase.

7.3.4 Effects of water on Cu_2O morphology

As mentioned earlier, water is the key to the formation of cubic morphology of Cu_2O in the present work. At room temperature, $Cu(NO_3)_2$ in the DMF solution can form the complex of $[CuNO_3(DMF)_5]^+$ (Mamantov and Popov, 1994). The redox chemical process for the formation of Cu_2O phase in DMF-water solvent system had been proposed in Chapter 6 (eq. 6.1, 6.2 and 6.3), where DMF solvent acts as a weak reducing agent in the synthesis and a small amount of water is incorporated into the synthesis through the starting reagent $Cu(NO_3)_2 \cdot 3H_2O$. Different from the formation of polycrystalline Cu_2O hollow spheres, surprisingly, single-crystal Cu_2O hollow cubes could be obtained with additional water which was deliberately added in the present work. The significant contrast in the latter crystal morphology can be attributed to a gain in stabilization of the {100}, {010}, and {001} crystal planes with more abundant water. Figure 7.13A, B show two possible surface terminations of the Cu_2O (100) plane. Whether a (100) surface is terminated with Cu^+ cations or with O^{2-} anions, there must be local unbalanced charged domains (e.g., atomic steps) on its surface. Therefore, surface adsorptions with ions in opposite charges and/or polar molecules will compensate the surface charges and thus stabilize the crystal planes. Consistent with this postulation, the stabilizing effect is indeed obtained when additional water is

added to the reactions, owing to more charged species in the products (e.g., $NH_2(CH_3)_2^+$ in eq. 6.2) and more polar solvent molecules (e.g., water) can interact with the Cu_2O (100) surfaces via direct charge compensation or through formations of different hydrogen bonding.

To demonstrate the effect of water, Figure 7.14 shows some TEM/SEM images of Cu_2O hollow cubes and large cubes prepared at different reaction temperatures and times. Figure 7.14A, B show the images of samples prepared at 170 ^oC for 26 h with 0.30 mL and 0.50 mL of H_2O in 30 mL of starting 0.005 M Cu^{2+} DMF solution (Expt. 8 and 10, Table 7.1). in this experiment, the volume of water only varied from 0.30 to 0.50 mL, but the Cu_2O crystal morphology was changed from small hollow cubes to large solid microcubes, accompanied by a drastic size change from 0.15 μm to 3-6 μm. Furthermore, Figure 7.14C, D are the SEM images of samples prepared at a higher temperature 190 ^oC for 11 h with 0.50 mL and 0.60 mL of H_2O in 30 mL of starting 0.005 M Cu^{2+} DMF solution (Expt. 20 and 21, Table 7.1). With a difference of 0.10 mL in water (0.5 mL versus 0.6 mL), the average size of cubes increases from 0.2 μm to 0.8 μm. When the reaction temperature is raised to 200 ^oC, very large cubes also begin to form with 0.6 mL water in the solution (Figure 7.14F). When the temperature is increased to 210 ^oC, an amount of 0.5 mL deionized water is sufficient to generate the large cubes, owing to the fast reaction rate at the even higher temperature (Figure 7.14G, H).

Based on these results, we observe that with the additional deionized water in starting DMF solution, the crystal morphology of Cu_2O change from hollow nanocubes to large solid microcubes. The optimal water volume for the formation of Cu_2O hollow cubes is around 0.4–0.5 mL under our general experimental conditions.

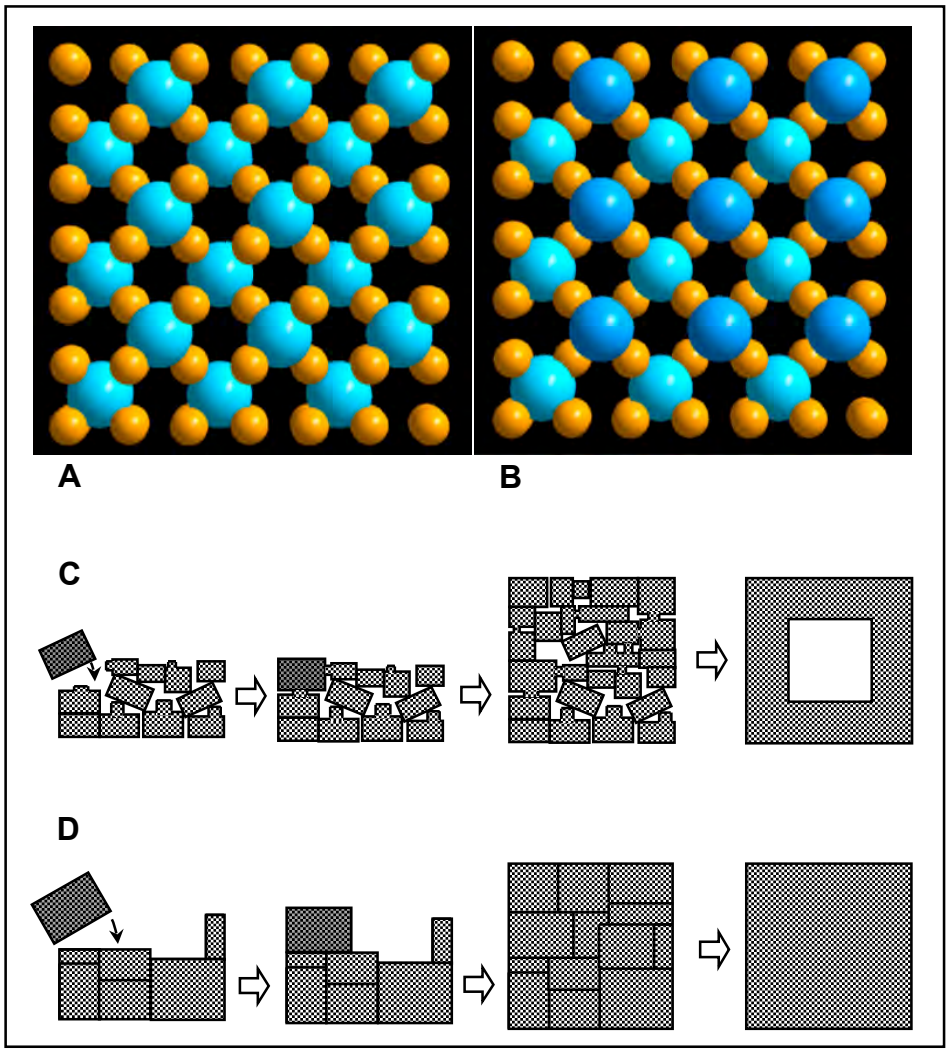

Figure 7.13 Surface models for the Cu_2O (100) crystal planes: (A) Cu^{+}-cation terminated plane (Cu in orange), and (B) O^{2-}-anion terminated plane (O^{2-} in blue and dark blue). Reductive formation of cubic structures: (C) under a low water content condition, the formed Cu_2O crystallites are smaller and the surfaces of Cu_2O (100) are rougher, leading to more mismatches among the crystallites and a lower packing density for the central void formation (via Ostwald ripening), and (D) with a higher content of water, the formed Cu_2O crystallites are larger and surface of Cu_2O (100) are smoother, resulting in a final crystal cubes. CuO crystallites attached to the forming Cu_2O cubes (in grey) are represented with darker rectangular blocks.

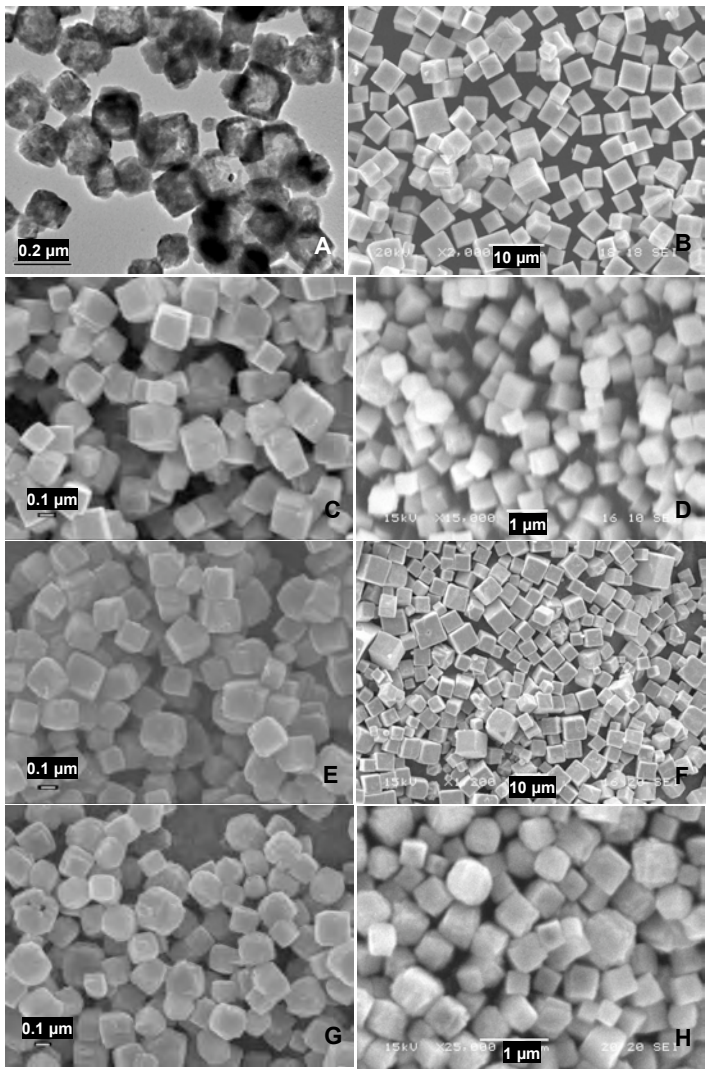

Figure 7.14 Cu_2O morphological changes with water: (A) hollow cubes: with 0.30 mL of H_2O at 170 ^oC for 26 h (Expt. 8), (B) large cubes: with 0.50 mL of H_2O at 170 ^oC for 26 h (Expt. 10), (C) hollow cubes: with 0.50 mL of H_2O at 190 ^oC for 11 h (Expt. 20), (D) large cubes: with 0.60 mL of H_2O at 190 ^oC for 11 h (Expt. 21), (E) hollow cubes: with 0.50 mL of H_2O at 200 ^oC for 6.5 h (Expt. 23), (F) large cubes: with 0.60 mL of H_2O at 200 ^oC for 6.5 h (Expt. 24), (G) hollow cubes: with 0.40 mL of H_2O at 210 ^oC for 5.5 h (Expt. 25) and (H) large cubes: with 0.50 mL of H_2O at 210 ^oC for 5.5 h (Expt. 26). A same amount of 30.0 mL of [Cu^{2+}] (0.005 M in DMF) was used in each of the above experiments (Table 7.1).

This optional amount of water is further addressed in Figure 7.13. With a limited amount of water, for example, the resultant Cu_2O crystallites are generally small and the surface of Cu_2O (100) may not be entirely smooth, which may lead to presence of more intercrystallite voids for the development of hollow interior (Figure 7.13C). With a larger amount of water present, on the other hand, bigger and smoother surfaces of Cu_2O (100) can be attained, which favors a faster reaction and formation of more compact crystallite aggregates, resulting in large solid Cu_2O microcubes (Figure 7.13D).

7.3.5 Effects of ethanol on Cu_2O morphology

To investigate the effort of solvent on the stability of Cu_2O (100) surface, weaker polar molecules such as ethanol are also examined in the synthesis (Table 7.2). Figure 7.15 shows the TEM images and SAED pattern of the Cu_2O nanocubes prepared with ethanol added. The formed cubes under this condition are uniform and the edge length of the cubes is smaller than 100 nm. Similar to Figure 7.4B, the spot array shows a four-fold axis that can be indexed with *hk0*, also indicating a cubic single crystal symmetry for Cu_2O nanocubes. Without adding ethanol to the synthesis, in contrast, only polycrystalline Cu_2O spheres could be formed. The stabilizing effect of ethanol on the Cu_2O (100) surface has thus been demonstrated.

Our XRD investigation of Figure 7.16 indicates that the product formed at 2 h is a mixture of CuO and Cu_2O. When the reaction time is prolonged to 3-6 h, pure Cu_2O products are obtained. From our XRD and TEM studies (Figure 7.17), it can be concluded that the synthetic process using DMF-ethanol is very similar to the process using DMF-water, that is, Cu^{2+} initially forms the CuO fine nanocrystallites in the

basic solutions and then CuO nanocrystallites are reduced and aggregate directly to Cu_2O cubes. Our present process is different from a process reported in literature, in which the Cu^{2+}salts in alkaline solution are reduced with hydrazine to intermediates of CuOH and then transformed into Cu_2O by the thermal decomposition (Gou and Murphy, 2003). However, when the CuO suspensions in an aqueous solution were used as the precursor to synthesize Cu_2O particles at 30 ^oC, the morphology of Cu_2O is uniform polycrystalline sphere with an average diameter of 0.27 μm (Muramatsu and Sugimoto, 1997). Comparing these results, we can see that the high temperature and polarity of the solvent are very important for the formation of Cu_2O single-crystalline nanocubes.

7.3.6 Formation of Cu nanocubes

In this work, the formed Cu_2O nanocubes were also used as solid precursors to fabricate metallic Cu hollow nanostructures. Owing to the weak reducing power of DMF, it takes a long time to reduce Cu^{2+} to Cu_2O and to Cu at low temperature (e.g., 20 h is needed at 180 ^oC; Expt. 37, Table 7.2). To overcome this process difficulty, a two-step method was devised (Expt. 38-41, Table 7.2): the experiments were conducted at 180 ^oC for 6 h and consecutively at 200 ^oC for 1-2 h, while the volume ratio of DMF to ethanol was still kept at 10:20. The Cu products were also confirmed by XRD method; Figure 7.16 shows the XRD pattern of the samples prepared with this method. In Figure 7.18A, B, the hollow interior of Cu nanoproducts is confirmed, noting that the formed Cu preserves the shape of the pristine Cu_2O nanocubes, and the sharp SAED ring pattern in Figure 7.18C demonstrates the high crystallinity for this metal product.

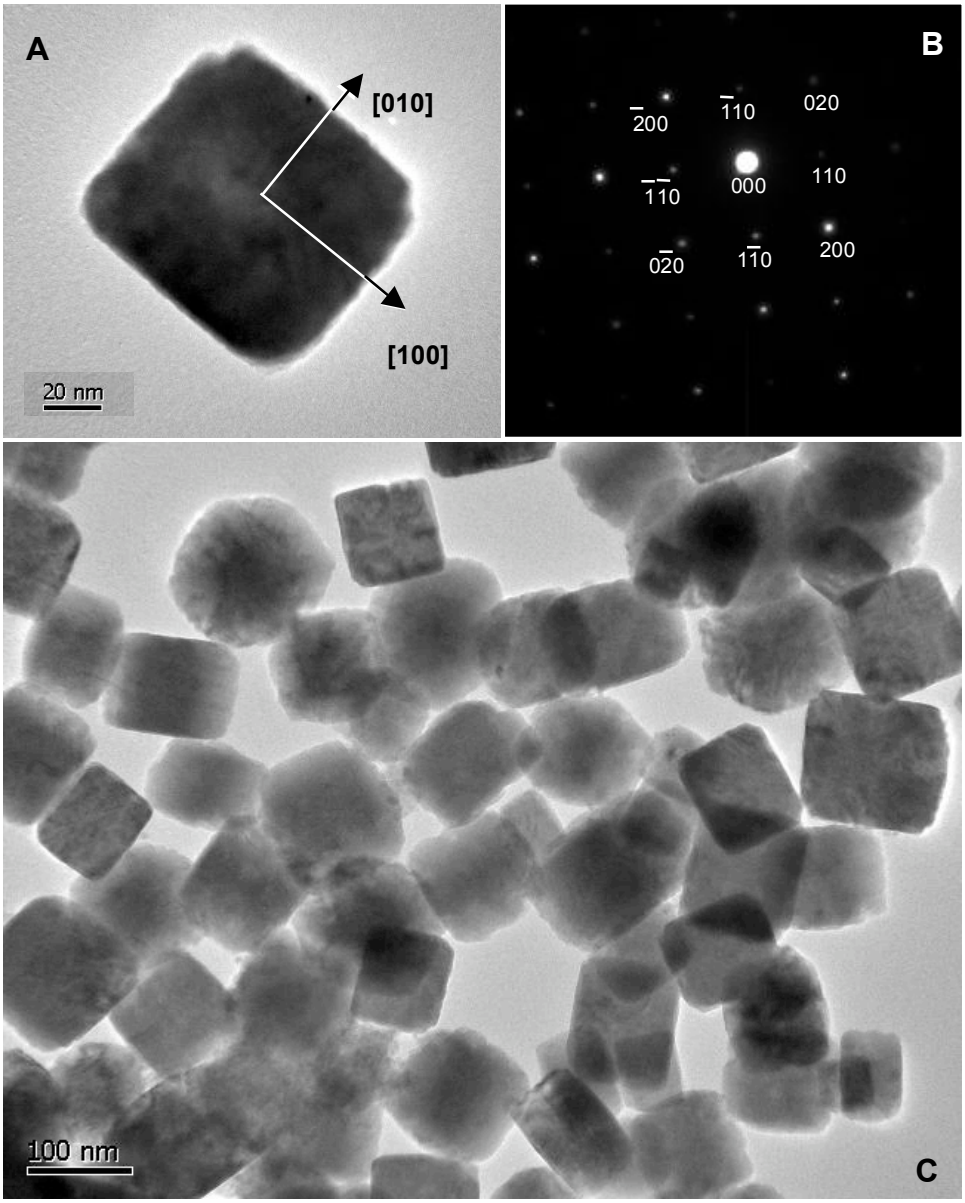

Figure 7.15 Crystal morphology of Cu_2O nanocubes: (A) detailed view on a crystal cube (note that there is a lighter center), (B) the SAED pattern of (A), and (C) general crystal morphology in a large scale. Experimental condition: 30.0 mL of $[Cu^{2+}]$ (0.005 M in DMF:EtOH = 10:20 mL/mL) at 180 ^{o}C for 6 h. (Table 7.2)

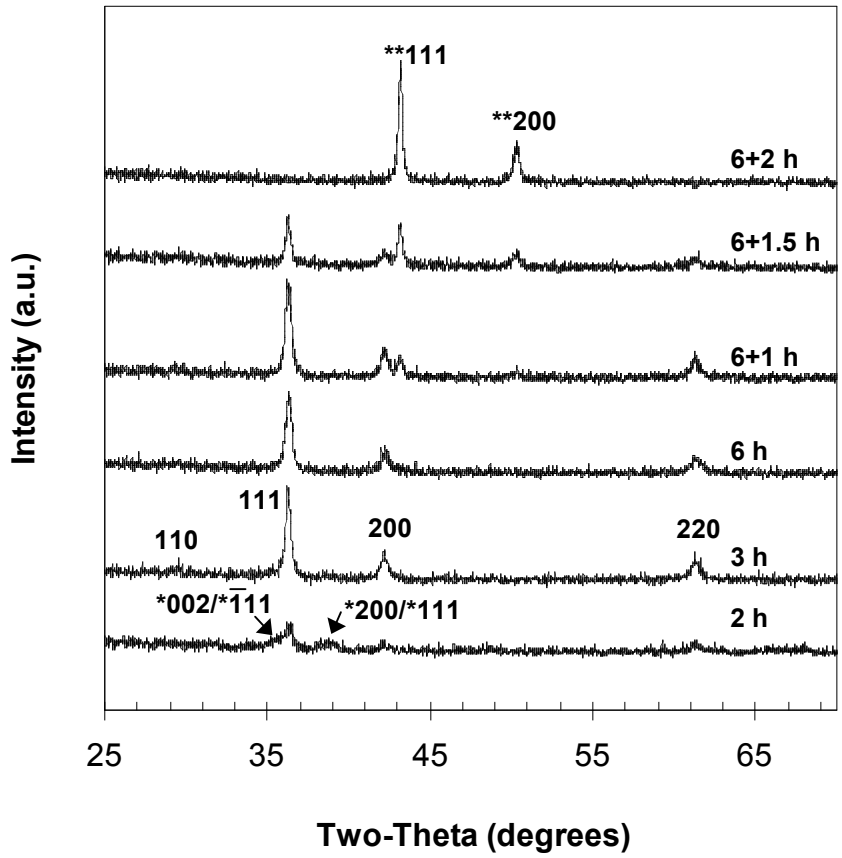

Figure 7.16 Powder XRD patterns of nanoproducts synthesized at 180 ^{o}C with different reaction times (2 to 6 h), and nanoproducts prepared with a two-step method at 180 ^{o}C for 6 h and consecutively at 200 ^{o}C for 1 to 2 h. Other experimental parameters used fro these samples: 30.0 mL of [Cu^{2+}] (0.005 M in DMF:EtOH = 10:20 mL/mL). Unmarked diffraction peaks are from Cu_2O phase, and single-asterisk (*) denotes CuO phase whilst the double-asterisk (**) represents metallic Cu phase.

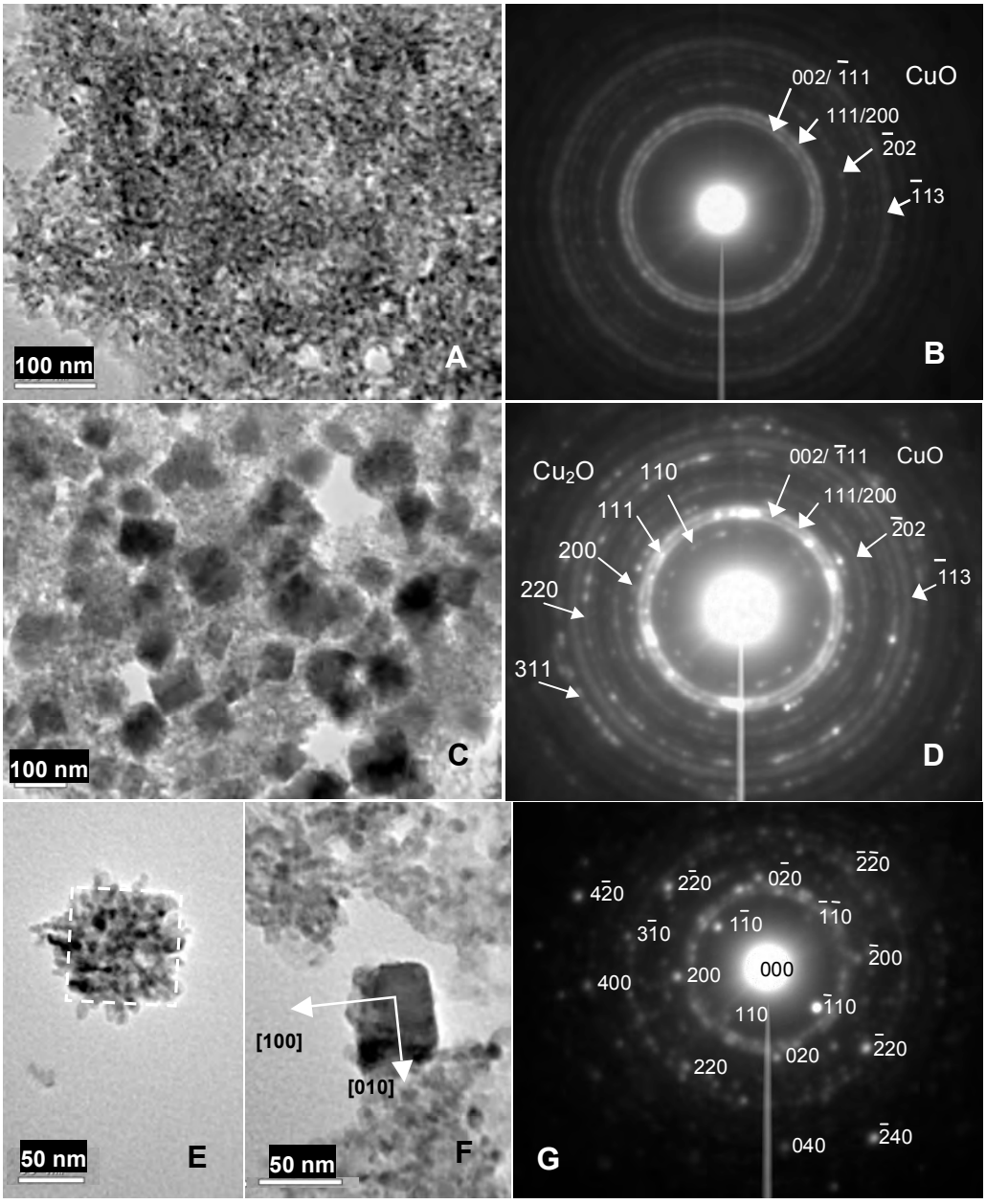

Figure 7.17 TEM/SAED characterization for the mixture of CuO and Cu_2O: (A, C, E and F): TEM images of mixture; (B): SAED pattern of (A); (D): SAED pattern of (C); (G): SAED pattern of (F). Experimental conditions: 30 mL of [Cu^{2+}] (0.005 M in DMF:Ethanol = 10:20 mL/mL) was heated at 180 ^{o}C for 2 h.

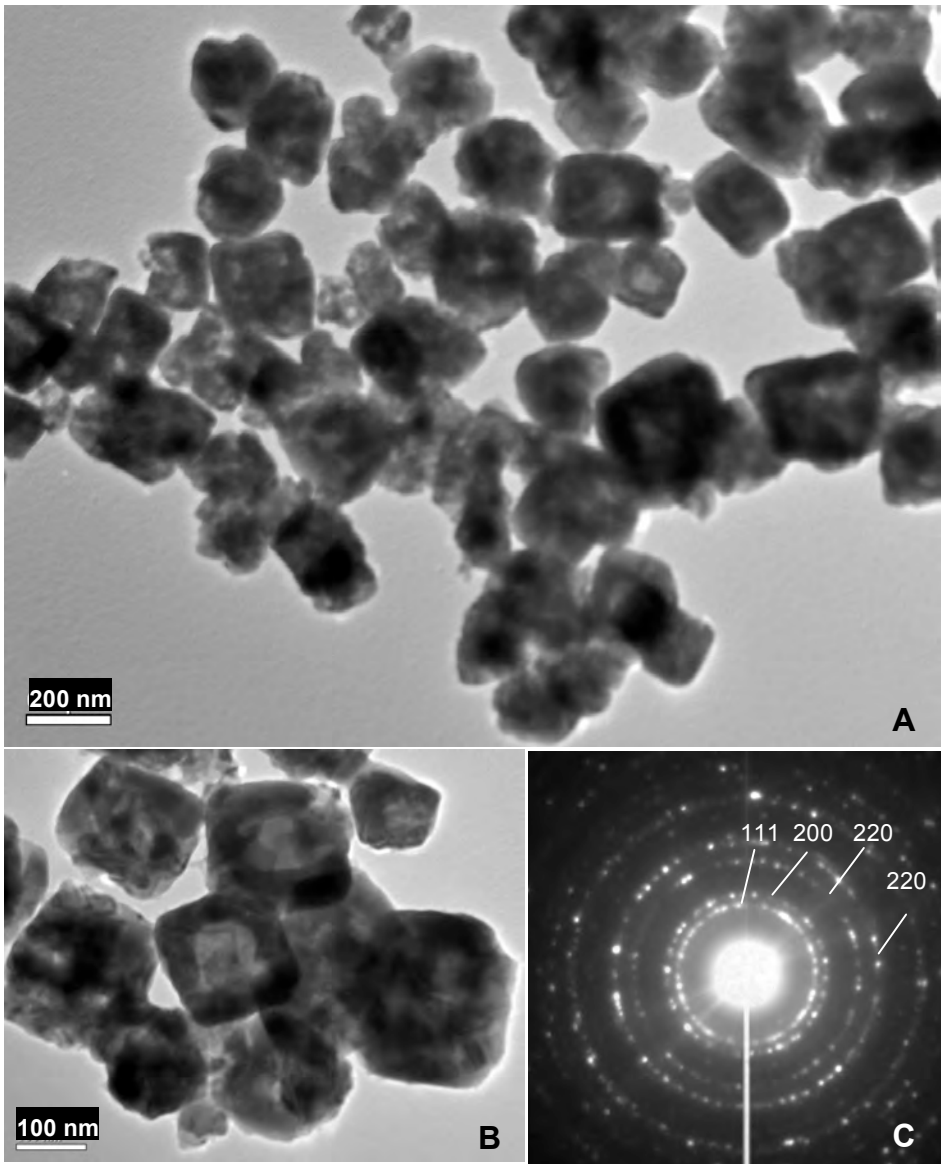

Figure 7.18 TEM/SAED charactrization for metallic Cu hollow nanocubes prepared by the two-step method: (A and B) TEM images; and (C) SAED pattern measured for (B). Experimental conditions: 30.0 mL of [Cu^{2+}] (0.005 M in DMF:Ethanol = 10:20 mL/mL) was heated at 180 ^{o}C for 6 h and consecutively at 200 ^{o}C for 2 h.

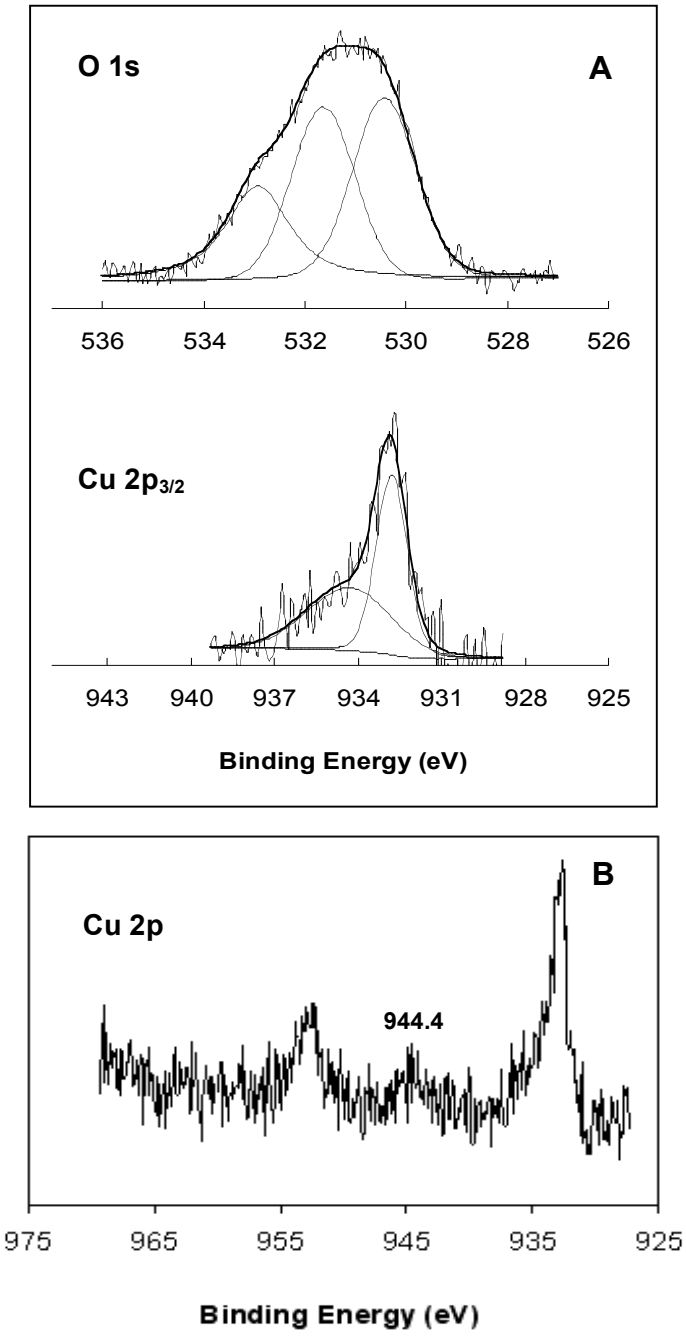

Figure 7.19 (A) Detailed XPS spectra of O 1s and Cu $2p_{3/2}$ for Cu hollow cubes, and (B) Overall XPS spectrum of Cu 2p. Experimental conditions: 30.0 mL of [Cu^{2+}] (0.005 M in DMF:Ethanol = 10:20 mL/mL) was heated at 180 ^{o}C for 6 h and consecutively at 200 ^{o}C for 2 h.

Table 7.5 Binding energies (eV) and relative contents (in parenthesis) of oxygen and copper.

O1s	CuO 530.4 (0.35)	OH^- and/or CO_3^{2-} 531.6 (0.39)	H_2O 532.9 (0.26)
Cu $2p_{3/2}$	Cu 932.8 (0.53)		CuO 934.3 (0.47)

Figure 7.19A shows the XPS spectra of O 1s and Cu $2p_{3/2}$ for the air-dried Cu hollow cubes prepared with the above two-step method. The BE positions of each component are detailed in Table 7.5. The Cu $2p_{3/2}$ XPS spectrum can also be deconvoluted into two peaks at 934.3 and 932.8 eV respectively. The peak at 934.3 eV belongs to the CuO, although it is higher than the reported energy of CuO (933.7 eV) (Wagner et al., 1979). However, it has been reported that when the ratio of CuO is decreased, the BE shifts from 933.6 eV to a higher value of 934.4 eV (Espinós et al., 2002). This suggests that a thin layer of CuO forms on the outermost surface of the sample. In Figure 7.19B, a weak split at 944.4 eV is the specific Cu 2p peak for surface CuO which indeed indicates the above oxidation. However, the Cu $2p_{3/2}$ BEs of Cu_2O and Cu are close to each other; the reported values are 932.5 eV and 932.6 eV (Wagner et al., 1979). Thus the peak at 932.8 eV cannot be confirmed only by Cu $2p_{3/2}$ XPS spectrum alone. The XPS spectrum of O 1s is also displayed in the Figure 7.19A, which can be deconvoluted into three peaks. The high BE component at 530.4 eV is due to the presence of CuO on the surface of Cu hollow particles. The next component at 531.6 eV can be attributed to the presence of hydroxyl groups and/or carbonate group. The final peak at 532.9 eV is due to the presence of H_2O adsorbed on the surface. From the O 1s spectrum, we can confirm that there exists no Cu_2O on the

outermost surface of the sample. Combining the Cu $2p_{3/2}$ XPS spectrum, it can be concluded that the Cu 2p BE of 942.8 eV belongs to metallic copper and only a thin layer of CuO exists on the outermost surface of the sample.

7.4 Conclusion

In this chapter, we developed a simple hydrothermal method to prepare single-crystalline Cu_2O hollow cubes. The crystal growth process was fully investigated, that is, the Cu^{2+} consecutively converts to CuO, to Cu_2O nanocubes and finally to Cu_2O hollow cubes *via* Ostwald ripening. The Cu_2O hollow cubes formed are about 200 nm. In this process, water has a great effect on the morphologies of Cu_2O products. With the increase of water in the starting solution, the morphologies of Cu_2O change from hollow spheres to hollow cubes and then to large cubes.

CHAPTER 8

LARGE-SCALE SYNTHESIS OF HIGHLY REGULATED ULTRALONG COPPER NANOWIRES

8.1 Introduction

In previous chapters, we have fabricated CuO and Cu_2O crystallites with different structures. In this chapter, we concentrate on the synthesis of ultronglong copper nanowire, as it has a great significence in the microelectronic industry.

The fabrication of one-dimensional (1D) copper nanomaterials (wires/cables/rods) has received considerable attention in recent years, and a number of methods have been available. The electrochemical deposition (ECD) is a commonly used method. When the reaction is completed, the template should be removed to obtain copper nanowires thus making the process complicated. In chemical vapor deposition (CVD) (Choi and Park, 2004) and vacuum vapor deposition (VVD) (Adelung et al., 2002; Liu[6] and Bando, 2003(a, b)) methods, copper nanowires can be synthesized without templates, but the reactions are conducted under high vacuums (0.1-1.0 Torr) and high temperatures. Surfactants and polymers are also adoped to synthesize copper nanowires, for example, SDBS (Liu[6] et al., 2003(c)), CTAB (Cao[2] et al., 2003), PEG (Cao[2] et al., 2003), and PVP (Liu[2] et al., 2003). Although the

significant research endeavor has been devoted, there is still lack of effective methods for large-scale production of high-quality nanostructured copper with precise morphological control. Major difficulties encountered in this area are short length, nonlinear morphology, polydispersivity, poor crystallinity, low yield, and process complexity. In this chapter, we demonstrate that highly regulated ultralong copper nanowires (all freestanding: 90–120 nm in diameter, 40-50 μm in length; aspect ratio > 350–450) can be synthesized in large-scale with a facile aqueous reduction route at low temperatures.

8.2 Experimental section

8.2.1 Materials preparation More than 60 experiments had been carried out in this research to fabricate copper nanowires. In each synthesis, 20–30 ml NaOH (3.5–15M) and 0.5–1.0 mL of $Cu(NO_3)_2$ (0.10 M) aqueous solution were added to a glass reactor (capacity 50 mL) (See Figure 8.6). Varying amounts of EDA (0.050–2.0 mL; 99 wt%) and hydrazine (0.020–1.0 mL; 35 wt%) were also added subsequentially, followed by a thorough mixing of all reagents with fierce shaking. The reactor was then placed in a water bath with temperature control over 25 ^{o}C–100 ^{o}C (optimized at 60 ^{o}C) for 15min to 15 hours. During the heating process, the solution was neither shaken nor stirred. After reaction, copper products were washed and harvested with centrifugation-radioperson cycles, with each successive up-clear solution being decanted and replaced with deionized water. Finally, the clean copper products were stored in a water–hydrazine

solution to prevent oxidation. Further details on the synthesis are listed in Table 8.1.

8.2.2 Materials characterization Crystallographic phases of the prepared copper samples were investigated by XRD method (Shimadzu XRD-6000, Cu K_α radiation). The dimension and morphology of the samples were examined using SEM (JSM-5600LV, JSM-6700), TEM (JEM 2010, 200 kV), and high resolution transmission electron microscopy with energy dispersive X-ray spectroscopy (HRTEM/EDX; JEM 3010, 300 kV). Surface chemical analysis of copper samples was performed by XPS.

8.3 Results and Discussion

8.3.1 Morphology and structure characterization of copper nanowires

In this work, more than 60 experiments were conducted and the composition of the prepared products was confirmed by XRD method. Figure 8.1 is the XRD patterns of some selected samples. The three peaks located at 2θ values of 42.9 ^{o}, 50.3 ^{o} and 73.9 ^{o} correspond to the characteristic diffractions of face-centred cubic (FCC) crystalline copper metal (JCPDS card no. 03-1005) although there is about 0.3^{o} excursion. This verifies that the samples are phase-pure copper metal. The three peaks are the diffraction of crystal faces of (111), (200) and (220) respectively. In the figure, some of the XRD patterns have weak diffraction intensities and it is the reason that a small amount of sample is used in the measurement.

Figure 8.2 shows product morphology of prepared copper wires. As shown,

Table 8.1 The detailed synthesis conditions for selected copper products.

Expt.	NaOH aqueous solution		$Cu(NO_3)_2$ aqueous solution		Volume of EDA (mL)	Volume of N_2H_4 (35 wt%) (μL)	Temperature (°C)	Time (h)	EDA:OH^-:Cu^{2+}:N_2H_4
	Volume (mL)	Concentration (Mol/L)	Volume (mL)	Concentration (Mol/L)					Molar ratio
A1	20	**15**	1.0	0.10	**0.15**	25.0	60	1	22.39 : 3000 : 1.0 : 2.76
A2	20	**15**	1.0	0.10	**0.125**	25.0	60	1	18.66 : 3000 : 1.0 : 2.76
A3	20	**15**	1.0	0.10	**0.10**	25.0	60	1	14.93 : 3000 : 1.0 : 2.76
A4	30	**7.0**	1.0	0.10	**0.50**	25.0	60	1	74.64 : 2100 : 1.0 : 2.76
A5	30	**3.5**	1.0	0.10	**0.50**	25.0	60	2	74.64 : 1050 : 1.0 : 2.76
B1	20	15	1.0	0.10	**2.00**	25.0	60	1.5	298.56 : 3000 : 1.0 : 2.76
B2	20	15	1.0	0.10	**1.00**	25.0	60	1	149.28 : 3000 : 1.0 : 2.76
B3	20	15	1.0	0.10	**0.50**	25.0	60	1	74.64 : 3000 : 1.0 : 2.76
B4	20	15	1.0	0.10	**0.30**	25.0	60	1	44.79 : 3000 : 1.0 : 2.76
B5	20	15	1.0	0.10	**0.20**	25.0	60	1	29.86 : 3000 : 1.0 : 2.76
B6	20	15	1.0	0.10	**0.075**	25.0	60	1	11.20 : 3000 : 1.0 : 2.76
C1	30	7.0	1.0	0.10	0.50	**25.0**	**100**	1	74.64 : 2100 : 1.0 : 2.76
C2	30	7.0	1.0	0.10	0.50	**30.0**	**55**	4	74.64 : 2100 : 1.0 : 3.32
C3	30	7.0	1.0	0.10	0.50	**60.0**	**50**	1.5	74.64 : 2100 : 1.0 : 6.64
D1	30	7.0	1.0	0.10	0.50	25.0	60	**0.5**	74.64 : 2100 : 1.0 : 2.76
D2	30	7.0	1.0	0.10	0.50	25.0	60	**0.75**	74.64 : 2100 : 1.0 : 2.76
D3	30	7.0	1.0	0.10	0.50	25.0	60	**3**	74.64 : 2100 : 1.0 : 2.76
D4	30	7.0	1.0	0.10	0.50	25.0	60	**4**	74.64 : 2100 : 1.0 : 2.76
D5	30	7.0	1.0	0.10	0.50	25.0	60	**13**	74.64 : 2100 : 1.0 : 2.76
E1	30	7.0	**0.50**	0.10	**0.35**	35.0	60	1	104.50 : 4200 : 1.0 : 7.74
E2	30	7.0	**0.50**	0.10	**0.30**	35.0	60	1	89.57 : 4200 : 1.0 : 7.74
E3	30	7.0	**0.50**	0.10	**0.20**	35.0	60	1	59.71 : 4200 : 1.0 : 7.74

Notes: The experiments are divided into different series. The parameters investigated in each set are indicated in bold font.

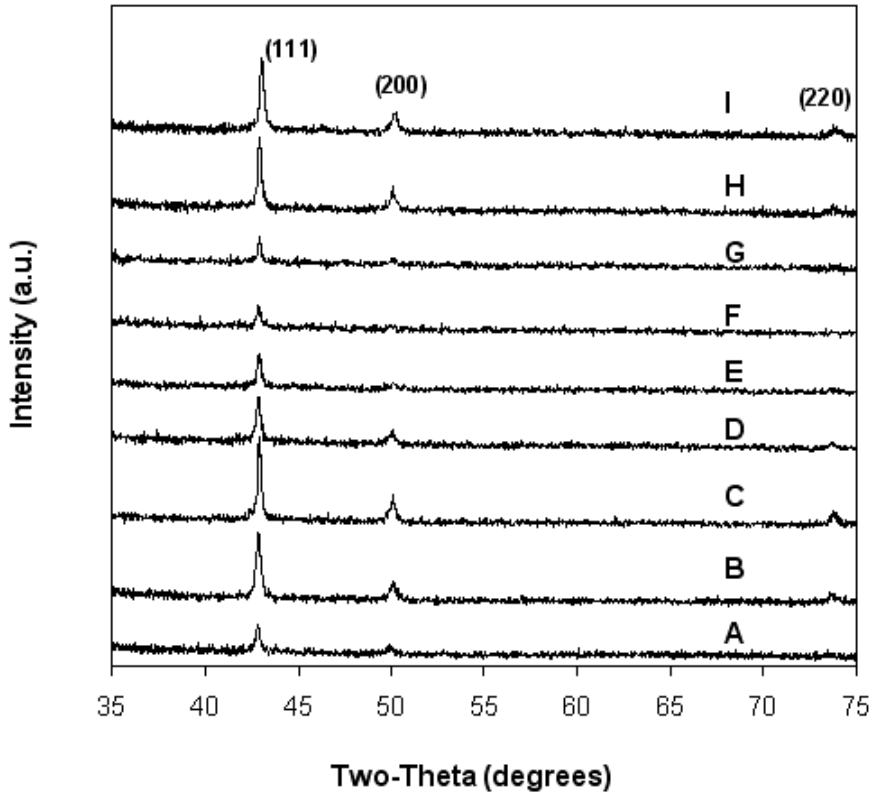

Figure 8.1 Representative XRD patterns of some selected copper metal samples (listed below). *Some of the above XRD patterns have weak diffraction intensities due to a small amount of sample used in the measurement in order to confirm the copper phase (i.e., the diffraction peak locations).

Expt.	NaOH solution		$Cu(NO_3)_2$ solution		Volume of EDA (mL)	Volume of N_2H_4 (35 wt%) (μl)	Temperature (°C)	Time (h)
	Volume (mL)	Concentration (Mol/L)	Volume (mL)	Concentration (Mol/L)				
A	30	7.0	1.0	0.10	0.30	40.0	60	1
B	30	7.0	1.0	0.10	0.35	40.0	60	1
C	30	7.0	1.0	0.10	0.35	60.0	45	3
D	30	7.0	1.0	0.10	0.35	70.0	45	3
E	30	7.0	1.0	0.10	0.40	40.0	60	1
F	30	7.0	1.0	0.10	0.50	25.0	100	1
G	30	7.0	1.0	0.10	0.50	25.0	60	1
H	30	7.0	1.0	0.10	0.50	25.0	60	3
I	30	7.0	1.0	0.10	0.50	40.0	60	1

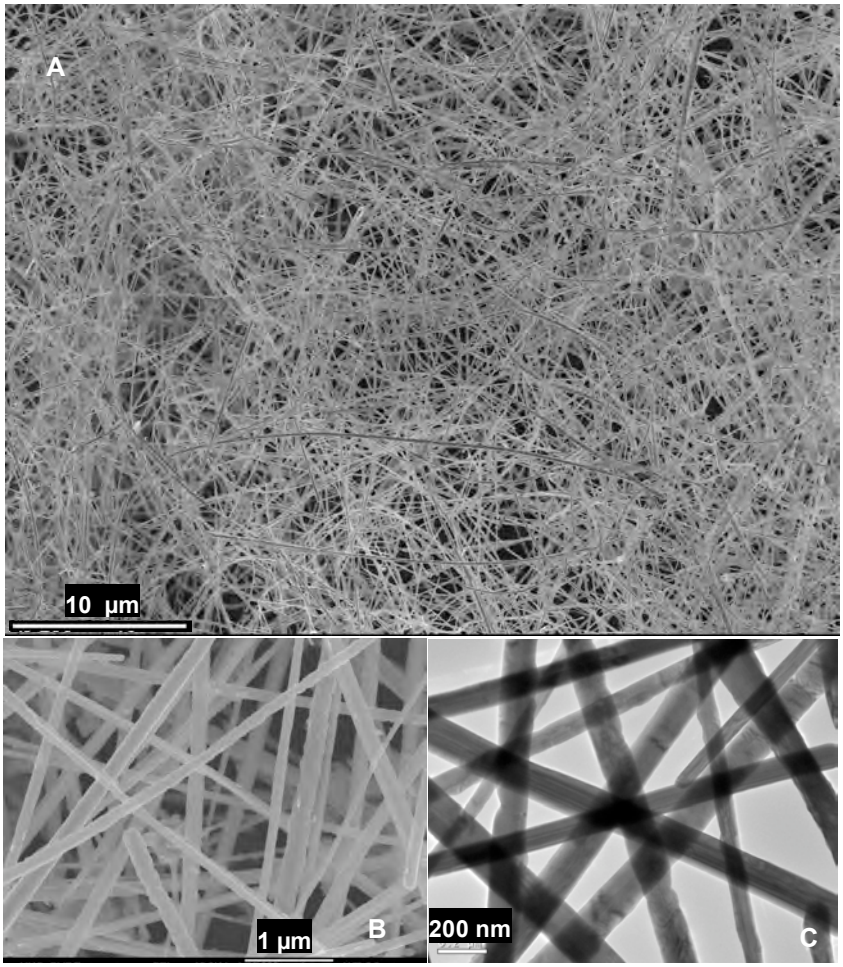

Figure 8.2 (A & B) FESEM images of general and detailed views of Cu nanowires; (C) TEM image of Cu nanowires. (A: Expt. A1; B&C: Expt.A4, see Table 8.1)

the nanowires are straight and highly regulated (Figure 8.2A & B), with constant diameters in the range of 60–160 nm (mostly in 90–120 nm). The wires are ultralong, having lengths of more than 40 μm, which virtually corresponds to an aspect ratio greater than 350! The nanowires obtained are single-crystalline with high lattice perfection (e.g., the lattice fringe d_{111} = 2.10±0.05Å), as shown in Figure 8.3A and B. the growth direction of these wires is along the <110> (Figure 8.3C), on the basis of SAED analysis (Figure 8.3D and Figure 8.4). But the SAED pattern of Figure 8.4B can be indexed to the [001] zone spots and it is scarce in all SAED patterns.

The chemical composition of the nanowires can be further confirmed with EDX technique. Figure 8.5A shows the EDX spectrum of copper nanowires (Figure 8.5B). The results are shown in Table 8.2. The molar ratio of Cu to O is close to 17:1. Considering the absorption of oxygen and oxidation in the drying process, the results demonstrate that the products are copper nanowires.

8.3.2 The reaction procedure

The reaction procedure is shown in Figure 8.6. The reduction of Cu^{2+} to metallic copper in this process is 100%, which is indicated in total disappearance of the Cu^{2+} light blue color. Interestingly, the as-prepared nanowires cake is lifted to the top of solution (Figure 8.6C) due to entrapping of nitrogen bubbles among the nanowires. The sticky solution of the high concentration of NaOH is the reason for nitrogen bubbles diffusing out from the copper nanowires cake. The formation of metallic

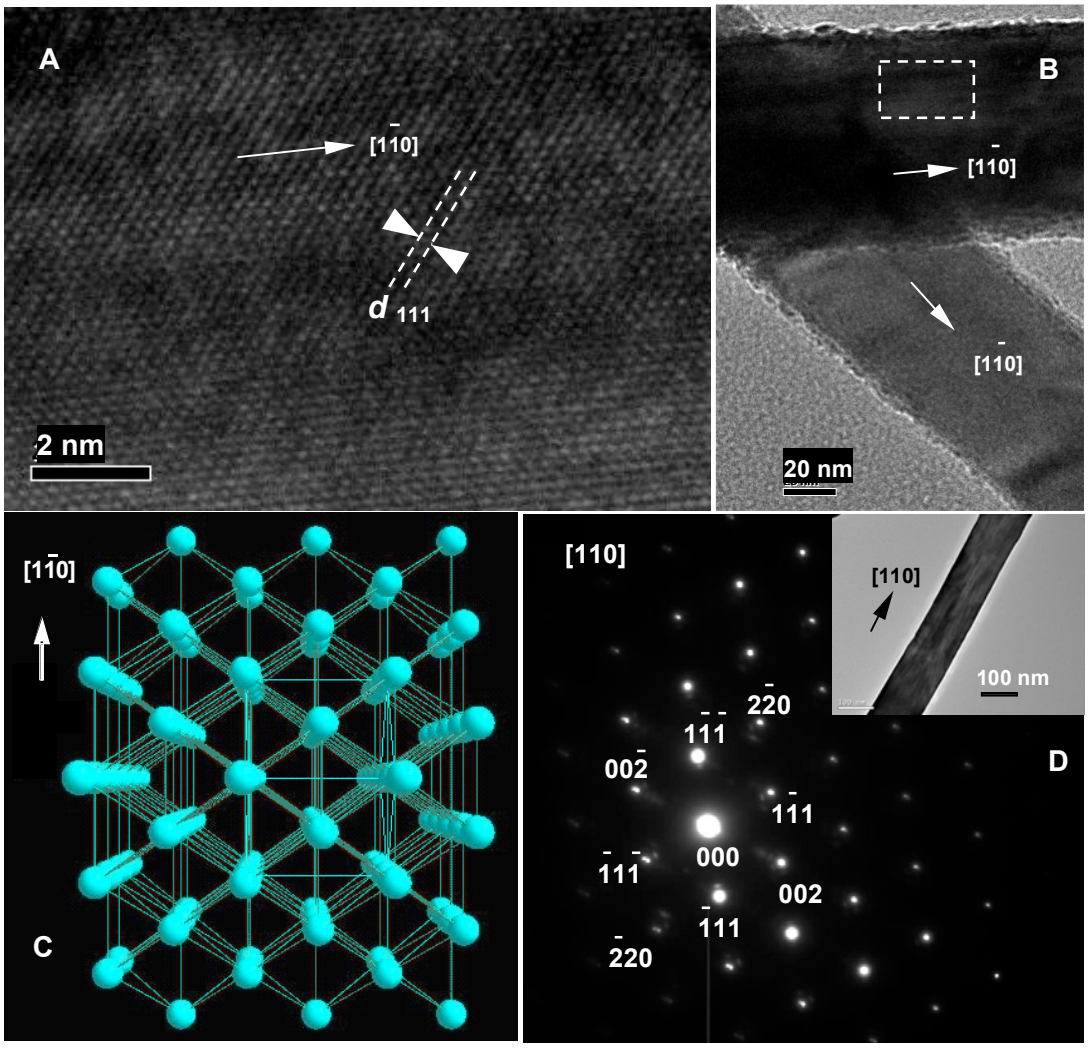

Figure 8.3 (A) HRTEM image of a Cu nanowire; (B) Location of examined area (indicated with a frame) in (A); (C) A bead-line model of the Cu (110) surface; (D) SAED pattern of a Cu nanowires (inset). (sample: Expt.A4, see Table 8.1)

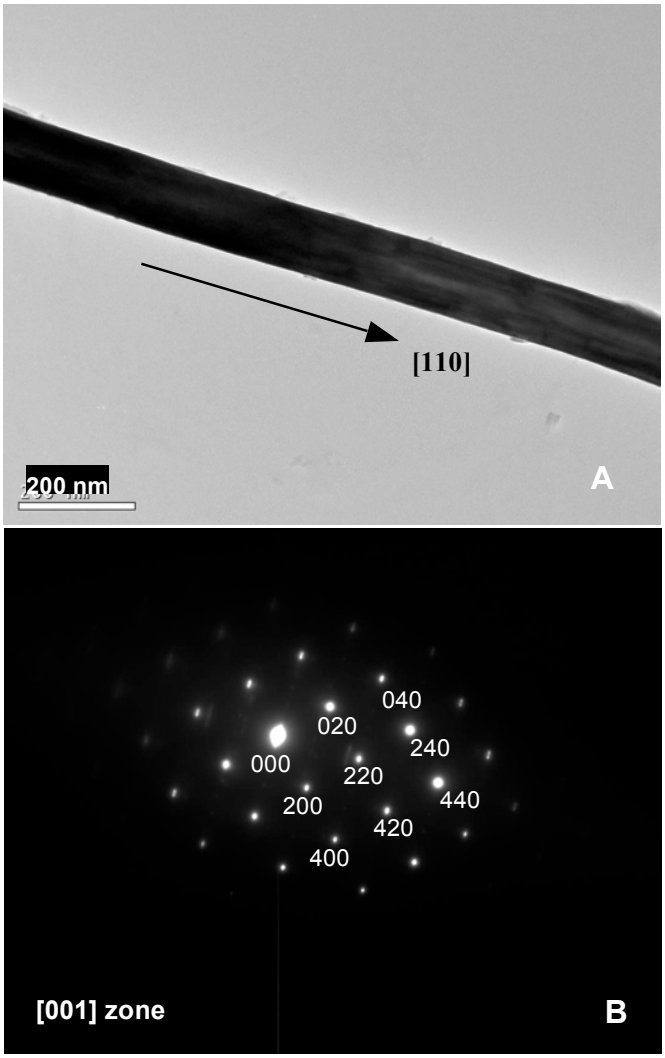

Figure 8.4 (A) TEM image of a Cu nanowire; (B) SAED pattern of the Cu nanowires shown in (A).

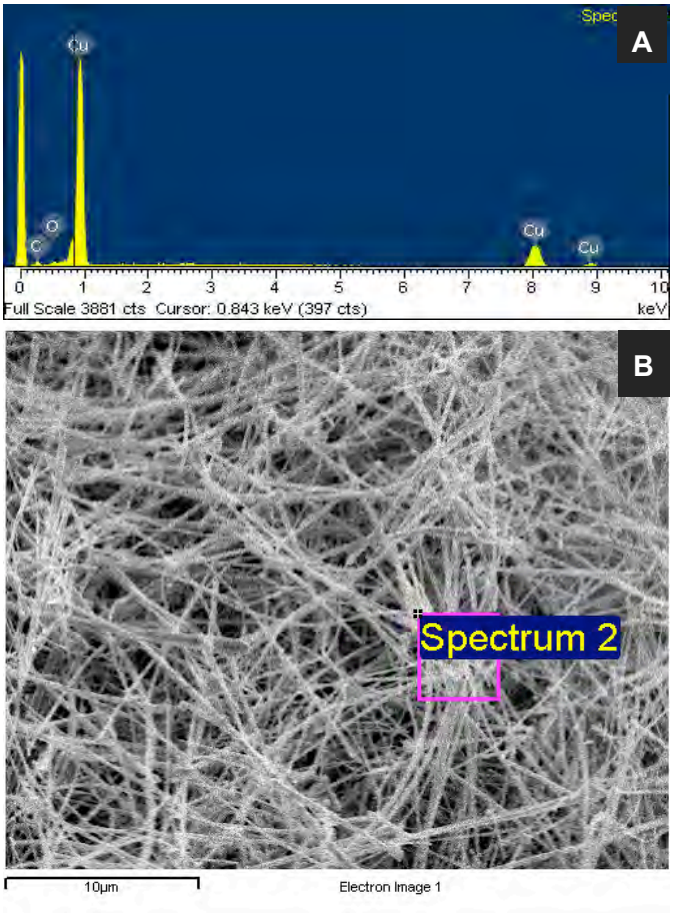

Figure 8.5 The EDX spectrum and corresponding SEM images for Cu nanowire (sample A1).

Table 8.2 EDX analysis result of copper nanowires. (Expt. A1, See Table 8.1)

Element	Weight%	Atomic%
C K	9.42	34.49
O K	1.37	3.77
Cu L	89.21	61.74
Totals	100.00	100.00

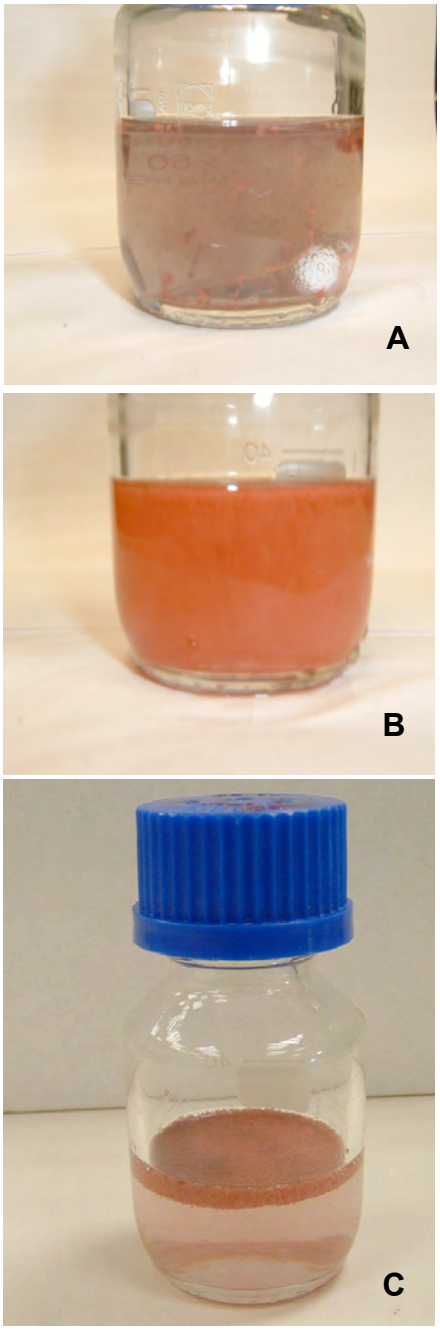

Figure 8.6 Color changing point at 30–40 min: (A) after 30 min at 60 ^{o}C (Expt. A4); (B) after 45 min at 60 ^{o}C. (Expt A4); (C) the final product in the solution after 1 h at 60 ^{o}C (Expt. A1).

copper in this work is based on the following reaction under basic condition:

$$2Cu^{2+} + N_2H_4 + 4OH^- \longrightarrow 2Cu + N_2 + 4H_2O \qquad (8.1)$$

8.3.3 The effects of NaOH and EDA on morphologies of Cu nanowires

Our experiments (Table 8.1) are conducted in high-concentration of NaOH solution and ethylenediamine (EDA) is also indispensable in the experiments. The Cu^{2+} displays a deep blue color in the NaOH high-concentration solution, indicating the formation of $[Cu(OH)_4]^{2-}$. Furthermore, it changes the chemical reaction route, that is, Cu^{2+} is directly reduced to metallic copper by hydrazine without appearance of the Cu_2O in the experiments. A high-concentration of NaOH ensures the formation of limited copper nuclei (seeds), owing to the high viscosity of the solution and diffusion boundary on the resulting nuclei; this nucleation step is crucial for a subsequent steady growth of nanowires. In addition to the control of seed population, the high concentration of this electrolyte also increases overall ion strength of the solution and slows down the growth rate of copper.

On the other hand, a certain amount of EDA is also indispensable to control product morphology. The interplay between NaOH and EDA has been recognized in this work. For example, with a high concentration of NaOH, a required amount of EDA is small, while for lower concentration of NaOH, the amount of EDA has to be increased accordingly in order to obtain high regularity for the 1D product. Table 8.1

(A1-A4) shows the optimized concentration of NaOH and EDA. In each case, there is an optimal molar ratio between the two chemicals. With a moderate amount of EDA, both wire- and disc-like morphologies could be obtained. When EDA was overused, however, the axial 1D growth of nanowires could be switched totally to a radial 2D growth. Figure 8.7 shows XRD patterns and a disc-like morphology of Cu at 100% morphological yield under such a condition. Figure 8.8 shows the morphology of Cu discs. The single-crystal discs also have <110> orientations, as determined by SAED method. Quite commonly, a seed in the center of disc can be identified.

The observed growth preference can be attributed to steric hindrance and charge restriction of starting copper complexes, such as $[Cu(OH)_4]^{2-}$, $[Cu(EDA)(OH)_2]$, and $[Cu(EDA)_2]^{2+}$ etc, on a growing crystal plane, and to synergetic effects of ligand (EDA) and electrolyte (NaOH) on a adsorption and deactivation of the grown part of a product morphology. For example, $[Cu(EDA)_2]^{2+}$ has a planar structure (Figure 8.9), which may guide the direction of $[Cu(EDA)_2]^{2+}$ closing a growing crystal plane.

8.3.4 The growth mechanism of Cu nanowires

According to reports (Liu[6] et al., 2003(c); Molares et al., 2001(a)), the Cu nanowires prepared grew along the <110> direction. In this work, we obtained the same result. Furthermore, the SAED patterns mostly show [110] zone spots, indicating that the copper nanowires settle on the copper grid by (110) plane. It might be deduced that the side face of copper nanowires also grow along (110) plane. These results

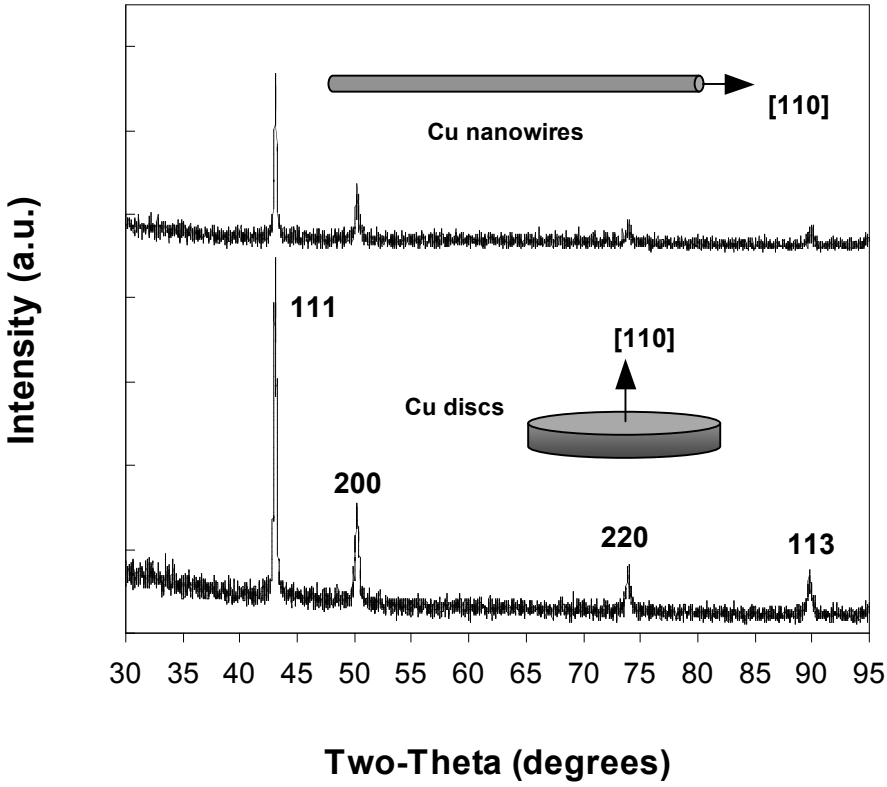

Figure 8.7 XRD patterns of Cu nanowires and discs.

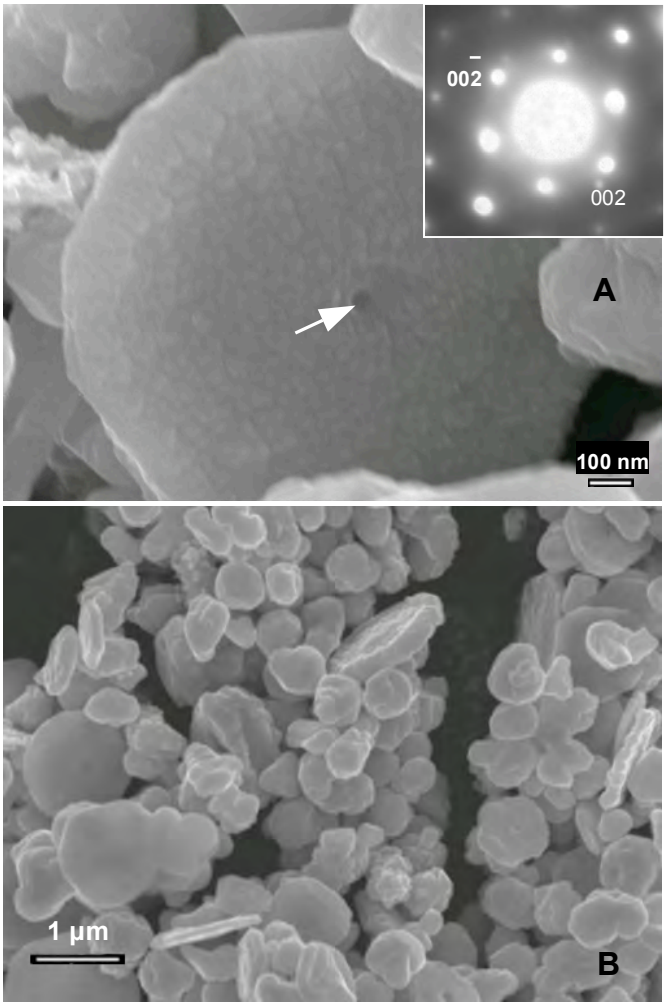

Figure 8.8 FESEM images of a large Cu disc; the white arrow indicates a seed in the center. Inset of (A) shows the [110] zone diffraction spots of Cu disc. (Expt. B2)

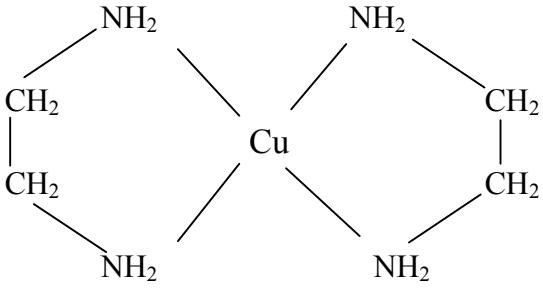

Figure 8.9 Structure of the five-membered ring for $[Cu(EDA)_2]^{2+}$.

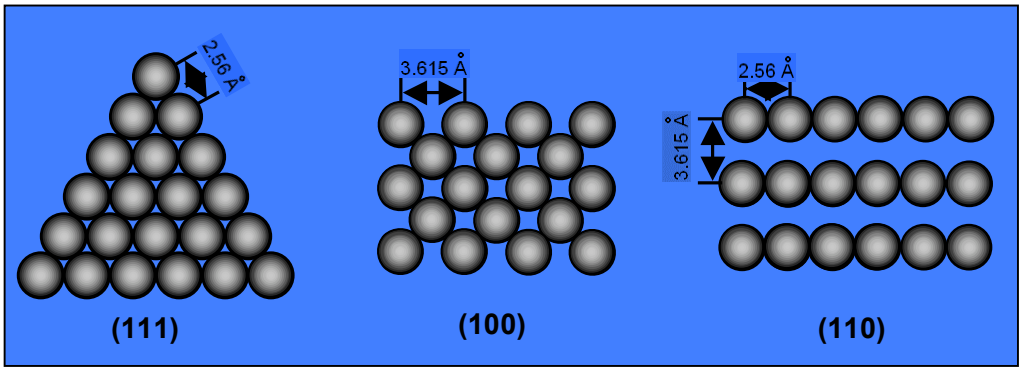

Figure 8.10 The ball model of Cu (111), (100) and (110) planes.

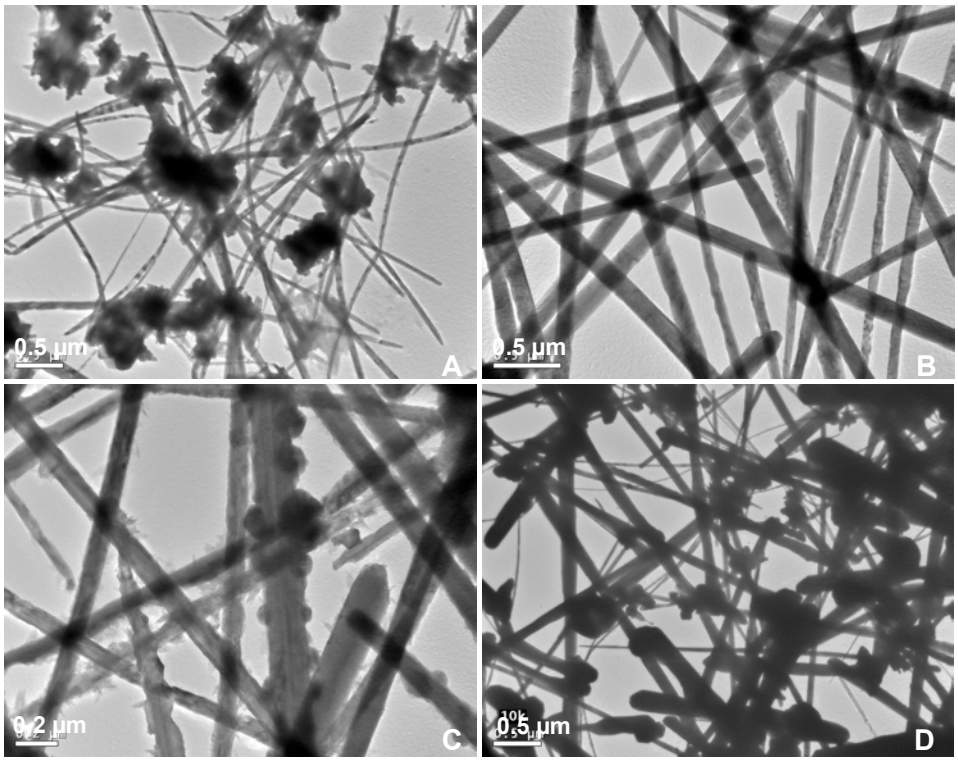

Figure 8.11 The effects of time on morphologies of products: (A) 0.5 h (Expt. D1); (B) 1 h (Expt. A4); (C) 4 h (Expt. D4); (D) 13 h (Expt. D5).

indicate that the (110) plane is a preference growing plane.

As known, the Cu crystal have face-centred cubic (FCC) structure (a_o = 3.615Å) and the radium of Cu atom is 1.28Å (Buchanan, 1997). Figure 8.10 is the ball model of the Cu (111), (100) and (110) planes. From the figure, we find that the atom density of copper is the lowest in (110) planes. Thus it needs the least amount of Cu atoms to form the (110) plane, or the (110) planes grow the fastest if the reducing rate of Cu^{2+} to Cu is same. From Cu crystal structure, we can further understand the growth of Cu nanowires.

In this work, the effect of reaction times on the Cu nanowires was studied. Figure 8.11A to D show the TEM images of samples obtained at 0.5 h, 1 h, 4 h, and 13h, with 7 M NaOH and 0.50 mL EDA in the solution. At 0.5 h, a large amount of Cu particles appear in the sample (Figure 8.11A) and these particles are mainly used as nanoparticle seeds. At the same time, many tenuous nanowires also appear. When the reaction time is prolonged to 1 h, a large amount of nanowires forms (Figure 8.11B) and the $Cu(NO_3)_2$ added is totally reduced to Cu nanowires. When the reaction time is prolonged to 4 h and 13 h, the nanowires obtained become thicker, and large particles are also observed with increase of size and numbers (Figure 8.11C and D). In this process, the Ostwald ripening plays a major role. These images indicate that the nanowire growth comes though the nucleation of the Cu nanoparticles and prolong of the nanowires from these nanoparticles. The results also indicate that the reaction for 1 h is appropriate in this temperature, that is, 60 ^oC.

8.3.5 Surface compositional analysis

XPS spectra of O 1s and Cu $2p_{3/2}$ for our air-dried Cu nanowires (Expt. A1) are displayed in Figure 8.12, and the binding energy (BE) positions of each component are detailed in Table 8.3.

Cu $2p_{3/2}$ XPS spectra is deconvoluted into two peaks (Figure 8.12) and the two copper peaks are at 932.3 and 934.0 eV. Generally, the Cu binding energies of Cu, Cu_2O and CuO peaks are about 932.7 eV, 932.5 eV and 933.6 eV respectively (Espinós et al., 2002). The binding energies of Cu and Cu_2O are very close, and therefore, we can not confirm the peak at 932.3 eV belongs to Cu or Cu_2O. For peak at 934.0 eV, it should attribute to the existence of CuO on the surface of Cu nanowires. The increase from 933.6 eV to 934.0 eV indicates the lower ratio of CuO on the surface, the same as the reported result (Espinós et al., 2002).

O 1s XPS spectra are also very important to confirm the atomic states of the sample surface. O1s XPS spectra can be deconvoluted into four peaks (Figure 8.12). The BE components at 529.5 eV and 530.7 eV, which is commonly known as the oxygen ions (O^{2-}) of metal oxides, could be attributed to the presence of CuO and Cu_2O on the surface. The next high component is at 531.6 eV with a high relative O ratio of 0.337, which is due to the presence of hydroxyl and carbonate groups (Xu[4] and Zeng, 2001; Zemlyanov et al., 1998). In my experiments, a high concentration of NaOH was used in the solution, so according to the O ratio it can be deduced that a

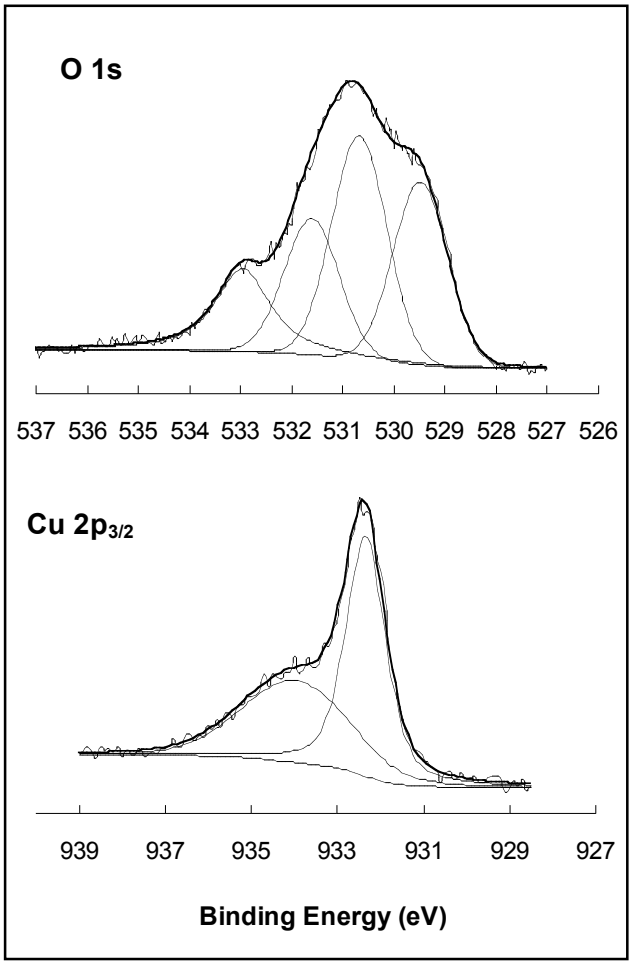

Figure 8.12 XPS spectra of O1s and Cu $2p_{3/2}$ for sample A1.

Table 8.3 Binding energies (BEs) of O 1s and Cu $2p_{3/2}$ and their relative percentage atomic ratios (indicated in parenthesis).

O1s	O in CuO 529.5 (0.276)	O in Cu_2O 530.7 (0.337)	CO_3^{2-} 531.6 (0.208)	H_2O 533.0 (0.177)
Cu $2p_{3/2}$	Cu and/or Cu_2O 932.3 (0.556)		CuO 934.0 (0.444)	

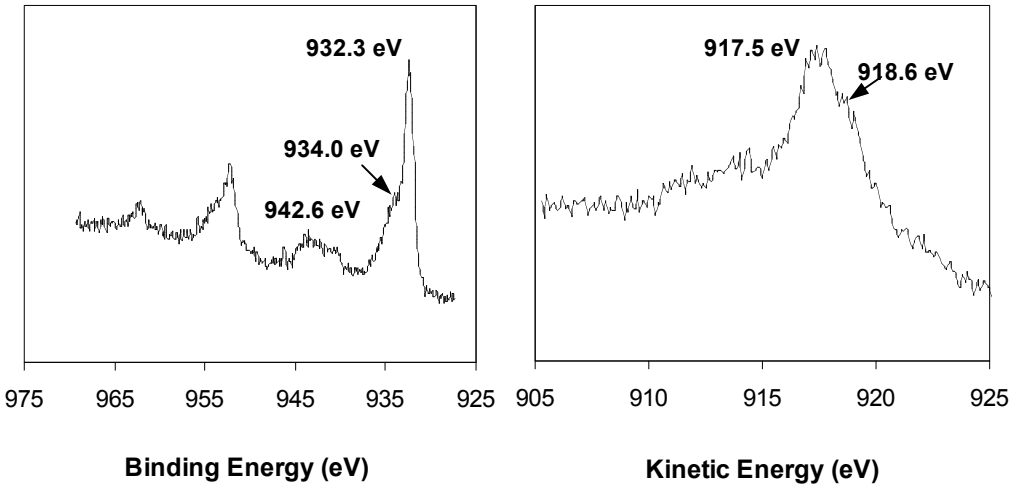

Figure 8.13 Cu 2p XPS spectrum and Cu L_3VV spectrum of sample A1.

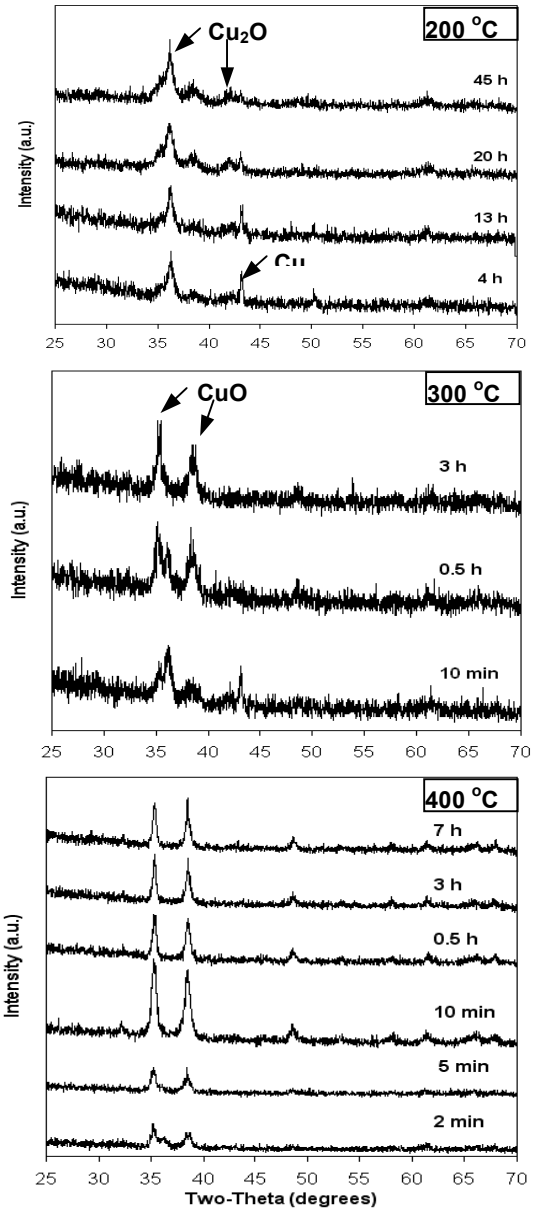

Figure 8.14 XRD pattern of samples obtained by heating Cu nanowires at 200 ^{o}C, 300 ^{o}C, and 400 ^{o}C in a muffled furnace for different times.

large amount of hydroxyl and carbonate groups are adsorbed on the outer layer. The final peak in 533.0 eV is due to the presence of H_2O on the surface (Espinós et al., 2002). From the results of O 1s XPS spectra, we can conclude that the Cu on the surface appear as CuO and Cu_2O. Thus the subpeak of 932.3 eV in Cu $2p_{3/2}$ XPS spectra can be attributed to the existence of Cu_2O.

The same results can be obtained from the Cu 2p XPS spectra and Cu L_3VV auger spectra (Figure 8.13). The binding energy of 932.3 eV and kinetic energy of 917.5 eV indicate the existence of Cu_2O although there are some differences with the values reported (Espinós et al., 2002). It can also be found that there is a week peak at 934.0 eV in the Cu 2p XPS spectra and a week peak at 918.6 eV in the Cu L_3VV auger spectra (Figure 8.13). It is the result of the existence of CuO on the surface of Cu nanowires. The weak split Cu $2p_{3/2}$ peak at 942.6 eV is the specific Cu 2p peak of CuO, which also demonstrates the existence of CuO.

From above analysis of O 1s, Cu 2p XPS and Cu L3VV auger spectra, we know that the Cu nanowires obtained are easily oxidized on the surface in the air, even in the air-drying process. Thus the Cu nanowires prepared are stored in dilute hydrazine solution to preventing the surface oxidation.

8.3.6 Fabrication of CuO nanotubes

The copper nanowires prepared can also be used as solid precursors for

fabrication of other nanostructures. In this work, the copper nanowires prepared were used to fabricate the CuO nanotubes through the direct metal oxidation.

The Cu nanowires prepared were heated at different temperatures (200 ^{o}C, 300 ^{o}C, and 400 ^{o}C) in a muffled furnace for different times. After heating, the samples were directly cooled down in the air. The reaction process is shown by XRD patterns (Figure 8.14). The peaks of Cu, Cu_2O and Cu are indicated in the XRD patterns. From the XRD pattern, we find that the heating temperature has a great influence on the oxidation process of Cu nanowires. At 200 ^{o}C, the Cu nanowires are mainly oxidized to Cu_2O and even heating for 45 h, the main phase is still Cu_2O. When the heating temperature is increased to 300 ^{o}C, the Cu nanowires are totally oxidized to CuO in 3 h, although the process still comes through the intermediate of Cu_2O. At higher heating temperature of 400 ^{o}C, the time of 5 min is enough for Cu nanowires to be totally oxidized to CuO.

Through the TEM analysis, we find that CuO samples prepared have the same morphology. Figure 8.15 shows the CuO nanotubes of one selected sample. From the SAED pattern (Figure 8.15B), it is confirmed that the CuO nanotubes are polycrystalline and still retain the original shape of Cu nanowires.

From XRD patterns (Figure 8.14), the hollowing mechanism may be explained. At 200 ^{o}C, the main phase is Cu_2O, which illustrates that the oxidation process is from Cu, to Cu_2O and then to CuO. The preformed surface Cu_2O may provide good starting points for metal out-diffusion, during which copper moves

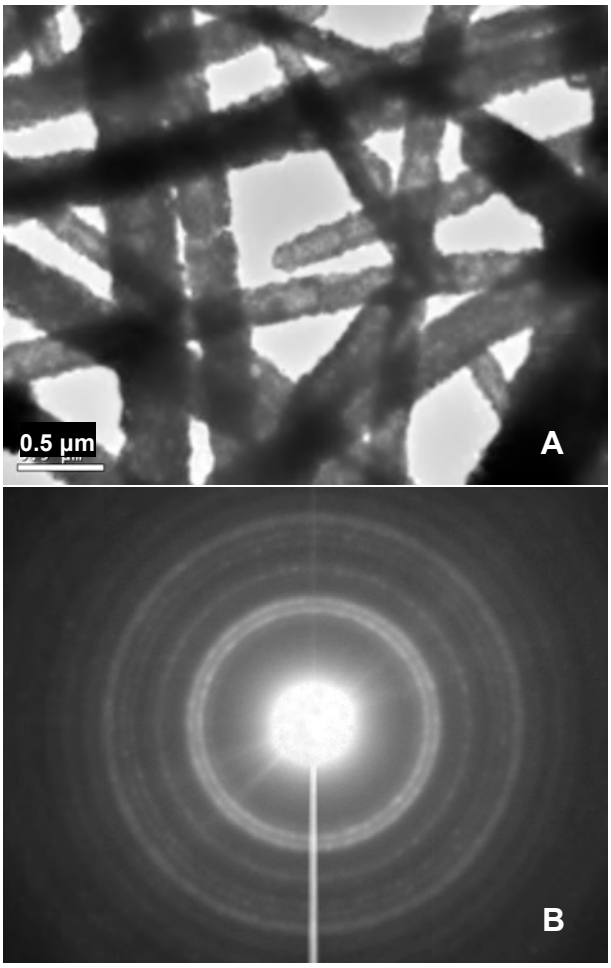

Figure 8.15 (A) TEM image of CuO nanotubes; (B) the SAED of CuO shown in (A).

preferentially toward surface region while oxygen anions on the surface are relatively immobile. The process is the same as the Kirkendall-type diffusion process (Yin[2] et al., 2004). Taking advantage of their interior void (Liu[1] and Zeng, 2004(a); Yin[2] et al., 2004), the polycrystalline CuO (a *p*-type oxide) nanotubes may find new applications in photocatalytic reactions such as water splitting with visible lights.

8.4 Conclusion

In summary, using low-cost starting chemicals, large-scale synthesis of highly regulated ultralong copper nanowires can be achieved under mild conditions, in which a high concentration of NaOH and a small amount of EDA are used to control the morphologies of Cu nanowires. The nanowires prepared are straight and highly regulated, with constant diameters in the range of 60–160 nm (mostly in 90–120 nm). The wires are ultralong, having lengths of more than 40 μm. The growth direction of these wires is along the <110>. The prepared copper nanowires can also be used as starting solid precursor for fabrication of polycrystalline oxide nanotubes via direct oxidation in air. The hollowing mechanism is discussed.

CHAPTER 9
CONCLUSION

9.1 Conclusion

This research studied the synthesis of CuO, Cu_2O and Cu crystallites and fabrication of their nanostructures. The influences of many factors, such as pH, temperature, coordination agents and capping agents, on the reducion and crystallization processes were discussed. Regarding to the research topic, new discoveries and applications presented in the thesis include:

1. One-dimensional CuO nanostructures in rod, wire, ribbon, platelet, and sheet morphologies can be fabricated with the present wet-chemical methods in which water-ethanol mixtures were used as solvents. Through the experiments, the crystal growth process of one-dimensional CuO nanostructures is clearly expanded. At first, single-crystalline monodispersed CuO nanorods with a breadth in the range of 5-15 nm formed by simply changing the starting copper ion concentration. Secondly, rigid or flexible long nanorods and nanoribbons up to 1 μm were prepared in the process of seeding and length growth along the 〈010〉 direction. Through the experiments and analysis of crystal structures, we also discussed the growth mechanism of one-dimensional CuO crystals. Upon the aging treatment, the morphology of formed one-dimensional CuO crystal can be further modified. The rod shortening has been observed due to Ostwald ripening. At the same time, the two-dimensional netted

structure formed owing to the self-assembly of one-dimensional CuO nanorod. Nanoplatelets or sheets of CuO can also be synthesized due to the self-assembly and Ostwald ripening. In this work, a wide variety of synthetic methods and process parameters were investigated, which allows us to fabricate CuO nanostructures with flexibility for the morphological and dimensional control.

2. We systematically studied the effects of pH on the synthesis and morphology of Cu_2O crystals. In acidic condition, the Cu^{2+} cations are directly reduced to Cu^{+} and the Cu_2O single crystals are formed in the reaction process. But in basic condition, the Cu^{2+} at first forms CuO crystallites and then these CuO crystallites aggregate together in the reduction process. Thus the Cu_2O nanoproducts with three different morphologies can be formed with the changes of the solvent. In this study, Cu_2O hollow spheres, hollow cubes and cubes were prepared.

3. In acidic condition, a variety of multipod frameworks of Cu_2O microcrystals were prepared through the careful control of synthetic parameters such as water content, reagent concentrations, and reaction time and temperature. The self-organization of these frameworks can be viewed in the following steps: (i) fractal growth of multipod frameworks from a nucleation center (space expansion), and (ii) attachment of microcrystal building units (space occupation). The greater importance is that the resultant microcrystal stacks (step (ii)) also provide a base for generation of intracrystal porosity and crystal self-amplification. These multipod framework structures of Cu_2O are important in the crystal growth. It not only explains many crystal phenomena, e.g., intracrystal porosity, but also provides instructions in crystal

growth process

4. Simple "one pot" approaches to prepare Cu_2O hollow spheres and hollow cubes through Ostwald ripening were also investigated. Based on the growth experiments and materials characterization, the formation mechanism is completely demonstrated with four different steps: (i) generation of primary nanocrystallites of CuO; (ii) spherical gathering of the primary CuO; (iii) reductive conversion of CuO to Cu_2O; and (iv) crystal aging of Cu_2O and formation of hollow nanospheres or nanocubes. It is an important finding that Ostwald ripening has been utilized in controlling crystallite size of shell structures, and thus for effectively tuning the optical band gap energy of Cu_2O (in the range of 2.405-2.170 eV).

5. In this thesis, a large-scale synthesis of highly regulated ultralong copper nanowires can be achieved under mild conditions. The nanowires prepared are straight and highly regulated, with constant diameters in the range of 60–160 nm (mostly in 90–120 nm). The wires are ultralong, having lengths of more than 40 μm. The growth direction of these wires is along the <110>. The prepared copper nanowires can also be used as starting solid precursor for fabrication of polycrystalline oxide nanotubes via direct oxidation in air.

It can be noted that the basic analysis techniques, such as XRD, TEM, HETEM, SEM, FESEM, AFM, XPS etc show great power in the characterization and determination of material structures and properties.

9.2 Direction for the future work

9.2.1 The synthesis of chiral copper oxide (CuO) nanoparticles

Most of the molecules in the world are chiral, and a wide range of biological and physical functions are related to the strict matching between chiral molecules (Dias, 2000). Thus the chiral selection of molecules has shown great challenges and tremendous potentials in medicinal chemistry and related disciplines. Compared to the stoichiometric use of chiral auxiliaries to separate chiral molecules, the asymmertric synthesis using chiral catalysts is one of the most attractive methods to obtain the pure chiral molecules, and therefore the synthesis of chiral catalysts has attacted more and more attention.

Cupric oxide (CuO, tenorite) is a chiral monoxide compound with monoclinic phase. As an important catalyst in many reactions (Chapter 2), the synthesis of chiral CuO nanoparticles has great significiance in nanochemistry. Recently the chiral CuO films have been electrodeposited on the Cu(111) and Au(001) (Switzer et al., 2003; Bohannan et al., 2004). In this thesis (Chapter 4), one-dimensional (1D) CuO nanostructures in rod, wire, ribbon, platelet, and sheet morphologies have been fabricated with wet-chemical methods. It is expected that CuO chiral single-crystal nanopartilces can be produced in the future study.

In order to synthesize the chiral CuO nanoparticles, tartaric and amino acids could be used as chiral agents (Calvo et al., 1993; Switzer et al., 2003; Bohannan et al., 2004; An et al., 2006). There are two possible approaches to synthesize CuO nanoparticles: (i) the CuO nanoparticles are fabricated directly from Cu^{2+} in chiral

agent solution; (ii) Cu^{2+} is at first tranfered into Cu (II) chiral precursor, and then the formed chiral precursor is decomposed into chiral CuO.

9.2.2 The effects of complexing agent on crystal growth

In Chapters 5-8, many complexing agents (e.g., formic acid, DMF, EDA) were used to control the morphologies and structures of copper and copper oxides. The effects of those complexants need to be confirmed in more details in the future. A systematical invetigation should be done to understand how the ligands coordinate with copper ions and how they activate or deactivate a crystal plane. A better understanding of these influences would help us stabilize certain crystallographic planes and control the crytal growth direction. Moreover, the knowledge accumulation would help us develop more novel methods to synthesize and assemble nanostructures of inorganic materials.

9.2.3 The application of Cu_2O nanoparticles in solar cells

In Chapter 6, Ostwald ripening has been utilized in controlling crystallite size of shell structures, and thus for effectively tuning the optical band gap energy of Cu_2O (in the range of 2.405-2.170 eV). Considering their unique hollow structure and facile tuning in band gap energy, the prepared Cu_2O nanospheres can be potentially used for harvesting solar energy in the visible range. Thus in further research, the application of Cu_2O hollow spheres in the solar cells should be studied.

At the same time, solid-solution redox reactions devised in this research may

also be extendable to future fabrication of Cu-Cu_2O nanocomposites and the application of these composites should also be studied.

9.2.4 Preparation of composite copper nanowires and then electrical measurement of obtained nanowires

In Chapter 8, the prepared copper nanowires are straight and highly regulated, with diameters range of 60–160 nm (populated in 90–120 nm). The wires are ultralong, having lengths of more than 40 μm. To prepare composite Cu nanowires, the surfaces coating with other metals deserves to be one of the future objectives. For example, Ni can be coated on the surface of copper wires *via* Ni-P electroless plating method to prevent the oxidation of pure Cu nanowires; Ag and Au can be coated on the surface of copper wires *via* Galvanic replacement reactions (Sun[3] and Xia, 2002(c); Chen[1] et al., 2005(a, b)) to increase the solderability of copper wires.

After surface coating with a thin layer of other metals, the electrical, thermal and mechanical properties of the composite copper nanowires will be measured to provide the necessary data for their applications in electronic micro-devices. The electrical measurement to individual naonostructures is a challenge to many existing testing techniques owing to the small size of nanostructures. In these years, many methods have developed to measure the nanostructures, for example, three-probe micromachined nanomanipulator for manipulation and *in-situ* characterization of nanomaterials in scanning electron microsope. Nanomeasurements by *in-situ* TEM and Scanning Tunneling Microscope (STM) (Wang[13] et al., 2000(a)) can also be used as

important approaches.

9.2.5 Ag, Au, Pt and Pd nanotubes or nanorods synthesis templated by copper nanowires

Metal nanostructures can be used in many areas, for examples, photography, catalysis, biological labelling, phontonics, optoelectrics, information storage et al (Sun[3] and Xia, 2002(c)). In Chapter 8, the fabricated copper wires have been successfully attempted to work as the templates in the fabrication of CuO nanotubes. In the future, it may also possible to use these copper nanowires as the templates to produce nanotubes or nanorods of other metals through Galvanic replacement reactions, such as Ag, Au, Pd or Pt (Sun[3] and Xia, 2002(c); Chen[1] et al., 2005(a, b)).

The above discussion acknowledges the limitation related to the present study. However, it provides us the new direction in the future research in this field. With the new research and development in this field, copper and copper oxdes (CuO and Cu_2O) will more greatly improve our living qualities.

REFERENCES

Adelung, R., W. Hargung and F. Ernst. Fabrication of Cu-induced networks of linear nanostructures on different length scales, Acta Mater., *50*, pp. 4925-4933. 2002.

Afanasiev, P. and I. Bezverkhy. Genesis of Vesicle-Like and Tubular Morphologies in Inorganic Precipitates: Amorphous Mo Oxysulfides, J. Phys. Chem. B, *107*, pp. 2678-2683. 2003.

Alexander, M.R., S. Payan and T.M. Duc. Interfacial Interactions of Plasma-polymerized Acrylic Acid and an Oxidized Aluminium Surface Investigated using XPS, FTIR and Poly(acrylic acid) as a Model Compound, Surf. Intersurface Anal., *26*, pp. 961-973. 1998.

An, H.-Y., E.-B. Wang, D.-R. Xiao, Y.-G. Li, Z.-M. Su and L. Xu. Chiral 3D Architectures with Helical Channels Constructed from Polyoxometalate Clusters and Copper-Amino Acid Complexes, Angew. Chem. Int. Ed., *45*, pp. 904-908. 2006.

Armstrong, A.R., J. Canales and P.G. Bruce. WO_2Cl_2 Nanotubes and Nanowires, Angew. Chem. Int. Ed., *43*, pp. 4899-4902. 2004.

Averback, R.S., J. Bernholc and D.L. Nelson. (ed). Clusters and Cluster-Assembled Materials, Materials Research Society, *26*, Pittsburgh. 1991.

Azarof, L.V. and M.J. Buerger. The Powder Method in X-Ray Crystallography, New York: McGraw-Hill Book Company. 1958.

Bakkers, E.P.A.M. and M.A. Verheijen. Synthesis of InP Nanotubes, J. Am. Chem. Soc., *125*, pp. 3440-3441. 2003.

Bala, T., S.K. Arumugam, R. Pasricha, B.L.V. Prasad and M. Sastry. Foam-based synthesis of cobalt nanoparticles and their subsequent conversion to $Co_{core}Ag_{shell}$ nanoparticles by a simple transmetallation reaction, J. Mater. Chem., *14*, pp. 1057-1061. 2004.

Balaev, D.A., K.A. Shaihutdinov, S.I. Popkov, D.M. Gokhfeld and M.I. Petrov. Magnetoresistive effect in bulk composites 1-2-3 YBCO+CuO and 1-2-3 YBCO+$BaPb_{1-x}Sn_xO_3$ and their application as magnetic field sensors at 77 K, Supercond. Sci. Technol., *17*, pp. 175-181. 2004.

Balamurugan, B. and B.R. Mehta. Surface-modified CuO layer in size-stabilized single-phase Cu_2O nanoparticles, Appl. Phys. Lett., *79*, pp. 3176-3178. 2001(a).

Balamurugan, B. and B.R. Mehta. Optical and structural properties of nanocrystalline copper oxide thin films prepared by activated reactive evaporation, Thin Solid Films, *396*, pp. 90-96. 2001(b).

Ballauff, M. and C.N. Likos. Dendrimers in Solution: Insight from Theory and Simulation, Angew. Chem. Int. Ed., *43*, pp. 2998-3020. 2004.

Balogh, L. and D.A. Tomalia. Poly(Amidoamine) Derdrimer-Templated Nanocomposites. 1. Synthesis of Zerovalent Copper Nanoclusters, J. Am. Chem. Soc., *120*, pp. 7355-7356. 1998.

Banerjee, I.A., L. Yu and H. Matsui. Cu nanocrystal growth on peptide nanobubes by biomineralization: size control of Cu nanocrystals by tuning peptide conformation, PNAS, *100*, pp. 14678-14682. 2003.

Barr, T.L. and S. Seal. Nature of the use of adventitious carbon as a binding energy standard, J. Vac. Sci. A, *13*, pp. 1239-1246. 1995.

Barrett, E.P., L.G. Joyner and P.C. Halenda. The Determination of Pore Volume and Area Distributions in Porous Substance. I. Computations from Nitrogen Isotherm, J. Am. Chem. Soc., *73*, pp. 373-380. 1951.

Becerril, H.A., R.M. Stoltenberg, C.F. Monson and A.T. Woolley, Ionic surface masking for low background in single- and double-stranded DNA-templated silver and copper nanorods, J. Meter. Chem., *14*, pp. 611-616. 2004.

Black, C.T., C.B. Murray, R.L. Sandstrom and S. Sun. Spin-Dependent Tunneling in Self-Assembled Cobalt-Nanocrystal Superlattices, Science, *290*, pp. 1131-1134. 2000.

Blanco, J., P. Avila, S. Suarez, M. Yates, J.A. Martin, L. Marzo and C. Knapp. CuO/NiO monolithic catalysts for NOx removal from nitric acid plant flue gas, Chem. Eng. J., *97*, pp. 1-9. 2004.

Bohannan, E.W., H.M. Kothari, I.M. Nicic and J.A. Switzer. Enantiospecific Electrodeposition of Chiral CuO Films on Single-Crystal Cu(111), J. Am. Chem. Soc., *126*, pp. 488-489. 2004.

Borgohain, K. and S. Mahamuni. Formation of single-phase CuO quantum particles, J. Mater. Res., *17*, pp. 1220-1223. 2002(a).

Borgohain, K., N. Murase and S. Mahamuni. Synthesis and properties of Cu_2O

quantum particles, J. Appl. Phys., *92*, pp. 1292-1297. 2002(b).

Bowden, N., A. Terfort, J. Carbeck and G.M. Whitesides. Self-Assembly of Mesoscale Objects into Ordered Two-Dimensional Arrays, Science, *276,* pp. 233-235. 1997.

Bravo, J., A. Karim, T. Conant, G.P. Lopez and A. Datye.Wall coating of a $CuO/ZnO/Al_2O_3$ methanol steam reforming catalyst for micro-channel reformers, Chem. Eng. J., *101*, pp. 113-121. 2004.

Breen, T.L., J. Tien, S.R.J. Oliver, T. Hadzic and G.M. Whitesides. Design and Self-Assembly of Open, Regular, 3D Mesostructures, Science, *284*, pp. 948-951. 1999.

Brookshier, M.A., C.C. Chusuei and D.W. Goodman. Control of CuO Particle Size on SiO_2 by Spin Coating, Langmuir, *15*, pp. 2043-2046. 1999.

Brunauer, S., P.H. Emmett and E. Teller. Adsorption of Gases in Multimolecular Layers, J. Am. Chem. Soc., *60*, pp. 309-319. 1938.

Brunauer, S., L.S. Deming, W.S. Deming and E. Teller. A Theory of the van der Waals Adsorption of Gases, J. Am. Chem. Soc., *62*, pp. 1723-1732. 1940.

Brundle, C.R., C.A. Evans and S. Wilson. Encyclopedia of Materials Characterization, Boston: Butterworth-Heinemann. 1992.

Buchanan, R.C. Materials crystal chemistry. pp. 105, 241. New York: Marcel Dekker. 1997.

Bulle-Lieuwma, C.W.T., W. Coene and A.F. de Jong. High-Resolution Electron Microscopy of Semiconductors and Metals, Adv. Mater., *3*, pp. 368-378. 1991.

Bush, A.A., V.Y. Shkuratov, A.B. Kuz'menko and E.A. Tishchenko. Growth and Morphological Study of Copper Oxide Single Crystals, Crystallogr. Rep., *47*, pp. 335-339. 2002.

Calcutt, V. Introduction to Copper, Innovations (www. copper. org), August 1st. 2001.

Calvo, R., C.A. Steren, O.E. Piro, T. Rojo, F.J. Zuñiga and E.E. Castellano. Crystal Structure and Magnetic Properties of Diaqua(L-aspartato)copper(II), Inorg. Chem., *32*, pp. 6016-6022. 1993.

Campbell, C.T., K.A. Daube and J.M. White, Cu/ZnO(0001) and Cu(111): Model Catalysts for Methanol Synthesis. Surf. Sci., 182, pp. 458-476. 1987.

Cao[1], M., C. Hu, Y. Wang, Y. Guo, C. Guo and E. Wang. A controllable synthetic

route to Cu, Cu_2O, and CuO nanotubes and nanorods, Chem. Commun., pp. 1884-1885. 2003(a).

Cao[1], M., C. Hu, G. Peng, Y. Qi and E.Wang.Selected-Control Synthesis of PbO_2 and Pb_3O_4 Single-Crystalline Nanorods**,** J. Am. Chem. Soc**.,** *125,* pp. 4982-4983. 2003(b)**.**

Cao[2], X., F. Yu, L. Li, Z. Yao and Y. Xie. Copper nanorod junctions templated by a novel polymer-surfactant aggregate, J. Cryst. Growth, *254*, pp. 164-168. 2003.

Carnes, C.L., J. Stipp, K.J. Klabunde and J. Bonevich. Synthesis, Characterization, and Adsorption Studies of Nanocrystalline Copper Oxide and Nickel Oxide, Langmuir, *18*, pp. 1352-1359. 2002.

Caruso[1], F. and R.A. Caruso. Nanoengineering of Inorganic and Hybrid Hollow Spheres by Colloidal Templating, Science, *282*, pp. 1111-1114. 1998.

Caruso[1], F., M. Spasova, A. Susha, M. Giersig and A.R. Caruso. Magnetic Nanocomposite Particles and Hollow Spheres Constructed by a Sequential Layering Approach, Chem. Mater., *13*, pp. 109-116. 2001(a).

Caruso[1], F. Nanoengineering of particle Surfaces, Adv. Mater., *13*, pp. 11-22. 2001(b).

Caruso[2], R.A., A. Susha and F. Caruso. Multilayered Titania, Silica, and Laponite Nanoparticle Coatings on Polystyrene Colloidal Templates and Resulting Inorganic Hollow Spheres, Chem. Mater., *13*, pp. 400-409. 2001.

Cason, J.P., M.E. Miller, J.B. Thompson and C.B. Roberts. Solvent Effects on Copper Nanoparticle Growth Behavior in AOT Reverse Micelle Systems, J. Phys. Chem. B, *105*, pp. 2297-2302. 2001.

Cheetham, A.K. and P. Day. Solid-state Chemistry: Techniques, Clarendon Press: Oxford, pp. 79. 1987.

Chemseddine, A. and T. Moritz. Nanostructuring Titania: Control over Nanocrystal Structure, Size, Shape, and Organization, Eur. J. Inorg. Chem., pp. 235-245. 1999.

Chen[1], J., S.-L. Li, F. Gao and Z.-L. Tao. Synthesis and Characterization of WS_2 Nanotubes, Chem. Mater., *15*, pp. 1012-1019. 2003.

Chen[1], J., Z.-L. Tao and S.-L. Li. Fabrication of Ru and Ru-Based Functionalized Nanotubes, J. Am. Chem. Soc., *126*, pp. 3060-3061. 2004.

Chen[1], J., B. Wiley, J. McLellan, Y. Xiong, Z.-Y. Li and Y. Xia. Optical Proerties of Pd-Ag and Pt-Ag Nanoboxes Synthesized via Galvanic Replacement reactions, Nano

Lett., *5*, pp. 2058-2062. 2005(a).

Chen[1], J., B. Wiley, Z.-Y. Li, D. Campbell, F. Saeki, H. Cang, L. Au, J. Lee, X. Li and Y. Xia. Optical Proerties of Pd-Ag and Pt-Ag Nanoboxes Synthesized via Galvanic Replacement reactions, Nano Lett., *5*, pp. 2058-2062. 2005(b).

Chen[2], S. and J.M. Sommers. Alkanethiolate-Protected Copper Nanoparticles: Spectroscopy, Electrochemistry, and Solid-State Morphological Evolution, J. Phys. Chem. B, *105*, pp. 8816-8820. 2001.

Chen[3], S.-J., X.-T. Chen, Z. Xue, L.-H. Li and X.-Z. You. Solvothermal preparation of Cu_2O crystalline particles, J. Crystal Growth, *246*, pp. 169-175. 2002.

Chen[4], Z.-Z., E.-W. Shi, Y.-Q. Zheng, W.-J. Li, B. Xiao and J.-Y. Zhuang. Growth of hex-pod-like Cu_2O whisker under hydrothermal conditions, J. Cryst. Growth, *249*, pp. 294-300. 2003.

Chen[5], M., Y. Xie, J. Lu, Y. Xiong, S. Zhang, Y. Qian and X. Liu. Synthesis of rod-, twinrod-, and tetrapod-shaped CdS nanocrystals using a highly oriented solvothermal recrystallization technique, J. Mater. Chem*., 12*, pp. 748-753. 2002.

Choi, H. and S.-H. Park. Seedless Growth of Free-Standing Copper Nanowires by Chemical Vapor Deposition, J. Am. Chem. Soc., *126*, pp. 6248-6249. 2004.

Collins, A.M., C. Spickermann and S. Mann. Synthesis of titania hollow microspheres using non-aqueous emulsions, J. Mater. Chem., *13*, pp. 1112-1114. 2003.

Cruccolini, A, R. Narducci and R. Palombari. Gas adsorption effects on surface conductivity of nonstoichiometric CuO, Sens. Actuators B, *98*, pp. 227-232. 2004.

Cullity, B.D. Elements of X-Ray Diffraction, 2nd ed, Massachusetts: Addison-Wesley. 1978.

Deki, S., K. Akamatsu, T. Yano, M. Mizuhata and A. Kajinami. Preparation and characterization of copper(I) oxide nanoparticles dispersed in a polymer matrix, J. Mater. Chem., *8*, pp. 1865-1868. 1998.

Deutscher, G. and Y. Lereah. Phase Separation by Coupled Single-Crystal Growth and Polycrystalline Fingering in Al-Ge: Experiment, Phys. Rev. Lett., *60,* pp. 1510-1513. 1988.

Dhas, N.A., C.P. Raj and A. Gedanken. Synthesis, Characterization, and Properties of Metallic Copper Nanoparticles, Chem. Mater., *10*, pp. 1446-1452. 1998.

Dias, L.C. Chiral Lewis Acid Catalyzed Ene-Reactions, Curr. Org. chem., *4*, pp. 305-342. 2002.

Dinsmore, A.D., M.F. Hsu, M.G. Nikolaides, M.Marquez, A.R. Bausch and D.A. Weits. Colloidosomes: Selectively Permeable Capsules Composed of Colloidal Particles, Science, *298*, pp. 1006-1009. 2002.

Dong, Y., Y. Li, C. Wang, A. Cui and Z. Deng. Preparation of Cuprous Oxide Particles of Different Crystallinity, J. Colloid Interface Sci., *243*, pp. 85-89. 2001.

Du, G.H. and G.V. Tendeloo. $Cu(OH)_2$ nanowires, CuO nanowires and CuO nanobelts, Chem. Phys. Lett., *393*, pp. 64-69. 2004.

Dumestre, F., B. Chaudret, C. Amiens, P. Renaud and P. Fejues. Superlattices of Iron Nanocubes Synthesized from $Fe[N(SiMe_3)_2]_2$, Science, *303*, pp. 821-823. 2004.

Ebisuzaki, Y. Preparation of Monocrystalline Cuprous Oxide, J. Appl. Phys., *32*, pp. 2027-2028. 1961.

Ermakova, L.L., V.V. Puzakov and A.D. Improving the manufacture of powderd copper (I) oxide, Lanskikh, Tsvetn. Met., *7*, pp. 35-37. 1986.

Espinós, J.P., J. Morales, A. barranco, A. Caballero, J.P. Holgado and A.R. González-Elipe. Interface Effects for Cu, CuO and Cu_2O Deposited on SiO_2 and ZrO_2, XPS determination of the Valence State of Copper in Cu/SiO_2 and Cu/ZrO_2 Catalysts, J. Phyc. Chem. B, *106*, pp. 6921-6929. 2002.

Fan, H., L. Yang, W. Hua, X. Wu, Z. Wu, S. Xie and B. Zou. Controlled synthesis of monodispersed CuO nanocrystals, Nanotechnology, *15*, pp. 37-42. 2004.

Faul, C.F.J. and M. Antonietti. Ionnic Self-Assembly: Facile Synthesis of Supramolecular Materials, Adv. Mater., *15*, pp. 673-683. 2003.

Feldman, L.C. and J.W. Mayer. Fundamentals of Surface and Thin Film Analysis, New York: North-Holland. 1986.

Feng, J. and H.C. Zeng. Size-Controlled Growth of Co_3O_4 Nanocubes, Chem. Mater., *15*, pp. 2829-2835. 2003.

Feng, X., L. Feng, M. Jin, J. Zhai, L.Jiang and D. Zhu. Reversible Super-hydrophobicity to Super-hydrophilicity Transition of Aligned ZnO Nanorod Films, J. Am. Chem. Soc.; *126*, pp. 62-63. 2004.

Fenoglio, R., P. Rolandi, P. Massa, J. Gonzalez and P. Haure. Characterization of

CuO/Al_2O_3 catalysts used in the oxidation of phenol solutions, Reaction Kinetics Catal. Lett., *81*, pp. 83-90. 2004.

Fernando, C.A.N., P.H.C. de Silva, S.K. Wethasinha, I.M. Dharmadasa, T. Delsol and M.C. Simmonds. Investigation of n-type Cu_2O layers prepared by a low cost chemical method for use in photovoltaic thin film solar cells, Renewable Energy, *26*, pp. 521-529. 2002.

Floriano, P.N., C.O. Noble, IV, J.M. Schoonmaker, E.D. Poliakoff and R.L. McCarley. Cu(0) Nanoclusters Derived from Poly(propylene imine) Dendrimer Complexes of Cu(II), J. Am. Chem. Soc., *123*, pp. 10545-10553. 2001.

Fu, A., C.M. Micheel, J. Cha, H. Chang, H. Yang, and A.P. Alivisatos. Discrete Nanostructures of Quantum Dots/Au with DNA, J. Am. Chem. Soc., *126*, pp. 10832-110833. 2004.

Fudouzi, H. and Y. Xia. Colloidal Crystals with Tunable colors and Their Use as Photonic Papers, Langmuir, *19*, pp. 9553-9660. 2003.

Fultz, B. and J. Howe. Transmission Electron Microscopy and Diffraction of Materials, New York: Springer. 2001.

Gao[1], F., Q. Lu, S. Xie and D. Zhao**.** A Simple Route for the Synthesis of Multi-Armed CdS Nanorod-Based Materials, Adv. Mater., *14,* pp. 1537-1540. 2002.

Gao[2], T., G. Meng, Y. Wang, S. Sun and L. Zhang. Electrochemical synthesis of copper nanowires, J. Phys.: Condens. Matter, *14*, pp. 355-363. 2002.

Gao[3], Y. and S.A. Elder. TEM study of TiO_2 nanocrystals with different particle size and shape, Mater. Lett., *44,* pp. 228-232. 2000.

García-Martínez, O., R.M. Rojas, E. Vila and J.L. Martın de Vidales. Microstructural characterization of nanocrystals of ZnO and CuO obtained from basic salts, Solid State Ionics, *63-65*, pp. 442-449. 1993.

Gates, B., Y. Wu, Y. Yin, P. Yang and Y. Xia. Single-Crystalline Nanowires of Ag_2Se Can Be Synthesized by Templating against Nanowires of Trigonal Se, J. Am. Chem. Soc., *123*, pp. 11500-11501. 2001.

Geissler, M. and Y. Xia. Patterning: Principles and Some New Developments, Adv. Mater., *16*, pp. 1249-1269. 2004.

Gillingham D.M., C. Müller and J.A. Bland. Spin-dependent quantum transport effects in Cu nanowires, J. phys.:Condens. Matter, *15*, pp. L291-296. 2003.

Goldberger, J., R. He, Y. Zhang, S. Lee, H. Yan, H.-J. Choi and P. Yang. Single-crystal gallium ntride nanotubes, Nature, *422*, pp. 599-602. 2003.

Golden, T.D., M.G. Shumsky, Y. Zhou, R.A. VanderWerf, R.A. Van Leeuwen and J.A. Switzer. Electrochemical Deposition of Copper(I) Oxide Films, Chem. Mater., *8*, pp. 2499-2504. 1996.

Göltner, C.G. Porous Solids from Rigid Colloidal Templates: Morphogenesis, Angew. Chem. Int. Ed., *38,* pp. 3155-3156. 1999.

Gou, L. and C.J. Murphy. Solution-Phase Synthesis of Cu_2O Nanocubes, Nano Lett., *3*, pp. 231-234. 2003.

Gou, L. and C.J. Murphy. Controlling the size of Cu_2O Nanocubes from 200 to 25 nm, J. Mater. Chem., *14*, pp. 735-738. 2004.

Gracias, D.H., J. Tien, T.L. Breen, C. Hsu and G.M. Whitesides. Forming Electrical Networks in Three Dimensions by Self-Assembly, Science, *289*, pp. 1170-1172. 2000.

Gredig, S.V., R.A. Köppel and A. Baiker. Synthesis of methylamines from carbon dioxide, hydrogen and ammonia over supported copper catalysts. Influence of support, J. Mol. Catal. A: Chemical, *127*, pp. 133-142. 1997.

Guo, L., Z.H. Wu, K. Ibrahim, T. Liu, Y. Tao and X. Ju. Research of nonlinear optical properties of copper nanoparticles, Eur. Phys. J. D, *9*, pp. 591-594. 1999.

Guo, L., Y.L. Ji, H. Xu, P. Simon and Z. Wu. Regularly Shaped, Single-Crystalline ZnO Nanorods with Wurtzite Structure, J. Am. Chem. Soc., *124*, pp. 14864-14865. 2002.

Guo, L., C. Liu, R. Wang, H. Xu, Z. Wu and S. Yang. Large-Scale Synthesis of Uniform Nanotubes of a Nickel Complex by a Solution Chemical Route, J. Am. Chem. Soc., *126*, pp. 4530-4531. 2004.

Guo[1], C.-W., Y. Cao, S.-H. Xie, W.-L. Dai and K.-N. Fan. Fabrication of mesoporous core-shell structured titania microspheres with hollow interiors, Chem. Commun., pp. 700-701. 2003.

Hagrman, P.J., D. Hagrman and J. Zubieta. Organic-Inorganic Hybrid Materials: From "Simple" Coordination Polymers to Organodiamine-Templated Molybdenum Oxides, Angew. Chem. Int. Ed., *38*, pp. 2638-2684. 1999.

Hah, H.J., J.S. Kim, B.J. Jeon, S.M. Koo and Y.E. Lee. Simple preparation of

monodisperse hollow silica particles without using templates, Chem. Commun., pp. 1712-1713. 2003.

Hamada, S., Y. Kudo and T. Tojo. Preparation and reduction kinetics of uniform copper particles from copper(I) oxides with hydrogen, Colloids and Surfaces, *67*, pp. 45-51. 1992.

Hames, Y. and S.E. San. CdO/Cu_2O solar cells by chemical deposition, Solar Energy, *77*, pp. 291–294. 2004.

Hammerschmidt, W., A. Baiker, A. Wokaun and W. Fluhr. Copper catalyzed synthesis of cyclic amines from aminoalcohols, Appl. Catal., *20*, pp. 305-312. 1986.

Hampden-Smith, M.J. and L.V. Interrante. Introductory Terms and Concept, pp. 1-18. Interrante, L.V. and M.J. Hampden-Smith (ed). Chemistry of Advanced Materials: An Overview, New York: Wiley-VCH. 1998.

He, Y. and Y. Zhu. Solvothermal Synthesis of Sodium and Potassium Tantaleate Perovskite Nanocubes, Chem. Lett., *33,* pp. 900-901. 2004.

Henglein, A. Formation and Absorption Spectrum of Copper nanoparticles from the Radiolytic Reduction of $Cu(CN)_2^-$, J. phys. Chem. B, *104*, pp. 1206-1211. 2000.

Hentze, H.P., S.R. Raghavan, C.A. McKelvey and E.W. Kaler. Silica Hollow Spheres by Templating of Catanionic Vesicles, Langmuir, *19*, pp. 1069-1074. 2003.

Hill, J.P., W. Jin, A. Kosaka, T. Fukushima, H. Ichihara, T. Shimomura, K. Ito, T. Hashizume, N. Ishii and T. Aida. Self–Assembled Hexa-*peri*-hexabenzocoronene Graphitic Nanotube, Science, *304*, pp. 1481-1483. 2004.

Hong, Z.S., Y. Cao and J.F. Deng. A convenient alcohothermal approach for low temperature synthesis of CuO nanoparticles, Mater. Lett., *52,* pp. 34-38. 2002.

Hsieh, C.-T., J.-M. Chen, H.-H. Lin and H.-C Shih. Synthesis of well-ordered CuO nanofibers by a self-catalytic growth mechanism, Appl. Phys. Lett., *82*, pp. 3316-3318. 2003.

Hsu, P.W., R. Yu and E. Matijević, Preparation and characterization of uniform particles of pure and coated metallic copper, Powder Technology, *63*, pp. 265-275. 1990.

Hu[1], J., Y. Bando, J. Zhan and D. Golberg. Sn-Filled Single-Crytalline Wurtzite-Type ZnS Nanotubes, Angew. Chem. Int. Ed., *43*, pp. 4606-4609. 2004.

Hu[2], Y., J. Chen, W. Chen, X. Lin and X. Li. Synthesis of Novel Nickel Sulfide Submicrometer Hollow Spheres, Adv. Mater., *15,* pp. 726-729. 2003.

Huang, C.L., R.E. Partch and E. Matijevic. Coating of Uniform Inorganic Particles with Polymers: II. Polyaniline on Copper Oxide, J. Colloid Interface Sci., *170*, pp. 275-283. 1995.

Huang, H.H., F.Q. Yan, Y.M. Kek, C.H. Chew, G.Q. Xu, W. Ji, P.S. Oh and S.H. Tang. Synthesis, Characterization, and Nonlinear Optical Properties of Copper Nanoparticles, langmuir, *13*, pp. 172-175. 1997.

Hwang, G.L., K.C. Hwang, Y.-T. Shieh and S.-J. Lin. Preparation of Carbon Nanotube Encapsulated Copper Nanowires and Their use as a Reinforcement for Y-Ba-Cu-O Superconductors, Chem. Mater., *15*, pp. 1353-1357. 2003.

Hyeon, T. Chemical synthesis of magnetic nanoparticles, Chem. Commun., pp. 927-934. 2003.

Iijima, S. Helical microtubules of graphitic carbon, Nature, *354*, pp. 56-58. 1991.

Ikkala, O. and G. ten Brinke. Functional Materials Based on Self-assembly of Polymeric Supramolecules, Science, *295*, pp. 2407-2409. 2002.

Ito, T. Simple Criterion for Wurtzite-Zinc-Blende Polytypism in Semiconductors, Jpn. J. Appl. Phys., *37*, pp. L1217-L1220. 1998(a).

Ito, T., H. Yamaguchi, K. Okabe and T. Masumi. Single-crystal growth and characterization of Cu_2O and CuO, J. Mater. Sci., *33*, pp. 3555-3566. 1998(b).

Jacobs, H.O., A.R. Tao, A. Schwartz, D.H. Gracias an G.M. Whitesides. Fabrication of a Cylindrical Display by Patterned Assembly, Science, *296*, pp. 323-325. 2002.

Jana, N.R., Y. Chen and X. Peng. Size- and Shape-Controlled Magnetic (Cr, Mn, Fe, Co, Ni) Oxide Nanocrystals via a Simple and General Approach, Chem. Mater., *16*, pp. 3931-3935. 2004.

Jiang[1], X.C., T. Herricks and Y.N. Xia. CuO Nanowires Can Be Synthesized by Heating Copper Substrates in Air, Nano Lett., *2*, pp. 1333-1338. 2002.

Jiang[1], X., B. Mayers, T. Herricks and Y. Xia. Direct Synthesis of Se@CdSe Nanocables and CdSe Nanotubes by Reacting Cadmium Salts with Se Nanowires, Adv. Mater., *15*, pp. 1740-1743. 2003.

Jiang[1], X., T. Herricks and Y. Xia. Monodispersed Spherical Colloids of Titania:

Synthesis, characterization, and Crystallization, Adv. Mater., *15*, pp. 1205-1209. 2003(a).

Jiang[2], X.Y., G.H. Ding, L.P. Lou, Y.X. Chen and X.M. Zheng. Catalytic activities of CuO/TiO_2 and $CuO\text{-}ZrO_2/TiO_2$ in NO+CO reaction, J. Molecular Catal. A, *218*, pp. 187-195. 2004.

Jiang[3], Y., Y. Wu, S. Zhang, C. Xu, W. Yu, Y. Xie and Y. Qian. A Catalytic-Assembly Solvothermal Route to Multiwall Carbon Nanotubes at a Moderate Temperature, J. Am. Chem. Soc., *122*, pp. 12383-12384. 2000.

Jin, R., Y. Cao, C.A. Mirkin, K.L. Kelly, G.C. Schatz and J.G. Zheng. Photoinduced Conversion of Silver Nanospheres to Nanoprisms, Science, *294*, pp. 1901-1904. 2001.

Jin, R., Y.C. Cao, E. Hao, G.S. Métraux, G.C. Schatz and C.A. Mirkin. Controlling Anisotropic Nanoparticle Growth Through Plasmon Excitation, Nature, *425*, pp. 487-490. 2003.

Jin, R., S. Egusa and N.F. Scherer. Thermally-Induced Formation of Atomic Au Clusters and Conversion into Nanocubes, J. Am. Chem. Soc., *126*, pp. 9900-9901. 2004.

Joseph, G. Copper: its trade, manufacture, use, and environmental status**.** pp. 331-371. Materials Park, Ohio : ASM International. 1999.

Jun, Y.W., S.M. Lee, N.J. Kang and J. Cheon. Controlled Synthesis of Multi-armed CdS Nanorod Architectures Using Monosurfactant System, J. Am. Chem. Soc*., 123*, pp. 5150-5151. 2001.

Jun, Y.W., Y.Y. Jung and J. Cheon. Architectural Control of Magnetic Semiconductor Nanocrystals, J. Am. Chem. Soc*., 124*, pp. 615-619. 2002.

Jung, C.R., J. Han, S.W. Nam, T.H. Lim, S.A. Hong and H.I. Lee. Selective oxidation of CO over $CuO\text{-}CeO_2$ catalyst: effect of calcination temperature, Catal. Today, *93-95*, pp. 183-190. 2004.

Kamata, K., Y. Lu and Y. Xia. Synthesis and Characterization of Monodispersed Core-Shell Spherical Colloids with Movable Cores, J. Am. Chem. Soc., *125*, pp. 2384-2385. 2003.

Kapoor, S. and T. Mukherjee. Photochemical formation of copper nanoparticles in poly(N-vinylpyrrolidone), Chem. Phys. Lett., *370*, pp. 83-87. 2003.

Katayama, J., K. Ito, M. Matusuoka and J. Tamaki. Performance of Cu_2O/ZnO solar

cell prepared by two-step electrodeposition, J. Appl. Electrochem., *34*, pp. 687–692. 2004.

Kato, T. Self-Assembly of Phase-Segregated Liquid Crystal Structure, Science, *295*, pp. 2414-2417. 2002.

Kellersohn, A., E. Knözinger, W. Langel and M. Giersig. Cu_2O Quantum-Dot Particles Prepared from Nanostructured Copper, Adv. Mater., *7*, pp. 652-655. 1995.

Kenane, S. and L. Piraux. Electrochemical self-assembly of Cu/Cu_2O nanowires, J. Mater. Res., *17*, pp. 401-406. 2002.

Kijeński, J., J. Burger and A. Baiker. Copper catalyzed disproportionation of benzylamine methyl derivatives, Appl. Catal., *11*, pp. 295-304. 1984.

Kijeński, J., P.J. Niedzielski and A. Baiker. Synthesis of cyclic amines and their alkyl derivatives from amino-alcohols over supported copper catalysts, Appl. Catal., *53*, pp. 107-115. 1989.

Kim[1], F., S. Connor, H. Song, T. Kuykendall and P. Yang. Patonic Gold Nanocrystals, Angew. Chem. Int. Ed., *43*, pp. 3673-3877. 2004.

Kim[2], J.Y., S.B. Yoon and J.S. Yu. Fabrication of nanocapsules with Au particles trapped inside carbon and silica nanoporous shells, Chem. Commun., pp. 790-791. 2003.

Kim[3], S.W., M. Kim, W.Y. Lee and T. Hyeon. Fabrication of Hollow Palladium Spheres and Their Successful Application to the Recyclable Heterogeneous Catalyst for Suzuki Coupling Reactions, J. Am. Chem. Soc., *124*, pp. 7642-7643. 2002.

Kim[4], M.H., S.H. Im and O.O. Park. Fabrication and Structural Analysis of Binary Colloidal Crystals with Two-Dimensional Superlattices, Adv. Mater., *17*, pp. 2501-2505. 2005.

Kinoshita, A. and T. Nakana. Production of Cuprous Oxide Single Crystal by Melt, Jpn. J. Appl. Phys., *5*, pp. 1121. 1966.

Kinoshita, A. and T. Nakano. Cu_2O Crystal Growth by Hydrothermal Technique, Jpn. J. Appl. Phys., *6*, pp. 656-657. 1967.

Kniep, R. and S. Busch. Biomimetic Growth and Self-Assembly of Fluorapatite Aggregates by Diffusion into Denatured Collagen Matrices, Angew. Chem., Int. Ed., *35*, pp. 2624-2626. 1996.

Kobayashi, S., N. Hamasaki, M. Suzuki, M. Kimura, H. Shirai and K. Hanabusa. Preparation of Helical Transition-Metal Oxide Tubes Using Organogelators as Structure-Directing Agents, J. Am. Chem. Soc., *124*, pp. 6550-6551. 2002.

Kolthoff, I.M. and G.E. Noponen. Studies on Aging of Fresh Precipitates. XIX. Aging of Freshly Precipitated Barium Sulfate in Dilute Barium and Sulfate Solutions[1], J. Am. Chem. Soc., *60*, pp. 499-505. 1938.

Kolthoff, I.M. and F.T. Eggertsen. Studies on Aging and Coprecipitation. XXXIV. The Aging of Freshly Precipitated Lead Chromate, J. Am. Chem. Soc., *63*, pp. 1412-1418. 1941.

Kolthoff, I.M. and R.C. Bowers. Studies on Aging and Coprecipitation. XLV. The Irreversible Flocculation of Colloidal Silver Bromide and the Aging in the Flocculated State[1], J. Am. Chem. Soc., *76*, pp. 1510-1515. 1954.

Konishi, Y., M. Motoyama, H. matsushima, Y. Fukunaka, R. Ishii and Y. Ito. Electrodeposition of Cu nanowire arrays with a template, J. Electroanalytical Chem., *559*, pp. 149-153. 2003.

Kothari, H.M., E.A. Kulp, S. Boonsalee, M.P. Nikiforov, E.W. Bohannan, P. Poizot, S. Nakanishi and J.A. Switzer. Enantiospecific Electrodeposition of Chiral CuO Films from Copper (II) Complexes of Tartaric and Amino Acids on Single-Crystal Au(001), Chem. Mater., *16*, pp. 4232-4244. 2004.

Kovtyukhova, N.I. and T.E. Mallouk. Nanowires as Building Blocks for Self-Assembling Logic and Memory Circuits, Chem. Eur. J., *8*, pp. 4354-4363. 2002.

Krumeich, F., H.-J. Muhr, M. Niederberger, F. Bieri, B. Schnyder and R. Nesper. Morphology and Topochemical Reactions of Novel Vanadium Oxide Nanotubes, J. Am. Chem. Soc., *121*, pp. 8324-8331. 1999.

Kulak, A., Y.J. Lee, Y.S. Park, H.S. Kim, S.L. Lee and K.B. Yoon. Anionic Surfactants as Nanotools for the Alignment of Non-spherical Zeolite Nanocrystals, Adv. Mater., *14*, pp. 526-529. 2002.

Kumar, R.V., Y. Diamant and A. Gedanken. Sonochemical Synthesis and Characterization of Nanometer-Size Transition Metal Oxides from Metal Acetates, Chem. Mater., *12,* pp. 2301-2305. 2000.

Kumar, R.V., R. Elgamiel, Y. Diamant, A. Gedanken and J. Norwig. Sonochemical Preparation and Characterization of Nanocrystalline Copper Oxide Embedded in Poly(vinyl alcohol) and Its Effect on Crystal Growth of Copper Oxide, Langmuir, *17*, pp. 1406-1410. 2001(a).

Kumar, R.V., Y. Mastai, Y. Diamant and A. Gedanken. Sonochemical synthesis of amorphous Cu and nanocrystalline Cu_2O embedded in a polyaniline matrix, J. Mater. Chem., *11*, pp. 1209-1213. 2001(b).

Kuzmenko, A.B., D. van der Marel, P.J.M. van Bentum, E.A. Tishchenko, C. Presura and A.A. Bush. Infrared spectroscopic study of CuO: Signatures of strong spin-phonon interaction and structural distortion, Phys. Rev. B, *63*, pp. 094303-094317. 2001.

Lao, J.Y., J. G. Wen and Z.F. Ren. Hierarchical ZnO Nanostructures, Nano Lett, *2*, pp. 1287-1291. 2002.

Lee[1], K., W.S. Seo and J.T. Park. Synthesis and Optical Properties of Colloidal Tungsten Oxide Nanorods**,** J. Am. Chem. Soc*., 125*, pp. 3408-3409. 2003.

Lee[2], S.-H., Y.-S. Her and E. Matijevic. Preparation and Growth Mechanism of Uniform Colloidal Copper Oxide by the Controlled Double-Jet Precipitation, J. Colloid Interface Sci., *186*, pp. 193-202. 1997.

Lehn, J.-M. Toward Self-organization and Complex Matter, Science, *295*, pp. 2400-2403. 2002.

Leopold, S., I.U. Schuchert, J. Lu, M.E.T. Molares, M. Herranen and J.-O. Carlsson. Electrochemical deposition of cylindrical Cu/Cu_2O microstructures, Electrochimica Acta, *47*, pp. 4393-4397. 2002.

Lereah, Y., G. Deutscher and E. Grunbaum. Formation of dense branching morphology in the crystallization of Al-Ge amorphous thin films, Phys. Rev. A, *44,* pp. 8316-8322. 1991.

Li[1], B., Y. Xie, J. Huang, Y. Liu and Y. Qian. Sonochemical Synthesis of Nanocrystalline Copper Tellurides Cu_7Te_4 and Cu_4Te_3 at Room Temperature, Chem. Mater., *12*, pp. 2614-2616. 2000.

Li[2], C.-C. and M.-H. Chang. Colloidal stability of CuO nanoparticles in alkanes via oleate modification, Mater. Lett., *58*, pp. 3903-3907. 2004.

Li[3], J., L. Liu, Y. Yu, Y. Tang, H. Li and F. Du. Preparation of highly photocatalytic active nano-size TiO_2–Cu_2O particle composites with a novel electrochemical method, Electrochem. Comm., *6*, pp. 940–943. 2004.

Li[4], N., X. Li, X. Yin, W. Wang and S. Qiu. Electroless deposition of open-end Cu nanotube arrays, Solid State Commum., *132,* pp. 841-844. 2004.

Li[5], Q., M. Shao, G. Yu, J. Wu, F. Li and Y. Qian. A solvent-reduction approach to tetrapod-like copper(I) chloride crystallites, J. Mater. Chem., *13*, pp. 424-427. 2003(a).

Li[5], Q. and C. Wang. Cu nanostructures formed via redox reaction of Zn nanowire and Cu^{2+} containing solutions, Chem. Phys. Lett., *375*, pp. 525-531. 2003(b).

Li[6], X., H. Gao, C.J. Murphy and L. Gou. Nanoindentation of Cu_2O Nanocubes, Nano Lett., *4,* pp. 1903-1907. 2004.

Li[7], Y., J. Wang, Z. Deng, Y. Wu, X. Sun, D. Yu and P. Yang. Bismuth Nanotubes: A Rational Low-Temperature Synthetic route, J. Am. Chem. Soc., *123*, pp. 9904-9905. 2001.

Li[7], Y., J. Shi, Z. Hua, H. Chen, M. Ruan and D. Yan. Hollow Spheres of Mesoporous Aluminosilicate with a Three-Dimensional Pore Network and Extraordinarily High Hydrothermal Stability, Nano Lett., *3*, pp. 609-612. 2003(a).

Li[7], Y., Y. Bando and D. Golberg. Single-Crystalline In_2O_3 Nanotubes Filled with In, Adv. Mater., *15*, pp. 581-585. 2003(b).

Li[7], Y., Y. Bando and D. Golberg. Quasi-Aligned Single-Crystalline $W_{18}O_{49}$ Nanotubes and Nanowires, Adv. Mater., *15*, pp. 1294-1296. 2003(c).

Liang[1], S.H., L. Fang and Z.K. Fan. Internal oxidation of Cr in Cu-Cr/Cu_2O composite powder prepared by mechanical activation, Mater. Sci. Eng. A, *374*, pp. 27-33. 2004.

Liang[2], Z., A. Susha and F. Caruso. Gold Nanoparticle-Based Core-Shell and Hollow Spheres and Ordered Assemblies Thereof, Chem. Mater., *15,* pp. 3176-3183. 2003.

Liang[3], Z.-H. and Y.-J. Zhu. Microwave-assisted of Single-crystalline CuO Nanoleaves, Chem. Lett., *33*, pp. 1314-1315. 2004.

Lifshitz, E., M. Bashouti, V. Kloper, A. Kigel, M.S. Eisen and S. Berger. Synthesis and Characterization of PbSe Quantum Wires, Multipods, Quantum Rods, and Cubes, Nano. Lett., *3*, pp. 857-862. 2003.

Lisiecki, I. and M.P. Pileni. Synthesis of Copper Metallic Clusters Using Reverse Micelles as Microreactors, J. Am. Chem. Soc., *115*, pp. 3887-3896. 1993.

Lisiecki, I. and M.P. Pileni. Copper Metallic Particles Synthesized “in Situ” in Reverse Micelles: Influence of Various Parameters on the Size of the Particles, J. phys. Chem., *99*, pp. 5077-5082. 1995(a).

Lisiecki, I., M. Björling, L. Motte, B. Ninham and M.P. Pileni. Synthesis of Copper

Nanosize Particles in Anionic Reverse Micelles: Effect of the Addition of a Cationic Surfactant on the Size of the Crystallites, Langmuir, *11,* pp. 2385-2392. 1995(b).

Lisiecki, I., F. Billludet and M.P. Pileni. Control of the Shape and the Size of Copper Metallic Particles, J. phys. Chem., *100*, pp. 4160-4166. 1996.

Lisiecki, I., H. Sack-Kongehl, K. Weiss, J. Urban and M.-P. Pileni. Annealing Process of Anisotropic Copper Nanocrystals. 1. Cylinders, Langmuir, *16*, pp. 8802-8806. 2000(a).

Lisiecki, I., H. Sack-Kongehl, K. Weiss, J. Urban and M.-P. Pileni. Annealing Process of Anisotropic Copper Nanocrystals. 2. Rods, Langmuir, *16*, pp. 8807-8808. 2000(b).

Lisiecki, I., A. Filankembo, H. Sack-Kongehl, K. Weiss, M.-P. Pileni and J. Urban. Structural investigation of copper nanorods by high-resolution TEM, Phys. Rev. B, *61*, pp. 4968-4974. 2000(c).

Liu[1], B. and H.C. Zeng. Hydrothermal Synthesis of ZnO Nanorods in the Diameter Regime of 50 nm, J. Am. Chem. Soc., *125,* pp. 4430-4431. 2003.

Liu[1], B. and H.C. Zeng. Mesoscale Organization of CuO Nanoribbons: Formation of "Dandelions", J. Am. Chem. Soc., *126*, pp. 8124-8125. 2004(a).

Liu[1], B., H.C. Zeng. Salt-Assisted Deposition of SnO_2 on α-MoO_3 Nanorods and Fabrication of Polycrystalline SnO_2 Nanotubes, J. Phys. Chem. B, *108,* pp. 5867-5874. 2004(b).

Liu[1], B. and H.C. Zeng. Fabrication of ZnO "Dandelions" via a Modified Kirkendall Process, J. Am. Chem. Soc., *126*, pp. 16744-16746. 2004(c).

Liu[1], B. and H.C. Zeng. Symmetric and Asymmetric Ostwald Ripening in Fabrication of Homogeneous Core-Shell Semiconductors, Small, *1*, pp. 566-571. 2005.

Liu[2], C.M., L. Guo, H.B. Xu, Z.Y. Wu and J. Weber, Seed-mediated growth and properties of copper nanoparticles, nanoparticle 1D arrays and nanorods, Microelectronic Engineering, *66*, pp. 107-114. 2003.

Liu[3], F.-K. and F.-H. Ko. Separation and Study of the Optical Properties of Silver Nanocubes by Capillary Electrophoresis, Chem. Lett., *33,* pp. 902-903. 2004.

Liu[4], R., F. Oba, E.W. Bohannan, F. Ernst and J.A. Switzer. Shape Control in Epitaxial Electrodeposition: Cu_2O Nanocubes on InP(001), Chem. Mater., *15*, pp. 4882-4885. 2003.

Liu[5] S., C. Wang, H. Zhai and D. Li. Hydrolysis of *N*,*N*-dimethylformamide catalyzed by the Keggin $H_3[PMo_{12}O_{40}]$: isolation and crystal structure analysis of $[(CH_3)_2NH_2]_3[PMo_{12}O_{40}]$, J. Mol. Structure, *654*, pp. 215-221. 2003.

Liu[6], Z. and Y. Bando. A Novel Method for Preparing Copper Nanorods and Nonowires, Adv. Mater., *15*, pp. 303-305. 2003(a).

Liu[6], Z. and Y. bando. Oxidation behaviour of copper nanorods, Chem. Phys. Lett., *378*, pp. 85-88. 2003(b).

Liu[6], Z., Y. Yang, J. Liang, Z. Hu, S. Li, S. Peng and Y. Qian. Synthesis of Copper Nanowires via a Complex-Surfactant-Assisted Hydrothermal Reduction Process, J. Phys. Chem. B, *107*, pp. 12658-12661. 2003(c).

Loison, J. L., M. Robino and C. Schwab. PROGRESS IN MELT GROWTH OF Cu_2O, J. Cryst. Growth, *50*, pp. 816-822. 1980.

Lossin, A. and F.-J. Westhoff. The Production and Application of Cuprous Oxide and Cupric Hydroxide, JOM, pp. 38-39. 1997.

Lou, X.W. and H.C. Zeng. Complex α-MoO_3 Nanostructures with External Bonding Capacity for Self-Assembly, J. Am. Chem. Soc., *125*, pp. 2697-2704. 2003.

Lu[1], C., L. Qi, J. Yang, D. Zhang, N. Wu and J. Ma. Simple Template-Free Solution Route for the Controlled Synthesis of $Cu(OH)_2$ and CuO Nanostructures, J. Phys. Chem. B, *108*, pp. 17825-17831. 2004.

Lu[2], J., P. Qi, Y. Peng, Z. Meng, Z. Yang, W. Yu and Y. Qian. Metastable MnS Crystallites through Solvothermal Synthesis, Chem. Mater., *13*, pp. 2169-2172. 2001.

Lu[3], Q., F. Gao and S. Komarneni. Biomolecule-Assisted Synthesis of Highly Ordered Snowflakelike Structures of Bismuth Sulfide Nanorods**,** J. Am. Chem. Soc.; *126*, pp. 54-55. 2004**.**

Lu[4], Z., J. Liu, Y. Tang and Y. Li. Hydrothermal synthesis of $CaSnO_3$ cubes, Inorganic Chemistry Commun., *7*, pp. 731-733. 2004.

Ma, R., T. Sasaki and Y. Bando. Layer-by-Layer Assembled Multilayer Films of Titanate Nanotubes, Ag- or Au-Loaded Nanotubes, and Nanotubes/Nanosheets with Polycations, J. Am. Chem. Soc., *126*, pp. 10382-10388. 2004.

Mahalingam, T., J.S.P. Chitra, S. Rajendran and P.J. Sebastian. Potentiostatic depositions and characterization of Cu_2O thin film, Semicond. Sci. Technol., *17*, pp. 565-569. 2002.

Mamantov, G. and A.I. Popov (ed). Chemistry of Nonaqueous Solutions, pp. 179-226, New York: VCH publishers, Inc. 1994.

Mandal, T.K., M.S. Fleming and D.R. Walt. Production of Hollow Polymeric Microspheres by Surface-Confined Living Radical Polymerization on Silica Templates, Chem. Mater., *12,* pp. 3481-3487. 2000.

Manna, L., E.C. Scher and A.P. Alivisatos. Synthesis of Soluble and Processable Rod-, Arrow-, Teardrop-, and Tetrapod-Shaped CdSe Nanocrystals, J. Am. Chem. Soc., *122*, pp. 12700-12706. 2000.

Manna, L., D.J. Milliron, A. Meisel and E.C. Scher. Controlled growth of tetrapod-branched inorganic nanocrystals, Nat. mater., *2,* pp. 382-385. 2003.

Marchetti, A.P., M.I. Freedhoff, P. Rodney and G.L. McLendon. Optical Properties of Semiconductor Nanocrystals: Cu_2O, Mater. Sci. Forum, *239-241*, pp. 679-682. 1997.

Matijević, E. Preparation and properties of uniform size colloids, Chem. Mater., *5*, pp. 412-416. 1993.

Matijević, E. Uniform Inorganic Colloid Dispersions. Achievements and Challenges, Langmuir, *10*, pp. 8-16. 1994.

Matsumoto, H., K.Saito, M.Hasuo, S. Kono and N. Nagasawa. Revived interest on yellow-exciton series in Cu_2O: An experimental aspect, Solid State Commun., *97,* pp. 125-129. 1996.

Matsuzawa, Y., M. Kogiso, M. Matsumoto, T. Shimizu, K. Shimada, M. Itakura and S. Kinugasa. Hydrophilic Interface-Directed Self-Assembly of Bola-Form Amide into Hollow Spheres, Adv. Mater., *15*, pp. 1417-1420. 2003.

Matter, P.H., D.J. Braden and U.S. Ozkan. Steam reforming of methanol to H_2 over nonreduced Zr-containing CuO/ZnO catalysts, J. Catal., *223*, pp. 340-351. 2004.

Mayers, B., X. Jiang, D. Sunderland, B. Cattle and Y. Xia. Hollow Nanostructures of Platinum with Controllable Dimensions Can Be Synthesized by Templating Against Selenium Nanowires and Colloids, J. Am. Chem. Soc., *125*, pp. 13364-13365. 2003.

McCafferty, E. and J.P. Wightman. Determination of the Concentration of Surface Hydroxyl Groups on Metal Oxide Films by a Quantitative XPS Method, Surf. Intersurface Anal.,26, pp. 549-564. 1998.

McCann, J.T., D. Li and Y. Xia. Electrospinning of nanofibers with core-sheath,

hollow, or porous structures, J. Mater. Chem., *15*, pp. 735-738. 2005.

McFadyen, P. and E.J. Matijevic. Copper Hydrous Sols of Uniform Particle Shape and Size, J. Colloid Interface Sci., *44,* pp. 95-106. 1973.

Medina-Valtierra, J., J. Ramírez-Ortiz, V.M. Arroyo-Rojas and F. Ruiz. Cyclohexane oxidation over Cu_2O–CuO and CuO thin films deposited by CVD process on fiberglass, Applied Catalysis A: General, 238, pp. 1–9. 2003.

Minami, T., H. Tanaka, T. Shimakawa, T. Miyata and H. Sato. High-Efficiency Oxide Heterojunction Solar Cells Using Cu_2O Sheets, Japan. J. Appl. Phys., *43,* pp. L 917–919. 2004.

Mishina, E.D., K. Nagai and S. Nakabayashi. Self-Assembled Cu/Cu_2O Multilayers: Deposition, Structure and Optical Properties, Nano Lett., *1*, pp. 401-404. 2001.

Molares, M.E.T., V. Buschmann, D. Dobrev, R. Neumann, R. Scholz, I.U. Schuchert and J. Vetter. Single-Crystalline Copper Nanowires produced by Electrochemical Deposition in Polymeric Ion Track Membranes, Adv. Mater., *13*, pp. 62-65. 2001(a).

Molares, M.E.T., J. Brötz, V. Buschmann, D. Dobrev, R. Neumann, R. Scholz, I.U. Schuchert, C. Trautmann and J. Vetter. Etched heavy ion tracks in polycarbonate as template for copper nanowires, Nucl. Instrum. Methods B, *185*, pp. 192-197. 2001(b).

Monson, C.F. and A.T. Woolley. DNA-Templated Construction of Copper Nanowires, Nano Lett., *3*, pp. 359-363. 2003.

Morea, P.S., Y.B. Khollama, S.B. Deshpandeb, S.K. Dateb, N.D. Salia, S.V. Bhoraskara, S.R. Sainkarb, R.N. Karekarc and R.C. Aiyera. Introduction of γ-Al_2O_3/Cu_2O material for H_2 gas-sensing applications, Materials Lett., *58*, pp. 1020–1025. 2004.

Moriarty, P. Nanostructured materials, Rep. Prog. Phys., *64*, pp. 297-381. 2001.

Motiei, M., J. Calderon-Moreno and A. Gedanken. The Formation of Carbon-Coated MgO Cubes and Carbon Cubes, Adv. Mater., *14*, pp. 1169-1172. 2002.

Muramatsu, A. and T. Sugimoto. Synthesis of Uniform Spherical Cu_2O Particles from Condensed CuO Suspensions, J. Colloid Interface Sci., *189*, pp. 167-173. 1997.

Murray, C.B., S. Sun, W. Gaschler, H. Doyle, T.A. Betley and C.R. Kagan. Colloidal synthesis of nanocrystals and nanocrytal superlattices, IBM J. Res. & Dev., *45*, pp. 47-56. 2001.

Musa, A.O., T. Akomolafe and M.J. Carter. Production of cuprous oxide, a solar cell material, by thermal oxidation and a study of its physical and electrical properties, Sol. Energ. Mater. Sol. Cells, *51*, pp. 305-316. 1998.

Na-Ranong, D., A. Jaree, R.R. Hudgins, H.M. Budman, P.L. Silveston and M. Menzinger. Amplification of periodic temperature disturbances in a packed-bed reactor: CO oxidation over a CuO/Al_2O_3 catalyst, Can. J. Chem. Eng., *81*, pp. 1215-1221. 2003.

Naik, S.P., A.S.T. Chiang, R.W. Thompson and F.C. Huang. Formation of Silicalite-1 Hollow Spheres by the Self-assembly of Nanocrystals, Chem. Mater., *15*, pp. 787-792. 2003.

Nakano, T., K. Ohtani, A. Kinoshita and T. Okuda. Growth of Cuprous Oxide (Cu_2O) Crystal, Jpn. J. Appl. Phys., *3*, pp. 124. 1964.

Nakashima, T. and N. Kimizuka. Interfacial Synthesis of Hollow TiO_2 Microspheres in Ionic Liquids, J. Am. Chem. Soc., *125*, pp. 6386-6387. 2003.

Nasibulin, A.G., E.I. Kauppinen, D.P. Brown and J.K. Jokiniemi. Nanoparticles Formation via Copper (II) Acetylacetonate Vapor Decomposition in the presence of Hydrogen and Water, J. Phys. Chem. B, *105*, pp. 11067-11075. 2001(a).

Nasibulin, A.G., P.P. Ahonen, O. Richard, E.I. Kauppinen and I.S. Altman. Copper and copper oxide nanoparticle formation by chemical vapor nucleation from copper (II) acetylacetonate, J. Nanoparticle Research, *3*, pp. 385-400. 2001(b).

Ni, Y., H. Liu, F. Wang, Y. Liang, J. Hong, X. Ma and Z. Xu. Shape Controllable Preparation of PbS Crystals by a Simple Aqueous Phase Route, Crystal Growth & Design, *4*, pp. 759-764. 2004.

Nishiyama, S., A. Ichikawa and T. Hattori. Thermoelectric Properties of CuO-added $AgSbO_3$ Ceramics, J. Ceram. Soc. Japn., *112*, pp. 298-300.2004.

Norris, D.J., E.G. Arlinghaus, L. Meng, R. Heiny and L.E. Scriven. Opaline Photonic Crystals: How Does Self-Assembly Work?, Adv. Mater., *16*, pp. 1393-1399. 2004.

Oh, J., Y. Tak and J. Lee. Electrodeposition of Cu_2O Nanowires Using Nanoporous Alumina Template, Electrochem. Solid-state Lett., *7*, pp. C27-C30. 2004.

Ohmori, M., and E.J. Matijević. Preparation and Properties of Uniform Coated Colloidal Particles. VII. Silica on Hematite, J. Coll. Interface Sci., *150*, pp. 594-598. 1992.

Olofsson, G., A. Hinz, and A. Andersson. A transient response study of the selective catalytic oxidation of ammonia to nitrogen on Pt/CuO/Al_2O_3, Chem. Eng. Sci., *59*, pp. 4113-4123. 2004.

Olynick, D.L., J.M. Gibson and R.S. Averback. In situ ultra-high vacuum transmission electron microscopy studies of nanocrystalline copper, Mater. Sci. Eng. A, *204*, pp. 54-58. 1995.

Olynick, D.L., J.M. Gibson and R.S. Averback. Trace oxygen effects on copper nanoparticle size and morphology, Appl. Phys. Lett., *68*, pp. 343-345. 1996.

Ono, S., K. Naitoh and T. Osaka. Initial propagation stage of direct copper plating on non-conducting substrates, Electrochimica Acta, *44*, pp. 3697-3705. 1999.

Orel, Z.C., E. Matijević and D.V. Goia. Conversion of uniform colloidal Cu_2O spheres to copper in polyols, J. Mater. Res., *18*, pp. 1017-1021. 2003.

Ostwald, W. Studien uber die Bildung und Umwandlung fester Korper, Z. Phys. Chem. *22*, pp. 289. 1897.

Ozaki, M. Preparation and Properties of Well-Defined Magnetic Particles, MRS BULLETIN, *14*, pp. 35-40. 1989.

Ozin, G.A. Nanochemistry: Synthesis in Diminishing Dimensions, Adv. Mater., *4*, pp. 612-649. 1992.

Pacholski, C., A. Kornowski and H. Weller. Self-Assembly of ZnO: From Nanodots to Nanorods, Angew. Chem., Int. Ed., *41*, pp. 1188-1191. 2002.

Palkar, V. R., P. Ayyub, S. Chattopadhyay and M. Multani. Size-induced structural transitions in the Cu-O and Ce-O systems, Phys. Rev. B, *53*, pp. 2167-2170. 1996.

Pang, Y.T., G.W. Meng, Y. Zhang, Q. Fang and L.D. Zhang. Copper nanowire arrays for infrared polarizer, Appl. Phys. A, *76*, pp. 533-536. 2003.

Pantarotto, D., R. Singh, D. McCarthy, M. Erhardt, J.-P. Briand, M. Prato, K. Kostarelos and A. Bianco. Functionalized Carbon Nanobubes for Plasmid DNA Gene Delivery, Angew. Chem. Int. Ed., *43*, pp. 5242-5246. 2004.

Papavasillou, J., G. Avgouropoulos and T. Ioannides. Production of hydrogen via combined steam reforming of methanol over CuO-CeO_2 catalysts, Catal. Commun., *5*, pp. 231-235. 2004.

Park[1], J.H., C. Oh, S.I. shin, S.K. Moon and S.G. Oh. Preparation of hollow silica

microspheres in W/O emulsions with polymers, J. Colloid Interface Sci., *266*, pp. 107-114. 2003.

Park[2], S., J.-H. Lim, S.-W. Chung and C.A. Mirkin. Self-Assembly of Mesoscopic Metal-Polymer Amphiphiles, Science, *303*, pp. 348-351. 2004.

Pastoriza-Santos, I. and L.M. Liz-Marzán. Reduction of silver nanoparticles in DMF. Formation of monolayers and stable colloids, Pure Appl. Chem., *72*, pp. 83-90. 2000.

Pastoriza-Santos, I. and L.M. Liz- Marzán. Synthesis of Silver Nanoprisms in DMF, Nano Lett., *2,* pp. 903-905. 2002.

Patzke, G.R., F. Krumeich and R. Nesper. Oxidic Nanotubes and Nanorods - Anisotropic Modules for a Future Nanotechnology, Angew. Chem., Int Ed., *41*, pp. 2446-2461. 2002.

Peng[1], Q., Y. Dong, Z. Deng, H. Kou, S. Gao and Y. Li. Selective Synthesis and Magnetic Properties of α-MnSe and $MnSe_2$ Uniform Microcrystals, J. Phys. Chem. B, *106,* pp. 9261-9265. 2002.

Peng[1], Q., Y. Dong and Y. Li. ZnSe Semiconductor Hollow Microspheres, Angew. Chem. Int. Ed., *42,* pp. 3027-3030. 2003.

Peng[2], T., A. Hasegawa, J. Qiu and K. Hirao. Fabrication of Titania Tubes with High Surface Area and Well-Developed Mesostructural Walls by Surfactant-Mediated Templating Method, Chem. Mater., *15*, pp. 2011-2016. 2003.

Penn, R.L. and J.F. Banfield. Imperfect Oriented Attachment: Dislocation Generation in Defect-Free Nanocrystals, Science, *281*, pp. 969-971. 1998.

Petrova, R.I. and J.A. Swift. Habit Changes of Sodium Bromate Crystals Grown form Gel Media, Crystal Growth & Design, *2*, pp. 573-578. 2002.

Pietryga, J.M., R.D. Schaller, D. Werder, M.H. Stewart, V.I. Klimov and J.A. Hollingswirth. Pushing the Band Gap Envelope: Mid-infrared Emitting Colloidal PbSe Quantum Dots, J. Am. Chem. Soc., *126*, pp. 11752-11753. 2004.

Pileni, M.P. and I. Lisiecki. Nanometer metallic copper particle synthesis in reverse micelles, Colloids Surf. A, *80*, pp. 63-68. 1993.

Pileni, M.P., T. Gulik-Krzywicki, J. Tanori, A. Filankembo and J.C. Dedieu. Template Design of Microreactors with Colloidal Assemblies, Control the Growth of Copper Metal Rods, Langmuir, *14*, pp. 7359-7363. 1998.

Prabhakaran, D., C. Subramanian, S. Balakumar and P. Ramasamy. Morphology and etching studies on YBCO and CuO single crystals, Phys. C, *319*, pp. 99-103. 1999.

Puntes, V.F., K.M. Krishnan and A.V. Alivisatos. Colloidal Nanocrystal Shape and Size Control: The Case of Cobalt, Science, *291*, pp. 2115-2117.2001.

Puzakov, V.V. and L.L. Ermakova. Homogeneous crystal nucleation of copper (I) oxide powder during electrolysis of chloride solution, Zh. Prikl. Khim., *64*, pp. 2567-2570. 1991.

Qi, P., A. Javey, M. Rolandi, Q. Wang, E. Yenilmez and H. Dai. Miniature Organic Transistors with Carbon Nanotubes as Quasi-One-Dimensional Electrodes, J. Am. Chem. Soc., *126*, pp. 11774-11775. 2004.

Ram, S. and C. Mitra. Formation of stable Cu_2O nanocrystals in a new orthorhombic crystal structure, Mater. Sci. Eng. A, *304–306*, pp. 805-809. 2001.

Ramírez-Ortiz, J., T. Ogura, J. Medina-Valtierra, S.E. Acosta-Oritz, P. Bosch, J.A. de los Reyes and V.H. Lara. A catalytic application of Cu_2O and CuO films deposited over fiberglass, Appl. Surf. Sci., *174*, pp. 177-184. 2001.

Rao[1], C.N.R. and A.K. Cheetham. Science and technology of nanomaterials: current status and future prospects, J. Mater. Chem., *11*, pp. 2887-2894. 2001.

Rao[1], C.N.R., G.U. Kulkarni, P.J. Thomas and P.P. Edwards. Size-Dependent Chemistry: Properties of Nanocrystals, Chem. Eur. J., *8*, pp. 28-35. 2002.

Rao[2], J.C., X.X. Zhang, B. Qin and K.K. Fung. High-resolution transmission electron microscopy study of epitaxial passive films on nanocubes of chromium, Philosophical Magazine Lett., *83,* pp. 395-401. 2003.

Reinhoudt, D.N. and M. Crego-Calama. Synthesis Beyond the Molecule, Science, *295*, pp. 2403-2407. 2002.

Remskar, M. Inorganic Nanotubes, Adv. Mater., *16*, pp. 1497-1504. 2004.

Roco, M.C. Nanotechnology: convergence with modern biology and medicine, Current Opinion in Biotechnology, *14*, pp. 337-346. 2003.

Runeberg, J., A. Baiker and J. Kijenski. Copper catalyzed amination of ethylene glycole, Appl. Catal., *17*, pp. 309-319. 1985.

Salzemann, C., I. Lisiecki, J. Urban and M.-P. Pileni. Anisotropic Copper Nanocrystals Synthesized in a Supersaturated Medium: Nanocrystal Growth, Langmuir, *20*, pp.

11772-11777. 2004.

Sampanthar, J.T. and H.C. Zeng. Arresting Butterfly-Like Intermediate Nanocrystals of ß-$Co(OH)_2$ via Ethylenediamine-Mediated Synthesis, J. Am. Chem. Soc., *124*, pp. 6668-6675. 2002.

Sanchez-Castillo, M.A., C. Couto, W.B. Kim and J.A. Dumesic. Gold-Nanotube Membranes for the Oxidation of CO at Gas-Water Interface, Angew. Chem. Int. Ed., *43,* pp. 1140-1142. 2004.

Savinova, E.R., A.L. Chuvilin and V.N. Parmon. COPPER COLLOIDS STABILIZED BY WATER-SOLUBLE POLYMERS PART I. PREPAREATON AND PROPERTIES, J. Mol. Catal., *48*, pp. 217-229. 1988.

Schmidt-Whitley, R. D., M. Martinez-Clemente and A. Revcolevschi. Growth and microstructureal control of single-crystal cuprous oxide, J. Cryst. Growth, *23*, pp. 113-120. 1974.

Schulz, K.H. and D.F. Cox. Photoemission and low-energy-electron-diffraction study of clean and oxygen-dosed Cu_2O (111) and (100) surfaces, Phys. Rev. B, *43*, pp. 1610-1621. 1991.

Shang, C.H. Pattern-formation study of macroscopic dense branching morphology in $Bi_{0.69}Al_{0.27}Mn$/SiO films, Phys. Rev. B, *53*, pp. 13759-13766. 1996.

Shao,W.Z., V.V. Ivanov, L. Zhen, Y.S. Cui and D.Z. Yang. Effect of porosity and copper content on compressive strength of Cu/Cu_2O cermet, J. Mater. Sci., *39***,** pp. 731–732. 2004.

Shevchenko, E.V., D.V. Talapin, H. Schnablegger, A. Kornowski, Ö. Festin, P. Svedlindh, M. Haase and H. Weller. Study of Nucleation and Growth in the Organometallic Synthesis of Magnetic Alloy Nanocrystals: The role of Nucleation Rate in Size Control of $CoPt_3$ Nanocrystals, J. Am. Chem. Soc., *125*, pp. 9090-9101. 2003.

Shiau, C.Y., S. Chen, J.C. Tsai and S.I. Lin. Effect of zinc addition on copper catalyst in isoamyl alcohol dehydrogenation, Appl. Catal. A: General, *198*, pp. 95–102. 2000.

Shimizu, T., T. Matsumoto, A. Goto, T.V.C. Rao, K. Yoshimura and K. Kosuge. Spin susceptibility and superexchange interaction in the antiferromagnet CuO, Phy.Rev. B, *68*, Art. No. 224433. 2003.

Sinha, P. and S. Roy. Barbier Reaction in the Regime of Metal Oxide: Carbonyl Allylation over β-SnO/Cu_2O and Surface Diagnostics, Organometallics, *23*, pp. 67-71.

2004.

Siripala, W., A. Ivanovskaya, T.F. Jaramillo, S.-H. Baeck and E.W. McFarland. A Cu_2O/TiO_2 heterojunction thin film cathode for photoelectrocatalysis, Solar Energy Materials & Solar Cells, *77*, pp. 229–237. 2003.

Son, S.U., I.K. Park, J. Park and T. Hyeon. Synthesis of Cu_2O coated Cu nanoparticles and their successful applications to Ullmann-type amination coupling reactions of aryl chlorides, Chem. Commun., pp. 778–779. 2004.

Song, X., S. Sun, W. Zhang and Z. Yin. A method for the synthesis of spherical copper nanoparticles in the organic phase, J. Colloid Interface Sci., *273*, pp. 463-469. 2004.

Spahr, M.E., P. Bitterli, R. Nesper, M. Müller, F. Krumeich and H.U. Nissen. Redox-Active Nanotubes of Vanadium Oxide, Angew. Chem. Int. Ed., *37*, pp. 1263-1265. 1998.

Steinbruchel, C. and B.L. Chin. Copper interconnect technology. Bellingham, WA: SPIE Optical Engineering Press, 2001.

Steinhart, m., R.B. Wehrspohn, U. Gösele and J.H. Wendorff. Nanotubes by Template Wetting: A Modular Assembly System, Angew. Chem. Int. Ed., *43*, pp. 1334-1344. 2004.

Sugimoto, T. Preparation and Characterization of Monodispersed Colloidal Particles, MRS BULLETIN, *14*, pp. 23-28. 1989.

Sumper, M. A Phase Separation Model for the Nanopatterning of Diatom Biosilica, Science, *295*, pp. 2430-2433. 2002.

Sun[1], K.P., W.W. Lu, M. Wang and X.L. Xu. Low-temperature synthesis of DME from $CO2/H_2$ over Pd-modified $CuO-ZnO-Al_2O_3-ZrO_2$/HZSM-5 catalysts, Catal. Commun., *5*, pp. 367-370. 2004.

Sun[2], X., X. Chen and Y. Li. Evaporation growth of multipod ZnO whiskers assisted by a Cu^{2+} etching technique, J. Crystal, Growth, *244,* 218-223. 2002.

Sun[2], X. and Y. Li. Size-controllable luminescent single crystal CaF_2 nanocubes, Chem. Commun., pp. 1768-1769. 2003.

Sun[3], Y., B.T. Mayers and Y. Xia. Template-Engaged Replacement Reaction: A One-Step Approach to the Large-Scale Synthesis of Metal Nanostructures with Hollow Inteiors, Nano Lett., *2*, pp. 481-485. 2002(a).

Sun[3], Y. and Y. Xia. Increased Sensitivity of Surface Plasmon Resonance of Gold Nanoshells Compared to That of Gold solid Colloids in Response to Environmental Changes, Anal. Chem., *74*, pp. 5297-5305. 2002(b).

Sun[3], Y. and Y. Xia. Shape-Controlled Synthesis of Gold and Silver Nanoparticles, Science, *298*, pp. 2176-2179. 2002(c).

Sun[3], Y., B.T. Mayers and Y. Xia. Metal Nanostructures with Hollow Interiors, Adv. Mater., *15*, pp. 641-646. 2003(a).

Sun[3], Y. and Y. Xia. Gold and silver nanoparticles: A class of chromophores with colors tunable in the range from 400 to 750 nm, Analyst, *128*, pp. 689-691. 2003(b).

Sun[3], Y., B. Wiley, Z.-Y. Li and Y. Xia. Synthesis and Optical properties of Nanorattles and Multiple-Walled Nanoshells/Nanotubes Made of Metal Alloys, J. Am. Chem. Soc., *168*, pp. 9399-9406. 2004.

Suryanarayana, C. and C.C. Koch. Non-Equilibrium Processing of materials, Netherlands: Pergamon Press. 1999.

Suzuki, T., Y. Utsumi, K. Sasaki and K. Shibuki. Growth of an oriented graphitic layer on a TiC nanocube, J. Appl. Phys. *77,* pp. 3450-3452. 1995.

Suzuki, T. ORIENTED GRAPHITIC LAYERS ON TiC NANOCUBE, Mol. Mat., *10,* pp. 181-184. 1998.

Switzer, J.A., M.J. Shane and R.J. Phillips. Electrodeposited Ceramic Superlattices, Science, *247*, pp. 444-446. 1990.

Switzer, J.A., R.P. Raffaelle, R.J. Phillips, C.J. Hung and T.D. Golden. Scanning Tunneling Microscopy of Electrodeposited Ceramic Superlattices, Science, *258*, pp. 1918-1921. 1992.

Switzer, J.A. and T.D. Golden. Scanning tunneling microscopy of nanoscale electrodeposited superlattices, Adv. Mater., *5*, pp. 474-476. 1993.

Switzer, J.A., C.J. Hung, B.E. Breyfogle, M.G. Shumsky, R. Vanleeuwen and T.D. Golden. Electrodeposited Defect Chemistry Superlattices, Science, *264*, pp. 1573-1576. 1994.

Switzer, J.A., C.J. Hung, E.W. Bohannan, M.G. Shumsky, T.D. Golden and D.C. Van Aken. Electrodeposition of quantum-confined metal/semiconductor nanocomposites, Adv. Mater., *9*, pp. 334-338. 1997.

Switzer, J.A., H.M. Kothari, P. Poizot, S. Nakanishi and E.W. Bohannan. Enantiospecific electrodeposition of a chiral catalyst, nature, *425*, pp. 490-493. 2003.

Tang, Q., J. Shen, W. Zhou, W. Zhang, W. Yu and Y. Qian. Preparation, characterization and optical properties of terbium oxide nanotubes, J. Mater. Chem., *13*, pp. 3103-3106. 2003(a).

Tang, Q., Z. Liu, S. Li, S. Zhang, X. Liu and Y. Qian. Synthesis of Yttrium hydroxide and oxide nanotubes, J. Crys. Growth, *259*, pp. 208-214. 2003(b).

Tang, Q., W. Zhou, W. Zhang, S. Ou, K. Jiang, W. Yu and Y. Qian. Size-Controllable Growth of Single Crystal $In(OH)_3$ and In_2O_3 Nanocubes, Cryst. Growth Des., *5*, pp. 147-150. 2005.

Tang[1], Z. and N.A. Kotov. One-dimensional Assemblies of Nanoparticles: Preparation, Properties, and Promise, Adv. Mater., *17*, pp. 951-962. 2005.

Tanori, J. and M.P. Pileni. Control of the Shape of Copper Metallic Particles by Using a Colloidal System as Template, Langmuir, *13*, pp. 639-646. 1997.

Tenne, R. Doping control for nanotubes, Nature, *431*, pp. 640-641. 2004.

Tian, Z.R., J.A. Voigt, J. Liu, B. Mckenzie and M.J. Mcdermott. Biomimetic Arrays of Oriented Helical ZnO Nanorods and Columns, J. Am. Chem. Soc., *124*, pp. 12954-12955. 2002.

Tian, Z.R., J. Liu, J.A. Voigt, B. Mckenzie and H. Xu. Hierarchical and Self-Similar Growth of Self-Assembled Crystals, Angew. Chem., Int. Ed., *42*, pp. 413-417. 2003(a).

Tian, Z.R., J. Liu, H. Xu, J.A. Voigt, B. Mckenzie and C.M. Matzke. Shape-Selective Growth, Patterning, and Alignment of Cubic Nanostructured Crystals via Self-Assembly, Nano Lett., *3*, pp. 179-182. 2003(b).

Torimoto, T., J.P. Reyes, K. Iwasaki, B. Pal, T. Shibayama, K. Sugawara, H. Takahashi and B. Ohtani. Preparation of Novel Silica-Cadmium Sulfide Composite Nanoparticles Having Adjustable Void Space by Size-Selective Photoetching, J. Am. Chem. Soc., *125,* pp. 316-317. 2003.

Torres, G.R., B. Agricole, P. Delhaes and C. Mingotaud. Crystallization of Prussian Blue Agalogs beneath Langmuir Films, Chem. Mater., *14,* pp. 4012-4014. 2002.

Toth, R.S., R. Kilkson and D. Trivich. Preparation of Large Area Single-Crystal Cuprous Oxide, J. Appl. Phys. *31*, pp. 1117-1121. 1960.

Trau, M., N. Yao, E. Kim, Y. Xia, G.M. Whitesides and I.A. Aksay. Microscopic patterning of orientated mesoscopic silica through guided growth, Nature, *390*, pp. 674-676. 1997.

Tremel, W. Inorganic Nanotubes, Angew. Chem. Int. Ed., *38*, pp. 2175-2179. 1999.

Trivich, D. and G.P. Pollack. Preparation of single crystal of cuprous oxide in an arc-image furnace, J. Electrochem. Soc., *117*, pp. 344-345. 1970.

Tsunekawa, S., T. Fukuda and A. Kasuya. Blue shift in ultraviolet absorption spectra of monodisperse CeO_{2-x} nanoparticles, J. appl. Phys., *87*, pp. 1318-1321. 2000.

Udrea, I. and C. Bradu. Ozonation of substituted phenols in aqueous solutions over $CuO\text{-}Al_2O_3$ catalyst, Ozone-Sci. Eng., *25*, pp. 335-343. 2003.

Urban, J.J., L. Ouyang, M.-H. Jo, D.S. Wang and H. Park. Synthesis of Single-Crystalline $La_{1-x}Ba_xMnO_3$ Nanocubes with Adjustable Doping Levels, Nano. Lett., *4*, pp. 1547-1550. 2004.

Valtchev, V. Silicalite-1 Hollow Spheres and Bodies with a Regular System of Macrocavities, Chem. Mater., *14*, pp. 4371-4377. 2002.

Vicsek, T. Fractal Growth Phenomena. Singapore: World Scientific. 1992.

Vitulli, G., M. Bernini, S. Bertozzi, E. Potzalis, P. Salvadori, S. Coluccia and G. Martra. Nanoscale Copper Particles Derived from Solvated Cu Atom in the Activation of Molecular Oxygen, Chem. Mater., *14*, pp. 1183-1186. 2002.

Vorobyova, S.A., A.I. Lesnikovich and V.V. Muchinskii. Interphase synthesis and some characteristics of stable colloidal solution of CuO in octane, Colloids Surf. A, *150*, pp. 297-300. 1999.

Vultier, R., A. Baiker and A. Wokaun. Copper catalyzed amination of 1, 6-hexanediol, Appl. Catal., *30*, pp. 167-176. 1987.

Wagner, C., W. Riggs, L. Davis and J. Moulder. Handbook of. X-ray Photoelectron Spectroscopy. Minnesota: Perkin Elmer Corporation, Eden Prairie. 1979.

Wan, Q., K. Yu, T.H. Wang and C.L. Lin. Low-field electron emission from tetrapod-like ZnO nanostructures synthesized by rapid evaporation, Appl. Phys. Lett., *83*, pp. 2253-2255. 2003.

Wang[1], C., K. Tang, Q. Yang, J. Hu and Y. Qian. Fabrication of BiTeI submicrometer

hollow spheres. J. Mater. Chem., *12*, pp. 2426-2429. 2002.

Wang[2], D. and F. Caruso. Polyelectrolyte-Coated Colloid Spheres as Templates for Sol-Gel Reactions, Chem. Mater., *14*, pp. 1909-1913.2002.

Wang[3], D., M. Mo, D. Yu, L. Xu, F. Li and Y. Qian. Large-Scale Growth and Shape Evolution of Cu_2O Cubes, Cryst. Growth Des., *3,* pp. 717-720. 2003.

Wang[4], H., J.Z. Xu, J.J. Zhu and H.Y. Chen. Preparation of CuO nanoparticles by microwave irradiation, J. Cryst. Growth, *244*, pp. 88-94. 2002.

Wang[5], J. and Y. Li. Rational Synthesis of Metal Nanotubes and Nanowires from Lamellar Structures, Adv. Mater., *15*, pp. 445-447. 2003.

Wang[6], M., X.Y. Liu, C.S. Strom, P. Bennema, W. van Enckevort and N.B. Ming. Fractal Aggregations at Low Driving Force with Strong Anisotropy, Phys. Rev. Lett., *80,* pp. 3089-3092. 1998.

Wang[7], P.-I., Y.-P. Zhao, G.-C. Wang and T.-M. Lu. Novel growth mechanism of single crystalline Cu nanorods by electron beam irradiation, Nanotechnology, *15*, pp. 218-222. 2004.

Wang[8], S., S. Yang, Z.R. Dai and Z.L. Wang. The crystal structure and growth direction of Cu_2S nanowire arrays fabricated on a copper surface, Phys. Chem. Chem. Phys., *3*, pp. 3750-3753. 2001.

Wang[8], S., Q. Huang, X. Wen, X.Y. Li and S. Yang. Thermal oxidation of Cu_2S nanowires: A template method for the fabrication of mesoscopic Cu_xO (x = 1,2) wires, Phys. Chem. Chem. Phys., *4*, pp. 3425-3429. 2002.

Wang[9], W., Y. Geng, Y. Qian, M. Ji and X. Liu. A Novel Pathway to PbSe Nanowires at Room Temperature, Adv. Mater., *10*, pp. 1479-1481. 1998.

Wang[9], W., Y. Geng, P. Yan, F. Liu, Y. Xie and Y. Qian. A Novel Mild Route to Nanocrystalline Selenides at Room Temperature, J. Am. Chem. Soc., *121*, pp. 4062-4063. 1999.

Wang[9], W., Y. Zhan and G. Wang. One-step, solid-state reaction to the synthesis of copper oxide nanorods in the presence of a suitable surfactant, Chem. Commun., pp. 727-728. 2001.

Wang[9], W., Y. Zhan, X. Wang, Y. Liu, C. Zheng and G. Wang. Synthesis and characterization of CuO nanowhiskers by a novel one-step, solid-state reaction in the presence of a nonionic surfactant, Mater. Res. Bull., *37*, pp. 1093-1100. 2002(a).

Wang[9], W., I. Germanenko and M.S. El-Shall. Room-Temperature Synthesis and Characterization of Nanocrystalline CdS, ZnS, and $Cd_xZn_{1-x}S$, Chem. Mater., *14*, pp. 3028-3033. 2002(b).

Wang[9], W., C. Lan, Y. Li, K. Hong and G. Wang. A simple wet chemical route for large-scale synthesis of $Cu(OH)_2$ nanowires, Chem. Phys. Lett., *366*, pp. 220-223. 2002(c).

Wang[9], W., G. Wang, X. Wang, Y. Zhan, Y. Liu and C. Zheng. Synthesis of Characterization of Cu_2O Nanowires by a Novel Reduction Route, Adv. Mater., *14*, pp. 67-69. 2002(d).

Wang[9], W., O.K. Varghese, C. Ruan, M. Paulose and C.A. Grimes, Synthesis of CuO and Cu_2O crystalline nanowires using $Cu(OH)_2$ nanowire templates, J. Mater. Res., *18*, pp. 2756-2759. 2003(a).

Wang[9], W., Z. Liu, Y. Liu, C. Xu, C. Zheng and G. Wang. A simple wet-chemical synthesis and characterization of CuO nanorods, Appl. Phys. A, *76*, pp. 417-420. 2003(b).

Wang[10]**,** X., J. Zhang, J. Chen, K. Zhou and Y. Li. Thermally Stable Silicate Nanotubes, Angew. Chem. Int. Ed., *43*, pp. 2017-2022. 2004.

Wang[11], Y., C. Ye, X. Fang and L. Zhang. A simple Method for Synthesizing Copper Nanotube Arrays, Chem. Lett., *33,* pp. 166-167. 2004.

Wang[12]**,** Z., X. Chen, J. Liu, M. Mo, L. Yang and Y. Qian. Room temperature synthesis of Cu_2O nanocubes and nanoboxes, Solid State Commun., *130,* pp. 585-589. 2004.

Wang[13], Z.L. (ed). Characterization of Nanophase Materials. pp. 37-79, Weinheim: WILEY-VCH. 2000.
Wang[13], Z.L., P. Poncharal and W.A. de Heer. Nanomeasurements of individual carbon nanotubes by *in situ* TEM, Pure Appl. Chem., 72, pp. 209-219. 2000(a).

Wang[13], Z.L., Y. Liu, and Z. Zhang (eds). Handbook of Nanophase and Nanostructured Materials. Vol. *1*, pp. 1. New York: Kluwer Academic/Plenum Publishers Press. 2003(a).

Wang[13], Z.L. New Developments in Transmission Electron Microscope for Nanotechnology, Adv. Mater., *15*, pp. 1497-1514. 2003(b).

Wang[13], Z.L., X.Y. Kong, X. Wen and S. Yang. In Situ Structure Evolution from

$Cu(OH)_2$ Nanobelts to Copper Nanowires, J. Phys. Chem. B, *107*, pp. 8275-8280. 2003(c).

Wayne-Richardson, H. Antifouling pigment, other applications and frontiers, pp. 395-419. Wayne-Richardson, H. (eds) Handbook of copper compounds and applications, New York: Marcel Dekker Inc. 1997.

Wen, X., W. Zhang and S. Yang. Synthesis of $Cu(OH)_2$ and CuO Nanoribbon Arrays on a Copper Surface, Langmuir, *19*, pp. 5898-5903. 2003.

Whitesides, G.M. and B. Grzybowski. Self-assembly at All Scales, Science, *295*, pp. 2418-2421. 2002.

Wijnhoven, J.E.G. and W.L. Vos. Preparation of Photonic Crystals Made of Air Spheres in Titania, Science, *281*, pp. 802-804. 1998.

Wojciechowska, M., M. Zielinski and M. Pietrowski. Reduction of NO by C_3H_6 over CuO-MnO/MgF_2 in the presence of H_2O, Catal. Today, *90*, pp. 35-38. 2004.

Wouters, D. and U.S. Schubert. Nanolithography and Nanochemistry: Probe-Related patterning Techniques and Chemical Modification for Nanometer-Sized Devices, Angew. Chem. Int. Ed., *43*, pp. 2480-2495. 2004.

Wu[1], G., L. Zhang, B. Cheng, T. Xie and X. Yuan. Synthesis of Eu_2O_3 Nanotubes Arrays through a Facile Sol-Gel Template Approach, J. Am. Chem. Soc., *126*, pp. 5976-5977. 2004.

Wu[2], H.Q., X.W. Wei, M.W. Shao, J.S. Gu and M.Z. Qu. Synthesis of copper oxide nanoparticles using carbon nanotubes as templates, Chem. Phys. Lett., *364,* pp. 152-156. 2002.

Wu[3], M., G. Wang, H. Xu, J. Long, F.L. Y. Shek, S.M.F. Lo, I.D. Williams, S. feng and R. Xu. Hollow Spheres Based on Mesostructured Lead Titanate with Amorphous Framework, Langmuir, *19*, pp. 1362-1367. 2003.

Wu[3], M., X. Pan, X. Qian, J. Yin and Z. Zhu. Solution-phase synthesis of Ag_2S hollow and concave nanocubes, Inorg. Chem. Commun., *7*, pp. 359-362. 2004.

Wu[4], S.-H. and D.-H. Chen. Synthesis of high-concentration Cu nanoparticles in aqueous CTAB solutions, J. Colloid Interface Sci., *273*, pp. 165-169. 2004.

Wu[5], Y., H. Yan, M. Huang, B. Messer, J.H. Song and P. Yang. Inorganic Semiconductor Nanowires: Rational Growth, Assembly, and Novel Properties, Chem. Eur. J., *8*, pp. 1260-1268. 2002.

Valtchev, V. Silicalite-1 Hollow Spheres and Bodies with a Regular System of Macrocavities, Chem. Mater., *14*, pp. 4371-4377. 2002.

Xia, Y. and G.M. Whitesides. Soft Lithography, Angew. Chem. Int. Ed., *37*, pp. 550-575. 1998.

Xia, Y., P. Yang, Y. Sun, Y. Wu, B. Mayers, B. Gates, Y. Yin, F. Kim and H. Yan. One-Dimensional Nanostructures: Synthesis, Characterization, and Applications, Adv. Mater., *15*, pp. 353-389. 2003.

Xiao, J., Y. Xie, R. Tang and W.Luo. Template-based synthesis of nanoscale Ag_2E (E = S, Se) dendrites, J. Mater. Chem., *12*, pp. 1148-1151. 2002.

Xiong, Y., Y. Xie, Z. Li, C. Wu and R. Zhang. A novel approach to carbon hollow spheres and vessels from CCl_4 at low Temperatures, Chem. Commun., pp. 904-905. 2003(a).

Xiong, Y., Z. Li, R. Zhang, Y. Xie, J. Yang and C. Wu. From Complex Chains to 1D Metal Oxides: A Novel Strategy to Cu_2O Nanowires, J. Phys. Chem. B, *107,* pp. 3697-3792. 2003(b).

Xu[1], A.-W., Y.-P. Fang, L.-P. You and H.-Q. Liu. A Simple Method to Synthesize $Dy(OH)_3$ and Dy_2O_3 Nanotubes, J. Am. Chem. Soc., *125*, pp. 1494-1495. 2003.

Xu[2], C., Y. Liu, G. Xu and G. Wang. Preparation and characterization of CuO nanorods by thermal decomposition of CuC_2O_4 precursor, Mater. Res. Bull., *37*, pp. 2365-2372. 2002.

Xu[3], J.F., W. Ji, Z.X. Shen, S.H. Tang, X.R. Ye, D.Z. Jia and X.Q. Xin. Preparation and Characterization of CuO Nanocrystals, J. Solid State Chem., *147*, pp. 516-519. 1999.

Xu[4], R. and H.C. Zeng. Synthesis of Nanosize Supported Hydrotalcite-like Compounds $CoAl_x(OH)_{2+2x}(CO_3)_y(NO_3)x\text{-}2y\cdot nH_2O$ on $\gamma\text{-}Al_2O_3$, Chem. Mater., *13*, pp. 297-303. 2001.

Xu[4], R. and H.C. Zeng. Mechanistic Investigation on Salt-Mediated Formation of Free-Standing Co_3O_4 Nanocubes at 95 ^oC, J. Phys. Chem. B., *107*, pp. 926-930. 2003.

Xu[4], R. and H.C. Zeng. Self-Generation of Tiered Surfactant Superstructures for One-Pot Synthesis of Co_3O_4 Nanocubes and Their Close- and Non-Close-Packed Organizations, Langmuir, *20*, pp. 9780-9790. 2004(a).

Xu[4], R. Synthesis and Investigation on Cobalt-Layered Hydroxide Compounds and their Related Nanostructured Materials. Ph.D Thesis, National University of Signapore. 2004(b).

Yada, M., M. Mihara, S. Mouri, M. Kuroki and T. Kijima. Rare Earth (Er, Tm, Yb, Lu) Oxide Nanobubes Templated by Dodecylsulfate Assemblies, Adv. Mater., *14*, pp. 309-313. 2002.

Yanagimoto, H., K. Akamatsu, K. Gotoh and S. Deki. Synthesis and characterization of Cu_2O nanoparticles dispersed in NH_2-terminated poly(ethylene oxide), J. Mater. Chem., *11*, pp. 2387-2389. 2001(a).

Yanagimoto, H., K. Akamatsu, K. Goto and S. Deki. Preparation of Cu_2O nanoparticles dispersed in NH_2-terminated polyethyleneoxide matrix, Eur. Phys. J. D, *16*, pp. 313-316. 2001(b).

Yang[1], H.G. and H.C. Zeng. Creation of Intestine-like Interior Space for Metal-Oxide Nanostructures with a Quasi-Reverse Emulsion**,** Angew. Chem. Int. Ed., *43,* pp. 5206-5209. 2004(a).

Yang[1], H.G. and H.C. Zeng. Preparation of Hollow Anatase TiO_2 Nanospheres via Ostwald Ripening**,** J. Phys. Chem. B, *108,* pp. 3492-3495. 2004(b).

Yang[2], M. and J.J. Zhu. Spherical hollow assembly composed of Cu_2O nanoparticles, Journal of Crystal growth, *256*, pp. 134-138. 2003.

Yang[3], R. and L. Gao. Novel Way to Synthesize CuO Nanocrystals with Various Morphologies, Chem. Lett., *33,* pp. 1194-1195. 2004.

Yang[4], Z., Z. Niu, Y. Lu, Z. Hu and C.C. Han. Templated Synthesis of Inorganic Hollow Spheres with a Tunable Cavity Size onto Core–Shell Gel Particles, Angew. Chem. Int. Ed., *42,* pp. 1943-1945. 2003.

Ye, C., G. Meng, Z. Jiang, Y. Wang, G. Wang and L. Zhang. Rational Growth of Bi_2S_3 Nanotubes from Quasi-two-dimensional Precursors, J. Am. Chem. Soc., *124*, pp. 15180-15181. 2002.

Yen, M.-Y., C.-W. Chiu, C.-H. Hsia, F.-R. Chen, J.-J. Kai, C.-Y. Lee and H.-T. Chiu. Synthesis of Cable-Like Copper Nanowire, Adv. Mater., *15*, pp. 235-237. 2003.

Yin[1], M. and S. O'Brien. Synthesis of Monodisperse Nanocrystals of Manganese Oxides, J. Am. Chem. Soc., *125*, pp. 10180-10181. 2003.

Yin[2], Y., Y. Lu, B. gates and Y. Xia. Synthesis and Characterization of Mesoscopic

Hollow Spheres of Ceramic Materials with Functionalized Interior Surfaces, Chem. Mater., *13*, pp. 1146-1148. 2001.

Yin[2], Y., R.M. Rioux, C.K. Erdonmez, S. Hughes, G.A. Somorjai and A.P. Alivisatos. Formation of Hollow Nanocrystals Through the Nanoscale Kirkendall**,** Science, *304*, pp. 711-714. 2004.

Yin[3], Z., Y. Sakamoto, J. Yu, S. Sun, O. Terasaki and R. Xu. Microemulsion-Based Synthesis of Titanium Phosphate Nanotubes via Amine Extraction System, J. Am. Chem. Soc., *126*, pp. 8882-8883. 2004.

Yong, C., B.C. Zhang, C.S. Seet, A. See, L. Chan, J.Sudijono, S.L. Liew, C.-H Tung and H.C. Zeng. Cool Copper Template for the Formation of Oriented Nanocrystalline α-Tantalum, J. Phys. Chem. B, *106*, pp. 12366-12368. 2002**.**

Yu[1], D. and V.W.-W. Yam. Controlled Synthesis of Monodisperse Silver Nanocubes in Water, J. Am. Chem. Soc., *126*, pp. 13200-13201. 2004.

Yu[2], J.Y., S. Schreiner and L. Vaska. Homogeneous catalytic production of hydrogen and other molecules from water—DMF solutions, Inorg. Chimica Acta, *170*, pp. 145-147. 1990.

Yu[3], S.H., M. Antonietti, H. Colfen and M. Giersig. Synthesis of Very Thin 1D and 2D $CdWO_4$ Nanoparticles with Improved Fluorescence Behavior by Polymer-Controlled Crystallization, Angew Chem., Int. Ed., *41,* pp. 2356-2360. 2002.

Yu[3], S.H., H. Colfen and M. Antonietti. The Combination of Colloid-Controlled Heterogeneous Nucleation and Polymer-Controlled Crystallization: Facile Synthesis of Separated, Uniform High-Aspect-Ratio Single-Crystalline BaCrO4 Nanofibers, Adv. Mater., *15*, pp. 133-136. 2003.

Yu[4], X.-F., N.-Z. Wu, Y.-C. Xie and Y.-Q. Tang. A monolayer dispersion study of titania-supported copper oxide, J. Mater. Chem., *10*, pp. 1629-1634. 2000.

Zaitseva, N., Z.R. Dai, F.R. Leon and D. Krol. Optical Properties of CdSe Superlattices, J. Am. Chem. Soc., *127*, pp. 10221-10226. 2005.

Zaric, S., G.N. Ostojic, J. Kono, J. Shaver, V.C. Moore, M.S. Strano, R.H. Hauge, R.E. Smalley and X. Wei. Optical Signatures of the Aharonov-Bohm Phase in Single-Walled Carbon Nanotubes, Science, *304*, pp. 1129-1131. 2004.

Zemlyanov, D.Y., E. Savinova, A. Scheybal, K. Doblhofer and R. Schlögl. XPS observation of OH groups incorporated in an Ag(111) electrode, Surf. Sci., *418*, pp. 441-456. 1998.

Zeng[1], H., P.M. Rice, S.X. Wang and S. Sun. Shape-Controlled Synthesis and Shape-Induced Texture of $MnFe_2O_4$ Nanoparticles, J. Am. Chem. Soc., *126*, pp. 11458-11459. 2004.

Zeng[2], H.C. and L.C. Lim. Secondary ionic forces in lead molybdate melt solidification, J. Mater. Res., *13,* 1426-1429. 1998.

Zhang[1], D.K., Y.C. Liu, Y.L. Liu and H. Yang. The electrical properties and the interfaces of Cu_2O/ZnO/ITO p-i-n heterojunction, Physica B, *351*, pp. 178-183. 2004.

Zhang[2], J. Formation of fractal patterns of MoO_3 crystals during phase transformation, Phys. Rev. B, *41*, pp. 9614-9616. 1990.

Zhang[3], L., J.C. Yu, A.-W. Xu, Q. Li, K.W. Kwong and S.-H. Yu. Peanut-shaped nanoribbon bundle superstructures of malachite and copper oxide, J. Crystal growth, *266*, pp. 545-551. 2004.

Zhang[4], R., L. Gao, J. Guo. Effect of Cu_2O on the fabrication of SiCp/Cu nanocomposites using coated particles and conventional sintering, Composites: Part A, *35*, pp. 1301–1305. 2004.

Zhao, M., L. Sun and R.M. Crooks. Preparation of Cu Nanoclusters within Dendrimer tempates, J. Am. Chem. Soc., *120*, pp. 4877-4878. 1998.

Zhao, M.L. and R.M. Crooks. Intradendrimer Exchange of Metal Nanoparticles, Chem. Mater., *11*, pp. 3379-3385. 1999.

Zheng, X.G., C.N. Xu, Y. Tomokiyo, E. Tanaka, H. Yamada and Y. Soejima. Observation of Charge Stripes in Cupric Oxide, Phys. Rev. Lett., *85*, pp. 5170-5173. 2000.

Zheng, X.G., T. Mori, K. Nishiyama, W. Higemoto, C.N. Xu. Dramatic Suppression of Antiferromagnetic Coupling in Nanoparticle CuO, Solid State Commun., *132*, pp. 493-496. 2004.

Zhong, Z., Y. Yin, B. Gates and Y. Xia. Preparation of Mesoscale Hollow Spheres of TiO_2 and SnO_2 by Templating Against Crystalline Arrays of Polystyrene Beads, Adv. Mater., *12*, pp. 206-209. 2000.

Zhou Y.C. and J.A. Switzer. Electrochemical deposition and microstructure of copper (I) oxide films, Scripta Materialia, *38*, pp. 1731-1738. 1998.

Zhu[1], C., C. Chen, L. Hao, Y. Hu and Z. Chen. Template-free synthesis of $Cu_2Cl(OH)_3$

nanoribbons and use as sacrificial template for CuO nanoribbon, J. Crystal Growth, 263, pp. 473-479. 2004.

Zhu[2], H., H. Shen, F. Gao, Y. Kong, L. Dong, Y. Chen, C. Jian and Z. Liu. A study of CuO/CeO2/Al-Zr-O in "NO plus CO", Catal. Commun., *5*, pp. 453-456. 2004(a).

Zhu[2], H., Y. Wang, N. Wang, Y. Li and J. Yang. Hydrothermal synthesis of indium hydroxide nanocubes, Mater. Lett., *58,* pp. 2631-2634. 2004(b).

Zhu[3], J., H. Chen, H. Liu, X. Yang, L. Lu and X. Wang. Needle-shaped nanocrystalline CuOprepared by liquid hydrolysis of $Cu(OAc)_2$, Mater. Sci. Eng. A, *384*, pp. 172-176. 2004(a).

Zhu[3], J., D. Li, H. Chen, X. Yang, L. Lu and X. Wang. Highly dispersed CuO nanoparticles prepared by a novel quick-precipitation method, Mater. Lett., *58*, pp. 3324-3327. 2004(b).

Zhu[4], J.W., H.Q. Chen, B. Xie, X.J. Yang, L. Lu and X. Wang. Preparation of nanocrystalline Cu_2O and its catalytic performance for thermal decomposition of ammonium perchlorate, Chinese J. Catalysis, *25*, pp. 637-640. 2004.

Zhu[5], Y., Y. Qian, M. Zhang, Z. Chen and D. Xu. Preparation and Characterization of Nanocrystalline Powders of Cuporous Oxide by Using γ-Radiation, Mater. Res. Bull., *29*, pp. 377-383. 1994.

Ziegler, K.J., C. Doty, K.P. Johnston and B.A. Korgel. Synthesis of Organic Monolayer-Stabilized Copper Nanocrystals in Supercritical Water, J. Am. Chem. Soc., *123*, pp. 7797-7803. 2001.

Ziegler, K.J., P.A. Harrington, K.M. Ryan, T. Crowley, J.D. Holmes and M.A. Morris. Supercritical fluid preparation of copper nanotubes and nanowires using mesoporous templates, J. Phys.: Condens. Matter, *15*, pp. 8303-8314. 2003.